A STUDY OF HEAVY METALS AND RADIONUCLIDES IN SCOTTISH FRESHWATER LOCH SEDIMENTS

CHARLOTTE L. BRYANT

PhD
UNIVERSITY OF EDINBURGH
1993

Declaration

The work presented in this thesis is entirely my own, except where reference is made to other sources. Some of the results have been published elsewhere, but the work has not been submitted, in part or in whole, for any other degree.

Acknowledgements

I am very grateful to my supervisors Dr John Farmer and Dr Gus MacKenzie for all their input, advice, discussion and effort throughout my PhD, which has helped me to learn a great deal about research and organisation.

At IFE I would like to thank my supervisor Dr Tony Bailey-Watts for his advice and encouragement, and Alex Kirika, who ensured that the fieldwork was always highly efficient and enjoyable.

I thank Tracy Shimmield for her help and advice with the γ-spectrometry. Thanks to Colin Robertson for help with γ-spectrometry, Elaine McDougall for CHN analysis, Tim Allott and Don Monteith (UCL) and Mr R. McMath and Mr R.Tippett (Glasgow University Field Station) for fieldwork co-operation, and the NERC for studentship funding.

Finally, I would like to thank all the people who have assisted me in various aspects of my work during the past four years: Sid and Margaret Bryant, Carol Sugden, Ali Sadler, Stuart Young, Lizzie Shepherd, Plaque Ball, Mick Blunt, Cecile Belmont, Iain Gunn, Karen Dews, Andrea Meachan, Lorna Boyd, Carolyn Peters, Suzanne Cameron.

Abstract

Heavy metals (Fe, Mn, Pb, Zn, Cu, Cd, Co and Ni) and radionuclides ^{210}Pb, ^{134}Cs and ^{137}Cs were studied in the sediments of Scottish freshwater lochs (acidified Round Loch of Glenhead, oligotrophic/mesotrophic Loch Lomond, eutrophic Loch Leven and Balgavies Loch and Loch Coire nan Arr in the remote north-west) to compare metal behaviour and associations in the different systems. Metal concentrations were determined in acid digested and sequentially extracted sediment and sediment porewaters. Radionuclide concentrations were measured to investigate sedimentation processes.

Redox cycling of Fe and Mn was important in all the lochs. In Balgavies Loch, porewater data for Fe and Mn were related to redox conditions at the time of sampling, whereas the solid phase concentrations were still changing in response to recent water column stratification. The association of Fe with organic matter was additionally important in surface sediment of Round Loch and Loch Coire nan Arr. Mn behaviour in Round Loch was also influenced by surface water acidification via post-depositional leaching of Mn from the sediment and/or a pH-related decrease in the efficiency of Mn sedimentation, resulting in increasing Mn concentration with depth.

Post-depositional mobility of Pb was not evident, despite the association of Pb with Fe oxides/hydroxides in sediments from all the lochs. This was supported by low, or non-detectable, porewater Pb concentrations and little change with depth in the relative concentrations of Pb in each fraction. Zn was generally more labile than Pb and, in Loch Coire nan Arr and Balgavies Loch, redox related release of Zn from the sediment and short-range mobility was apparent. In Round Loch, Zn concentrations, decreasing sharply towards the sediment surface, were explained by historical trends in pollutant Zn deposition to the loch, as well as a pH-related decrease in the efficiency of Zn deposition to the sediment. Similar concentration profiles of Cd and Zn in Loch Coire nan Arr and Round Loch suggested that Cd was influenced by the same processes as Zn. Cu was significantly associated with organic matter in all the lochs but only in Loch Coire nan Arr was there any evidence for minor release and reprecipitation, within the surface sediment.

^{210}Pb and radiocaesium data showed sediment mixing occurring in all five lochs. Mixing was intense in Balgavies Loch, Loch Leven and the central basin of Loch Lomond, precluding sediment dating and a historical interpretation of metal concentration trends. In Round Loch, Loch Coire nan Arr and Loch Lomond (southern basin), core chronologies indicated broad agreement between Pb and Zn (and Cd) concentration trends and historical changes in atmospheric pollution. Unlike

in Round Loch and Loch Lomond, Cu concentration patterns in Loch Coire nan Arr were not attributable to historical trends.

'Excess' pollutant metal inventories (g m^{-2}) for Pb and Zn were similar in Loch Leven (mean = 0.47 and 0.69 respectively) and nearby Balgavies Loch (0.47 and 0.84), and highest in Loch Lomond (S. basin) (5.4 and 11.5), which is close to urban and industrial areas. Coarser grained sediment in the central basin of Loch Lomond resulted in lower inventories of 1.59 (Pb) and 3.10 (Zn). Cu inventories ranged between 0.072 for Loch Leven and 0.38 for Loch Lomond (S. basin).

Radiocaesium inventories, separated into fallout sources from weapons testing and Chernobyl, showed a wide range of values, due to varying fallout inputs and behaviour of radiocaesium in the lochs. Estimated Chernobyl inventories in the organic-rich sediments of Round Loch were low (4.7-7.4 kBq m^{-2}) compared with reported fallout deposition to the area (20-38 kBq m^{-2}), because of inefficient deposition of radiocaesium to the sediment and/or post-depositional losses to the water column, followed by loss from the loch via hydraulic flushing. Radiocaesium was highly mobile via downwards diffusion in Round Loch sediment and historical trends were obscured at site 1. There was some radiocaesium movement in Loch Coire nan Arr sediments, probably due to diffusion and/or mixing, but calculated inventories (Chernobyl ^{137}Cs 0.13 - 0.52 kBq m^{-2}) were within the range of recorded deposition values. Calculated ^{137}Cs inventories for Loch Leven and Loch Lomond (0.78 and 2.6 - 6.8 kBq m^{-2} respectively, for Chernobyl fallout) agreed well with reported values, as radiocaesium was efficiently bound by the clay-rich sediment. In Loch Lomond, peaks due to radiocaesium fallout maxima were clearly discernible and, in the southern basin, the peak positions agreed with ^{210}Pb-derived dates. In contrast, intense sediment mixing in Loch Leven and Balgavies Loch had obscured the records of historical trends in fallout deposition.

Contents

List of Tables **page no.**

List of Figures

Chapter 1 Introduction

1.1 Sources and fates of metals in aquatic ecosystems: background to study

Sources of heavy metals (*e.g.* Pb, Zn, Cu, Cd) in the aquatic environment may be natural or anthropogenic. The natural processes of erosion and weathering of rock deposits result in mobilisation and cycling of metals in the environment. Anthropogenic sources of heavy metals include mining activities such as smelting, fossil fuel combustion (including alkyl lead petrol additives) and waste from industrial processes (Table 1.1). Metals from these sources may be introduced into aquatic systems by atmospheric deposition (dry and/or wet), direct inflow or industrial waste dumping and runoff from surrounding land. Since the Industrial Revolution there has been a marked increase in releases of heavy metals to the environment (Nriagu, 1979; Nriagu, 1990; Foster *et al.*, 1991) and a corresponding increase in metal loading to aquatic ecosystems. Table 1.2 shows worldwide emissions of various metals to the atmosphere from natural and anthropogenic sources, the main metal pollutants in terms of factor enhancement being Pb, Zn, Cd and V. While there has been a marked increase in pollutant metal inputs since the Industrial Revolution (*ca.* 1750), Pb concentrations in Greenland ice and snow began increasing as a result of human activities several thousand years ago (Ng and Patterson, 1981). By 1970, there had been a 200-fold enhancement overall. Ng and Patterson (1981) also concluded that by 1970 more than 99% of Pb in the troposphere of the northern hemisphere originated from human activities, largely from the use of alkyl leaded petrol. A more recent study (Boutron *et al.*, 1991), has shown that Pb concentrations in Greenland snow have decreased by a factor of 7.5 since the limitation in use of petrol Pb additives from about 1970 onwards. Over the same time period Cd and Zn concentrations have decreased by a factor of 2.5, whereas Cu concentrations have remained relatively constant.

The behaviour and distribution of metals in the aquatic environment is an important area of study as:

i) In high concentrations, many metals are toxic to living organisms, although in trace concentrations some of these elements may also be essential (Moore, 1991; Dave, 1992).

ii) Metal concentration profiles in sediments have traditionally been interpreted in terms of a historical record of metal deposition, which in the light of evidence of post-depositional metal mobility may not always be valid (Farmer, 1991; Allen et al., 1990).

Table 1.1 Worldwide atmospheric emissions of metals from anthropogenic sources in 1983 (Nriagu and Pacyna, 1988).

element	thousand tonnes per year							
	energy production	mining	smelting and refining	manufacturing processes	commercial uses[1]	waste incineration	transportation	total[2]
Sb	1.30	0.10	1.42			0.67		3.5
As	2.2	0.06	12.3	1.95	2.02	0.31		19
Cd	0.79		5.43	0.60		0.75		7.6
Cr	12.7			17.0		0.84		31
Cu	8.04	0.42	23.2	2.01		1.58		35
Pb	12.7	2.55	46.5	15.7	4.50	2.37	248	332
Mn	12.1	0.62	2.55	14.7		8.26		38
Hg	2.26		0.13			1.16		3.6
Ni	42.0	0.80	3.99	4.47		0.35		52
Se	3.85	0.16	2.18			0.11		6.3
Ta	1.13			4.01				5.1
Sn	3.27		1.06			0.81		5.1
V	84.0		0.06	0.74		1.15		86
Zn	16.8	0.46	72.0	33.4	3.25	5.90		132

[1]including agricultural uses
[2]totals are rounded

Table 1.2a Worldwide emissions of metals to the atmosphere from natural and anthropogenic sources in 1983 (Nriagu, 1991).

element	thousand tonnes per year		
	natural sources	anthropogenic sources	anthropogenic/ natural
Sb	2.6	3.5	1.3
As	12	19	1.6
Cd	1.4	7.6	5.4
Cr	43	31	0.72
Cu	28	35	1.2
Pb	12	332	28
Hg	2.5	3.6	1.4
Mo	3.0	6.3	2.1
Ni	29	52	1.8
Se	10	5.1	0.51
V	28	86	3.1
Zn	45	132	2.9

Table 1.2b Rationale for choice of metals studied

metal	reason for study
Fe and Mn	to provide information on the presence/extent of redox-driven diagenesis (and the redox regime in the sediment) of these metals, which might influence the behaviour of other metals;
Pb, Zn, Cu and Cd	significant pollutant inputs of these metals to aquatic systems (Pb and Cd highest emissions from pollutant sources to atmosphere in terms of factor enhancement over natural sources); in high concs., possible toxic effects on biota; commonly chosen in other studies of metal behaviour;
Co and Ni	behaviour of these metals reported to be related to Fe and/or Mn redox cycling;

iii) The biogeochemistry of metals should be fully understood in order for rational decisions to be made about environmental management.

The rationale for choice of metals studied is shown in Table 1.2b.

1.1.1 Factors influencing metal behaviour in the water column of aquatic systems

The chemical speciation of an element in water is an important determinant of its mobility and bioavailability. Metal species may be conveniently sub-divided in terms of their size (Fergusson, 1990). Species < 0.45 μm are arbitrarily defined as soluble, > 0.45 μm as solids. Fig. 1.1 illustrates the variations in species with size for Pb and Cd.

Various factors can influence the speciation of metals in water, including: solubility of metal compounds, metal oxidation state, availability of complexing agents in the water, complex formation, ion-pair formation, adsorption onto or desorption from particulate material, and the redox and pH conditions of the environment. The properties of the metals themselves are important in determining their particular form or association in the aquatic environment.

Eh-pH diagrams are graphical ways of displaying information on equilibrium solubility as a function of pH values and redox conditions (Drever, 1982; Salomons and Förstner, 1984). Fig. 1.2 shows an Eh-pH diagram for Zn in the system $Zn+CO_2+S+H_2O$. While such diagrams may be useful for predicting the occurrence of metals in different forms and their associations and concentrations in different environmental conditions, their validity may be limited because they are based on experimental laboratory data, which may not necessarily be extendable to natural situations.

Properties and geochemistry of metals in freshwaters

Summarised below are the associations of some metals in freshwater, based largely on the work of Moore (1991). Table 1.3 outlines the oxidation states and forms of selected metals,which may be found in freshwaters. Factors which influence the mobility and cycling of trace metals include solution characteristics (pH, Eh, ligand concentrations) and the nature of the solid biotic and abiotic surfaces encountered (such as sediment porosity, scavenging capacity *etc.*). These factors will affect both the behaviour of metals in the water column, whether metal deposition to the sediments occurs (or whether the metal remains in the water column and is eventually flushed out of the lake) and, if so, mechanisms of transfer to the bottom and post-depositional behaviour.

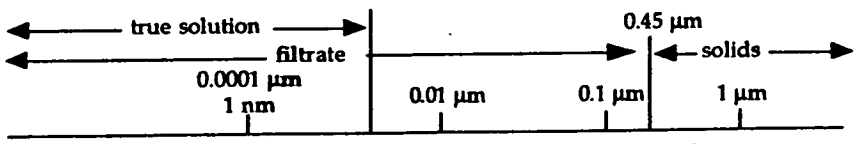

Species	Free metal ion	Ion-pairs, metal chelates	Organic complexes	Metal species attached to high molecular weight organics	Metal species sorbed to colloids	Metal species in organic material	Inorganic solids, sorption, precip-itation
Lead & cadmium	Pb^{2+} Cd^{2+}	$PbCO_3$ $PbHCO_3^+$ PbNTA $PbCl^+$ $CdCO_3$ $CdCl^+$ $CdCl_2$	Pb, Cd-fulvic acid complexes	Pb, Cd-humic acid complexes	Pb, Cd-$Fe(OH)_3$ Pb, Cd-MnO_2	Pb, Cd-amino acids Pb, Cd-organic complexes	Pb, Cd-clays $PbCO_3(s)$ $CdCO_3(s)$ $Pb_3(OH)_2(CO_3)_2$ CdS

Fig. 1.1 Pb and Cd species in water with respect to size (Andreae, 1986 in Fergusson, 1990)

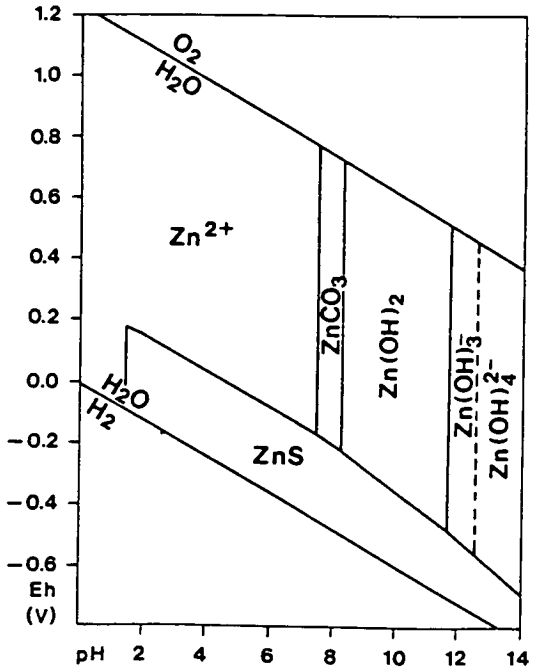

Fig. 1.2 Fields of stability of solids and dissolved Zn species in the system $Zn+CO_2+S+H_2O$ at 25°C and 1 atm. in water (from Hem, 1972 in Salomons and Förstner, 1984)

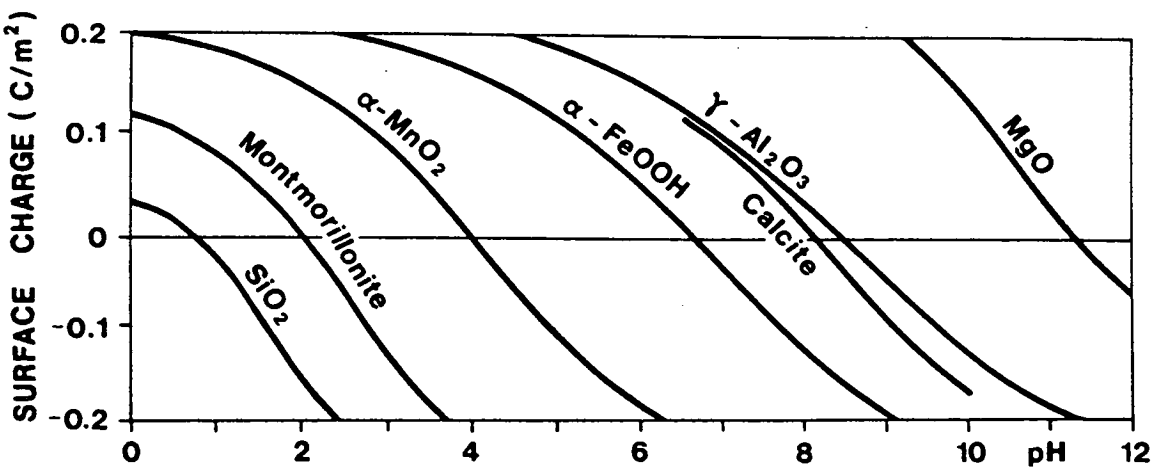

Fig. 1.3 The effect of pH on the surface charge of inorganic particles (Stumm and Morgan, 1981)

Table 1.3 Oxidation states and forms of selected metals found in the water column of freshwaters (Moore, 1991)

metal	oxidation state	metal form
Fe	+2, +3	Fe^{3+} generally in aerobic waters & relatively insoluble salts; Fe^{2+} soluble under sufficiently anoxic conditions;
Mn	various (-3 to +7) +2 and +4 most important	Mn^{2+} highly soluble in anaerobic conditions; Mn^{4+} insoluble; Mn compounds incl. hydroxides, sulphides, carbonates, oxides, phosphates: sparingly soluble; nitrate, chloride, sulphate salts: relatively soluble;
Pb	+2, +4	various low solubility complexes with many anions incl. hydroxides, carbonates, sulphides, less frequently sulphates; moderately strong chelates formed with humic and fulvic acids;
Zn	+2	aerobic conditions: Zn^{2+} dominant at acidic pH, $Zn(OH)_2$ at pH 8-11; anaerobic conditions: ZnS formation (irrespective of pH); binds readily with many organic ligands, esp. in presence of N or S donor atoms;
Cd	+2	homologous chemistry to Zn; oxyphilic and sulphophilic; relatively mobile, as Cd^{2+}, $Cd(OH)_{2aq}$, $Cd(OH)_3^-$, $Cd(OH_4)^{2-}$, $CdCO_3$, various other organic and inorganic complexes; ligand affinity to complex with Cd often decreases with increasing pH, due to formation of solid $Cd(OH)_2$; sorption onto suspended solids, *e.g.* clay minerals, important; occasionally co-precipitation with hydrous Fe, Al & Mn oxides and carbonate minerals is more dominant;
Cu	+2	organic and inorganic ligand complexes; at circumneutral pH most inorganic Cu complexes in solution as carbonate, nitrate, sulphate & sulphide, rather than hydrated divalent cupric ion; neutral ligands, *e.g.* ammonia, ethylenediamine and pyridine, form strong 4 - co-ordinated complexes; insoluble sulphide complexes; stable complexes with humic acids may dominate;
Ni	+2 (primarily)	reducing conditions: relatively insoluble sulphides, if S available in excess; aerobic conditions and pH <9: complexes with sulphates & naturally occurring ligands; reversibly binds with Al and Mn compounds.;
Co	+2, +3	dominant species: Co^{2+}, $CoCO_3$, $Co(OH)_3$ & CoS; Co co-ordination compound, cyanocobalamin (Vitamin B12), can also occur; may form chelates of moderate stability;

Equilibrium-solubility control

Metal concentrations in solution may be regulated by equilibrium with respect to a solid phase containing the metal as a major component. Ion activity products in waters can be compared with solubility products of mineral constituents of the solid phase to determine whether the solubility of the solid phase influences the solution concentration of the metal. If equilibrium between the solid and solution phase is controlling the concentration of a dissolved metal, then the ion activity product of the dissolved mineral constituents should be close to the solubility product of the solid phase. If an element occurs in a different oxidation state in the solid from that in solution (*e.g.* Fe^{2+} - Fe_2O_3, Mn^{2+} - MnO_2), the solubility product must take account of the redox potential pE. Generally, solubility equilibria provide upper limits to the concentrations of dissolved trace metals. It is unusual for water to be supersaturated with respect to a solid phase by more than 3 orders of magnitude (i.e. observed concentration > 1,000x equilibrium concentration) (Drever, 1982).*

Adsorption and co-precipitation

The concentrations of dissolved metals in natural waters are often much lower than would be expected on the basis of either equilibrium solubility calculations or of supply to the water from various sources. The most common reason for this is adsorption of the element onto a solid phase (Drever, 1982). Adsorption occurs when a dissolved ion or molecule becomes attached to the surface of a pre-existing solid substrate. Generally, adsorption does not occur at very low pH, whereas at high pH all cations are strongly adsorbed. The pH range over which no adsorption to complete adsorption occurs is different for each ion and, to some extent, for different substrates (Fig.1.3). Co-precipitation occurs when a dissolved species is incorporated as a minor component in a solid phase as that phase itself is precipitated. Adsorption may be sub-divided on the basis of the following processes (Fergusson, 1990):

i) Physical sorption

This occurs by non-specific electrostatic attraction, involving an electric double layer set up between the charged surface (*e.g.* on a clay or Fe/Mn hydrous oxide, described below) and the sorbed species (which may be ionic or polar). The charged surface changes as a result of the adsorption and this may influence subsequent processes. The zero point charge (ZPC) is the pH at which the surface has zero charge and the charge alters from positive to negative at pH values above or below the ZPC. Table 1.4 lists the ZPCs of some common environmental materials. At pH values sufficiently far from the ZPC, repulsion of the like-charged solid surfaces maintains

* see Corrigenda, page 365

Table 1.4 Zero point charges for some environmental materials (from Förstner, 1980)

material	pH at ZPC
α-Al_2O_3	9.1
α-$Al(OH)_3$	5.0
γ-Fe_2O_3	6.7
$Fe(OH)_3$ amorphous	8.5
MnO_2	2 - 4.5
SiO_2	2.0
Kaolinite	4.6
Montmorillonite	2.5
Calcite	8 - 9.5

dispersion of the particulate material, but as the ZPC is approached flocculation and coagulation occur because the repulsion is reduced.

ii) Chemisorption and co-precipitation

Sorption of heavy metals onto clays is controlled by the number of free sorption sites on the clay surface. The pH, and nature of the metal species (*i.e.* their charge and hydration) also affect sorption. Different clays vary in their ability to accumulate heavy metals, related to the potential of the clay to expand, which effectively increases its surface area and therefore heavy metal uptake. (Drever, 1982).

Adsorption by hydrous Mn and Fe oxides

Hydrous Mn and Fe oxides are almost ubiquitous in sediment and water column particulates where conditions are not strongly reducing (Drever, 1982). They occur as coatings around silicate grains and as discrete grains of oxide mineral. The hydrous Fe oxide is often amorphous and Mn generally occurs as poorly crystallised birnessite or todorokite. (ibid.) Both Mn and Fe hydrous oxides are very fine-grained, with surface areas often around 200 $m^2\ g^{-1}$ giving high adsorption capacities and affinities for heavy metals. Chemisorption, and eventual co-precipitation, of metals with the hydrous oxides of Mn and Fe is a major process for metal accumulation by particulates. Heavy metals may be sorbed to the surface of the hydrous oxides and then exchange for protons or other metal ions. As the particle size increases the metal ions can become incorporated into the lattice of the hydrous oxide. If the oxides are dissolved by reduction, then any adsorbed metals would be released to solution and may become associated with another phase, such as sulphide. The surface charge of Mn and Fe oxides becomes more negative with increasing pH (Fig. 1.3).

Adsorption by silicates

Cation exchange reactions involving clay minerals and zeolites may also result in heavy metal uptake, although it would not be expected to be an important process because the major cations (Ca^{2+}, Mg^{2+}, K^{+} and Na^{+}) should compete with the metals for adsorption sites and displace them into solution. However, the selectivity of an exchanger for a particular ion may be so great that the ion is removed from solution even if only present in a low concentration. In oxidising environments adsorption of metals by Mn and Fe oxides appears to be a more important process (Drever, 1982).

Adsorption by organic matter and uptake by living organisms

The association of metals with organic matter is generally important in lake systems. Metals may associate with living organisms (such as phytoplankton and zooplankton) by direct uptake of bioavailable metal species or by sorption onto the surfaces of the organisms. In addition, organic compounds produced by degradation of organic matter can complex metals in the water (and subsequently in the sediment) and because of this are important ecologically, since they may increase the bioavailablity of a metal. Many of these compounds are not fully characterised or named, but are generally termed 'humic substances' with high molecular weights (700 to $>2x10^6$), such as polysaccharides, proteins and phenols, containing organic groups, which readily co-ordinate metal ions. Humic substances are grouped according to their solubility properties as follows (Saar and Weber, 1982):

Humic acid - soluble in basic solution, insoluble in acid solution and ethanol

Fulvic acid - soluble in acid and basic solution

Humin - soluble in neither acid nor basic solution

Metals may associate with these organic compounds by forming chelates, and humic substances may also be adsorbed by Fe oxides via exchange of humic anions for H_2O and the surface hydroxyl groups (Tipping, 1981). In a particular humic or fulvic acid the number and types of metal complexing functional groups will be similar and at any particular site, the ease and strength of its interaction with a metal ion will depend on the following (Livens, 1991):

i) The affinity of the metal for the binding site

ii) Stereochemical factors, which can be affected by the position of the site within the humic or fulvic acid molecule and by the size of any other ligands on the metal.

iii) The nature of the functional groups around the actual complexing group, *e.g.* an aliphatic hydroxyl group is much less acidic, and therefore a much weaker ligand than a phenolic hydroxyl group.

The physico-chemical properties of humic substances are still poorly understood, however, so that while metal associations with such substances have frequently been observed, the precise nature of the associations, *e.g.* characterisation of the binding site, can only be inferred, often by using models and chemical extraction (Nriagu and Coker, 1980; Tipping, 1993).

This Section (1.1) has, briefly and generally, covered the topics of metal introduction to lakes, and speciation, behaviour, uptake and removal mechanisms in lake waters. Before proceeding with a review of the literature on the behaviour of metals in specific systems, including metal and radionuclide behaviour in bottom

sediments, a discussion of lake characteristics and classification follows to provide a background to the subsequent sections.

1.1.2 Lake characteristics and limnological classification

The biological productivity and chemical composition of natural lake systems (*i.e.* sediments and water column) depend on a number of factors, such as (Wetzel, 1975):

1. Catchment area - catchment bedrock (or underlying rock type if, for example, glacial deposits overly the bedrock) plays an important role in the formation of soil type and, together with the the catchment soil, determines to what extent nutrient or metal leaching occurs. Additionally, the catchment composition is important in determining the buffering capacity of the lake, *e.g.* in response to acid deposition. Catchment soils and vegetation influence the nature and amount of allochthonous (catchment-derived) organic matter in a lake. Surrounding land-use may also be significant *e.g.* whether the land is used for agricultural purposes which may involve the use of fertilisers, potentially affecting the system by run-off of excess nutrients into the lake. ×
2. Streams/rivers flowing into the lake may bring nutrients, metals and suspended particulates.
3. Environmental factors such as light, temperature, wind, oxygen supply and gaseous exchange between the atmosphere and the water.
4. Lake morphometry *e.g.* bathymetry.
5. The lake sediments, which may be sources and/or sinks of various nutrients and metals.

Because of the interaction of metals with biological material and the influence of biological productivity on lake processes and chemistry, it is important in a study of metal behaviour in lakes to have an understanding of the different biological processes which may occur. These are related to lake structure (Fig.1.4) and the biological productivity of lakes is used for limnological classification.

Different parts of lakes have different nutrient, oxygen, light and thermal regimes and are inhabited by characteristic plant and animal communities. On this basis, the region under water extending to the maximum depth of rooted vegetation is divided into major life zones (Fig. 1.4), collectively known as the littoral zone. The extent of this zone is very variable in different lake types and is determined primarily by the lake profile *e.g.* steeply shelving lakes have a narrow littoral zone. In open waters (the limnetic region), light intensity decreases with depth and is dependent upon the water type (*i.e.* clear, muddy *etc.*). At some depth, determined by local

× See Corrigenda, page 365

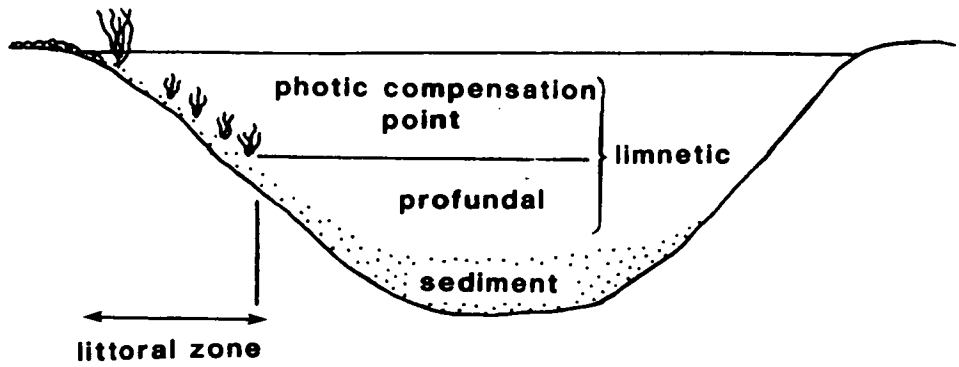

Fig. 1.4 Different zones of a lake (from Anderson, 1981)

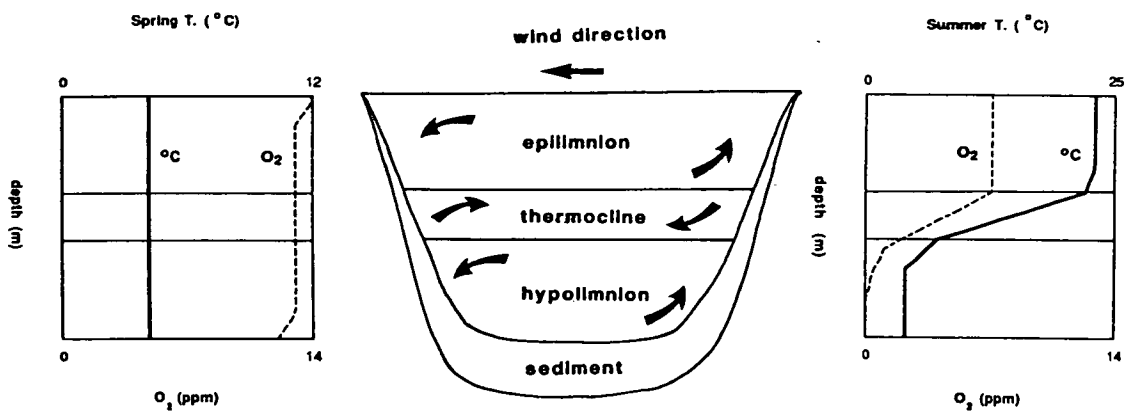

Fig. 1.5 Thermal stratification in a north temperate lake (from Anderson, 1981)

conditions, light intensity decreases to the 'compensation level' below which no photosynthetic activity occurs (the profundal zone). The compensation level usually coincides with the lower limits of the littoral zone. In the sunlit photic zone, photosynthetic activity is carried out by phytoplankton (predominantly unicellular algae and diatoms) which support a major herbivore sub-system (zooplankton and predatory fish). It is generally assumed that production exceeds community respiration in the photic zone and that dead material sinks below the compensation level to the profundal zone where respiration (bacterial mineralisation of dead material) exceeds production. In the profundal zone, no photosynthetic activity occurs and heterotrophs are supported by detritus produced in the photic zone (autochthonous detritus) or by terrestrial litter washed in by streams (allochthonous detritus).

Stratification

The functioning of lake systems is extremely variable in space and time, particularly in the limnetic region (Fig. 1.4) where the seasonal availability of oxygen and nutrients is determined by the thermal properties of the water. (Anderson, 1981) The maximum density of water is reached at 3.94°C and water at any other temperature will be layered on top unless external physical forces (*e.g.* wind action) cause mixing. This may cause stratification in a water column. (ibid.) To illustrate this (Fig. 1.5), a deep temperate lake in Spring may have water uniformly at 4°C. Throughout the water column, oxygen concentration is constant, except for a small decrease at depth due to bacterial activity in the sediments and slightly higher levels at the surface due to enhanced absorption by ripples. As the year progresses, heat is absorbed by the surface waters, causing a rise in temperature, but little heat is conducted to depth and the deep waters remain at approximately 4°C. In an absolutely still lake the temperature would decrease with depth down to the compensation level and then remain constant. Wind passing over the surface of the lake can cause mixing of the low density waters which may circulate independently of the deeper waters. When this occurs, the lake has become thermally stratified into an upper epilimnion and a lower hypolimnion, separated by the thermocline, which is the region of maximum change in temperature with depth (Fig.1.5). Contra-rotating currents may be set up in the hypolimnion in response to the wind induced currents in the epilimnion, but neither oxygen nor chemical species are significantly exchanged across the thermocline. If the bottom sediments of the lake have a high biochemical oxygen demand (BOD) and bacterial degradation of detritus continues in the hypolimnion, oxygen levels in the hypoliminion can decrease until anaerobic conditions are established. In temperate, stratified lakes when the surface waters cool in late summer, heat is lost from the water

faster than it is absorbed and finally the epilimnion and hypolimnion equilibrate and the water column can then mix or overturn under the influence of autumn winds. Stratification may also occur if the surface of the lake is frozen, with cold (< 3.94°C) surface waters of the epilimnion overlying hypolimnetic waters at approximately 4°C (Anderson, 1981). Shallow lakes do not show thermal stratification and, if wind action is sufficient, even deep lakes may not stratify to the point where a redox gradient occurs (although this is also dependent on the lake productivity and, therefore, hypolimnetic BOD). This applies to many of the Scottish lochs, few of which have been reported as developing anoxia in the hypolimnion, although they may be thermally stratified (A.Lyle, pers. comm.).

Trophic status

The trophic status of lakes has been discussed by Anderson (1981) who indicates that lakes under natural conditions may be broadly classified into oligotrophic and eutrophic types according to their nutrient status and associated features. Although there is no strict classification system for lakes, Table 1.5 shows some characteristics of the different types, though not all lakes fit into this scheme and additional types are recognised (*e.g.* saline, ultra-eutrophic).

Typical oligotrophic (low nutrient-status) lakes are clear, deep water bodies, usually found in regions of acid igneous rock. Nutrient input from the catchment is low, as is the primary productivity, and phytoplankton do not show marked seasonal blooms, because of the low availability of nitrogen and phosphorus. Phosphorus becomes bound by iron/humus colloidal complexes and is only released under anaerobic conditions when Fe is reduced. Although oligotrophic lakes may become thermally stratified, anoxia in the hypolimnion is rarely achieved because the low organic matter content of the surface sediments has insufficient BOD to deoxygenate the bottom waters. Eutrophic (nutrient-rich) lakes are found in lowland regions and are comparatively shallow. Primary production by macrophytes and phytoplankton is at least ten times higher than in oligotrophic lakes, due to a larger nutrient capital and input from the surrounding land. Thermal stratification may occur and anaerobic conditions usually prevail at, or near, the sediment surface, from which phosphorus is mobilised. Algae may then become so prolific that the lake waters turn green at certain times of the year. Oligotrophy and eutrophy are the extremes of a continuum of lake types and mesotrophy is recognised as the intermediate.

Table 1.5 Typical ranges of characteristics for different types of lakes (from Whittaker 1975, in Anderson, 1981)

	Oligotrophic	Mesotrophic	Eutrophic
Net primary productivity ($g\ m^{-2}\ y^{-1}$)	15-50	50-150	150-500
Phytoplankton biomass ($mg\ m^{-3}$)	20-200	200-600	600-10,000
Total organic matter ($mg\ l^{-1}$)	1-5	2-10	10-100
Chlorophyll a ($\mu g\ l^{-1}$)	0.3-3	2-15	10-500
Light penetration (m)	20-120	5-40	3-20
Total phosphorus ($\mu g\ l^{-1}$)	<1-5	5-10	10-30
Inorganic nitrogen ($\mu g\ l^{-1}$)	<1-200	200-400	300-650
Total inorganic solutes ($mg\ l^{-1}$)	2-20	10-200	100-500

1.1.3 The influence of lake characteristics on metal behaviour

In view of the range of factors which can affect their speciation and associations, metals might be expected to show different behaviour in different lake types. For example, in a recent review article, Livett (1988) illustrated some of the different factors important in the sediments of diverse lake systems:

1. Lake acidification has been reported to cause remobilisation of some metals from surface sediments.
2. In very reducing, organic-rich sediments, such as those found in deep, permanently anoxic basins, heavy metals can form highly stable complexes with transformed organic matter and are therefore retained in porewaters.
3. In seasonally anoxic, eutrophic sediments, insoluble sulphides are an important sink for metals as organic matter decomposes. Release of some metals to the overlying water may result from periodic oxidation of sulphide to sulphate.
4. In well-mixed, oxygenated lakes, and/or those low in productivity, generally the co-precipitation of metals with Fe/Mn oxides is a more important metal sedimentation mechanism than sulphide formation. Extended aerobic periods in the bottom waters can lead to deposition of Fe and Mn at the sediment surface, forming crusts, which can also act as a focus for metal accumulation due to the scavenging capacity of their oxides.

Whilst the above points generalise the biogeochemical behaviour of metals which may have very different properties, they provide a convenient grouping of aquatic systems into similar types in which metal behaviour can be studied.

Acidification

Wet and dry deposition of acidic substances emitted to the atmosphere by anthropogenic activities, such as fossil fuel combustion, has been significant throughout the world in recent decades. This acidic deposition has resulted, in the northern temperate zone, in average rainwater pH values of less than 4.5 (Likens, 1989) and has caused widespread ecological damage to lakes and streams, many of which are unable to support viable populations of fish and other aquatic organisms (Maitland, *et al.* 1987). Acid deposition may affect the behaviour of metals in lakes both directly, by increasing metal solubility, or indirectly, due to its effects on mobilisation of metals in the catchment, nutrient cycling, microbial processes and growth and survival of aquatic organisms.

In a review of literature on the effects of acidic deposition on lakes, Likens (1989) commented that the response of any single lake is highly individualistic, depending on a variety of complex, interacting factors. Catchment characteristics, such as soil vegetation type and different lake morphometries and flushing rates, different water chemistry and productivity, may all influence the extent to which a lake is affected by acidic inputs. However, there is unequivocal historical evidence of acidification, such as diatom-inferred pH changes (*e.g.* Battarbee *et al.*, 1989), in many lakes exposed to acid deposition in sensitive areas (*i.e.* those with hard bed-rock, thin, acid soils and little acid neutralising capacity). Such lakes show the following general effects of acid deposition (Likens, 1989):

1. Increase in sulphate, and possibly nitrate, concentration in the water column. The increase in sulphate may be associated with an increased deposition of sulphides to the sediment (e.g. with iron).
2. Decrease in alkalinity and/or the pH of the water column and the surface of the sediments.
3. Increase in heavy metal concentrations in the water column (*e.g* due to mobilisation of metals from the catchment or due to increased atmospheric deposition associated with the combustion of fossil fuels), which may result in greater deposition of metals to the sediments.
4. Greater range of chemical conditions in the water column or at the sediment-water interface, *e.g.* due to episodic acidic pulses from snowmelt.
5. Possible increase in the transparency of the water column.
6. Physical and biological changes at the sediment surface, such as increased growth of algal mats and moss and decreased diversity (and possibly abundance) of invertebrates.

Some, or all, of the above points may have an impact on metal behaviour and there are two basic approaches to the study of this: by laboratory or field-based experiments and direct observation of the natural system. Experimental studies of the effects of acidification on metal behaviour have focused either on laboratory investigations of release of metals from sediment at different pH values, or use of experimental acidfication or radiotracer techniques directly in lakes.

Trefry and Metz (1984) used leaching of Mississippi river sediments and particulates at pH values of 2.2-6.0 as an experimental approach to studying the release/uptake processes of metals in sediment as a function of pH. They found that depending on sample and metal type, metal removal in the leachate from the sediment increased linearly or exponentially with surface water pH. For pH values comparable with surface water pH of acidified lakes (pH 4-6) concentrations of leachable Mn, Cd

and Zn were considerably enhanced relative to pH 6 leachates, but there was negligible enhancement in concentrations of Fe, Cu and Pb. Mobilisation of metals from sediments from Ramsey Lake near Sudbury, Ontario (Arafat and Nriagu, 1986) was simulated by experimental lowering of pH in water overlying sediment cores over a period of 12 months. The long-term pH-induced release from sediment to water for each metal increased exponentially with a decrease in pH below a threshold value, which, for Cu, Ni, Zn and Cd, was around 3-4. In a similar study, enclosures in Lake 223 of the Canadian Experimental Lakes Area were acidified to pH 5.7 and 5.1 respectively, using H_2SO_4. Control enclosures were maintained at pH 6.7-6.8 (Schindler *et al.*, 1980). Al, Mn, Zn and Fe were found to be released from sediments at pH 5 and 6. Using radiotracers, acidification was found to increase the solubility of several heavy metals, including Fe, Co, Mn and Zn. In contrast, V and Hg solubility decreased with increasing acidity. Loss to the sediments was slowed by acidification for Mn and Zn , but enhanced for Cs and V (Schindler *et al.*, 1980).

Different species of diatoms are characteristic over narrow pH ranges and identification of their remains from dated sediment cores has enabled a correlation to be established between diatom species and historical changes in the pH of the surface water. (Battarbee et al., 1985) Heavy metal concentration-depth profiles in sediments have been used in surface water acidification studies (*e.g.* Battarbee *et al.*, 1985) on the assumption that the deposition history of acidic precipitation is broadly accompanied by that of several heavy metals, such as Zn and Pb. This enables a history of contamination to be established, as shown by Rippey (1990) using dated sediment cores from lakes in areas of high and low acid depostion. Metal contamination was found to increase this century in areas of high acid deposition although, in some cases, heavy metal fluxes dropped over the past 10-30 years. While this trend agreed well with evidence from sediment cores of historical atmospheric contamination changes in sulphur and organic pollutants, as well as the diatom-inferred pH changes, the possibility of surface water acidification altering the historical record of metal contamination in the sediment should be considered.

White and Driscoll (1987a) observed elevated concentrations of Zn in acidic Darts Lake, USA. Zn was found to be a conservative solute, as indicated by a low transport of particulate-bound Zn, and inputs closely balancing efflux of Zn from Darts Lake. They also noted that the deposition of particulate Mn to sediment traps was similar to that of Zn, contrasting with Pb and Al, which showed 60-100x higher deposition rates. Laboratory based sediment leaching studies were additionally used to show that there was a marked increase in the retention of Zn by particulate matter (and in the distribution coefficient K_D) with an increase in solution pH from 3.5 to 6.0.

This change in Zn behaviour as a function of pH has implications for the interpretation of sedimentary Zn profiles.

In another study of Darts Lake (White and Driscoll, 1985), the cycling of Pb was investigated. In-lake chemical transformations, such as the association of Pb with Al oxides, were found to be important in determining the behaviour of Pb. The authors suggested that the effects of acidification, such as the mobilisation of Al and the formation of particulates, may vary through time (especially in Darts Lake, which receives acidic pulses due to snowmelt) resulting in temporal changes in the retention of Pb in the waters and sediments of low ionic strength lakes. Therefore, the frequently reported increase in the rate of Pb deposition to sediments of acidic lakes may not be due solely to increasing atmospheric Pb deposition, but also to an increase in Pb scavenging by particulates. However, as particulate formation and Pb concentration in Darts lake were enhanced during stratified periods, caution must be exercised in extending this interpretation to other acidic lakes, which may not stratify or receive acidic pulses.

Deposition of Mn to the sediments of Darts Lake (White and Driscoll, 1987b) was also affected by significant temporal and spatial changes in dissolved O_2 and pH. Mn was highly conservative (*i.e.* influx closely balanced efflux) in the system and the effect of decreasing pH causing decreased K_D (determined by sediment trap and water column concentrations, as well as sediment adsorption studies) showed that Mn behaviour was apparently due to the acidic conditions in Darts Lake.

Consistent with the results from Darts Lake, metal concentrations in a severely acidified Black Forest lake sediment core showed a highly significant negative correlation between diatom-inferred pH and Pb and Al concentrations, and a highly positive correlation in the case of Mn. While the historical increase in Pb concentration with decreasing pH could be a result of greater anthropogenic Pb deposition associated with fossil fuel combustion, the vertical pattern of Mn decreasing towards the sediment surface is probably explicable in terms of reduced deposition of Mn to the sediment with increasing surface water acidity, as suggested by Bendell-Young *et al.* (1989). A similar Mn concentration profile shape was also found in acidified Lake Gårdsjön, Sweden (Renberg, 1985). In this lake Cd and Zn were apparently affected by acidification as the net fluxes of these metals (determined from the 'pollutant' metal concentrations and sedimentation rate) at the time of sampling were similar to those in the early 1900's, deduced from flux calculations, as above. This did not agree with documented trends in fall-out history, despite the slight decrease reported for the atmospheric loading of these metals during the few years preceding the sampling date. This pattern could have been caused by post-depositional leaching of Zn and Cd from

the surface sediment as a result of lowered surface water pH or disturbed sedimentation mechanism (decreased deposition of Zn and Cd to the sediments). The authors considered the former explanation unlikely in view of higher pH values in the porewaters relative to the overlying waters.

Sub-surface peaks in total Zn concentration in the sediments of acid lakes have often been attributed to changes in atmospheric deposition of this metal and/or post-depositional release of Zn from sediment due to acidity. Considerably lower dissolved Zn concentrations in the anoxic porewaters of two acid lakes, relative to the overlying waters, were reported by Carignan and Tessier (1985), who concluded that the observed sub-surface total Zn concentration peaks result from downward diffusion of Zn through the porewaters, followed by formation of relatively insoluble Zn sulphide minerals. The same interpretation was used by Carignan and Nriagu (1985) to explain solid and solution phase Cu and Ni profiles in the sediments of acid Clearwater lake. Developing the work on Zn in the two acid lakes, Tessier *et al.* (1989) measured Zn concentrations in oxic sediments, associated porewaters and overlying waters at 40 littoral stations of lakes covering a large range of surface water pH from 4-8.4. Again, large concentration gradients were found at the sediment-water interface of acid lakes (pH <6), implying downward diffusion of Zn from the water column to the porewaters. A model describing the distribution of labile Zn between the water column and sedimentary Fe oxyhydroxides as a function of pH, predicted that most of the mobile Zn should be present in the water column at pH <5 and in the surficial sediments above pH7. This would therefore mean that the diagenetic diffusion-precipitation of Zn at depth (Carignan and Tessier, 1985) is an indirect effect of recent acidification.

In-situ alkalinity generation

Buffering of acidic deposition to lakes (including their catchments) may occur by chemical weathering processes, such as cation exchange with Ca and Al. This may be very slow in soft-water, hard bedrock areas in which the cation-exchange capacity is easily depleted, leading to acid sensitivity, *i.e.* the lake is unable to buffer the effects of acid deposition. In addition to chemical weathering, biological alkalinity production by sulphate, and nitrate reduction by bacteria, can occur (Rudd et al., 1986). Rates of microbially-mediated sulphate reduction and denitrification have been measured in the sediments of unacidified as well as experimentally and atmospherically acidified lakes in North America and Norway (Rudd *et al.*, 1986). In all of the lakes, H^+ was actively consumed by both sulphate reducers and denitrifiers and this occurred in sediments irrespective of whether they were overlain by oxygenated or anoxic water.

Acidification did not detectably inhibit the activity of the two types of bacteria, even at pH 4.5. Evidence was found that sediments with higher organic carbon contents per unit volume had greater potential for microbial alkalinity production. As atmospheric acid deposition is a result of the formation of nitric and sulphuric acids from the gases emitted during fossil fuel combustion, the associated nitrate and sulphate inputs to lakes may be important in mitigating the impact of acid precipitation in the sediments. On an annual basis, Rudd *et al.* (1986) also found that in lakes receiving significant inputs of both nitric and sulphuric acids, the alkalinity production from denitrification was at least 4-5x greater than that produced by sulphate reduction. Similar results were found by Norton *et al.* (1990) in artificially acidified Lake 223 of the Experimental Lakes Area. They noted too, that the reduction of Mn and Fe in anoxic sediments is an H^+ consuming process. As a result of in-situ alkalinity production the porewaters of acidified lakes may remain circumneutral (Rudd *et al.*; 1986, Herlihy and Mills, 1986).

The extent of alkalinity generation may vary according to the location within the lake (Schafran and Driscoll, 1990). The pH values of near-shore sediment porewaters of acidified Darts Lake were more variable than those in the deeper parts of the lake, in which sediment porewaters were of a higher pH relative to the overlying water. Groundwater seepage appeared to account for much of the variability in the near-shore sites, some of which had acidic porewaters elevated in Al.

Redox cycling

During early diagenesis (*i.e.* a post-depositional change in the composition of recently deposited sediments, as opposed to long-term changes such as metamorphism) of recently deposited sediments, changes in porewater composition may result from the series of reactions which accompany the microbial decomposition of organic matter. Bacteria and other microorganisms obtain energy by oxidising organic compounds and can use a variety of inorganic oxidising agents, *e.g.* O_2 during aerobic decomposition of organic matter via overall reactions of the type:

$$CH_2O + O_2 \longrightarrow CO_2 + H_2O$$

where CH_2O represents organic compounds (Berner, 1980). In sediments with an organic content greater than 0.5%, the concentration of dissolved oxygen in the porewaters is insufficient for complete aerobic oxidation of the organic carbon, leading (in oxygenated water columns) to anoxic conditions below depths of a few cm. Other inorganic oxidising agents are then used (predominantly the electron acceptors NO_3^-, MnO_2, $Fe(OH)_3$, SO_4^{2-}) to oxidise organic matter in the following thermodynamically favourable sequence (from Berner, 1980):

	Reaction	ΔG^o (kJmol^{-1} of CH_2O)
dissolved oxygen	$CH_2O + O_2 \longrightarrow CO_2 + H_2O$	-475
nitrate	$5CH_2O + 4NO_3^- \longrightarrow 2N_2 + 4HCO_3^- + CO_2 + 3H_2O$	-448
Mn oxides	$CH_2O + 3CO_2 + H_2O + 2MnO_2 \longrightarrow 2Mn^{2+} + 4HCO_3^-$	-349
Fe hydroxides	$CH_2O + 7CO_2 + 4Fe(OH)_3 \longrightarrow 4Fe^{2+} + 8HCO_3^- + 3H_2O$	-114
sulphate	$2CH_2O + SO_4^{2-} \longrightarrow H_2S + 2HCO_3^-$	-77
dispro-portionation	$2CH_2O \longrightarrow CH_4 + CO_2$	-58

Where ΔG^o is the standard free energy change for the bacterially-mediated reactions and data for CH_2O and MnO_2 are for sucrose and birnessite respectively.

i) Conceptual models

As a result of organic matter degradation described above, redox gradients develop. In the case of sediments below well-oxygenated water columns, a redoxcline (region of large change in redox potential with depth) will occur, usually a few cm below the sediment-water interface. In a stratified water body, with anoxic bottom waters (hypolimnion), the redoxcline may exist at the oxic/anoxic boundary of the water column, rather than in the sediment. The transport of redox-sensitive elements can be controlled by such redox gradients and, to illustrate this, Mn and Fe redox cycling will be considered, particularly as the oxides/hydroxides of these metals are important scavengers of other elements and therefore play a role in other geochemical cycles. Davison (1985) has discussed the conceptual model for Mn and Fe transport at a redox boundary. A simple illustration of this transport (Fig. 1.6) was shown for a system in which the redox gradient is determined by the oxic/anoxic boundary and a supply of oxidised metal from the oxic region is reduced to the soluble Fe^{2+} or Mn^{2+} form on reaching the anoxic region (Fe^{2+} and Mn^{2+} usually dominate in the reduced form, although other species such as $FeOH^+$ and $FeCl^+$ may also exist). This model produces M^{2+} at the oxic/anoxic boundary and, for a simple one-dimensional example, M^{2+} diffuses away from this point in upward and downward directions. As reduction occurs over a finite distance, the soluble M^{2+} concentration peak is usually rounded, rather than sharp. To maintain the above steady-state profile, there must be a removal mechanism for the soluble species produced. Below the redoxcline, formation of

Fig.1.6 Model for the transport of soluble Fe and Mn at a redox boundary (Davison,1985). (M = metal)

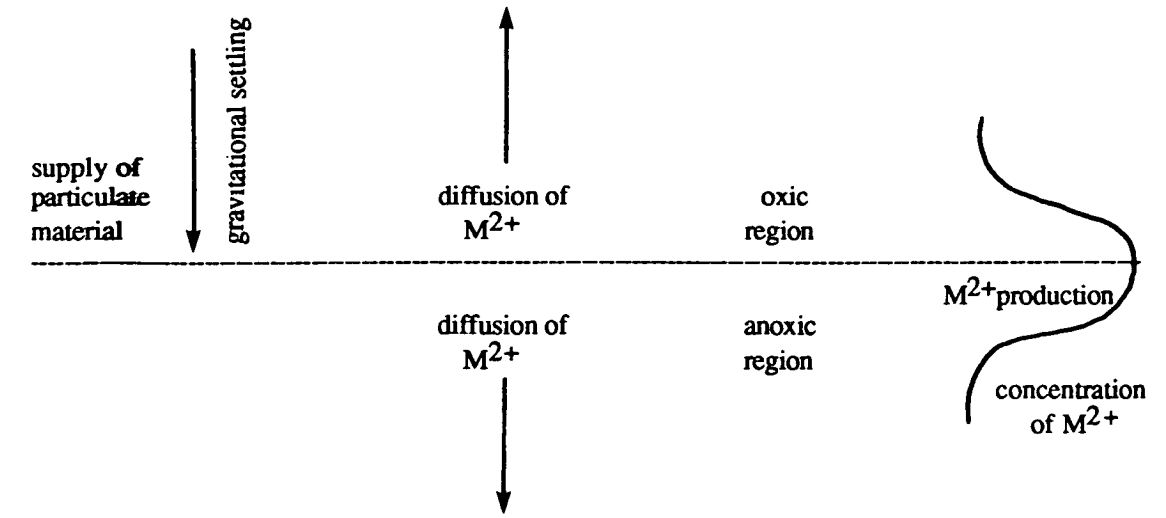

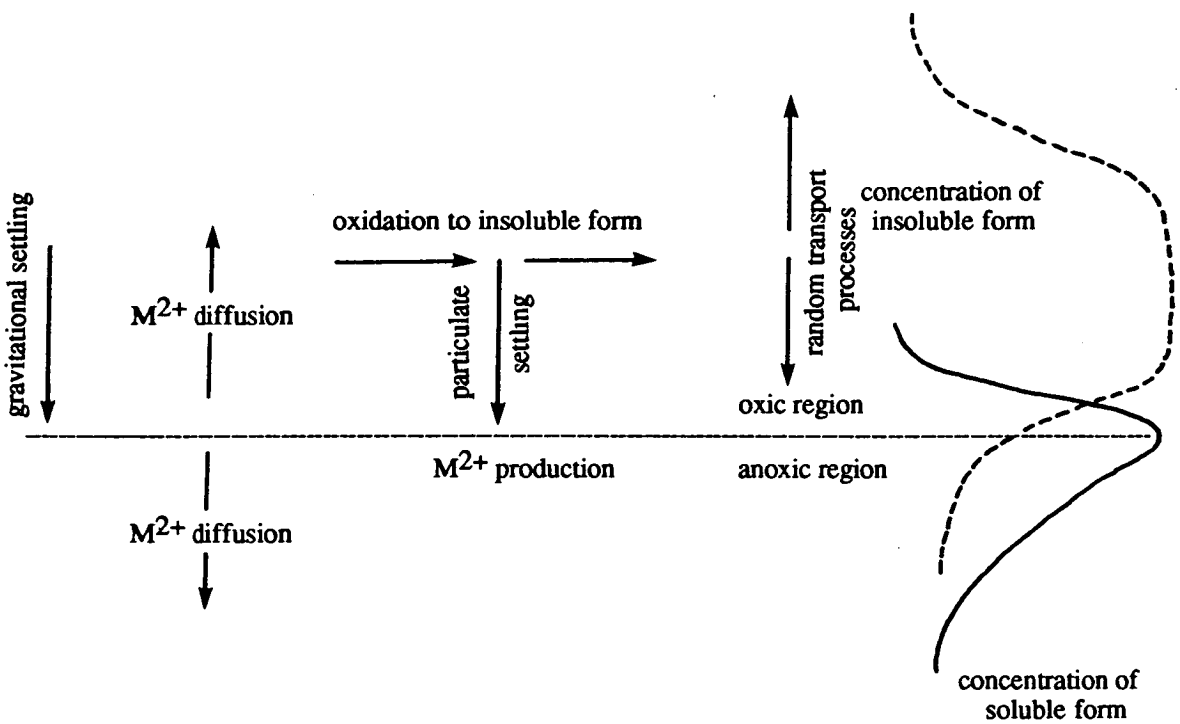

(random transport processes and gravitational sinking are only relevant in the water column).

Fig.1.7 Model for the transport of soluble and solid phase Fe and Mn at a redox boundary (Davison,1985) (M = metal)

minerals, such as MnS and $MnCO_3$, can occur while removal above the redoxcline is usually by oxidation of the divalent metal and precipitation of insoluble oxides.

Davison (1985) lists six factors which could modify the simple model illustrated in Fig.1.6.

1. Inadequate sampling - *e.g.* if only the sediment (and not the water column) is sampled, this may not represent the whole of the generalised profile shape.
2. Horizontal transport - the model assumes transport is restricted to one dimension and for lake sizes other than very large basins, the horizontal transport component may be significant.
3. Variation in vertical transport rate - if the diffusion rates in anoxic and oxic regions differ greatly (as at a sediment-water interface) the concentration profile of M^{2+} would not be symmetrical around the redoxcline.
4. Gradual change in redox environment - the model assumes a distinct and discrete redox boundary, but if this is not so, differences in the shapes of the Fe and Mn profiles are observed due to their different redox potentials and reaction rates.
5. Steady-state conditions may not apply - especially for systems controlled by seasonal events, in which the position of the redoxcline can move quickly and the associated chemistry does not respond on the same time-scale.
6. Authigenic (within lake) mineral formation depends on the lake chemistry. If the solubility product of the divalent cation is exceeded with respect to some anion, such as sulphide or carbonate, the resultant mineral may form, with removal of the cation from solution.

Profile shapes may also appear to be more complicated at sediment-water interfaces, because of the marked differences in the rates of transport operating in the porewaters and overlying waters. Porewater transport can be approximated by molecular diffusion, whereas eddy diffusion (usually 1,000 times faster) is dominant in water columns. Further complications arise if the redox boundary is also situated at the sediment-water interface, because, in this case, most of the solubilised metal is returned to the water column and may not show a high concentration there, due to dispersion by rapid mixing of the water. Similarly, a maximum in the soluble metal concentration may be so sharp that the sampling interval may be insufficiently detailed to show it.

A similar generalised model to that in Fig. 1.6 can also be derived to incorporate associated profiles of the insoluble forms of Fe and Mn (Fig.1.7). In field situations this simplistic model is not usually found, *e.g.* because the position of the redox boundaries is not usually so well-defined in space or time. In addition, Mn and Fe concentration profiles (solid and solution phase) are usually different for the two

metals: generally the Mn concentration peaks are displaced upwards, relative to those of Fe. This is due to the differences in both thermodynamic (Mn is more readily reduced than Fe) and kinetic factors, (Mn is oxidised about fifty times more slowly than Fe in typical aquatic environments; Stumm and Morgan, 1981). The latter means that Mn solubilised in reduced sediment layers is capable of diffusing further than Fe^{2+} through oxic strata before being reoxidised. The degree of enhancement in the solid phase is usually more marked for Mn than for Fe, because much of the total sedimentary Fe is bound within stable mineral lattices and is not mobile under most environmental conditions.

ii) Evidence from field data

Many studies in various lake types have been carried out to investigate the redox-controlled cycling of Fe and Mn and were found to be interpretable in terms of the conceptual models for Fe and Mn transport described above. Subsequent work has been undertaken to examine possible effects of the redox cyling of Fe and Mn on other elements, which may be associated with the solid, oxidised compounds of Fe and Mn, known to be important metal scavengers due to their adsorptive properties.

One of the earliest studies of metal redox cycling, which has formed the basis for much of the work on Fe and Mn redox chemistry in lakes, was that of Mortimer (1941, 1942) on Esthwaite Water, a small productive lake in north-west England. Davison *et al.* (1982) have since observed the dynamics of Fe and Mn in Esthwaite Water by direct flux measurement, using sediment traps, and their work clearly illustrates the differences in thermodynamically- and kinetically-controlled behaviour between Fe and Mn during summer stratification.

Fe and Mn cycling has also been shown to take place in Loch Lomond sediments (Farmer and Lovell, 1984) with a near-surface enrichment of the trace element As clearly related to the dissolution-diffusion-precipitation cycle of Fe (Farmer and Lovell, 1986), as has also been found in a range of Canadian lakes (Belzile and Tessier, 1990).

iii) Influence of Fe/Mn redox cycling on metal behaviour

Changes in the position of the redoxcline in lakes, such as during seasonal stratification and anoxia, have been used to evaluate the effect of Fe/Mn diagenesis on the biogeochemistry of other metals. In the seasonally anoxic Lake Sammamish, Washington, Balistrieri *et al.* (1992a, 1992b) found that changes in Co, Ni, Cu and Cr concentrations in the dissolved and particulate phases occurred during stratification. Bottom water inventories, concentrations and partitioning of Co between dissolved

and particulate phases, were strongly linked to the seasonal cycle of the lake and the cycling of Mn. Particulate Co was mostly associated with the Mn-oxide phase in the epilimnion, but was correlated with particulate Fe in the hypolimnion. Ni cycling was more closely linked with Mn cycling in the water column, but Cd, Cu and Zn were not significantly affected by the cycling of Fe and Mn. A correlation between reactive Si and total acid soluble Zn concentrations suggested the role of biological activity (*i.e.* diatom production and regeneration) in Zn cycling.

In seasonally anoxic Esthwaite Water: concentrations of Fe and Mn in the water column and porewaters changed seasonally, but there were no comparable concentration changes for Cd, Cu, Pb and Zn (Morfett *et al.*, 1988). Throughout the year, the sediments acted as a sink for these metals, which were not released from the sediments at any time of the year. Again, biological uptake and release of Zn, and also Cu, appeared to be an important process and enhanced concentrations of these metals at the sediment-water interface observed during summer stratification were attributed to release from biological material.

Mn and Fe cycling related to sedimentary redox conditions has also been well-established in marine systems, *e.g.* in sediments of the eastern equatorial Atlantic (Froelich *et al.*, 1979). Metal accumulation mechanisms were investigated in Californian coastal sediments by Shaw *et al.* (1990), who found that diagenesis with downcore variations in sediment redox conditions, decoupled the mechanisms of metal transport to the sediments from acccumulation, resulting in solid phase metal concentration profiles that were not interpretable in terms of historical deposition changes. The behaviour of Ni and Co was closely associated with Mn cycling processes - release in the Mn reduction zone, followed by upward migration in the porewaters and scavenging and adsorption by Mn oxides. In contrast, Cr, V and Mo accumulation was enhanced by in-situ reduction, with release to solution occurring under oxic conditions. These metals appeared to be transported to the sediments within biological material. Cu was also transported to the sediments with biogenic material, released upon degradation of the organic matter and generally rapidly removed onto solids.

Gobeil *et al.* (1987) investigated the diagenesis of Cd in Laurentian Trough sediments in relation to Fe and Mn cycling. However, the diagenetic behaviour there was found to be linked to aerobic degradation of organic matter, followed by diffusion of Cd in the porewaters upwards (to the water column) and downwards (to be precipitated, probably as sulphides). In a further study of the Laurentian Trough sediments, Gobeil and Silverberg (1989) explained a near-surface dissolution of Pb as release from organic matter, but a second zone of Pb release was attributed to Fe redox

cycling. Ridgway and Price (1987) have also suggested that Pb is subject to post-depostional mobility, via organic matter degradation, particularly in the sulphate reducing zone in the sediments of Loch Etive, a sea loch on the west coast of Scotland.

The possibility of Pb mobility has implications for the use of ^{210}Pb for sediment dating (Section 1.2.3), since a fundamental assumption of this technique is that Pb is not mobile once deposited in the sediments. Benoit and Hemond (1990) studied the behaviour of ^{210}Pb in an oligotrophic, dimictic lake (*i.e.* the water column overturns, following stratification, twice a year) and showed that releases of ^{210}Pb and ^{210}Po from the sediment occurred, apparently linked to the diagenetic cycling of Fe, and possibly that of Mn. In contrast, Crusius and Anderson (1989) produced evidence from some lakes in the Experimental Lakes Area of ^{210}Pb immobility, showing good agreement between ^{210}Pb-based sedimentation rates and corresponding rates based on other radionuclides and varves. ^{210}Pb mobility has also been evaluated in-situ (Crusius and Anderson, 1990) under anoxic, moderately sulphidic conditions in Black Sea sediments. This was done by examining ^{210}Pb activity across a turbidite of low ^{210}Pb activity surrounded, above and below, by pelagic sediments of much higher ^{210}Pb activity. No evidence was found for significant ^{210}Pb mobility in these conditions.

The redox-controlled diagenesis of Fe and Mn therefore appears to be an important process in a variety of systems and warrants further attention to evaluate its possible effects on the distribution and behaviour of other metals.

Eutrophication

During the past few decades concern over pollution by inorganic substances has grown and is now a central issue in the control of water pollution (Mason, 1981). Eutrophication can be defined as an increase in the rate of input of nutrients (Edmundson, 1974), which may be considered as artificial or cultural if the increase is caused by human activities, or natural if a result of non-human processes, such as forest-fire.

In the majority of lakes phosphorus is normally the limiting factor to algal growth (although nitrate availability may be limiting during peak times of algal growth in the summer), so that an increase in phosphorus in the water will result in an increase in productivity. (Mason, 1981) If nitrate becomes limiting, some blue-green algae are able to fix atmospheric nitrogen and continue to grow, provided phosphorus is not limiting. Most of the polluting nutrients enter lakes and watercourses in effluents from sewage treatment works, in untreated sewage, or from farming activities. (ibid.) Roosting waterfowl excrement may also be a significant source of phosphorus in lakes (Bailey-Watts and

Kirika, 1987). Phosphorus is present in the water in both soluble and particulate form and, once deposited in the sediment, may undergo remobilisation due to redox changes. As a consequence of the seasonal increase in algal productivity in eutrophic lakes, especially where marked algal blooms occur, there may be an impact on the behaviour of metals, *e.g.* due to an uptake of metals by algae or an increase in particulates (algae) in the water column.

Sediment mixing

Sediment transport (and therefore metal transport) may be influenced by physical or biological mixing. Physical mixing is mainly by focusing (greater sediment accumulation in the deeper parts of lakes), slumping (periodic accumulation of sediment from slopes in deeps) or disturbance of the sediment by wave action. Bioturbation involves the disturbance of sediment by organisms, usually benthic invertebrates (such as tubificid worms), which burrow in the near-surface sediment causing reworking of the sediment (Robbins, 1982), horizontally or vertically. Benthic organisms may also irrigate their burrows, influencing the interaction between the porewater and the water column and deposition of fecal pellets at the sediment surface can affect sedimentary metal concentrations by bringing older material in contact with new material (Reynoldson, 1987). Disturbance of sediment by bioturbation or physical means results in a distortion of the historical sedimentary record and is further discussed in Section 1.2.3.

1.2 The investigation of metal behaviour in aquatic systems: requirements for sampling and analysis

Lakes are dynamic systems and in order to study the behaviour of metals within such systems, interactions between different phases in the lake must be considered. The sediment-water interface is an important 'boundary' between the water column and sediment and it is therefore necessary to obtain undisturbed samples of this interface. Water column samples should also be collected and filtered through a suitable filter size to obtain information on the distribution of metals between the dissolved phase and suspended particulates. As conditions such as suspended particulate load, oxygen concentration and temperature can vary throughout the water column, especially if stratification occurs, samples should be taken at different depths in the water.

Collection of sediment cores is an essential part of the study of metal behaviour in lake systems as metal concentrations are generally much greater in sediments than in

the overlying water column and this may have ecotoxicological implications as bottom-feeding benthic invertebrates form the diet of some fish. Sediments can act as both sources or sinks of metals within a lake system. If sediment has not been disturbed since deposition, a suitably sampled core can provide information on the historical changes of metal input to the lake, using acid digestion of sediment to evaluate metal concentrations. Sequential extraction techniques can be used to establish geochemical associations of metals and whether changes occur in such associations with depth in the sediment, as a result of changing conditions. Analysis of metals in porewaters provides a link between processes influencing metals in the water column and those occurring in the sediment, and may also provide evidence for metal mobility (*e.g.* by diffusion) and/or establishment of equilibria with solid mineral phases.

In addition to metal analysis in the sediment column, an important feature in the study of metal behaviour is to obtain information on the sedimentation processes, such as the rate of sedimentation (accumulation), to enable full interpretation of the metal data. This is frequently achieved using naturally occurring ^{210}Pb and the anthropogenic radiocaesium isotopes, ^{134}Cs and ^{137}Cs, which are useful for establishing sedimentation rates, core chronology and mixing characteristics.

With the above requirements for sampling and analysis in mind, some of the currently available techniques are discussed in the following sections.

1.2.1 Field sampling

Sediment core collection

In any investigation of the vertical distribution of pollutants in sediments, the collection of undisturbed sediment, including the sediment-water interface, is of primary importance. There is a range of devices available for sediment coring, not all of which are suitable for collection of undisturbed sediment. Baxter *et al.* (1981) have shown that while radionuclide and metal concentration data obtained from a sediment core, collected with a small diameter gravity corer, appeared plausible when considered in isolation, comparison with data from an adjacent core collected with a soft-landing, hydraulically damped Craib corer (Craib, 1965) indicated that loss of surface sedimentary material and possible distorting effects can occur with the gravity corer.

The Jenkin Surface-Mud Sampler (Ohnstad and Jones, 1982) was designed to collect undisturbed sediment cores, as well as the water immediately overlying the sediment. In suitable sediment (soft ooze sediments), the corer has been observed in action by divers, confirming that its use causes minimal disturbance of the surface

sediment (ibid.). If disturbance does occur however, because of non-vertical entry into the mud or poorly controlled lowering of the apparatus, sediment disturbance is easily observed (via the perspex core tube) as particles or cloudiness in the overlying water. Similarly, the Mini-Mackereth corer (Mackereth, 1969), which may be used to collect sediment cores of around 1 m length, has been developed with consideration given to minimal disturbance of the sediment-water interface and, again, any disturbance would be observed in the overlying water. Finally a third device, the modified Kajak corer (Brinkhurst *et al.*, 1969), also suits the requirements for sediment core collection and has the advantage of being a small apparatus, useful for operating from small boats.

All three corers have been used extensively in studies requiring undisturbed sediment and overlying water and are therefore suitable for use in this study. The choice of which device to use is based largely on suitability for each particular site and the available facilities, such as size of boat from which to sample. For example, while the Mini-Mackereth is useful for collecting long cores, which may show important changes in metal geochemistry at depths greater than those sampled by the other corers, the necessary equipment (*e.g.* compressed air cylinders) prevents its use at remote sites where equipment may have to be carried to the loch by hand.

Coring location

For a comparative inter-loch investigation of metals and radionuclides, where minimal disturbance to the sediment occurs, the optimum coring site will be one of maximum water depth, so that sediment grain size and disturbance by wave action are minimised, whilst also avoiding steep gradients, where slumping or focusing of sediment could complicate the sedimentation process. The choice of sites in this study was based on previous coring work (where available), the extensive bathymetric survey of Scottish lochs by Murray and Pullar (1910), and occasionally, use of an echo-sounder.

Porewater sampling

Microbial decomposition of organic matter in the sediment, and in the hypolimnion of stratified lakes, results in a decrease in the redox potential leading to anoxic conditions. Various studies (*e.g.* Troup *et al.*, 1974; Loder *et al.*, 1978) have emphasised the importance of sampling sediment porewaters under oxygen-free conditions, to avoid oxidation of soluble Fe^{2+} to Fe^{3+} resulting in the formation of solid oxides/hydroxides, which occurs if oxygen is present during sampling. Dissolved Mn is also oxidised in the presence of oxygen and as both Fe and Mn

oxyhydroxides are good scavengers of trace metals, the sampling procedure could potentially affect concentrations of these metals.

Several techniques have been developed for the sampling of sediment porewaters in oxygen-free conditions, but, as Carignan *et al.* (1985) have pointed out, no particular porewater trace metal sampling procedure can be considered artefact-free and so concentration measurements should be regarded as operationally defined until it is shown that independent procedures consistently yield similar results. There are three basic approaches to lake sediment porewater sampling:

1. Dialysis (Hesslein, 1976)
2. Sectioning of sediment cores in a N_2 purged atmosphere (glovebox or glovebag) followed by

a. centrifugation and filtration of supernatant via membrane filters

or

b. squeezing sediment directly via membrane filters

3. Syringe method (Davison *et al.*, 1982).

The dialysis or 'peepers' method involves in-situ diffusion of dissolved porewater constituents across a membrane into N_2-purged distilled water in the sampler compartments, which are spaced at required sampling intervals. The dialyzer is inserted into the sediment and allowed to equilibrate, often for several days. Carignan (1984) has drawn attention to several potential sources of error in the use of this technique, including the type of membrane used, construction material of the sampler, chemical state of the initial filling water, general design of the dialyzer and selection of an appropriate equilibration time. Physical breakdown of cellulose-based membranes lead to the underestimation or overestimation of porewater solutes, and polycarbonate was unsuitable for dialyzer construction because of Fe precipitation problems. Equilibration times of 15-20 days were found adequate for most sediments and the initial elimination of O_2 in the compartments was essential in the collection of representative samples. Davison *et al.* (1982) also observed that porewater equilibration using dialysis membranes is unsuitable for sediment rich in Fe and S, because FeS may precipitate inside the membrane, so total analysis for Fe and S does not give equilibrium concentrations in solution.

In a comparison of the dialysis and centrifugation-filtration techniques, Carignan *et al.* (1985) concluded that the two methods give comparable results, but because dialysis is performed *in situ*, problems due to temperature changes and exposure to atmospheric oxygen during porewater extraction by other methods are minimised. Furthermore, dialysis was less time consuming and relatively simple.

A recent modification of the dialysis method has been developed (Davison *et al.*, 1991) to allow chemical measurements to be made at high spatial resolution (<1 mm), which may be necessary to show detailed trends in dissolved metal concentrations, particularly near the sediment-water interface of oxygenated waters. The technique involves initial insertion of a thin film of gel into the sediment. Diffusive equilibrium is established within minutes and, on removal of the gel, the dissolved components are fixed, allowing measurements to be made. The method, although used for Fe measurement only and with a previously collected sediment core, has potential for use with other metals and in-situ dialysis.

The syringe method of porewater extraction involves collection of a sediment core using a core tube previously drilled with holes at required sampling intervals. The holes are sealed with tape during coring, after which the tape is successively removed from the holes, through which sediment is withdrawn via a large diameter needle into a N_2-purged syringe. The sediment is then passed via an Ar-flushed membrane filter and the porewater collected in a second syringe below the filter. This relatively simple method has been used successfully on Loch Lomond sediments for the measurement of dissolved Fe, Mn and As concentrations (Lovell, 1985).

1.2.2 Sequential extraction methods

Measurement of total metal concentrations in sediment yields little information on the mobility, availability, uptake and transport of metals. Knowledge of how metals are bound is necessary for the accurate assessment of potential modes of transport and environmental impact of metals. To address this problem, a number of sequential extraction schemes have been developed (Pickering, 1986), aiming to mimic environmental conditions which might be encountered in nature and to remove metals from the mineral phases with which they may be associated (Mahan *et al.*, 1987).

The sequential extraction scheme was developed principally by Tessier *et al.* (1979) and involves a five step extraction of sediment with increasingly vigorous chemical extractants to remove metals from the following fractions:

1. Exchangeable - changes in ionic composition of water are likely to affect sorption-desorption processes and therefore metals adsorbed on the surfaces of clays, hydrated oxides of Fe and Mn and humic acids may be susceptible to such changes.
2. Bound to carbonates or 'specifically sorbed' - this fraction would be influenced by pH changes.

3. Bound to Fe and Mn oxides - these oxides are excellent trace metal scavengers under oxidising conditions, but are thermodynamically unstable under anoxic conditions (low Eh).
4. Bound to organic matter/present as sulphides - metals may be associated with organic matter by complexation and peptization (particularly humic and fulvic acids), while certain living organisms bioaccumulate metals. Organic matter can be degraded in natural waters and sediments, leading to a release of soluble trace metals. The formation of metal sulphides generally occurs in the sulphate reducing zone (Section 1.1.3)
5. Residual - once the first four fractions have been removed, the residual solid should contain mainly primary and secondary minerals, which may have trace metals bound within their crystal structure. Over a reasonable time span and under normal environmental conditions, these metals would not be expected to be released to solution.

Whilst Tessier *et al.* (1979) concluded that the precision and accuracy of their method were good, the technique has potential disadvantages and the evaluation of these has led to considerable controversy over the validity of this method. Kheboian and Bauer (1987) have drawn attention to two possible sources of error in the sequential extraction technique:
1. Non-selectivity - the minerals are not uniquely attacked by a particular reagent
2. Redistribution - trace metals liberated by one extractant have the opportunity to reassociate with remaining undissolved components.
Both of these factors could obscure the true metal association and so present problems in the interpretation of data. To evaluate these effects, Kheboian and Bauer (1987) used the Tessier extraction scheme for analysis of synthetic sediments of known composition and metal associations. None of the trace metals was removed at the stage predicted according to the extraction scheme. Pb and Cu were removed later than predicted due to redistribution and Zn earlier because of non-selective extraction. It was concluded that information from the extraction scheme could not be reliably interpreted because of the problem of elemental redistribution. For the purposes of comparative studies (*i.e.* using the same extraction procedure on sediments from different sources), the information obtained could again be unreliable as a result of observed trends being due to different degrees of redistribution during extraction, influenced by variations in sediment composition.

These conclusions were disputed by Belzile *et al.* (1989) who used a standard addition technique to examine the degree of readsorption of As, Cd, Cu, Ni, Pb and Zn during various extractions of oxic lake sediments. The results showed that

previous critiques of extraction methods had overestimated the general importance of readsorption during partial extraction of natural sediments. Kersten and Förstner (1987) examined the effect of sample pre-treatment on the reliability of solid phase speciation data for heavy metals, with implications for the study of early diagenetic processes. They emphasised that anoxic sediments should be extracted in field moist, oxygen-free conditions.

Opinion varies as to the usefulness of sequential extraction techniques (Pickering, 1986; Martin *et al.*, 1987; Campbell and Tessier, 1989), but it does appear that they can be useful in showing changes in metal associations which may occur vertically in the sediment, provided data so obtained are treated with caution, as being operationally defined rather than definitive of absolute geochemical associations. In a comparative study, variations or similarities in metal fractions between different types of lakes are also of value and may be important in characterising the particular system.

1.2.3 Radiometric assessment of sedimentation processes

^{210}Pb geochemistry

^{210}Pb ($t_{1/2}$ = 22.35 y) is a member of the ^{238}U natural decay series (Fig.1.8) and is useful in the study of mixing, accumulation rates and geochronology of recent sediments. In undisturbed sediment, chronologies over the last 100-150 years can be reliably established, which can be of value in the interpretation of concentration profiles of pollutant heavy metals. (Krishnaswami et al., 1971)

In lake sediments, ^{210}Pb generally originates from two sources.(ibid.):

1. Supported ^{210}Pb - from in-situ decay of ^{226}Ra in minerals and rock fragments. The ^{210}Pb is in secular equilibrium with ^{226}Ra (as long as the intermediate gaseous ^{222}Rn remains immobile).
2. Unsupported (or 'excess') ^{210}Pb - ^{226}Ra in soils and rocks decays to ^{222}Rn, some of which diffuses into the atmosphere where it remains until it decays to ^{210}Pb. Rapid removal of the ^{210}Pb (5-10 days residence time in the atmosphere; Turekian *et al.*, 1977) to land and lake surfaces by both dry and wet deposition provides a flux of ^{210}Pb unsupported by ^{226}Ra. Pb is highly reactive in the aquatic environment, by hydrolysis and uptake on solid surfaces, and is therefore dominantly associated with particulate matter. As a consequence, unsupported ^{210}Pb deposited to lake surfaces is relatively rapidly removed from the water column with suspended particulates which settle to the sediment surface. There may also be a contribution of ^{210}Pb from the catchment, including run-off and river/stream inputs, but direct atmospheric deposition tends to be most important.(Appleby and Oldfield, 1978).

Fig.1.8 ^{238}U decay series showing radionuclide half-lives (based on Friedlander et al., 1981).

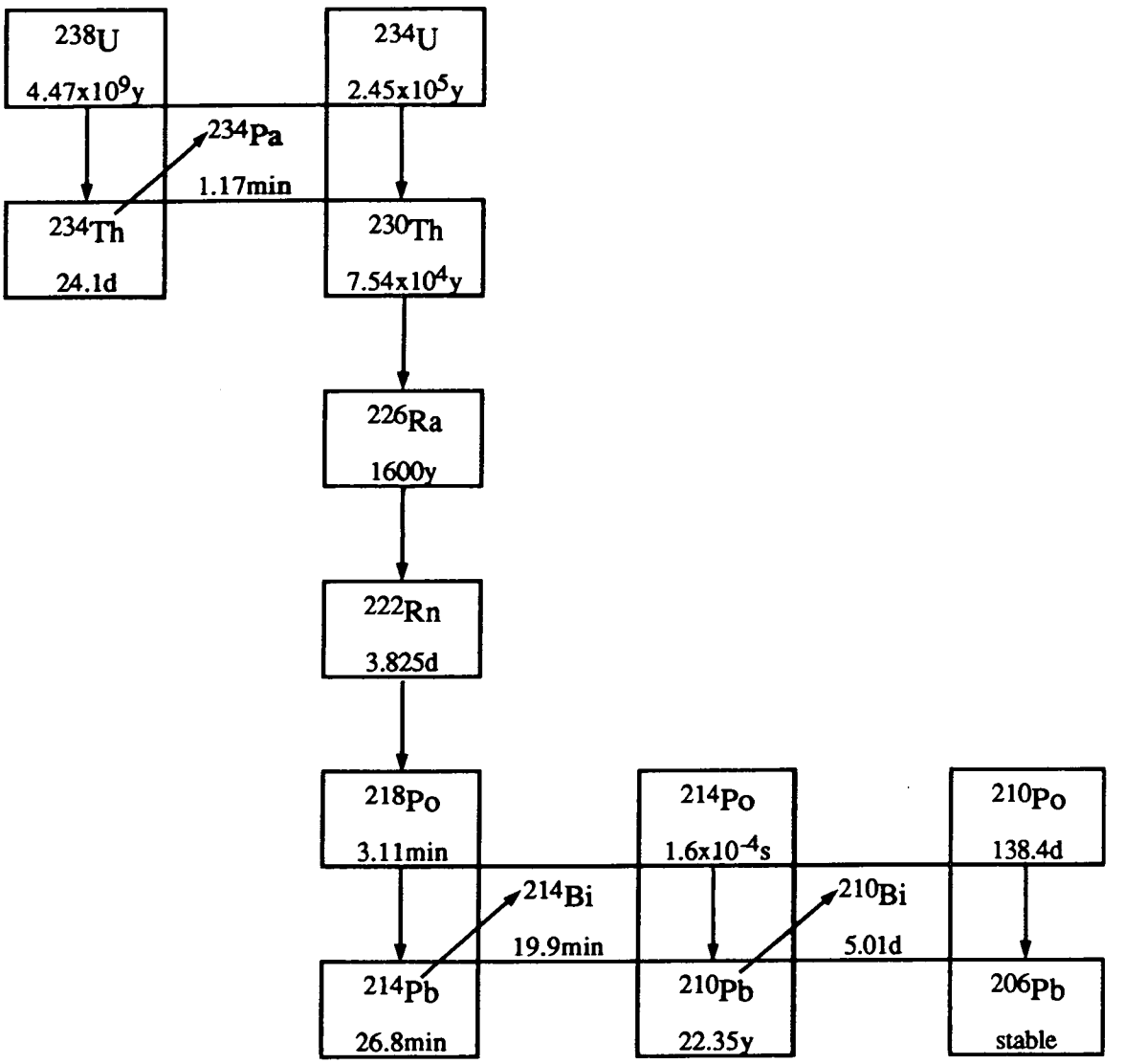

The average flux of ^{210}Pb to a particular sampling location (Bq m^{-2} y^{-1}) can be determined by multiplying the total unsupported ^{210}Pb inventory (Bq m^{-2}) by the decay constant ($\lambda = \ln 2/t_{1/2}$).

Sediment dating

Sedimentation rates can be estimated from the decay of unsupported ^{210}Pb with increasing depth in accumulating sediments (Oldfield and Appleby, 1984). The unsupported ^{210}Pb concentration is calculated by subtraction of supported ^{210}Pb from total ^{210}Pb activity, with the supported component being estimated either by ^{226}Ra analysis or by observation of a constant ^{210}Pb concentration at depth in the sediment (*i.e.* at depths where unsupported ^{210}Pb has decayed away).

Two models are used in ^{210}Pb dating, the constant initial concentration (CIC) (Krishnaswami and Lal, 1971) and the constant rate of supply (CRS) (Appleby and Oldfield, 1978). The CIC model assumes that ^{210}Pb is immobile in the sediment and that the ^{210}Pb flux to the sediment surface and the sediment accumulation rate are both constant. Under these circumstances, radioactive decay of ^{210}Pb results in an exponential decrease in the unsupported ^{210}Pb concentration with depth in the sediment. If the natural logarithms (ln) of the unsupported ^{210}Pb concentrations are plotted against depth (generally as cumulative weight of dry sediment per unit area, to compensate for effects of sediment compaction), a gradient (m) of $-s/\lambda$ is obtained, where s is the sedimentation rate, so a sedimentation rate can then be calculated via $s = -\lambda m$.

In the CRS model, as for the CIC calculation, it is assumed that ^{210}Pb is immobile and the ^{210}Pb flux is constant, but the models then diverge, because the CRS model does not require a constant sedimentation rate. The model was developed by Appleby and Oldfield (1978) because they had found situations where the unsupported ^{210}Pb concentration *increased* with depth at certain levels and they interpreted the increases as being a result of a decrease in the sediment accumulation rate, giving higher concentrations of ^{210}Pb. In this case, the age of each sampled layer is determined from the equation below and the sedimentation rate can then be determined by dividing the cumulative sediment weight per unit area by the age of interval i.

$$t_i = 1/\lambda \ \ln A_o/A_i$$

where t_i = age at base of interval i
λ = ^{210}Pb decay constant

Ao = total cumulative unsupported ^{210}Pb (*i.e.* integrated accumulation of unsupported ^{210}Pb throughout the length of the core)

Ai = cumulative unsupported ^{210}Pb below interval i

Dating by both CRS and CIC models and external dating methods on sediments from Lough Earne in Northern Ireland and the New Guinea Highlands (Oldfield *et al.*, 1978) and annually laminated lake sediments from Finland (Appleby *et al.*, 1979) have indicated that where sedimentation rates have varied through time, the CRS model provided a better approximation to true age than other ^{210}Pb models. In a later assessment of ^{210}Pb data from sites with varying sediment accumulation rates, Appleby and Oldfield (1983) concluded that no single model will give a reliable ^{210}Pb chronology in all cases and that each data set must be considered independently for consistency with the dating models.

Other factors influencing sediment may result in non-linear ^{210}Pb profiles, such as mixing (Nittrouer *et al.*, 1983/1984) outlined in Section 1.1.3. If the sediment mixing is rapid, relative to the sedimentation rate, the observed ln ^{210}Pb concentration will be constant over the mixing zone (Fig. 1.9b), whereas if mixing is slow, the ln ^{210}Pb concentration profile will appear as a change in sedimentation rate (Fig. 1.9c). Below the mixing zone a normal radionuclide decay pattern is observed. Sediment mixing has important implications for dating sediments, but reliable chronologies may still be obtainable. In the case of the ln ^{210}Pb concentration profile affected by rapid mixing of near-surface sediment (Fig. 1.9b), the CIC model may be used to calculate a sedimentation rate, by linear regression of data from the base of the mixing zone downwards. Similarly, the CRS model could be applied to the same data, where A_o would be the total cumulative excess ^{210}Pb, with increasing depth from the base of the mixing zone. Where slow mixing of the surface sediment has occurred (Fig. 1.9c), the data may be unsuitable for dating, since it may not be possible to distinguish between the effects of mixing and a change in sedimentation rate.

Sediment mixing can also alter the profiles of other elements and care must be taken when interpreting the profiles of elements which have not been deposited to the lake by a steady-state process. For example, the deposition to Scottish lochs of radiocaesium in fallout from the Chernobyl reactor accident can be considered a single event, with most of the deposition occurring over a short period of time (days). Rapid sediment mixing (Fig. 1.9b) would effectively mix the radiocaesium, deposited at the sediment surface, downward to older sediment at the base of the mixing zone and thus increase the *apparent* time elapsed since the deposition event. In contrast, atmospheric deposition of pollutant heavy metals has taken place largely since the onset of the

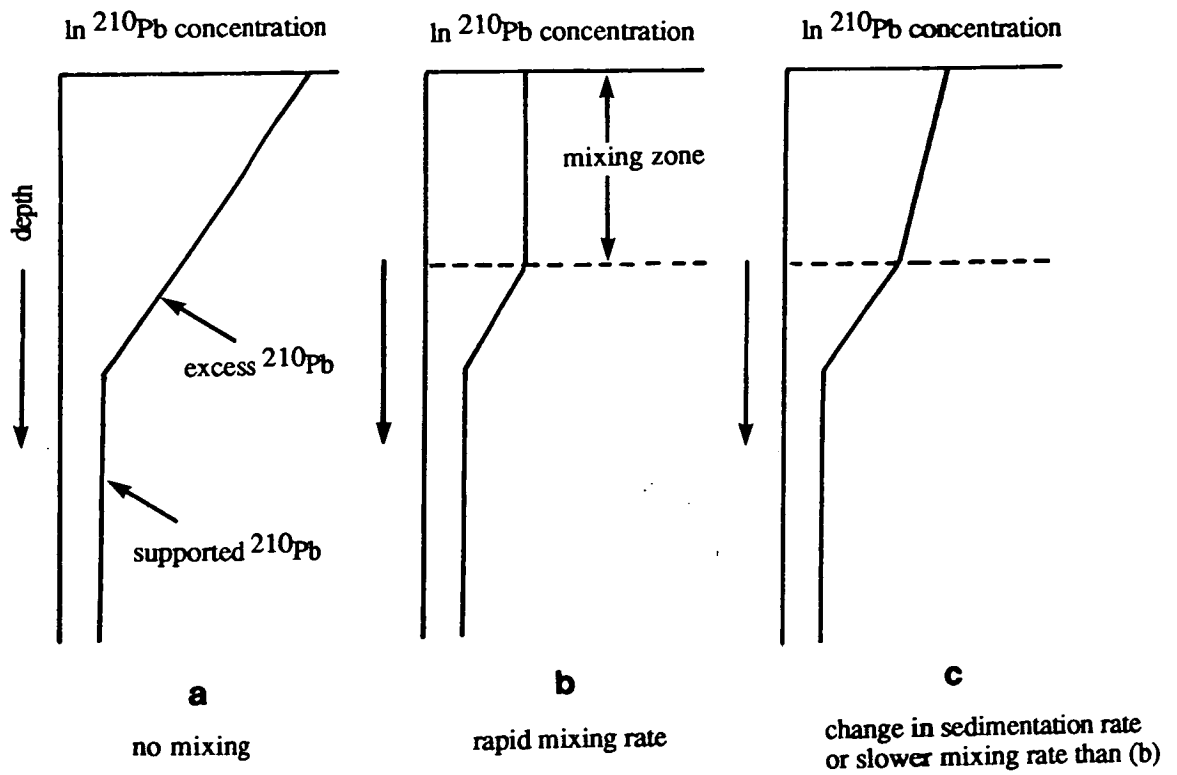

Fig. 1.9 Profiles of sedimentary ln ^{210}Pb concentrations against depth: (a) no mixing; (b) rapid (complete) mixing; (c) partial mixing or change in sedimentation rate

Industrial Revolution, about 250 years ago, with variations in the metal fluxes during this time. If the sedimentation rate is rapid, relative to the mixing rate, then transient variations in solid phase metal concentrations will have a defined structure, partly related to input trends. On the other hand, if the mixing rate is rapid relative to the sedimentation rate, then the mixing process will effectively smooth out short-term variations in any inputs over the mixing depth. The effects of partial mixing will therefore be to preserve the position of a pollutant peak, but to damp the magnitude, and complete (rapid) mixing will displace peak pollutant metal fluxes and the onset of increase in pollutant inputs by the depth of sediment (and corresponding number of years) in the mixed zone.

Gubala *et al.* (1990) examined the effects of Fe cycling on ^{210}Pb dating of sediments in an Adirondack lake (USA) and identified potential errors in dating because of sediment mass changes induced by post-depositional Fe remobilisation and precipitation. Significant deviations between Fe-corrected and uncorrected dating were not found and unless sediment accumulation rates were low with high Fe enrichment, the deviations for CIC and CRS models were unlikely to be greater than those due to analytical error alone.

Radiocaesium dating

Radiocaesium nuclides are artificial in origin and occur as widespread environmental pollution. ^{137}Cs ($t_{1/2}$ = 30.23 y) is a fission product, introduced into the environment by nuclear weapons testing and planned or accidental releases from nuclear industry facilities (*e.g.* reactors and fuel reprocessing plants). ^{134}Cs ($t_{1/2}$ = 2.05 y) is only produced in significant amounts in nuclear reactors, as it is formed by the time-dependent process of neutron activation (MacKenzie and Scott, 1984) and is not produced by fission, as it is shielded in the ^{134}Cs chain by ^{134}Xe. Introduction of radiocaesium to the atmosphere from the testing of nuclear weapons occurred mainly during the late 1950's and early 1960's (Cambray *et al.*, 1982). In April 1986 the Chernobyl nuclear reactor accident occurred and fallout from this was deposited onto Britain in May 1986 as a single event, with a characteristic $^{134}Cs/^{137}Cs$ activity ratio of about 0.55 (Horrill *et al.*, 1988). Radiocaesium in Scottish freshwater lochs originates from fallout from weapons testing and the Chernobyl reactor accident and ^{137}Cs may be separated into these two fallout sources by dividing the measured $^{134}Cs/^{137}Cs$ activity ratio in a sediment section by the characteristic Chernobyl-derived ratio (corrected for decay to the sampling date), to obtain the fraction of ^{137}Cs due to Chernobyl fallout. The weapons testing ^{137}Cs contribution can then be calculated by

subtracting the Chernobyl-derived ^{137}Cs from the total ^{137}Cs concentrations for each sediment section.

Radiocaesium from nuclear weapons testing has been used to date sediment cores by correlation of peak activities at depth in the sediment with the time of maximum atmospheric deposition of radiocaesium in 1959-1963. Sedimentation rates established in this way often show good agreement with ^{210}Pb dating information (*e.g.* Pennington *et al.*, 1973; Edgington *et al.*, 1991). In principle, the deposition of radiocaesium from Chernobyl fallout can also be used to date sediments. Use of radiocaesium as a dating tool is only valid, however, if the radiocaesium has been deposited relatively rapidly from the water column to the sediment and has not subsequently undergone any significant remobilisation or redistribution. There is evidence that these criteria may not always be met, and factors such as delays in deposition of radiocaesium to the sediment, continuing catchment inputs after the fallout event, disturbance of the sediment by physical (*e.g.* wave action, sediment focusing or slumping) or biological (*e.g.* burrowing animals) means and post-depositional mobility of radiocaesium within the sediment are all potentially capable of affecting the radiocaesium profile (Robbins *et al.*, 1977; Davis *et al.*, 1984; Comans *et al.*, 1989) and therefore distorting the historical record of fallout deposition (Farmer, 1991). The principal mechanism by which radiocaesium is bound in the sediments is uptake by clay minerals (*e.g.* Benes *et al.*, 1989; Petersen *et al.*, 1990) and various studies have shown that mobility of radiocaesium occurs in sediments with a low clay content (*e.g.* Evans *et al.*, 1983; Davis *et al.*, 1984; Torgersen and Longmore, 1984) by diffusion in porewaters. In considering whether radiocaesium is a useful dating tool, it is therefore necessary to bear in mind these possible influences on the profile shape.

1.3. Approach to study

In order to understand the behaviour of metals in lake systems, it is necessary to view the lake as a whole, taking into account interactions between the water column and sediments (solid and solution phase), inputs from the catchment area and the atmosphere, and the influence of seasonal changes.

The basic approach to this study (Fig. 1.10) was to choose a range of lakes which would provide a variety of conditions of potential importance in terms of metal behaviour and distribution. Sediments and overlying water samples were collected from the lochs. Coring sites were chosen carefully, taking bathymetry and location in the loch into account. Analyses of sediments (solid and solution phase) were

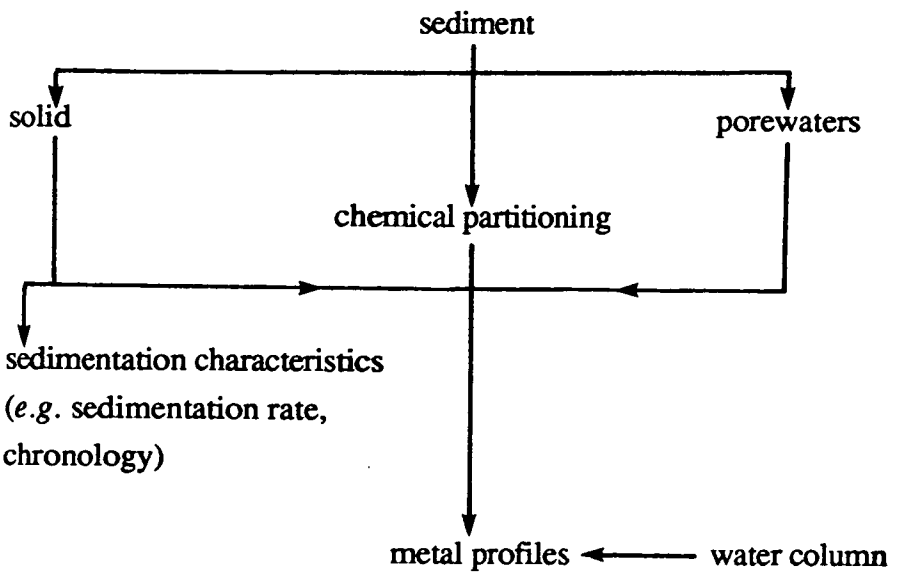

Fig. 1.10 Approach to the study of metals and radionuclides in different lake types

performed to obtain metal concentration profiles, including the distribution of metals between different sedimentary fractions. Radionuclide activities (^{226}Ra, ^{210}Pb, ^{134}Cs and ^{137}Cs) in the sediment were measured to establish sedimentation rates and chronologies. Radionuclide data can also shed light on any mixing processes occurring at the sampled sites, as well as enabling a comparison of the behaviour and distribution of radionuclides in the different systems.

1.3.1 Choice of sampling locations

With more than 91% of the freshwater in Britain, Scotland provides a good location for a comparative study of metal behaviour in different lake types. There are diverse lochs in relatively close proximity, most of which have been characterised in terms of bathymetry in an extensive survey of Scottish lochs by Murray and Pullar (1910). Five lochs were chosen in this project, to cover a range of conditions, such as acidification, trophic status and sediment type. The reasons for choosing these five lochs (Fig.1.11) and some of their characteristics (Table 1.6), are described below.

Round Loch of Glenhead

Round Loch of Glenhead lies in the Galloway region of south-west Scotland, overlying granite bedrock, with a peaty catchment and, as a consequence, organic-rich sediments. The loch has been the focus of detailed investigations into aspects of surface water acidification (*e.g.* Flower and Battarbee, 1983; Jones *et al.*, 1989; Battarbee *et al.*, 1989) and is part of the Acid Waters Monitoring Network (Patrick *et al.*, 1991).

Palaeolimnological studies, largely using diatom-inferred pH (*e.g.* Jones *et al.*, 1989; Battarbee *et al.*, 1989), have indicated that, while the loch was acid throughout the post-glacial period (due to the nature of its catchment), a stable pH of *ca.* 5.5 in the water column declined rapidly, from around 1870, by one pH unit during the next 100 years. This dramatic decrease has resulted from acid deposition associated with fossil fuel combustion. Although there is some evidence of an improvement in the past 20 years to a mean pH of 4.9 by 1989 (Flower *et al.*, 1990; Allott *et al.*, 1992), the loch remains acidified.

Palaeolimnological studies of this loch have included trace metal analyses of sediments (Cu, Zn and Pb) (Battarbee et al., 1989). As the loch is remote from any point sources of these metals, anthropogenic contributions are attributable to atmospheric inputs. Rippey (1990) found that the pattern of trace metals, sulphur and PAH concentration-depth

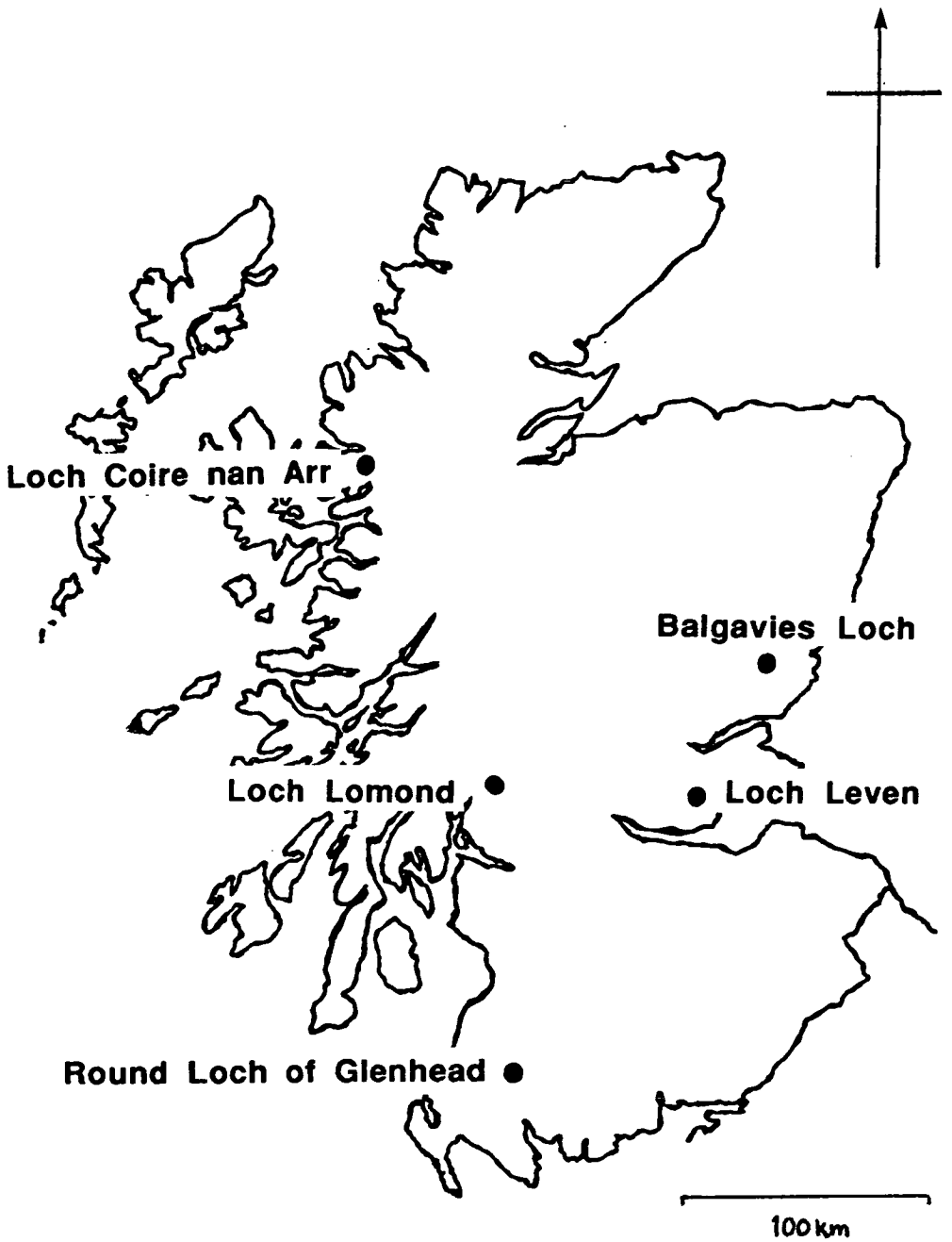

Fig.1.11 Location of sampled lochs in Scotland

Table 1.6 A summary of chosen sampling locations and their characteristics

sampling location	bedrock	characteristics	mean pH of water column
Round Loch of Glenhead	granite	acidified, organic-rich sediments, oligotrophic	4.9
Loch Lomond	upper loch (north): metamorphic mica-schists, schistose grits and slates; lower loch (south): Carboniferous and Devonian sedimentary rocks;	meso-/oligotrophic, redox-cycling of Fe, Mn and As	6.6 (upper loch) 7.6 (lower loch)
Loch Leven	sand and gravel, overlying boulder clay	eutrophic	7.2-9.3
Balgavies Loch	worked glacial deposits, overlying Lower Old Red Sandstone	hard water, seasonal stratification, eutrophic	8.3
Loch Coire nan Arr	Torridonian sandstones	acid sensitive, organic-rich sediments, oligotrophic	6.3

profiles in the sediment cores gave the same qualitative description of contamination, indicating that the metal inputs are indeed associated with fossil fuel combustion.

In view of the extensive work on acidification of this loch, together with palaeolimnological studies of metals in dated sediment cores, further investigation of this loch would be of value in terms of metal behaviour, particularly as there has been evidence from other acid lakes suggesting effects which could modify the historical record of anthropogenic metal input.

Loch Lomond

This loch is the largest freshwater body in the U.K. (71 km^2) and lies 30 km north-west of Glasgow. It is a glacial loch with two regions (upper and lower loch), with four basins (Maitland, 1981). The lower loch to the south overlies Carboniferous and Devonian sedimentary rocks and is wide, with a relatively shallow depth of <31 m. The southern and central basins of the lower loch are more biologically productive (mesotrophic) than the narrow, deeper (max. 200m) oligotrophic basins to the north, where the bedrock consists of metamorphosed Dalradian mica-schists and schistose grits and slates (Slack, 1954). Dissolved oxygen is high (>72%) throughout the loch at all times of the year (Maulood and Boney, 1980).

Solid and solution phase concentrations of Fe, Mn and As in sediment cores from various sites in Loch Lomond have shown that redox-driven diagenesis has altered the patterns of historical deposition of these elements to the sediment (Farmer and Lovell, 1984 and 1986). Surface enhancements of Mn up to 9.1% in the near-surface sediment and of As up to 675 mg kg^{-1} (compared with 15-50 mg kg^{-1} background concentrations) were found (Farmer and Lovell, 1986). This redox-cycling could perhaps involve other elements, such as pollutant metals, due to the high scavenging capacity of Fe/Mn oxyhydroxides for metals.

A continuation of the work already carried out in Loch Lomond, where redox-driven diagenesis is known to be an important factor in Fe, Mn and As geochemistry, therefore seemed appropriate with respect to evaluation of the behaviour and distribution of additional metals.

Loch Leven

Loch Leven lies approximately 35 km north of Edinburgh and occupies the central part of a natural bedrock depression. It is a drift basin, formed in sand and gravel deposits which overlie boulder clay. Catchment land-use is predominantly agricultural and phosphorus run-off from the land, together with treated sewage effluent inputs, roosting wildfowl and a now ceased process of effluent input to the

loch from a woollen mill, have contributed to the eutrophication of this loch (Bailey-Watts and Kirika, 1987). Summer algal blooms are common and are a subject of concern due to potential harmful effects of toxins released by blue-green algae in this loch, which is famous for trout fishing. Stratification is relatively uncommon in Loch Leven and affects only the deeper areas with a generally poorly defined hypolimnion. The loch is therefore typically isothermal with an oxygen concentration approaching saturation (Smith, 1974).

Loch Leven is regarded as a shallow, eutrophic system and the total phosphorus loading (which includes an internal phosphorus contribution due to release from the sediments) (Bailey-Watts and Kirika, 1987), and consequent eutrophication, provide a suitable site for investigation of metal behaviour in a eutrophic lake system. A pilot project (Murray, 1989) on heavy metals and radionuclides in Loch Leven sediments has provided some background to the work, *e.g.* a surface enhancement of Mn indicated redox cycling as an operative process of metal cycling in the lake and phosphorus release from the sediments has been shown to be related to release of Fe to the water column (Scott, 1990).

Balgavies Loch

Balgavies Loch is a glacial loch in central Scotland, appoximately 10 km east of Forfar in the Angus District. Catchment soils are basic, nutrient rich and intensively farmed (Harper and Stewart 1987). As with Loch Leven, this eutrophic loch has been significantly enriched in nutrients, characterised by various algal blooms during the summer, but in contrast to Loch Leven, Balgavies Loch has an unusually high concentration of $CaCO_3$.

This site was chosen for sampling as it was found to be stratified, with anoxic bottom waters in the west basin during the summer of 1991, and a change in the position of the redoxcline from the sediment to the overlying water has possible implications for diagenetic redox-driven remobilisation of metals.

Loch Coire nan Arr

This loch lies on the Torridonian sandstones of the Applecross area in north-west Scotland. It is a clearwater loch, which is part of the UK Acid Waters Monitoring Network, as is Round Loch of Glenhead. It has a mean pH of 6.34 (Patrick *et al.*, 1991) and, despite acid sensitivity (*i.e.* low buffering capacity of the loch or catchment to acid deposition) similar to Round Loch (Battarbee, 1988), palaeolimnological evidence has shown no pH change at this site.

Sampling of this site could provide interesting information on metal behaviour in a clearwater loch, as well as a comparison with Round Loch, similar in acid sensitivity and sediment type (organic-rich) but apparently unaffected by recent acid deposition.

1.3.2 Project aims

There have been relatively few comparative studies of metal behaviour and associations in different lake types and none using the described approach for the comparison of Scottish freshwater lochs. The aim of this project was to investigate metal behaviour in diverse freshwater lake systems. Specific objectives of the study were:

1. To establish metal concentrations in acid digested sediment, operationally-defined sediment fractions (using a sequential extraction scheme), sediment porewaters and the water column.
2. To derive sedimentation rates and information on sediment mixing, using the radionuclides ^{210}Pb, ^{226}Ra and radiocaesium, and to study the behaviour of the radionuclides in the different lake types.
3. To determine whether heavy metals are mobile in the sediments of the different lakes, which would challenge the traditionally held view that concentration profile trends of pollutant metals can be viewed as a historical record of atmospheric metal pollution input to the lake. Within this objective, metal mobility was to be investigated in terms of possible effects of:
   i. Redox-cycling of Fe/Mn, since the oxides/hydroxides of these metals are efficient scavengers of heavy metals.
   ii. Acidification
   iii. Eutrophication
4. To evaluate fluxes, inventories and, where possible, historical records of pollutant metals and radionuclides in a fairly comprehensive Scotland-wide study.

Chapter 2 Materials and Methods

2.1 Field sampling

2.1.1 Coring techniques

In studying the behaviour of metals in a lake system, the sediment-water interface is important, as it is an area over which movement of metal species (*e.g.* deposition, sorption, exchange, release) between the sediment and the water column occurs. Any coring device used in such a study must therefore collect a sediment core in which the vertical integrity and an undisturbed sediment-water interface are preserved. Of the various devices available for collecting sediment cores, three corers were used in the present work, all of which satisfied the above criteria and were suitable for sampling silty sediment and additionally had individual advantages which suited the sampling requirements, *e.g.* the Mini-Mackereth corer was used where possible to obtain longer sediment cores, whereas the less cumbersome Kajak corer is suitable for sampling remote areas. In all three cases the corer was lowered and raised manually from an anchored (or otherwise steadied) boat and sediment cores were collected in cylindrical perspex tubes. The main features of the design and operation of the corers are described below.

Upon collection, cores were transported to the lakeside and water overlying the sediment in the core tube was syphoned off to within a few cm above the sediment surface where, using a syphon or syringe, a sample was collected and transferred to acid-washed (Section 2.2.1), sample-rinsed bottles. The sediment was then extruded and sectioned as described below. At most sites (refer to Chapters 3-7), at least three cores were collected in close proximity. Coring sites were chosen by referring to the lake bathymetry. Sites should ideally be relatively deep and away from steep slopes.

Jenkin Surface-Mud Sampler
(Ohnstad and Jones, 1982) (Fig. 2.1i)

This corer collects a sediment core of approximately 20 cm length. The apparatus sinks into the sediment and, when the core tube (internal diameter = 6.9 cm) is sufficiently filled, tension on the attached rope is released, triggering the spring mechanism and causing two rubber plates to seal the tube. The device can then be pulled vertically out of the water. After collection of a core and syphoning off of overlying water, a piston is inserted into the bottom of the core tube and the sediment

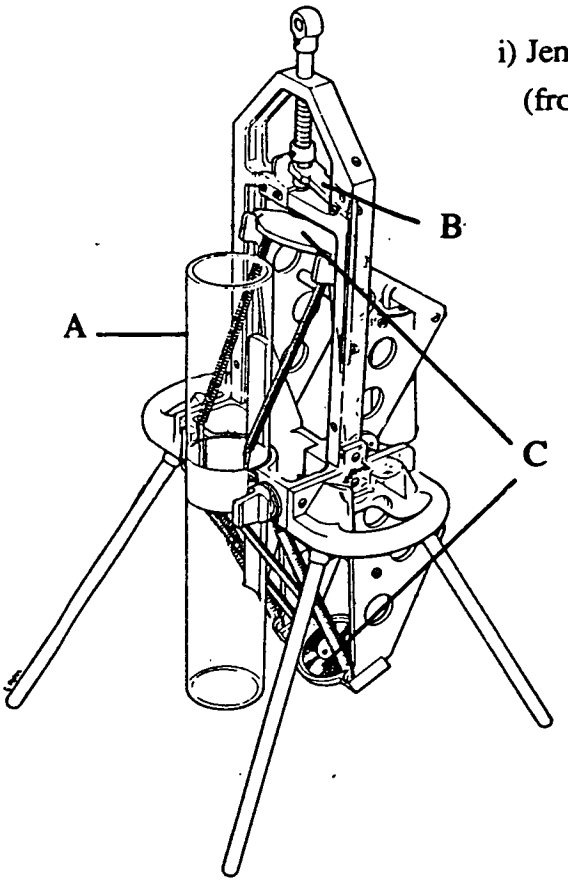

i) Jenkin Surface-Mud sampler
(from Ohnstad and Jones, 1982)

A-core tube
B-spring mechanism catch
C-core tube lids

ii) Modified Kajak corer

A-core tube
B-bung
C-shaft of closing mechanism

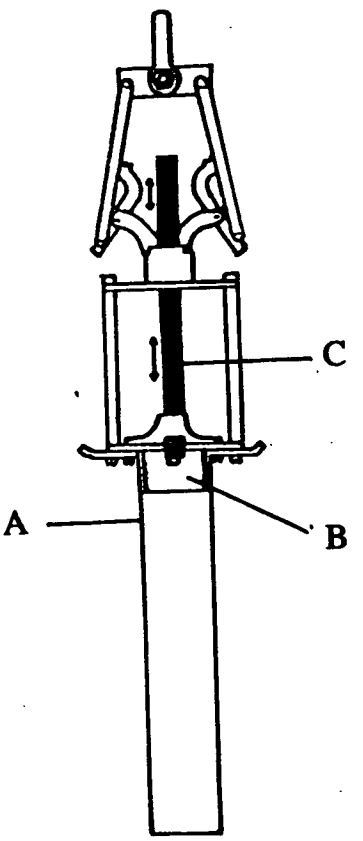

Fig. 2.1 Coring devices

iii) Mini-Mackereth corer

A-core tube

B-air line

C-piston driving core tube

D-rubber ball

E-valves

F-anchor chamber

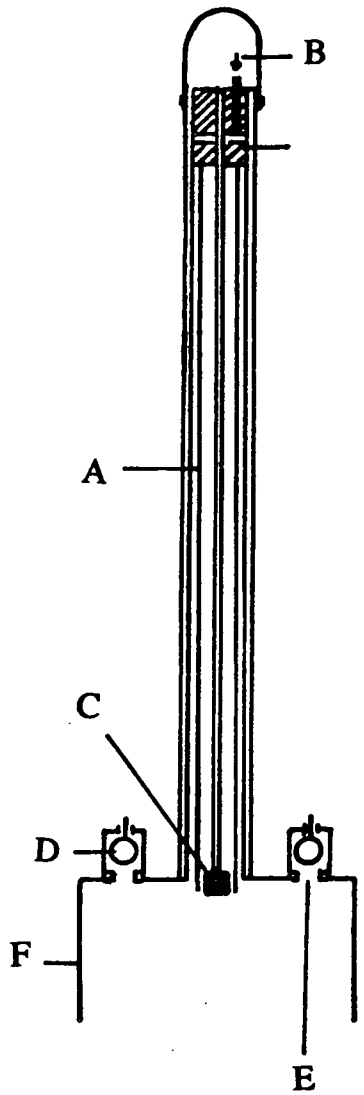

Fig. 2.1 Coring devices (cont.)

can then be extruded using a simple hydraulic pump, which drives the piston up the core tube.

In this study sediment was then sectioned at the desired vertical intervals by measuring the height of sediment extruded at the top of the core into a graduated perspex ring of the same diameter as the core tube and slicing the sediment below the ring, using either a stainless steel or perspex plate. Sediment sections were placed into labelled plastic bags, which were sealed and stored in a freezer box until return to the laboratory.

Modified Kajak Corer

(Brinkhurst *et al.*, 1969) (Fig. 2.1ii)

Operation of this corer is similar in principle to the Jenkin Surface-Mud Sampler, but the apparatus is less bulky. Sediment cores of approximately 30 cm length (core tube internal diameter = 5.1 cm) are collected. The core tube penetrates into the sediment and, once sufficiently filled, release of tension on the attached rope causes the rubber bung to seal the top of the core tube and this holds the sediment in the tube by suction. The apparatus can then be pulled to the surface, inserting a bung into the bottom of the core tube before it is removed from the water to prevent loss of the sediment.

Sediment collected in this study was extruded manually by pushing the core tube down onto a piston, which was attached to a rod. A small metal bar placed through holes drilled at measured intervals in the piston rod, allowed sections of known depths to be removed from the top of the core and collected as described for sediment collected with the Jenkin Sampler.

Mini-Mackereth Corer

(Mackereth, 1969) (Fig 2.1iii)

The Mini-Mackereth corer is designed to collect sediment cores of around 1 m length (core tube internal diameter = 6.5 cm). Unlike the previously described corers which use the weight of the corer to drive the tube into the sediment, the Mini-Mackereth core tube is forced into the sediment by applying pressure from a compressed air cylinder on the boat, via an air hose attached to the top of the outer tube.[x] The corer is lowered to the sediment surface and the anchor chamber allowed to sink into the sediment, causing the ball valves to lift and allowing water to escape from the chamber. These valves close again once the chamber stops sinking. The anchor chamber holds the apparatus in position while the core tube is driven into the sediment by opening the air valve to *ca.* 6.8 atm above hydrostatic pressure. After switching the

[x] See Corrigenda, page 365

air supply off, the apparatus is pulled vertically out of the water. Upon recovery, the core tube is sealed by inserting bungs at both ends to prevent loss of the sediment.

The extrusion method used in this study involved inserting a piston and plastic "follower" into the bottom of the core tube, followed by sediment extrusion using a hand-operated hydraulic pump to drive the piston upwards. The sediment was sectioned at desired intervals and stored as previously described.

2.1.2 Glovebox sectioning of sediment

Sectioning of sediment in oxidising conditions (*i.e.* in air) can alter its redox potential and may change the associations of metals from their pre-sampled state. To overcome this problem, some of the sediment cores collected were sectioned in a specially designed, perspex glovebox (Fig. 2.2), which was positioned as near as possible to the sampled site. A piston was inserted into the core tube below the sediment, sealing the sediment from the air, and the tube was inserted into the glovebox via a port beneath the box. The core tube fitted closely in the port and was isolated from the outside atmosphere by an o-ring compression seal at the bottom of the port. The port itself was finally bolted to the glovebox and sealed by an o-ring compression seal. With the latex gloves secured to the front of the box and oxygen-free nitrogen flowing into the purged glovebox (the inlet pipe was positioned over the sediment) at continuous positive pressure (felt at the outlet), the glovebox provided an oxygen free atmosphere. Water overlying the sediment in the core tube (referred to hereafter as 'overlying water') was removed using a syringe and discarded, except for a sample of water collected as near to the sediment surface as possible without disturbing the sediment-water interface and transferred to an acid-washed (Section 2.2.1), sample-rinsed bottle. A sub-sample of the overlying water was passed through a membrane filter. Pore sizes of membrane filters, for the filtration of overlying water and porewater samples, varied. The aim of the filtration was to gain information about soluble metal concentrations, however pore sizes of membrane filters are generally assigned the following limits to the term 'soluble':

0.45 μm	particulates removed but not some fine particulates / micro-organisms
0.2 μm	particulates and micro-organisms removed
25,000 M.W.	colloids removed

Initially in this study a pore size of 0.45 μm (Millipore HAWP 03700) was used and then, to prevent micro-organisms and fine particulates passing the filter, 0.1 μm filters

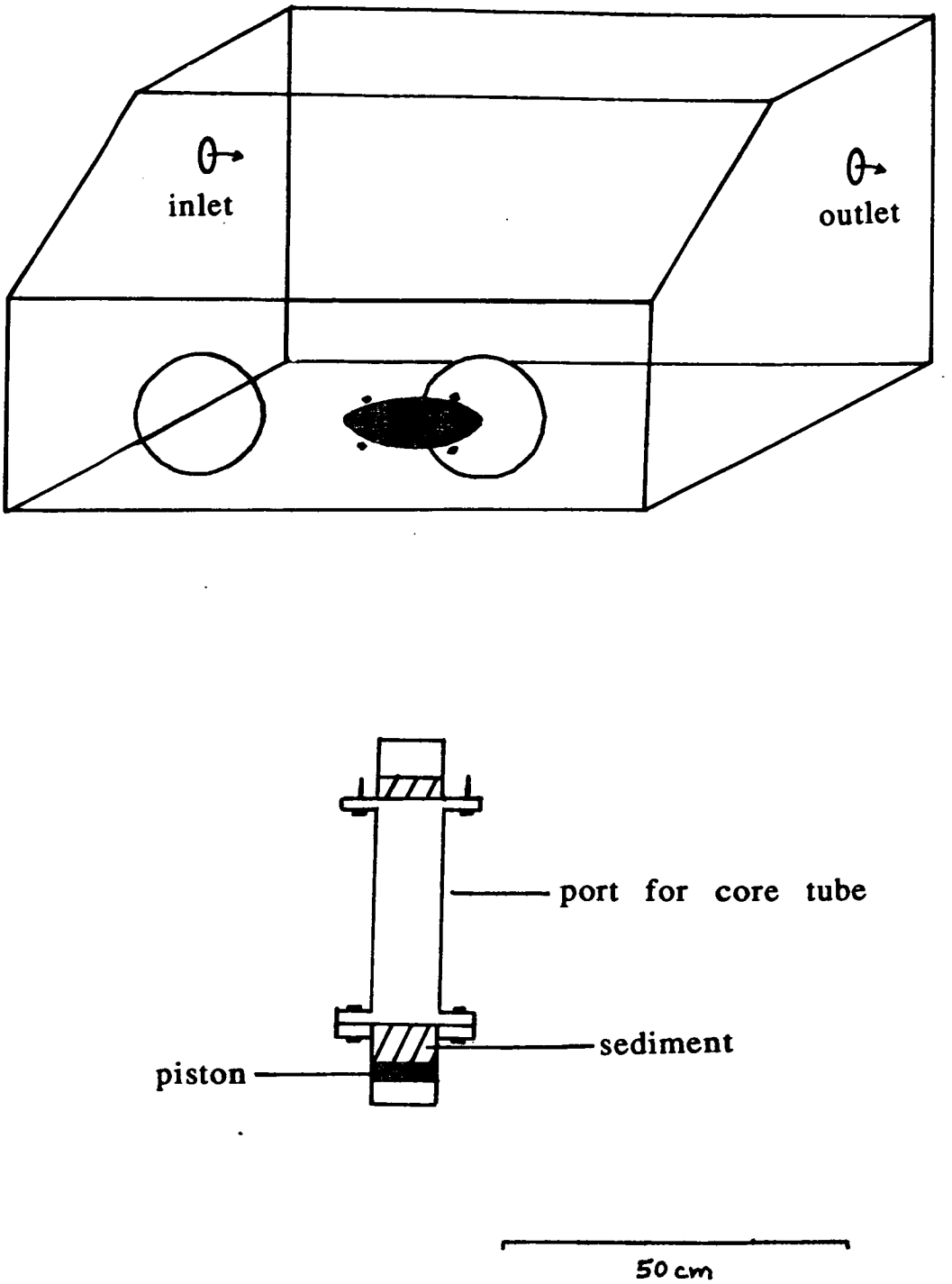

Fig. 2.2 Perspex glovebox for sediment sectioning under nitrogen

(Millipore SX 0001300) were used, which proved unsuitable due to rapid clogging of the pre-filter with particles. Finally, membrane filters of 0.22 μm (Millipore GSWP 03700) pore size were used and were found to be most suitable in terms of ease of use and sampling aims. Details of which filters were used are given in the individual Chapters (3-7).

Sediment was extruded manually by pushing the piston upwards, using a rod, into 1 cm depth perspex rings of the same diameter as the core tube. Perspex plates were used to slice the sediment below the rings and a clean perspex ring and plate were used for each section to prevent cross-contamination and the need for washing within the glovebox. Treatment of the sectioned sediment is described later.

2.1.3 Porewater sampling

Various established methods of obtaining porewater samples were used as follows:

Syringe method (based on Davison *et al.*, 1982)

Sediment cores were collected (using either a Jenkin Surface-Mud Sampler or a modified Kajak corer) in core tubes in which 0.5 cm diameter holes had been drilled in a spiral at 1 cm vertical intervals. The holes had been taped over with insulating tape prior to coring. Once on shore, the core tube was held vertically and overlying water was removed by syphon from water *ca.* 5 cm above the sediment-water interface and transferred to an acid-washed (Section 2.2.1), sample-rinsed polyethylene bottle. Each drilled hole was exposed successively by removing the tape, so that a 0.5 cm diameter stainless steel or teflon needle, attached to a 20 ml syringe (neoprene or teflon stopper), could be introduced to withdraw sediment. The stainless steel needle and neoprene syringe stoppers were found to be a source of zinc contamination and were subsequently replaced by a teflon needle and teflon syringe stoppers. Sediment was withdrawn via each hole and porewaters were obtained by hand-forced filtration of the sediment, using an argon-flushed membrane filter and filter holder (Millipore 0.45 μm HAWP 03700, 0.22 μm GSWP 03700 or 0.1 μm SX 0001300). The porewater was collected by a second syringe below the filter holder and samples were stored in acid washed containers (Section 2.2.1) after acidifying with 16 M nitric acid (AristaR, BDH) 1:1000 v/v. Two blanks were prepared with each sampling by passing MilliQ deionised water via an Ar-flushed membrane filter, acidifying as for the samples. The deionised water was purified by reverse osmosis and ion exchange to a resistivity of 18.3 MΩ (Millipore Milli-Q SP reagent water system) and is hereafter referred to as MilliQ deionised water.

Glovebox method

Using the previously described glovebox method for sediment sectioning (Section 2.1.2), porewater samples were obtained by one of the following methods:

1. In the glovebox, wet sediment was placed into plastic bags and, by cutting the corner off the bag, was squeezed into a 20 ml syringe (teflon stopper). Porewater samples were collected in a second 20 ml syringe by hand-forced filtration through a membrane filter (Millipore 0.45 μm or 0.1 μm). Blanks were prepared by passing MilliQ deionised water through filters as for the porewaters.
2. In the glovebox, 1 cm sections of wet sediment were placed in acid-washed (Section 2.2.1), screw-top polyethylene centrifuge tubes (50 ml, Falcon). The tube tops were securely sealed with insulating tape to prevent air entering when the tubes were removed from the glovebox and centrifuged for 5 min (Gellman Junior centrifuge, speed 5). After replacing the tubes in the glovebox and purging with nitrogen, the tubes were opened and the supernatant liquid was passed via 0.1 μm or 0.22 μm filters. Two blanks were prepared with each sample batch by processing MilliQ deionised water in the same way as the sediment.

All samples and blanks prepared by the above methods were acidified with 16 M nitric acid (AristaR, BDH) 1:1000 v/v and stored at 4°C in acid-washed containers until analysed.

2.1.4 Water column sampling

The total water depth was determined at each site using a plumb line, and water column samples were collected using either a Friedinger sampler or a van Dorn sampler. These devices are similar in design and operation, consisting of a tube with lids at either end, which are held open while the sampler is lowered to the required depth by an attached rope. A messenger weight is then dropped along the rope, causing the lids to shut and seal the tube, after which the apparatus is pulled to the surface and the sample collected.

All samples were emptied into acid-washed (Section 2.2.1), sample-rinsed 500 ml polyethylene bottles. On return to the laboratory, 250 ml sub-samples were filtered via 0.45 μm membrane filters (Millipore HAWP 04700), using a Gelman filtration kit and were acidified with 16 M nitric acid (AristaR, BDH) 1:1000 v/v and maintained at 4°C until analysed.

Using a hand-held meter (Checkmate, Ciba-Corning), pH, conductivity, temperature and dissolved oxygen measurements were made on surface water and water overlying

the sediment in the core tubes. Secchi disc readings were also recorded. pH, conductivity, temperature, dissolved oxygen and depth at various depths in the water column at some of the sites were measured with the multiprobe Windermere Profiler 2 (IFE, Windermere), instead of the Checkmate.

2.2 Chemical pre-treatment of sediment

2.2.1 Acid washing

All glassware was thoroughly acid-washed to minimise sample contamination by heating in 8 M nitric acid (SLR, BDH) in a 5 l glass beaker for 2-3 h at 90°C. After cooling, the glassware was rinsed in MilliQ deionised water before transferring to a 5 l beaker of MilliQ deionised water and reheated for 2-3 h at 90°C. Plastic ware was cleaned as described for glassware, except the acid was not heated and the equipment remained in the acid overnight. (Lovell, 1985).

Sediment pre-treatment

Total wet weights were determined for each sediment section and, depending on requirements, were treated as follows:

2.2.2 Acid digestion

Sediment samples were oven-dried at approximately 40°C for one week after which their weights were recorded and each section was homogenised by grinding with a glass pestle and mortar (wiped between each sample and starting with the deepest section to prevent cross-contamination).

A nitric/hydrochloric (HNO_3/HCl) acid digestion method was used to remove metals from all but the most resistant fractions of sediment (such fractions being minerals, which could only be broken down by total digestion using hydrofluoric/perchloric acids). Using acid-washed glassware (Section 2.2.1), 8 M nitric acid (AnalaR, BDH; 20 ml) was added to accurately weighed samples of approximately 0.5 g dried, ground sediment and boiled gently on a hotplate for 2 h in 100 ml beakers, covered with watchglasses. 11.6 M hydrochloric acid (AnalaR, BDH; 10 ml) was added and the mixture boiled for a further 1 h. The beakers were removed from the hotplate and the samples were allowed to cool, after which they were filtered via Whatman No.40 filter paper, washing the residues with 1 M hydrochloric acid (AnalaR, BDH). The solutions were re-heated on the hotplate and

dissolved completely in hydrochloric acid by addition of 11.6 M hydrochloric acid (AnalaR, BDH) until no further brown fumes of nitrogen dioxide were emitted, *i.e.* when all nitric acid had been removed. After evaporation to near-dryness, the samples were taken up in 1 M hydrochloric acid and made up to 25 ml in volumetric flasks. Duplicate samples were digested for each sediment section. Two blanks were prepared with each sample batch, by using the reagents as in the digestion procedure, without the sediment. Samples and blanks were stored in 30 ml plastic Sterilin universal bottles prior to analysis.

2.2.3 Sequential extraction of sediment

This technique uses a five step sequential extraction of wet sediment, with the aim of removing metals from different operationally defined sediment fractions. The scheme chosen was one used for the sequential extraction of soils (Gibson and Farmer, 1986), which was based on the widely used extraction scheme of Tessier (1979).

Using acid-washed (Section 2.2.1) equipment throughout, wet sediment samples (0.1-1 g equivalent dry weight) were weighed into plastic, screw-topped centrifuge tubes (50 ml, Falcon) in duplicate for each sediment section. The remaining wet sample was weighed, oven-dried at 40°C for one week and reweighed to determine the dry:wet ratio, so equivalent dry weights for the extracted samples could be determined. Each sample, and two blanks per sample batch (centrifuge tubes with no sediment), was treated with the reagents listed below (all AnalaR, BDH). Between each step, the tubes were centrifuged for 5 min. (Gellman Junior centrifuge, speed 5). The supernatant was decanted and made up to 25 ml in volumetric flasks, using the respective extraction reagent for each step.

I. Exchangeable fraction

1 M ammonium acetate, pH7 (20 ml), shaken for 4 h (20°C).

II "Carbonate-bound"/specifically sorbed

1 M sodium acetate (acidified to pH5 with acetic acid) (15 ml), shaken for 5 h (20°C).

III. Easily reducible

0.1M hydroxylammonium chloride/0.01 M nitric acid (20 ml), shaken for 0.5 h (20°C).

IV. Moderately reducible

1M hydroxylammonium chloride/4.4 M acetic acid (20 ml), shaken for 4 h (20°C).

V. Organic fraction/sulphides

The sediment was transferred to 100 ml glass beakers. 0.02 M nitric acid (3 ml) and 30% w/v hydrogen peroxide (adjusted to pH2 with nitric acid) (5 ml) were added. Samples, covered by watchglasses, were heated to 85 ± 2°C for 2 h in a waterbath with occasional agitation. The samples were allowed to cool, before addition of further 30% (w/v) hydrogen peroxide (pH2) (5 ml) and reheated to 85 ± 2°C for 3h. On cooling, the sediment was transferred back to the centrifuge tubes and shaken with 3.2 M ammonium acetate in 3.2 M nitric acid (15 ml) for 0.5 h.

2.2.4 Sequential extraction under nitrogen

As previously mentioned (Section 2.1.2), the association of metals with different sediment fractions may be redox-dependent. For this reason, sequential extraction of sediment in an inert atmosphere may minimise post-sampling changes to the sediment due to altered redox conditions, and so give a better representation of in-situ metal associations. Some of the sediments sampled (refer to methods Chapters 3-7) were sequentially extracted under nitrogen.

As soon as possible after collection (*i.e.* in the field, where practicable) sediment cores were sectioned in the glovebox (Section 2.1.2) and the wet sediment placed into tightly sealed plastic bags. The bags were shut into screw-top, plastic tubs, the tub tops of which were further sealed with insulating tape, before removal from the glovebox. Samples were then transported to the laboratory in a freezer-box.

In an air-purged, nitrogen-filled glovebag (Aldrich Z10,608-9), the tubs were opened and wet sediment (equivalent dry weight 0.2-1.3 g) weighed into screw-top centrifuge tubes. The first sequential extraction reagent (Section 2.2.3) was purged with nitrogen, to remove oxygen, before addition to the samples. The centrifuge tubes were closed and sealed with insulating tape, before removal from the glovebag to be shaken. Thereafter, fractions II-IV were extracted in the same way, always opening the tubes and adding the air-purged reagents within the glovebag. Fraction V was extracted in air as described in Section 2.2.3.

2.3 Metal, carbon and nitrogen analysis

Flame and graphite furnace atomic absorption spectrophotometry (AAS), employed extensively in this study, are well-established methods of determining metal concentrations (*e.g.* Metcalfe, 1987; L'vov, 1991) and the following section is

therefore restricted to a description of the instrumentation and operating conditions used.

2.3.1 Flame AAS

A Pye Unicam SP9-800 flame AAS with a Pye Unicam SP9 computer was used to determine metal concentrations in solutions from the acid digests and sequential extractions, and in some porewater and water column samples. Operating conditions used are listed in Table 2.1 and specific conditions used for the different sample solutions are given in Table 2.2. An air/acetylene flame was used for all analyses in a ratio of approximately 2:1 (SP9 flowmeter: air 38 mm/acetylene 20 mm). A slotted tube atom trap (STAT, PU 9423 390 35021) was used when increased sensitivity was required, in which case a 50 mm slot burner was used. For all other analyses, the 100 mm slot burner was used. Single element hollow cathode lamps were used. Background correction, employing a deuterium arc hollow cathode lamp as the continuum source, was used at wavelengths less than 278 nm to correct for non-specific or background absorption (Metcalfe, 1987).

The SP9 computer recorded the mean of three integrated absorbance readings (integration time 1-3 s). At least four standard concentrations were prepared, covering the range of sample concentrations, by dilution of BDH Spectrosol standards (1000 mg l^{-1}) with the sample reagents. Standards were run regularly throughout the procedure. Sample solution concentrations (ranges listed in Table 2.3) were determined by calibration with the known standard concentrations. A standard addition method was used on a representative number of samples to assess for matrix effects, which were not found to be significant, sample concentrations determined by standard addition being generally within ± 10% of the concentration determined by calibration only. However, for some of the sequential extraction reagents (notably for fraction II, the sodium acetate extractant) the baseline value, measured between each sample, was obtained using the sample reagent rather than MilliQ deionised water. Two previously analysed samples were measured with each new sample batch to ensure reproducibility between analyses and the between-run precision was usually < ± 5%. Details of detection limits and sample solution concentration ranges are given in Table 2.3.

Table 2.1 Operating conditions for flame atomic absorption spectrophotometry

	element	wavelength (nm)	bandpass (nm)	background correction	lamp current (mA)	other conditions*
1	Cd	228.8	0.5	yes	3-4	STAT
2	Co	240.7	0.2	yes	8	
3	Cu	324.8	0.5	no	4	
4a	Fe	248.3	0.2	yes	10-12	
b		302.1	0.2	no	12	burner rotation[1]
c		346.6	0.2	no	12	"
d		372.0	0.2	no	12	"
5a	Mn	279.5	0.2	no	11	
b		403.1	0.2	no	10-12	burner rotation
6a	Ni	232.0	0.2	yes	10	
b		341.5	0.2	no	8	
7	Pb	217.0	0.5	yes	5	STAT used for some samples
8	Zn	213.9	0.5	yes	7	

Table 2.2 Atomic absorption spectrophotometry: sample analysis indicating elements analysed in the different samples and conditions used, by reference to Tables 2.1 and 2.4[2]

samples	Flame AAS (Table 2.1)	GFAAS (Table 2.2)
acid digests	Cd (1), Co (2), Cu (3), Fe (4c,d), Mn (5a,b), Ni (6a,b), Pb (7), Zn (8)	
sequential extraction	Cu (3), Fe (4a,b,c,d), Mn (5a,b), Pb (7), Zn (8)	
water column (incl overlying water)	Fe (4a), Mn (5a), Zn (8) for some samples	Cd, Cu, Fe, Mn, Pb, Zn
porewater	Fe (4a), Mn (5a), Zn (8) for some samples	Cd, Cu, Fe, Mn, Pb, Zn

* burner height: 8-12 mm (100 mm slot burner), 15-18 mm(50 mm slot burner)

[1]the 100 mm slot burner was rotated (1-70^{o}) to decrease sensitivity for some of the samples at the wavelength shown

[2]numbers in brackets refer to the different conditions in Table 2.1

Table 2.3 Detection limits and sample solution concentration ranges for flame and graphite furnace atomic absorption spectrometry.

	Fe	Mn	Pb	Zn	Cu	Cd	Co	Ni
FAAS								
detection limit (mg l^{-1})	0.05	0.03	0.1 (0.03 with STAT)	0.01	0.02	0.01 (0.003 with STAT)	0.05	0.04
sample solution concentration range (mg l^{-1})	BDL-1,600	BDL-700	BDL-2.5	BDL-6.0	BDL-1.3	BDL-0.02	BDL-0.6	BDL-1.0
GFAAS								
detection limit (mg l^{-1})	0.005	0.002	0.003	0.001	0.005	$1x10^{-4}$	not analysed	
sample concentration range (mg l^{-1})	BDL-34	BDL-34	BDL-0.06	BDL-0.06	BDL-0.15	BDL-$7x10^{-4}$		
uncorrected sample peak heights (mm)	0-140 some solutions diluted	0-140	0-40	0-140	0-60	0-25		
blank peak heights (mm)	0-3	0-4	0-4	0-10*	0-2*	0-5		

BDL = below detection limit

* Results from samples with blank concentrations > 0.006 mg l^{-1} (Zn) and $3x10^{-4}$ mg l^{-1} (Cd) were discarded

2.3.2 Graphite furnace AAS

Concentrations of Cd, Cu, Fe, Mn, Pb and Zn in acidified water column and porewater samples were determined using a Perkin Elmer PE-306 atomic absorption spectrometer attached to an HGA-400 graphite furnace, with an AS-1 autosampling system. Samples were injected in 20 µl aliquots into ordinary (uncoated) graphite tubes (PE 3007 0699). Each standard or sample was injected three times and the mean value calculated from peak heights recorded on a potentiometric recorder (RE 511, Venture). Instrument operating conditions employed for each element are indicated in Table 2.4 and elements analysed in different samples are listed in Table 2.2. A four step procedure was programmed to dry and ash the sample, to atomise with gas interrupt as required and finally to clear the graphite tube before injection of the following sample. Ramp time indicates the time set for the graphite tube to heat to the required temperature and hold time the length of time at which the temperature was held constant for each step. Argon was used as purge gas at an inlet pressure of 2.8 bar. Single element hollow cathode lamps were used below the maximum recommended currents on the lamps and a deuterium arc lamp was used to correct for background or non-specific absorption at wavelengths below 300 nm. A minimum of four standard concentrations was used, by dilution of BDH Spectrosol standard solutions (1000 mg l^{-1}) with 0.01 M nitric acid (AristaR, BDH), and were introduced regularly during a sample run. Sample solution concentrations (ranges listed in Table 2.3) were determined (after blank correction, where necessary, by subtraction of the blank peak height from the sample peak height) by calibration with the known standard concentrations.

2.3.3 Carbon and nitrogen analysis

The total % carbon and nitrogen contents of dried, ground sediment samples were determined by CHN analysis (Perkin Elmer 2400 CHN Elemental Analyzer). The principles of operation of the CHN analyser are described in the users manual for the above instrument (Culmo, 1988), but in summary, the technique involves complete combustion of samples, contained in tin or aluminium vials, in the presence of excess O_2 and combustion reagents to form CO_2, H_2O and N_2 gases. These combustion products are then passed to a gas control zone, where they are thoroughly homogenised and then selectively retained by frontal chromatography, after which the gases are detected stepwise as they pass through a thermal conductivity detector system.

Table 2.4 Graphite furnace atomic absorption spectrophotometry: operating conditions

element	Fe	Mn	Pb	Zn	Cu	Cd
wavelength (nm)	248.3	279.5	283.3	213.9	324.8	228.8
slit setting (nm)	0.7	0.7	0.7	0.7	0.7	0.7
background correction	yes	yes	yes	yes	no	yes
drying						
temp. (°C)	120	120	120	120	120	120
ramp time (s)	2	2	2	2	2	2
hold time (s)	20	20	20	20	20	20
ashing						
temp. (°C)	1200	1000	500	400	900	250
ramp time (s)	1	1	1	1	1	1
hold time (s)	20	20	20	20	20	20
atomising						
temp. (°C)	2700	2100	2100	2200	2250	2100
ramp time (s)	1	1	1	1	1	1
hold time (s)	5	5	5	5	5	5
clearing						
temp. (°C)	2700	2700	2700	2700	2700	2700
ramp time (s)	1	1	1	1	1	1
hold time (s)	3	3	3	3	3	3
gas interrupt	miniflow/ none	miniflow/ none	stopflow	miniflow/ none	stopflow	stopflow

2.3.4 Sediment porosity measurements

Sediment porosities were determined as follows, to give a rough guide to changes in sediment grain size in cores:

$$\text{porosity (\%)} = \frac{V_W \times 100}{V_W + V_S} = \frac{M_W/D_W \times 100}{M_W/D_W + M_S/D_S}$$

where: V_W (V_S) = volume of water (volume of solids) (cm^3)
M_W (M_S) = mass of water (mass of solids) (g)
D_W (D_S) = density of water (density of solids) ($g\ cm^{-3}$)

Water density was assumed = 1. Sediment density was estimated by assuming dry organic matter density = 1.4 g cm^{-3} and dry inorganic sediment density = 2.5 g cm^{-3} (El-Daoushy, 1990) and, using results from the carbon analysis (Section 2.3.3), calculating the overall density of sediment samples by using the quoted sediment densities in the proportion of organic to inorganic matter obtained for sediment from each sampling site.

2.4 Radionuclide analysis

2.4.1 Principles of γ-spectrometry

Interaction of γ radiation with matter

Gamma (γ) radiation consists of high energy photons of electromagnetic radiation, which are emitted as nucleii undergo transitions from higher energy state(s) to lower excited states or the ground state. The γ photons have a low probability of interaction with atoms encountered and the initial energy of the photon is retained until interaction with an absorber occurs, by one of the following processes:

1. Photoelectric effect - this involves transfer of all the γ-photon energy to a bound electron in an atom of the absorber, which causes ejection of the electron as an energetic photoelectron and complete dissappearance of the γ ray. The photoelectric effect is more efficient for lower photon energies and is related to $E^{-7/2}$ (for E<1 MeV) and at higher energies to 1/E and the probability of occurrence is approximately proportional to Z^5 (where Z = atomic number) of the absorber (but decreases at higher γ energies). This mode of interaction contributes to the 'full energy peak' in the recorded pulse height spectrum and provides the best method for measuring the original γ-ray energy.

2. Compton scattering - during this process a photon transfers only part of its energy to an electron, which may be bound or free. The photon is degraded in energy and is also deflected from its original path. The probability of scattering depends on the number of electrons available and therefore is proportional to Z. For energies > 0.5 MeV it is approximately proportional to E^{-1} and, consequently, Compton scattering falls off much more slowly than photoelectric absorption with increasing energy, at least at moderate energies of up to 1 or 2 MeV. The scattering gives rise to electrons with a continuous distribution of energies absorbed in the detector and gives the observed 'Compton continuum' extending in the spectrum from the lowest energy to a maximum energy transferred to the electrons, which is called the 'Compton edge'.
3. Pair production - this effect is less common than the other two and only occurs for γ photons of energy > 1.022 MeV. γ rays are transformed upon interaction with matter resulting in the formation of an electron - positron pair and involving a transfer of the residual γ photon energy to the pair as kinetic energy. This process is always followed by annihilation of the positron by combination with an electron, resulting in emission of two γ photons of 0.511 MeV, observable in the spectrum and known as the 'annihilation peak'. The probability of pair production is proportional to Z^2 of the absorber and increases with increasing photon energy.

Interaction of γ photons with matter by these three mechanisms causes ionization in the absorber and determination of this forms the basis for γ spectrometric dectection.

Detection of γ radiation

High-purity semi-conductor germanium (Ge) crystals are widely used as detectors for γ-spectroscopy. Principles of γ-spectroscopy and operation of detectors have been described extensively (*e.g.*. Friedlander *et al.*, 1981; EG & G Ortec, 1993), but the main components of the detection system are outlined below and illustrated in Fig. 2.3.

Interaction of γ radiation with the Ge detector, by one of the processes described above, promotes electrons into the conduction band and for the photoelectric effect, the number of electrons migrating into this band is proportional to the energy of the incident radiation. The charge pulse is collected by application of a high voltage (3,500 V) to the crystal and is then amplified, converted to a digital pulse by an analogue to digital converter (ADC) and the signal is then stored in a multi-channel buffer. The information stored in the buffer may be accessed by computer on demand.

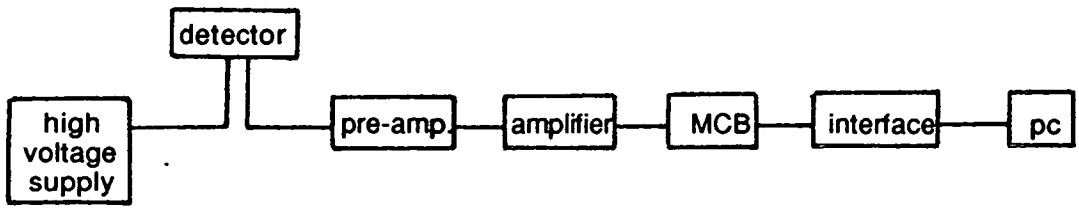

MCB = multi-channel buffer containing the ADC

Fig. 2.3 The main components of a typical γ-spectrometer

2.4.2 Instrumentation

γ-spectra were recorded using a Tennelec co-axial, n-type intrinsic Ge detector with a thin aluminium window. The detector has a 35% relative efficiency and a resolution (full width at half peak maximum) of 1.8 keV at 1333 keV, with a selected energy range 10 keV - 2 MeV. The high purity Ge detector element (impurity concentration $< 3x10^{10}$ cm^{-3}) is a single crystal of Ge, made into a diode. The detector is mounted within a vacuum cryostat and cooled with liquid nitrogen to reduce leakage current and thermal noise. The detector is surrounded by 10 cm of Pb to shield it from background radiation. A Cd-Cu metal lining is used to shield from fluorescent x-rays produced by γ interactions with the Pb shielding. Even with this arrangement, background counts are still recorded and appropriate correction was made to spectra on the basis of detector background recorded over two weeks. Background spectra were recorded throughout the period of research (Table 2.5).

The analysis system comprised an EG & G Ortec 919 ADCAM multi-channel buffer unit, interfaced with an IBM compatible PC. Spectra were analysed using the Ortec software package MINIGAM 2. Energy calibration of the system was performed using a ^{226}Ra calibration source to generate a spectrum with peaks of known energy, from which the MINIGAM 2 programme created a calibration file via linear regression analysis of energy against channel number.

2.4.3 Sample preparation and analysis

Dried, ground sediment samples were weighed into clear, polystyrene containers. Where sufficient sample was available (> 5 g), (from Loch Lomond and Loch Leven) sediment was pelletised by compressing under 10 tonnes in a metal die (diameter = 4.8 cm) in order of decreasing depth (*i.e.* working up the core) and the die was wiped clean between pressing to minimise cross-contamination. Pelletised samples provided better counting geometries, as counting efficiency decreases with distance from the detector (at distance d, the detection efficiency for a point souce is proportional to $1/d^2$) and therefore height of the sample. Sample height was recorded, so that suitable standard geometries could be prepared.

In order to obtain the maximum detection efficiency, samples were placed directly on the detector, the face of which was covered with a thin layer of polythene to avoid contamination, and counted for approximately two days to minimise statistical uncertainty. Sample count rates were recorded at 46.5 keV (^{210}Pb), 185 keV (^{226}Ra), 661.6 keV (^{137}Cs) and 604.7 and 796 keV (^{134}Cs), corrected for background and the

Table 2.5 Two week background count rates for ^{210}Pb, ^{226}Ra and radiocaesium

radionuclide	counts per second (cps)	1 σ (%)
^{210}Pb (46.5 keV)	6.86×10^{-3}	7.93
^{226}Ra (185 keV)	1.16×10^{-3}	4.85
^{137}Cs (661.6 keV)	1.44×10^{-3}	20.18
^{134}Cs (796 keV)	1.04×10^{-3}	41.5
^{134}Cs (604.7 keV)	no counts	

1σ (%) = relative uncertainty, based on 1σ counting statistics

Table 2.6 Standard solutions (Amersham International) used to prepare solutions for spiked standards.

radionuclide	date of initial preparation	certified activity (A_o) ($Bq\ ml^{-1}$)
^{210}Pb	23.10.89	63.1
^{226}Ra	1991	22.7
^{134}Cs	16.03.89	18.65×10^2
^{137}Cs	14.10.89	3.541×10^2

value obtained time-corrected to the date of coring (equation 2, Section 2.4.4). The final radionuclide concentration in the sample was then given by:

$$S = (C \times 100/E) / W$$

where: S = sample radionuclide concentration (Bq kg^{-1})
C = count rate (cps)
E = absolute detection efficiency (%)
W = sample weight (kg)

2.4.4 Standard preparation and analysis

The relationship between radiation detected and distance from the detector ($1/d^2$) and the dependence of photoelectric absorption of γ-photons on Z^5 (where Z = atomic number), Compton effect on Z and pair production on Z^2 of the absorber, means that variations in the height, density and atomic composition of the samples must be taken into account when making standards used to determine absolute detection efficiency.

To correct for distance of sample from the detector and self-absorption effects, one of two methods was used to prepare standards comparable with the samples, using spike solutions, prepared by dilution of primary standard solutions, supplied by Amersham International and certified to $< \pm$ 1% accuracy for radionuclide content (Table 2.6).

1. For highly organic, loose (unpelletised) sediment samples, a mixture of vermiculite and cellulose was used as standard material, cellulose being used to mimic the Z value of the organic-rich sediment samples and vermiculite to obtain the comparable sample density. Depending on standard height, using a 0.1 ml pipettor, 0.1-0.4 ml of spike solution (Table 2.6) was applied evenly to four layers of vermiculite/cellulose mixture, which were separated by thin polythene discs. ^{210}Pb standards were prepared separately from the other radionuclides to avoid obscuring the photopeak at 46.5 keV by Compton Scattering from higher energy γ photons (particularly radiocaesium).
2. Standards for samples with higher clay content were prepared using dried, ground sediment which was a mixture of deep (> 6 m) Glasgow clay and Loch Lomond sediment, collected from depths below 70 cm, and this sediment was assumed to contain no radiocaesium or unsupported ^{210}Pb. 10 ml of each spike solution (Table 2.6) was added to 117.9298 g of sediment for ^{210}Pb standards and 113.6327 g of sediment for ^{226}Ra, ^{137}Cs and ^{134}Cs standards and mixed thoroughly with water to distribute the spike homogenously. The sediment was then freeze-dried and

appropriate quantities weighed into containers or pelletised, as described above for the samples. To mimic the Z value of samples with moderate %C contents (but less than the highly organic sediments mentioned above) cellulose was added to aliquots of spiked sediment and thoroughly mixed.

Blanks were prepared using unspiked sediment (pelletised and loose) or cellulose/vermiculite mixture and appropriate correction was made to the observed standard count rates.

Absolute efficiency for detection was determined for each radionuclide by:

$$E=C/A \times 100 \quad (1)$$

where: E = detection efficiency (%)
C = standard count rate (cps g^{-1}) (cps = counts per second)
A = actvity (Bq g^{-1})

Standard count rates were corrected for background radiation (or blank sediment counts, whichever was greater). Correction for the decay of spike since preparation was made by

$$A_t = A_o e^{-\lambda t} \quad (2)$$

where: A_t = activity at time of analysis (Bq)
A_o = activity at time of spike preparation (Bq)
$\lambda = \ln 2/t_{1/2}$ ($t_{1/2}$=half life of radionuclide(y))
t = time elapsed since preparation of spike solution

Accuracy and precision

The precision for standard preparation was assessed by making triplicate standards using the spiked sediment. Activities and detection efficiencies generally agreed well between the standards (Table 2.7), although the ^{226}Ra results have rather high errors, which is probably due to insufficient volume of spike solution being used in the standard preparation. Accuracy was determined by measuring ^{210}Pb and ^{226}Ra in the IAEA marine sediment reference material (SD-A-1) with a certified activity correct to 1.1.87. Reference material was pelletised as previously described and counted for 72 h. The ^{210}Pb and ^{226}Ra measurements agreed with the certified activity (Table 2.8) within the uncertainties at the 95% confidence limit. No reference material was available for the organic rich sediments.

Table 2.7 Reproducibility of standards used for determining detection efficiency

standard code	standard weight (g)	detection efficiency (%) ^{210}Pb 46.5 keV	^{226}Ra 185 keV	^{137}Cs 661.6keV	^{134}Cs 796 keV	^{134}Cs 604.7 keV
RPb-1	2.1484	0.758 ±0.018				
RPb-2	1.8678	0.873 ± 0.028				
RPb-3	2.0216	0.867 ± 0.022				
RCs-1	2.2617		0.766 ± 0.243	3.458 ± 0.044	2.974 ± 0.033	4.325 ± 0.047
RCs-2	2.2072		0.624 ± 0.272	4.491 ± 0.050	2.863 ± 0.031	4.253 ± 0.045
RCs-3	2.1050		0.659 ± 0.123	4.502 ± 0.046	2.934 ± 0.030	4.307 ± 0.044

Table 2.8 Determination of ^{210}Pb and ^{226}Ra in IAEA marine sediment reference material (SD-A-1)

pellet weight (g)	activity (Bq kg^{-1}) ^{210}Pb (46.5 keV)	^{226}Ra (185 keV)
4.4662	73 ± 24	113 ± 47
9.7862	74 ± 18	97 ± 23
14.8028	82 ± 12	82 ± 12
19.0428	90 ± 10	71 ± 13

Error is a fully propagated error, based on 1σ counting statistics

Certified activities

^{210}Pb 70 Bq kg^{-1} (range at 95% confidence limit = 58-88 Bq kg^{-1})

^{226}Ra 75 Bq kg^{-1} (range at 95% confidence limit = 55-85 Bq kg^{-1})

The detection limit for peaks recorded in the spectra is defined as three times the uncertainty on the Compton continuum under the photopeak (*i.e.* 3 σ where 1 $\sigma = N^{1/2}$ and N = no. of counts).

2.5 Summary of sediment pre-treatment and analyses

The pre-treatment of sediment and analyses performed on the samples collected during the research and described in this Chapter are summarised in Fig. 2.4.

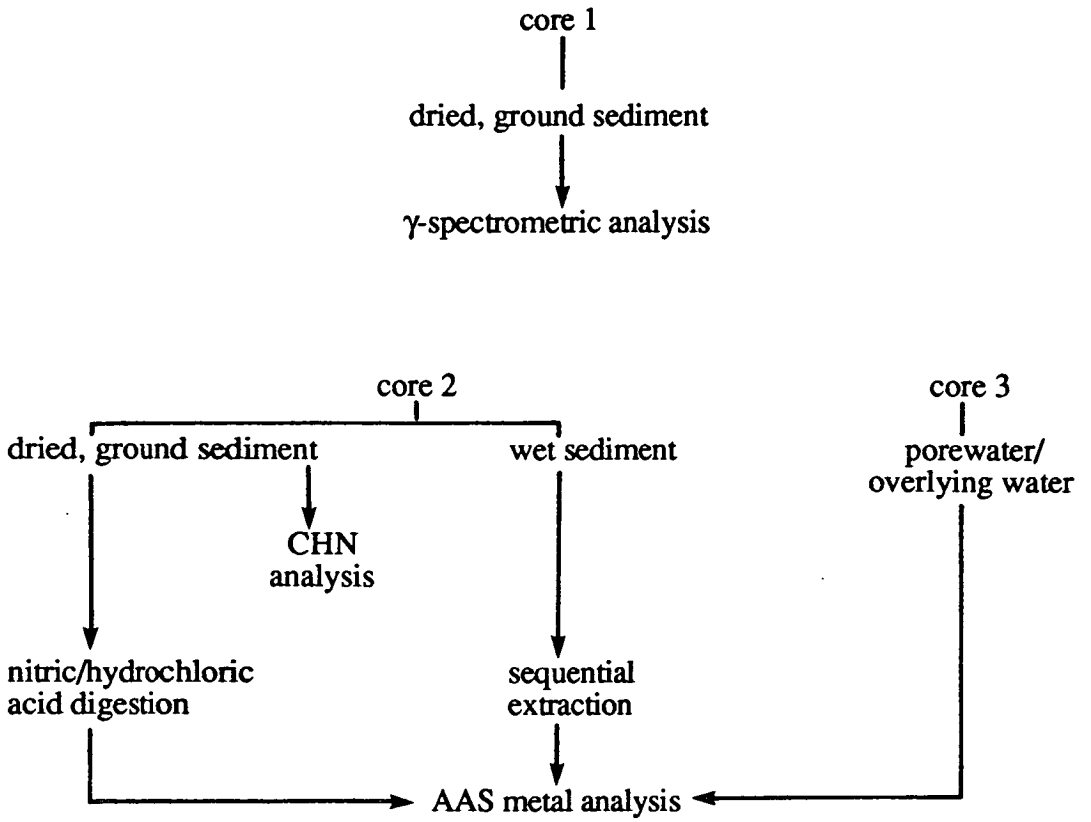

Fig. 2.4 Summary of sediment pre-treatment and analysis

Chapter 3 Round Loch of Glenhead

3.1 Study Area

As briefly discussed in Chapter 1, Round Loch of Glenhead in the Galloway region of south-west Scotland (OS grid ref. NX 450 804) is an acid loch which has been extensively studied (*e.g.* Flower *et al.*, 1987; Battarbee *et al.*, 1989; Jones *et al.*, 1989) with respect to the acidification of surface water, due to deposition of acid precipitation, resulting from fossil fuel combustion (Chapter 1).

The loch and its catchment of 95.1 ha with the Cliffs of Craiglee to the north and north-east (at an altitude of 531 m) have been designated a Site of Special Scientific Interest (SSSI). The underlying bedrock is the Loch Doon granite intrusion and catchment soils are mainly deep peats and peaty podsols, with skeletal soils and bare rock on the steepest slopes (Patrick *et al.*, 1991). The catchment is unafforested, unlike many areas in the region, and the moorland vegetation is dominated by *Molinia, Erica* and *Trichophorum* with other species commonly associated with upland blanket mires, such as *Calluna, Nardus, Potentilla* and *Narthecium*. The community is maintained by periodic burning and sheep grazing (Jones *et al.*, 1989).

Round Loch of Glenhead (Fig. 3.1) lies at an altitude of 295 m, receiving high rainfall (*ca.* 2,700 mm in 1988) and high acid deposition (Table 3.1). Drainage into the loch is from the blanket peats of the catchment and minor streams with the outflow draining to the south-west into Glenhead Burn and Loch Trool. The ecology of the loch is characteristic of oligotrophic and low pH conditions with impoverished communities of macrophyte flora and macroinvertebrate fauna (Patrick *et al.*, 1991). Macrophyte flora are characterised by *Littorella uniflora, Lobelia dortmanna, Isoetes lacustris* and *Juncus bulbosus* var. *fluitans* with local abundance of liverworts in shallow water. Of the macroinvertebrate fauna, only the most acid tolerant mayfly *Leptophlebia vespertina*, a few beetles and corixids and *Chironomidae* (which may burrow in the sediment) are present. Brown trout (*Salmo trutta* L.) have been found in the loch, but the population is low in density compared with less acidified lakes (Maitland *et al.*, 1987).

Sediments are organic-rich (*ca.* 20% C) and remnants of terrestrial plant remains are observed in the dark brown coloured sediment. Further details of sediment characteristics are described in Section 3.4.1 (Discussion).

Table 3.1 summarises the main features of Round Loch and its catchment.

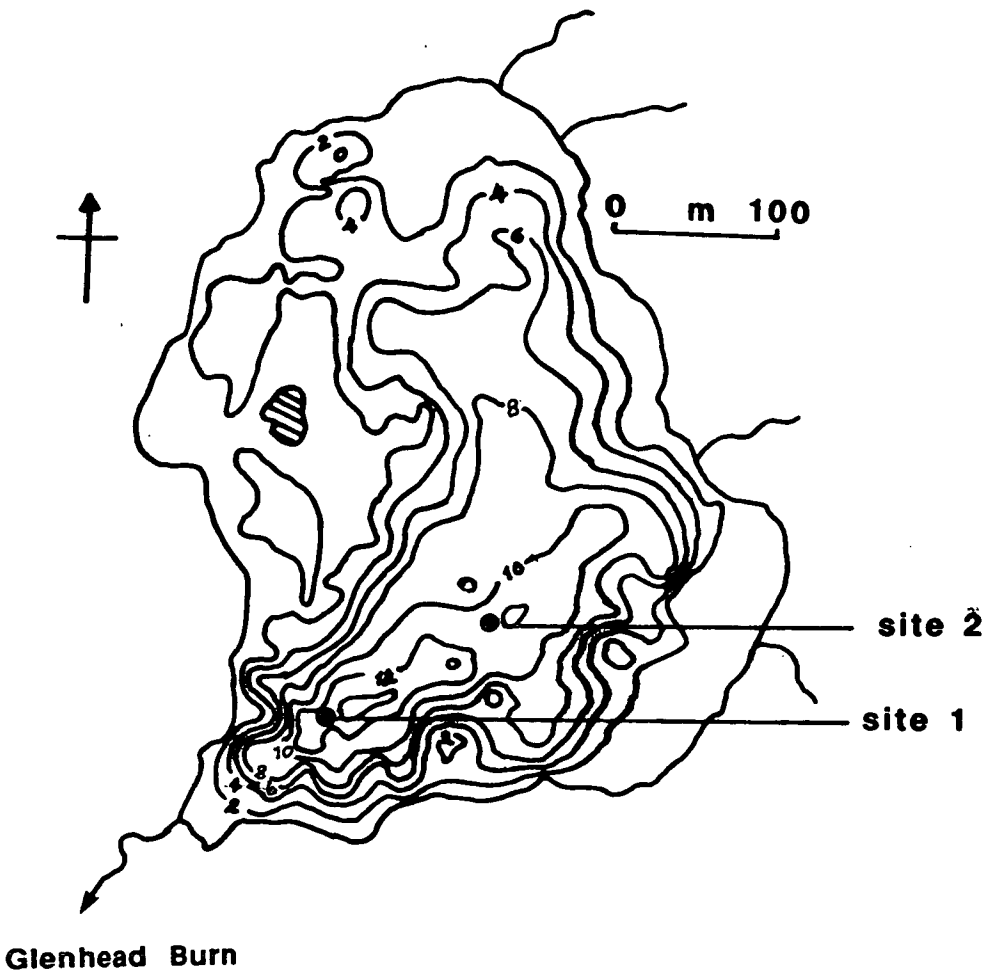

Fig. 3.1 Round Loch of Glenhead bathymetry and sampled sites (●). Contour depths in metres.

Table 3.1 Round Loch of Glenhead site characteristics (Patrick *et al.*, 1991)

Loch altitude	295 m
Maximum depth	13.5 m
Mean depth	4.28 m
Volume	0.53×10^6 m^3
Loch area	12.5 ha
Catchment geology	tonalite/granite
Catchment soils	peat, peaty podsols
Catchment vegetation	100% moorland
Catchment area	95.1ha (excluding loch)
Ratio of catchment:loch area	7.5:1
Mean annual rainfall	*ca.* 2,700 mm (1988)
Wet deposited acidity	0.5 kg H^+ ha^{-1} y^{-1} (1988)
Wet deposited non-marine sulphate	21.73 kg S ha^{-1} y^{-1} (1988)

3.2 Sampling and analysis

3.2.1 Site 1

Sampling was carried out on 4.6.90 in the southern part of the loch (Fig. 3.1). Three sediment cores (RLG1-A, RLG1-B, RLG1-C) were collected at a water depth of 13 m, using a modified Kajak corer (Chapter 2). All sediment cores were uniformly dark brown with unconsolidated surface material and *Molinia* was observed in two of the cores. One of the cores (RLG1-C) was collected in a pre-drilled core tube for porewater sampling using the syringe method as described in Chapter 2. Porewater was extracted by hand-forced filtration using a stainless steel syringe and filtered via 0.45 μm filters (Chapter 2). Filtered porewater samples were collected in 20 ml self-sealing glass vials and were acidified prior to analysis, once the vial tops had been removed. The remaining two cores of 25 cm and 32 cm length were extruded manually and sectioned at 1 cm vertical intervals. Core RLG1-A was used for γ-spectrometric analysis and RLG1-B (sectioned at 2 cm intervals below 20 cm) for sequential extraction and nitric/hydrochloric acid digestion, followed by metal analysis (Chapter 2). Table 3.2 summarises the core codes and purposes of core collection.

Water overlying the sediment in the core tube (referred to as 'overlying water') was removed with a syphon and treated as described for the water column samples. Water column samples were collected at depths of 0 m, 5 m and 10 m using a Friedinger sampler (Chapter 2). Sub-samples were filtered via 0.45 μm filters and both filtered and unfiltered samples were acidified. Details are described in Chapter 2.

Surface water characteristics (Table 3.3) were measured with the Ciba-Corning Checkmate probes (Chapter 2).

3.2.2 Site 2

Three cores (with lengths between 23 and 26 cm) were collected (RLG2-1A, RLG2-1B, RLG2-1C), using a Jenkin Surface-Mud sampler (Chapter 2) on 25.1.91 at a water depth of 12.5 m in the southern part of the loch in the basin adjacent to that sampled at site 1. One of the cores (RLG2-1C) was collected using a pre-drilled core tube, but this time the porewater samples were stored in 30 ml acid-washed plastic Sterilin Universal bottles, with the aim of minimising problems due to Zn and Cd contamination encountered with use of the self-sealing vials. Sediment from the other cores (RLG2-1A and RLG2-1B) was extruded hydraulically and treated and analysed as for material from site 1 (Table 3.2).

Table 3.2 Core codes, sampling dates and purpose of core collection from Round Loch of Glenhead

code	location	sampling date	purpose of core
RLG1-A	site 1	4.6.90	γ-spectrometry
RLG1-B	"	"	chemical digestion
RLG1-C	"	"	porewater analysis
RLG2-1A	site 2	25.1.91	γ-spectrometry
RLG2-1B	"	"	chemical digestion
RLG2-1C	"	"	porewater analysis
RLG2-2A	site 2	23.5.92	porewater analysis
RLG2-2B	"	"	"

Table 3.3 Surface water characteristics in Round Loch of Glenhead

sampling date	pH	cond. (µS)	O_2(%)	T. (^oC)
4.6.90	4.7	50.0	89	12.0
25.1.91	5.1	54.8	98	2.0

Water samples were collected every 2 m from the surface to 12 m depth, using a Friedinger sampler. Overlying water was collected by syphon and all water samples were treated as for those at site 1.

Site 2 was further sampled on 23.5.92 for the collection of sediment porewaters, as no data had been obtained for Zn concentrations from previous sampling trips, due to high concentrations of Zn in the blanks. Two cores (RLG2-2A and RLG2-2B) were collected with spirally-drilled core tubes at a water depth of 12.5 m, using a Jenkin Surface-Mud sampler and porewaters were collected using the syringe method (Chapter 2). On this occasion, however, an acid-washed teflon needle was used in place of the stainless-steel needle and the syringes had teflon stoppers instead of neoprene stoppers. Porewater was passed via 0.22 µm filters (Chapter 2) and the samples stored in 30 ml Nalgene 'low metal' bottles. Overlying water and surface water samples were collected and sub-samples passed via 0.22 µm filters before acidifying.

Surface water characteristics (Table 3.3) were measured with the Ciba-Corning Checkmate probes (Chapter 2).

3.3 Results

Data are listed in Tables 3.4-3.23. Figures containing some of this information are presented in the Discussion (Section 3.4).

1. Tables 3.4-3.7 contain wet and dry sediment section weights, mid-section cumulative weights (g cm^{-2}) and porosities (using an assumed solid sediment density of 2.28 g cm^{-3}) for sediment cores RLG1-A, RLG1-B, RLG2-1A and RLG2-1B. Total carbon content and C/N ratios were measured in sediment from cores RLG1-A and RLG2-1A and results are listed in Tables 3.4 and 3.6.

2. Tables 3.8 and 3.9 contain total ^{210}Pb, ^{226}Ra and excess ^{210}Pb concentrations for sediment cores RLG1-A and RLG2-1A.

3. Radiocaesium concentrations (at the time of sampling) and $^{134}Cs/^{137}Cs$ ratios for sediment cores RLG1-A and RLG2-1A are presented in Tables 3.10 and 3.11. ^{134}Cs concentrations, calculated using the 605 keV and 796 keV γ lines, are shown along with the mean (x ^{134}Cs) value given at each depth.

4. Metal concentrations for HNO_3/HCl acid digested sediment and in sequentially extracted sediment for cores RLG1-B and RLG2-1B are listed in Tables 3.12-3.18, in which column headings I-V refer to the following fractions and extractants:

I. 1 M ammonium acetate, pH 7, 20°C (exchangeable fraction)

II. 1 M sodium acetate, pH 5 with acetic acid, 20°C ("carbonate-bound"/specifically sorbed)

III. 0.1 M hydroxylammonium chloride/0.01 M nitric acid, 20°C (easily reducible)

IV. 1 M hydroxylammonium chloride/4.4 M acetic acid, 20°C (moderately reducible)

V. 30% w/v hydrogen peroxide, pH 2, 85 +/- 2°C; 3.2 M ammonium acetate in 3.2 M nitric acid (organic fraction/sulphides)

Sum I-V refers to the sum of metal concentrations in all fractions.

5. Porewater and water column data are listed in Tables 3.19-3.23a No results are presented for Zn and Cd in samples collected during field work on 4.6.90 and 25.1.91, due to high concentrations of these metals detected in the blanks (Zn ≥ 0.01 mg l^{-1}, Cd ≥ 5 x 10^{-4} mg l^{-1}). Data for Pb and Cu in porewaters are not presented as most of the samples were below detection limits of 0.003 mg l^{-1} and 0.008 mg l^{-1} respectively and the few detectable results were ≤ 0.02 mg l^{-1} for both metals.

6. (BDL) is entered where samples were below detection limit, and (...) where a result was not available.

Table 3.4 Some physical characteristics, carbon content and carbon/nitrogen ratios of Round Loch of Glenhead sediment core RLG1-A[1]

section depth (cm)	wet section weight (g)	dry section weight (g)	mid-section cumulative weight (g cm^{-2})	porosity (%)	carbon content (%)	C/N ratio
0-1	19.651	0.936	0.024	97.8	19.0	13
1-2	20.299	1.250	0.080	97.2	19.7	14
2-3	21.568	1.403	0.147	97.0	20.6	14
3-4	21.313	1.426	0.219	97.0	20.1	15
4-5	22.115	1.561	0.295	96.8	20.5	15
5-6	22.463	1.613	0.376	96.7	19.1	16
6-7	20.737	1.587	0.458	96.5	21.4	17
7-8	20.595	1.784	0.543	96.0	23.1	16
8-9	22.513	1.866	0.636	96.2	22.2	18
9-10	21.723	1.872	0.732	96.0	21.8	17
10-11	22.522	1.996	0.830	95.9	22.4	19
11-12	22.060	2.031	0.933	95.7	23.4	16
12-13	20.287	1.894	1.033	95.7	23.5	16
13-14	22.223	2.071	1.134	95.7	25.2	20
14-15	22.625	2.165	1.242	95.6	25.8	19
15-16	22.695	2.331	1.356	95.2	22.8	19
16-17	23.202	2.360	1.476	95.3	21.5	18
17-18	23.847	2.379	1.596	95.4	21.7	18
18-19	21.799	2.243	1.714	93.2	23.9	18
19-20	22.481	2.258	1.829	95.3	...	...
20-21	22.201	2.300	1.945	95.2	...	...
21-22	23.637	2.506	2.067	95.0	...	...

[1]core cross-section area = 19.63 cm^2

Table 3.5 Some physical characteristics of Round Loch of Glenhead sediment core RLG1-B[2]

section depth (cm)	wet section weight (g)	dry section weight (g)	mid-section cumulative weight ($g\ cm^{-2}$)	porosity (%)
0-1	25.701	0.961	0.024	98.3
1-2	16.448	1.032	0.075	97.1
2-3	17.355	1.160	0.131	97.0
3-4	21.037	1.430	0.197	96.9
4-5	19.374	1.383	0.269	96.7
5-6	19.568	1.388	0.339	96.8
6-7	20.509	1.409	0.410	96.9
7-8	19.096	1.401	0.482	96.6
8-9	19.656	1.617	0.559	96.2
9-10	21.289	1.728	0.644	96.3
10-11	20.769	1.722	0.732	96.2
11-12	20.175	1.782	0.821	95.9
12-13	21.216	1.838	0.913	96.0
13-14	20.661	1.851	1.007	95.9
14-15	19.323	1.740	1.099	95.8
15-16	20.273	1.890	1.191	95.7
16-17	20.638	2.030	1.291	95.4
17-18	18.027	1.806	1.389	95.3
18-19	22.613	2.169	1.490	95.6
19-20	21.656	2.156	1.600	95.4
20-21	19.895	2.000	1.706	95.3
21-22	19.641	1.971	1.807	95.3
22-23	21.486	2.080	1.910	95.5
23-24	19.971	2.031	2.015	95.3
24-25	20.937	2.125	2.121	95.3
25-26	21.304	2.132	2.230	95.3
26-27	20.735	2.145	2.338	95.2
27-28	20.661	2.092	2.446	95.3
28-29	22.496	2.314	2.559	95.2
29-30	21.555	2.345	2.677	94.9
30-31	16.708	1.894	2.785	94.7
31-32	24.991	3.152	2.914	94.0

[2]core cross-section area = 19.63 cm^2

Table 3.6 Some physical characteristics, carbon content and carbon/nitrogen ratios of Round Loch of Glenhead sediment core RLG2-1A[3]

section depth (cm)	wet section weight (g)	dry section weight (g)	mid-section cumulative weight (g cm^{-2})	porosity (%)	carbon content (%)	C/N ratio
0-1	46.718	0.630	0.008	99.4	21.4	13
1-2	27.124	1.080	0.031	98.2	22.0	13
2-3	43.587	2.258	0.076	97.7	19.7	12
3-4	41.619	2.616	0.141	97.1	19.0	12
4-5	41.998	2.752	0.213	97.0	18.8	14
5-6	40.032	2.892	0.288	96.7	19.4	15
6-7	45.883	3.421	0.373	96.6	20.6	16
7-8	45.563	3.658	0.467	96.3	23.1	19
8-9	43.290	3.570	0.564	96.2	21.6	19
9-10	34.787	3.547	0.659	95.2	21.9	18
10-11	43.077	3.759	0.757	96.0	...	
11-12	52.112	4.624	0.869	95.9	...	
12-13	37.058	3.928	0.983	95.0	...	
13-14	38.724	3.490	1.083	95.8	...	
14-15	38.257	3.440	1.175	95.8	...	

[3]core cross-section area = 37.39 cm^2

Table 3.7 Some physical characteristics of Round Loch of Glenhead sediment core RLG2-1B[4]

section depth (cm)	wet section weight (g)	dry section weight (g)	mid-section cumulative weight ($g\ cm^{-2}$)	porosity (%)
0-1	47.424	1.515	0.020	98.6
1-2	37.019	2.156	0.069	97.4
2-3	40.085	2.533	0.132	97.1
3-4	43.866	2.808	0.203	97.1
4-5	44.550	3.442	0.287	96.4
5-6	39.257	3.058	0.374	96.4
6-7	44.683	3.475	0.461	96.4
7-8	38.045	3.312	0.552	96.0
8-9	38.641	3.396	0.642	95.9
9-10	36.304	3.185	0.730	96.0
10-11	35.148	2.882	0.811	96.2
11-12	43.901	3.833	0.901	96.0
12-13	39.239	3.311	0.996	96.1
13-14	39.020	3.525	1.088	95.8
14-15	44.902	4.093	1.190	95.8
15-16	44.477	3.991	1.298	95.8
16-17	39.960	3.590	1.399	95.8
17-18	37.118	3.489	1.494	95.6
18-19	38.920	3.740	1.590	95.5
19-20	36.933	3.548	1.688	95.5
20-21	38.324	3.676	1.784	95.6
21-22	38.213	3.849	1.885	95.3
22-23	34.760	3.589	1.984	95.2

[4]core cross-section area = 37.39 cm^2

Table 3.8 Total ^{210}Pb, ^{226}Ra and excess ^{210}Pb concentrations in Round Loch of Glenhead sediment core RLG1-A (4.6.90)

section depth (cm)	mid-section cumulative weight (g cm^{-2})	total ^{210}Pb (Bq kg^{-1})	^{226}Ra (Bq kg^{-1})	excess ^{210}Pb (Bq kg^{-1})
0-1	0.024	900 ± 100	BDL	818 ± 45
1-2	0.080	781 ± 66	78 ± 46	699 ± 73
2-3	0.147	707 ± 97	BDL	625 ± 102
3-4	0.219	715 ± 71	"	633 ± 78
4-5	0.295	648 ± 69	75 ± 44	566 ± 76
5-6	0.376	496 ± 65	97 ± 45	414 ± 72
6-7	0.458	441 ± 73	BDL	359 ± 80
7-8	0.543	218 ± 55	79 ± 37	136 ± 63
8-9	0.636	210 ± 75	BDL	128 ± 81
9-10	0.732	160 ± 61	"	BDL
10-11	0.830	150 ± 52	80 ± 37	"
11-12	0.933	158 ± 56	122 ± 43	"
12-13	1.033	92 ± 56	178 ± 39	"
13-14	1.134	BDL	133 ± 41	"
14-15	1.242	"	BDL	"
15-16	1.356	85 ± 41	99 ± 33	"
16-17	1.476	77 ± 44	126 ± 32	"
17-18	1.596	BDL	110 ± 36	"
18-19	1.714	"	123 ± 34	"
19-20	1.829	"	118 ± 32	"

Table 3.9 Total ^{210}Pb, ^{226}Ra and excess ^{210}Pb concentrations in Round Loch of Glenhead sediment core RLG2-1A (25.1.91)

section depth (cm)	mid-section cumulative weight (g cm^{-2})	total ^{210}Pb (Bq kg^{-1})	^{226}Ra (Bq kg-1)	excess ^{210}Pb (Bq kg^{-1})
0-1	0.008	680 ± 100	BDL	540 ± 104
1-2	0.031	1,103 ± 92	"	963 ± 97
2-3	0.076	956 ± 47	"	816 ± 56
3-4	0.141	948 ± 51	153 ± 66	808 ± 59
4-5	0.213	734 ± 47	BDL	594 ± 56
5-6	0.288	517 ± 48	"	377 ± 57
6-7	0.373	482 ± 65	"	342 ± 72
7-8	0.467	344 ± 46	130 ± 49	204 ± 55
8-9	0.564	237 ± 62	108 ± 58	BDL
9-10	0.659	123 ± 52	191 ± 65	"
10-11	0.757	123 ± 29	140 ± 32	"
11-12	0.869	140 ± 29	159 ± 33	"
12-13	0.983	107 ± 27	154± 34	"
13-14	1.083	113 ± 32	184 ± 37	"
14-15	1.175	105 ± 34	BDL	"

Table 3.10 Radiocaesium concentrations and $^{134}Cs/^{137}Cs$ activity ratios* in Round Loch of Glenhead sediment core RLG1-A (4.6.90)

section depth (cm)	^{137}Cs 661 keV (Bq kg^{-1})	^{134}Cs 605 keV (Bq kg^{-1})	^{134}Cs 796 keV (Bq kg^{-1})	x^{134}Cs (Bq kg^{-1})	$^{134}Cs/^{137}Cs$
0-1	1,322 ± 13	214 ± 11	205 ± 26	210 ± 14	0.159 ± 0.011
1-2	1,075 ± 12	150 ± 6	149 ± 19	150 ± 10	0.140 ± 0.009
2-3	797 ± 19	105 ± 12	117 ± 35	111 ± 18	0.139 ± 0.023
3-4	644 ± 12	93 ± 8	88 ± 26	90 ± 14	0.140 ± 0.020
4-5	778 ± 12	128 ± 7	112 ± 23	120 ± 12	0.154 ± 0.015
5-6	707 ± 11	98 ± 7	99 ± 17	98 ± 9	0.138 ± 0.013
6-7	402 ± 12	66 ± 7	50 ± 19	58 ± 10	0.144 ± 0.026
7-8	190 ± 7	30 ± 5	20 ± 15	25 ± 8	0.132 ± 0.041
8-9	119 ± 8	26 ± 6	BDL		0.218 ± 0.052
9-10	108 ± 9	25 ± 7	"		0.231 ± 0.067
10-11	84 ± 8	BDL	"		
11-12	46 ± 7	"	"		
12-13	58 ± 8	"	"		
13-14	36 ± 9	"	"		
14-15	37 ± 10	"	"		
15-16	45 ± 8	"	"		
16-17	30 ± 9	"	"		
17-18	22 ± 9	"	"		
18-19	16 ± 8	"	"		

Table 3.11 Radiocaesium concentrations and $^{134}Cs/^{137}Cs$ activity ratios in Round Loch of Glenhead sediment core RLG2-1A (25.1.91)

section depth (cm)	^{137}Cs 661 keV (Bq kg^{-1})	^{134}Cs 605 keV (Bq kg^{-1})	^{134}Cs 796 keV (Bq kg^{-1})	x^{134}Cs (Bq kg^{-1})	$^{134}Cs/^{137}Cs$
0-1	1,702 ± 29	228 ± 13	220 ± 37	224 ± 20	0.132 ± 0.012
1-2	3,499 ± 49	480 ± 17	480 ± 28	480 ± 16	0.137 ± 0.005
2-3	4,566 ± 56	614 ± 10	637 ± 14	625 ± 9	0.137 ± 0.002
3-4	1,605 ± 23	188 ± 8	207 ± 13	197 ± 8	0.123 ± 0.005
4-5	903 ± 14	89 ± 6	108 ± 12	99 ± 7	0.109 ± 0.008
5-6	551 ± 12	51 ± 13	38 ± 8	45 ± 8	0.081 ± 0.014
6-7	384 ± 9	34 ± 7	39 ± 12	37 ± 7	0.095 ± 0.018
7-8	270 ± 7	22 ± 4	22 ± 10	23 ± 6	0.084 ± 0.021
8-9	192 ± 8	19 ± 5	BDL		0.099 ± 0.026
9-10	127 ± 7	BDL	"		
10-11	104 ± 4	12 ± 3	"		0.115 ± 0.029
11-12	80 ± 4	9.2 ± 2.9	"		0.115 ± 0.037
12-13	52 ± 3	7.6 ± 2.8	"		0.146 ± 0.054
13-14	33 ± 4	9.0 ± 3.0	"		0.273 ± 0.097
14-15	22 ± 4	7.6 ± 3.5	"		

* where ^{134}Cs was BDL at 796 keV, but detectable at 605 keV, concentrations from the latter energy were used to calculate $^{134}Cs/^{137}Cs$

Table 3.12 Fe, Mn, Pb, Zn, Cu, Cd, Co and Ni concentrations in HNO_3/HCl acid digested Round Loch of Glenhead sediment core RLG1-B

depth (cm)	Fe %	Mn mg kg^{-1}	Pb mg kg^{-1}	Zn mg kg^{-1}	Cu mg kg^{-1}	Cd mg kg^{-1}	Co mg kg^{-1}	Ni mg kg^{-1}
0-1	3.49	210	199	62	26	0.8	BDL	12
1-2	1.26	91	232	75	26	1.0	4	21
2-3	0.94	97	263	122	28	1.2	4	19
3-4	0.94	100	298	174	30	1.7	4	20
4-5	1.04	110	272	164	30	1.3	4	20
5-6	0.97	120	280	132	31	1.7	5	22
6-7	0.90	120	284	197	29	2.2	4	17
7-8	0.94	130	282	199	27	1.7	4	18
8-9	0.92	150	298	168	28	1.7	4	17
9-10	0.97	150	360	196	31	2.1	4	17
10-11	0.91	150	347	210	27	1.7	4	14
11-12	0.98	180	346	147	26	1.6	4	15
12-13	1.00	190	354	179	24	1.8	5	14
13-14	1.00	210	338	165	23	1.6	5	14
14-15	1.15	230	337	150	21	1.7	8	18
15-16	1.25	250	331	112	19	1.4	10	20
16-17	1.20	250	303	101	17	1.4	7	16
17-18	1.20	280	266	104	14	1.6	6	16
18-19	1.18	300	211	82	12	1.1	6	14
19-20	1.21	310	174	62	10	1.0	5	14
20-21	1.22	330	160	57	10	0.9	5	14
21-22	2.04	460	134	44	9	0.9	8	13
22-23	1.17	350	113	30	9	0.9	5	12
23-24	1.19	350	132	41	9	0.8	5	14
24-25	1.22	400	86	26	8	0.7	5	14
25-26	1.21	390	79	28	8	0.7	6	14
26-27	1.22	390	65	23	8	0.7	6	12
27-28	1.24	400	60	29	8	0.7	5	13
28-29	1.28	430	51	29	8	0.6	6	13
29-30	1.32	460	50	29	8	0.7	7	12
30-31	1.50	490	38	26	8	0.7	6	13
31-32	1.16	370	94	29	8	0.8	4	14

Table 3.13 Fe, Mn, Pb, Zn, Cu, Cd, Co and Ni concentrations in HNO_3/HCl acid digested Round Loch of Glenhead sediment core RLG2-1B

depth (cm)	Fe %	Mn mg kg^{-1}	Pb mg kg^{-1}	Zn mg kg^{-1}	Cu mg kg^{-1}	Cd mg kg^{-1}	Co mg kg^{-1}	Ni mg kg^{-1}
0-1	5.96	123	197	73	22	0.5	BDL	13
1-2	1.93	111	242	73	24	0.8	"	17
2-3	1.48	110	270	136	28	1.0	"	20
3-4	1.47	134	276	181	28	1.1	5	18
4-5	1.37	140	255	131	28	1.2	4	16
5-6	1.33	166	303	167	30	1.4	4	16
6-7	1.28	177	289	152	29	1.0	6	12
7-8	1.38	219	299	132	25	1.0	7	15
8-9	1.36	232	333	168	20	1.4	6	15
9-10	1.43	250	308	144	19	1.2	5	13
10-11	1.38	270	260	124	16	1.1	5	12
11-12	1.39	294	215	86	14	0.8	8	12
12-13	1.40	329	169	53	12	0.8	5	12
13-14	1.40	357	152	54	11	0.6	5	12
14-15	1.44	400	133	47	10	0.4	7	13
15-16	1.45	412	128	39	10	0.5	6	14
16-17	1.50	465	109	33	10	0.6	7	14
17-18	1.49	477	94	31	10	0.4	6	12
18-19	1.47	492	80	28	10	0.4	6	12
19-20	1.53	517	78	36	10	0.4	6	13
20-21	1.60	527	69	46	14	0.5	8	14
21-22	1.57	502	74	37	12	0.5	7	12
22-23	1.61	468	...	56	13	0.6	7	13

Table 3.14 Fe and Mn concentrations in sequentially extracted Round Loch of Glenhead sediment core RLG1-B

	Fe (%) fractions						Mn (mg kg^{-1}) fractions					
depth (cm)	I	II	III	IV	V	sum I-V	I	II	III	IV	V	sum I-V
0-1	0.025	0.32	0.33	1.90	1.84	4.41	26	BDL	34	60	71	191
1-2	0.009	0.061	0.069	0.30	0.62	1.06	23	"	BDL	BDL	40	63
2-3	0.007	0.034	0.047	0.15	0.48	0.72	35	"	"	"	34	69
3-4	0.006	0.058	0.069	0.18	0.51	0.82	50	"	"	"	42	92
4-5	0.006	0.059	0.074	0.20	0.53	0.87	52	16	"	"	35	103
5-6	0.004	0.054	0.082	0.23	0.62	0.99	61	23	"	"	38	122
6-7	0.004	0.065	0.083	0.19	0.51	0.86	63	BDL	"	"	39	102
7-8	0.004	0.053	0.083	0.23	0.49	0.86	60	21	"	"	35	116
8-9	0.003	0.057	0.071	0.25	0.51	0.89	73	23	"	"	42	138
9-10	0.004	0.059	0.072	0.18	0.50	0.82	65	28	25	"	40	158
10-11	0.007	0.063	0.087	0.22	0.44	0.82	69	26	20	"	31	146
11-12	0.006	0.076	0.080	0.23	0.49	0.88	61	29	72	"	36	198
12-13	0.004	0.086	0.092	0.24	0.58	1.00	73	37	65	"	40	215
13-14	0.004	0.084	0.096	0.25	0.48	0.92	71	35	56	"	33	195
14-15	0.004	0.092	0.085	0.26	0.63	1.08	55	37	87	18	43	240
15-16	0.004	0.088	0.093	0.27	0.70	1.16	57	42	104	17	42	262
16-17	0.003	0.083	0.089	0.26	0.66	1.09	50	40	99	14	42	245
17-18	0.003	0.082	0.090	0.24	0.52	0.93	66	39	97	12	41	255
18-19	0.003	0.092	0.087	0.26	0.62	1.07	78	51	110	17	46	302
19-20	0.005	0.090	0.089	0.30	0.60	1.08	93	59	92	23	40	307
20-21	...	...	...	...	...	...	...	...	...	...	...	...
21-22	0.005	0.110	0.103	0.32	0.56	1.09	117	66	82	26	40	331
22-23	...	...	...	...	...	...	...	...	...	...	...	...
23-24	0.005	0.120	0.108	0.39	0.49	1.11	256	97	57	17	48	475
24-25	...	...	...	...	...	...	...	...	...	...	...	...
25-26	0.005	0.120	0.131	0.39	0.58	1.22	136	67	125	35	49	412
26-27	...	...	...	...	...	...	...	...	...	...	...	...
27-28	0.004	0.082	0.095	0.29	0.54	1.01	184	94	110	20	43	451
28-29	...	...	...	...	...	...	...	...	...	...	...	...
29-30	0.003	0.120	0.114	0.40	0.58	1.22	178	99	95	24	43	439
30-31	...	...	...	...	...	...	...	...	...	...	...	...
31-32	0.004	0.100	0.098	0.33	...	...	109	79	138	40	72	438

Table 3.15 Pb and Zn concentrations in sequentially extracted Round Loch of Glenhead sediment core RLG1-B

depth (cm)	Pb (mg kg^{-1}) fractions I	II	III	IV	V	sum I-V	Zn (mg kg^{-1}) fractions I	II	III	IV	V	sum I-V
0-1	14	80	BDL	95	21	210	BDL	18	5	17	15	55
1-2	39	100	"	92	26	257	"	15	6	25	24	70
2-3	68	120	"	54	26	268	"	24	10	39	27	100
3-4	67	140	"	77	26	310	"	40	14	89	73	216
4-5	68	120	"	80	26	294	"	39	15	65	42	161
5-6	66	150	"	109	35	360	"	25	13	52	53	143
6-7	76	140	"	82	28	326	"	31	14	85	86	216
7-8	69	140	"	75	26	310	"	29	14	75	87	205
8-9	75	140	"	81	30	326	"	30	14	61	65	170
9-10	74	160	"	96	37	367	"	28	14	67	90	199
10-11	96	160	"	94	23	373	"	31	13	92	74	210
11-12	81	150	"	95	31	357	"	38	13	63	75	189
12-13	77	180	"	102	32	391	"	26	11	73	50	160
13-14	63	150	"	88	26	327	"	21	13	69	50	153
14-15	70	170	"	98	23	401	"	18	13	63	51	145
15-16	60	160	"	100	20	340	"	15	10	44	39	108
16-17	53	140	"	93	28	314	"	18	9	45	29	101
17-18	42	110	"	69	21	242	"	18	7	36	31	82
18-19	28	100	"	54	19	201	"	11	5	30	34	80
19-20	18	80	"	57	18	173	"	8	2	20	28	58
20-21	...	...	...	...	...		...	...	...	...	...	
21-22	BDL	50	BDL	60	18	128	BDL	5	4	13	11	33
22-23	...	...	...	...	...		...	...	...	...	...	
23-24	18	40	BDL	47	26	113	BDL	7	4	16	17	44
24-25	...	...	...	...	...		...	...	...	...	...	
25-26	BDL	20	BDL	37	18	75	BDL	12	4	19	18	53
26-27	...	...	...	...	...		...	...	...	...	...	
27-28	BDL	20	BDL	25	12	57	BDL	6	2	12	21	41
28-29	...	...	...	...	...		...	...	...	...	...	
29-30	BDL	20	BDL	32	9	61	BDL	4	3	13	13	33
30-31	...	...	...	...	...		...	...	...	...	...	
31-32	BDL	5	BDL	25	8	38	BDL	6	2	14	21	43

Table 3.16 Fe and Mn concentrations in sequentially extracted Round Loch of Glenhead sediment core RLG2-1B

	Fe (%) fractions						Mn (mg kg^{-1}) fractions					
depth (cm)	I	II	III	IV	V	sum I-V	I	II	III	IV	V	sum I-V
0-1	0.39	0.46	0.46	1.67	3.36	6.34	9	10	22	19	46	106
1-2	0.006	0.15	0.16	0.16	1.18	1.66	24	21	16	7.1	45	113
2-3	0.003	0.12	0.12	0.32	0.96	1.52	30	30	12	7.2	44	123
3-4	0.003	0.11	0.11	0.28	0.99	1.49	44	37	18	10	46	155
4-5	0.002	0.09	0.08	0.23	0.89	1.29	45	36	19	9.2	42	151
5-6	0.002	0.09	0.09	0.23	0.80	1.21	51	44	24	12	42	173
6-7	0.002	0.08	0.08	0.26	0.84	1.26	62	54	27	16	47	206
7-8	0.002	0.08	0.08	0.24	0.82	1.22	62	56	37	20	48	223
8-9	0.002	0.09	0.08	0.25	0.85	1.27	60	60	55	30	53	258
9-10	0.001	0.09	0.08	0.26	0.81	1.24	72	74	52	29	51	278
10-11	0.001	0.10	0.09	0.26	0.84	1.29	91	75	53	29	55	303
11-12	0.001	0.09	0.09	0.26	0.82	1.17	111	83	58	28	54	234
12-13	0.001	0.10	0.09	0.31	0.80	1.30	135	105	51	32	52	375
13-14	0.003	0.11	0.09	0.28	0.74	1.22	155	118	40	28	49	390
14-15	0.003	0.10	0.10	0.31	0.82	1.33	171	124	53	32	54	434
15-16	0.003	0.11	0.10	0.37	0.92	1.50	187	160	68	46	63	524
16-17	0.002	0.10	0.10	0.33	0.90	1.43	200	163	78	43	62	506
17-18	0.005	0.11	0.09	0.35	0.76	1.32	224	159	58	39	54	534
18-19	0.003	0.12	0.10	0.36	0.89	1.47	219	166	67	44	68	564
19-20	0.002	0.12	0.08	0.31	0.83	1.34	231	164	59	39	63	556
20-21	0.002	0.12	0.10	0.33	0.90	1.45	214	167	88	51	69	589
21-22	0.005	0.12	0.10	0.34	0.91	1.47	239	182	60	40	66	587
22-23	0.002	0.10	0.09	0.34	0.93	1.46	207	168	77	47	66	565

Table 3.17 Pb and Zn concentrations in sequentially extracted Round Loch of Glenhead sediment core RLG2-1B

	Pb (mg kg^{-1}) fractions						Zn (mg kg^{-1}) fractions					
depth (cm)	I	II	III	IV	V	sum I-V	I	II	III	IV	V	sum I-V
0-1	BDL	37	5	113	51	206	4	21	10	14	26	75
1-2	16	74	12	116	76	294	3	14	13	26	44	100
2-3	22	103	16	127	97	365	2	11	14	34	110	171
3-4	29	109	19	140	106	403	2	13	24	49	161	249
4-5	23	88	16	117	102	346	0.9	7.4	17	34	104	163
5-6	30	109	20	186	118	463	1	8.1	20	41	155	225
6-7	33	113	18	152	121	437	1	6.9	16	43	155	222
7-8	26	106	17	145	120	414	0.6	3.9	13	36	96	150
8-9	28	121	17	156	134	456	0.6	4.4	12	33	158	208
9-10	23	109	12	132	103	379	0.6	3.0	8.9	27	105	144
10-11	24	97	9	123	96	349	0.7	5.1	8.5	27	114	155
11-12	15	68	9	97	74	263	BDL	2.4	3.6	13	73	92
12-13	10	51	5	89	65	220	"	BDL	1.9	10	49	61
13-14	BDL	44	3	72	58	177	"	"	1.1	6.8	49	57
14-15	"	34	4	70	61	169	"	"	2.0	11	46	59
15-16	"	34	4	73	61	172	"	"	1.2	8.1	34	43
16-17	"	27	3	55	54	139	"	"	1.4	6.8	35	43
17-18	"	22	BDL	52	41	115	"	"	0.6	4.6	29	34
18-19	"	18	"	43	39	100	"	"	1.0	5.7	30	37
19-20	"	15	"	36	34	85	"	"	0.8	6.2	29	36
20-21	"	19	"	39	34	92	"	"	1.8	6.8	40	49
21-22	"	18	"	34	34	86	"	"	0.9	7.1	35	43
22-23	"	18	"	41	42	101	"	"	1.4	7.4	35	44

Table 3.18 Cu concentrations in fraction V of Round Loch of Glenhead sediment cores RLG1-B and RLG2-1B*.

	Cu (mg kg^{-1})	
depth (cm)	RLG1-B	RLG2-1B
0-1	22	17
1-2	21	24
2-3	24	29
3-4	24	32
4-5	24	27
5-6	28	28
6-7	26	28
7-8	27	23
8-9	26	20
9-10	26	18
10-11	24	15
11-12	24	11
12-13	22	9
13-14	18	8
14-15	15	8
15-16	17	8
16-17	14	9
17-18	12	7
18-19	10	8
19-20	8	8
20-21	...	9
21-22	9	9
22-23	...	9
23-24	9	...
25-26	10	...
27-28	7	...
29-30	7	...
31-32	7	...

* Cu was not detectable in fractions I-IV

Table 3.19 Concentrations of Fe and Mn in porewaters from Round Loch of Glenhead.sediment cores RLG1-C and RLG2-1C.

	Fe ($mg\ l^{-1}$)		Mn ($mg\ l^{-1}$)	
depth (cm)	RLG1-C	RLG2-1C	RLG1-C	RLG2-1C
0-1	...	0.70	...	0.061
1-2	1.1	0.24	0.030	0.061
2-3	1.1	2.0	0.039	0.051
3-4	0.96	...	0.035	...
4-5	0.90	0.14	0.032	0.046
5-6	0.90	...	0.062	0.03
6-7	1.1	0.35	0.086	0.032
7-8	1.3	...	0.082	0.028
8-9	1.3	0.34	0.086	0.016
9-10	0.84	0.63	0.090	0.010
10-11	0.65	0.56	0.072	0.021
11-12	0.98	0.96	...	...
12-13	...	0.40	0.093	0.024
13-14	1.0	0.33	0.093	0.083
14-15	1.8	0.20	0.14	0.035
15-16	3.0	0.25	0.26	0.021
16-17	...	...	0.26	...
17-18	3.9	1.07	0.22	0.040
18-19	1.6	...	...	0.072
19-20	2.9	0.95	0.22	0.050
21-22	...	0.57	...	0.045
23-24	...	0.18	...	0.026

Table 3.20 Fe and Mn concentrations in water column samples and water overlying Round Loch of Glenhead sediment core RLG1-C.

	Fe ($mg\ l^{-1}$)		Mn ($mg\ l^{-1}$)	
sample	u/filt.	filt.	u/filt.	filt.
surface	0.023	...	0.024	0.024
5 m	0.022	0.018	0.023	0.023
10 m	0.036	0.029	0.025	0.022
RLG1-C	0.64	0.35	0.049	0.044

u/filt. (filt.) - unfiltered (filtered) sample

Table 3.21 Fe and Mn concentrations in water column samples from site 2 and water overlying Round Loch of Glenhead sediment core RLG2-1C.

	Fe ($mg\ l^{-1}$)		Mn ($mg\ l^{-1}$)	
sample	u/filt.	filt.	u/filt.	filt.
surface	0.035	0.028	0.017	0.017
2 m	0.039	0.039	0.020	0.017
4 m	0.034	0.032	0.017	0.014
6 m	0.072	0.028	0.017	0.015
8 m	0.036	0.036	0.016	0.016
10 m	0.046	0.044	0.015	0.015
12 m	0.053	0.039	0.015	0.015
RLG2-1C	0.64	0.050	0.020	0.020

Table 3.22 Fe, Mn and Zn concentrations in porewaters from Round Loch of Glenhead sediment cores RLG2-2A and RLG2-2B.

	Fe ($mg\ l^{-1}$)		Mn ($mg\ l^{-1}$)		Zn ($mg\ l^{-1}$)	
depth (cm)	RLG2-2A	RLG2-2B	RLG2-2A	RLG2-2B	RLG2-2A	RLG2-2B
0-1	0.42	0.49	0.022	0.024	0.007	0.002
1-2	0.66	1.0	0.024	0.030	0.012	0.005
2-3	...	0.99	...	0.031	...	0.005
3-4	0.66	1.2	0.039	0.036	0.004	0.005
4-5	0.68	0.84	0.044	0.034	0.004	0.003
5-6	0.82	1.4	0.071	0.057	0.008	0.006
6-7	0.79	1.1	0.057	0.059	...	0.007
7-8	0.68	...	0.059	...	0.006	...
8-9	0.92	0.92	0.10	0.068	0.007	0.005
9-10	0.88	1.2	0.046	0.065	0.014	0.009
10-11	0.94	...	0.12	...	0.010	...
11-12	0.90	...	0.12	...	0.010	...
12-13	0.72	...	0.090	...	0.018	...
13-14	1.4	...	0.12	...	0.019	...

Table 3.23a Fe, Mn and Zn concentrations in water column samples from site 2 and water overlying Round Loch of Glenhead sediment cores RLG2-2A and RLG2-2B

	Fe ($mg\ l^{-1}$)		Mn ($mg\ l^{-1}$)		Zn ($mg\ l^{-1}$)	
	u/filt.	filt.	u/filt.	filt.	u/filt.	filt.
surface	0.032	0.022	0.009	0.008	0.006	0.003
RLG2-2A	...	0.037	0.012	0.010	0.020	0.009
RLG2-2B	0.070	0.031	0.042	0.029	0.066	0.027

u/filt. (filt.) - unfiltered (filtered) sample

3.4 Discussion

3.4.1 Sediment core characteristics

Sediment porosities from cores RLG1-A, RLG1-B, RLG2-1A and RLG2-1B (Tables 3.4-3.7) are similar and though a downcore decrease occurs, remain fairly high throughout the cores (max. 99.4% at 0-1 cm in core RLG2-1A to a minimum of 93.2% at 18-19 cm in core RLG1-A). Total %C contents for cores RLG1-A and RLG2-1A (Tables 3.4 and 3.6) can be regarded as organic C contents, since the presence of carbonates is unlikely at the pH of the surface water and in view of the bedrock (granite) and soil type (peaty) of the catchment. Carbon contents are high at both sites, ranging from 18.8-25.8%. The C/N ratios range from 12-20 and in both cores increase downcore, resulting from preferential degradation of planktonic debris (with a low C/N ratio) relative to peaty, catchment-derived organic matter.

Full interpretation of the results from chemical extraction and digestion of sediment requires knowledge of the sedimentation characteristics (deposition rates, mixing *etc.*) and so the radionuclide data will be discussed first.

3.4.2 Radionuclide data for Round Loch of Glenhead

^{210}Pb and radiocaesium at site 1

Total ^{210}Pb concentrations in sediment from core RLG1-A (Table 3.8, Fig. 3.2) decrease downcore from a surface (0-1 cm) maximum of 900 Bq kg^{-1} to 77 Bq kg^{-1} at 16-17 cm. Values between 13 and 15 cm are below the detection limit (70 Bq kg^{-1}) due to small sample sizes. ^{226}Ra was undetectable in many of the samples, but ranged from 75-178 Bq kg^{-1} where detectable, concentrations increasing slightly downcore. The plot of total ^{210}Pb and ^{226}Ra concentration against depth (as cumulative weight / area, to compensate for sediment compaction) (Fig.3.2), shows that below 9 cm,the total ^{210}Pb concentrations are fairly constant, so although ^{226}Ra was near the detection limit, there is a detectable supported ^{210}Pb component. A value for supported ^{210}Pb of 82 ± 10 Bq kg^{-1} (similar to the minimum ^{210}Pb concentration) was obtained by taking the mean of ^{226}Ra concentrations above 10 cm. The excess ^{210}Pb concentrations agree (within the counting uncertainty) within the top 4 cm, implying that mixing occurs to this depth. The total excess ^{210}Pb inventory is 3.1 kBq m^{-2} and, if steady-state conditions are assumed, a calculated ^{210}Pb flux of 95.1 Bq m^{-2} y^{-1} is obtained (inventory x λ). The plot of ln (excess ^{210}Pb) against depth

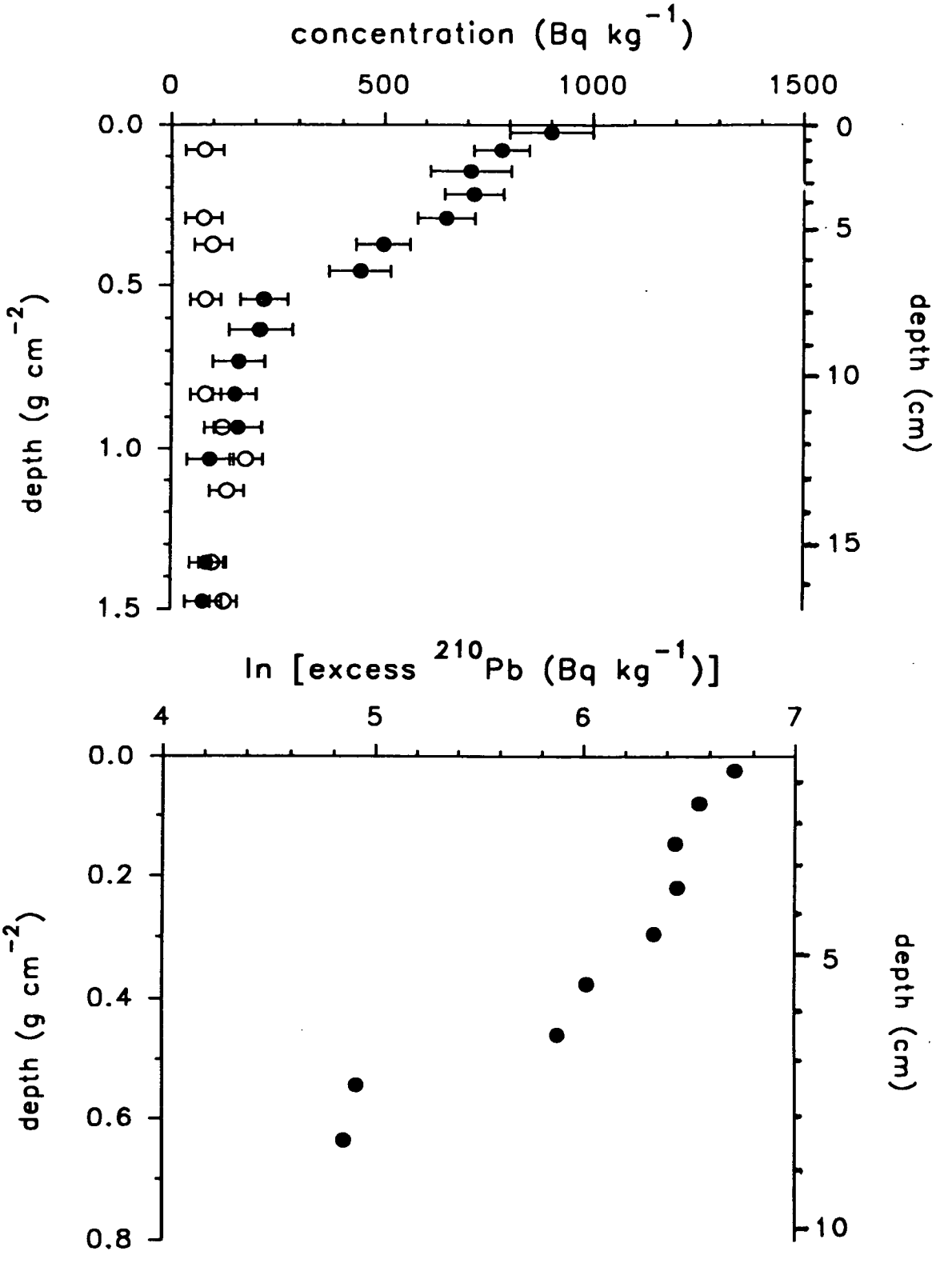

Fig. 3.2 Plots of total ^{210}Pb (•) and ^{226}Ra (o) and ln (excess ^{210}Pb) in Round Loch of Glenhead sediment core RLG1–A against depth

(cumulative weight/area) (Fig. 3.2) does not show a clear linear decrease in ln (excess ^{210}Pb) below the mixed zone discussed above, which makes calculation of a sedimentation rate difficult at this site. The following sedimentation rates were calculated using linear regression of ln (excess ^{210}Pb) between the depths shown:

0-9 cm	10.2 mg cm^{-2} y^{-1}
3-9 cm	7.25 mg cm^{-2} y^{-1}
3-7 cm	12.3 mg cm^{-2} y^{-1}

If the ^{210}Pb flux is divided by the highest excess ^{210}Pb value of 818 Bq kg^{-1} (taking this value to be equivalent to the concentration of settling particulates), a sedimentation rate of 11.6 mg cm^{-2} y^{-1} is derived. This sedimentation rate is close to the upper limit calculated using the CIC model and to values obtained in this loch by Appleby *et al.* (1990) of 11.3-12.0 mg cm^{-2} y^{-1}. The sedimentation rates calculated from 3-9 cm and 3-7 cm should be taken as upper and lower limits, since it does not appear valid to assign more importance to either of the values obtained and so a ^{210}Pb chronology based on one sedimentation rate cannot be established (Table 3.23b).

The ^{137}Cs concentration profile for core RLG1-A (Table 3.10, Fig. 3.3) shows an exponential decrease from 1,322 Bq kg^{-1} at the surface (0-1 cm), with a sub-surface enhancement in the depth range 4-7 cm, below which concentrations decrease to a minimum of 16 Bq kg^{-1} at the maximum depth measured (18-19 cm). Initially, it might be thought that the ^{137}Cs distribution could be attributed to weapons testing fallout at 4-7 cm with overlying higher concentrations as a result of Chernobyl fallout deposition. The depth to which ^{137}Cs penetrates corresponds to at least 1860, on the basis of the highest ^{210}Pb-derived sedimentation rate of 12.3 mg cm^{-2} y^{-1} and assuming mixing has occurred to the base of 4 cm (which could have caused downward smearing of the ^{137}Cs). Since this date is long before the use of nuclear technology, the ^{210}Pb chronology provides evidence that ^{137}Cs has moved downwards in the sediment. The enhanced ^{137}Cs concentrations in the 4-7 cm depth range may therefore be due to downward mixing of the sediment.

Concentrations of ^{134}Cs (Table 3.10, Fig.3.3) decrease from a surface maximum of 210 Bq kg^{-1} (0-1 cm) to 24 Bq kg^{-1}, below which ^{134}Cs was less than the detection limit of 22 Bq kg^{-1}. $^{134}Cs/^{137}Cs$ activity ratios (Table 3.10) are all within error of the value of 0.15 appropriate to Chernobyl fallout, after decay correction to the sampling date. This means that weapons testing fallout cannot be identified (within error) in the top 10 cm, confirming that the sub-surface maximum in the ^{137}Cs profile does not correspond to weapons testing fallout and therefore that Chernobyl radiocaesium penetrates to at least a depth equivalent to 1951 (in terms of

Table 3.23b ^{210}Pb-derived chronology range for Round Loch of Glenhead sediment cores RLG1-A and RLG1-B*

	RLG1-A		RLG1-B	
section depth (cm)	mid-section date range	base-section date range	mid-section date range	base-section date range
0-1	1987-1988	1983-1986	1987-1988	1983-1986
1-2	1979-1983	1975-1981	1980-1984	1976-1982
2-3	1970-1978	1965-1975	1972-1979	1968-1977
3-4	1960-1972	1955-1969	1963-1974	1958-1971
4-5	1949-1966	1944-1963	1953-1968	1948-1965
5-6	1938-1959	1932-1956	1943-1962	1938-1960
6-7	1927-1953	1921-1950	1933-1957	1928-1954
7-8	1915-1946	1909-1942	1924-1951	1919-1948
8-9	1902-1938	1896-1934	1913-1945	1907-1941
9-10	1889-1930	1883-1927	1901-1938	1895-1934
10-11	1876-1923	1868-1918	1889-1930	1883-1927
11-12	1861-1914	1854-1910	1877-1923	1870-1920
12-13	1848-1906	1841-1902	1864-1916	1858-1912
13-14	1834-1898	1826-1894	1851-1908	1844-1904
14-15	1819-1889	1811-1885	1838-1901	1832-1897
15-16	1803-1880	1795-1875	1826-1893	1819-1889
16-17	1786-1870	1778-1865	1812-1885	1805-1881
17-18	1770-1860	1761-1855	1798-1877	1792-1873
18-19	1754-1851	1746-1846	1784-1869	1777-1864
19-20	1738-1841	1730-1837	1769-1860	1762-1855
20-21	1722-1832	1714-1827	1755-1851	1748-1847
21-22	1705-1822	1696-1817	1741-1843	1734-1839
22-23			1727-1835	1719-1830
23-24			1712-1826	1705-1822
24-25			1697-1817	1690-1813
25-26			1682-1809	1675-1804
26-27			1668-1800	1660-1795
27-28			1653-1791	1645-1787
28-29			1637-1782	1629-1777
29-30			1621-1772	1612-1767
30-31			1606-1764	1599-1760
31-32			1588-1753	1577-1747

* based on limits to sedimentation rate of 7.25-12.3 mg cm^{-2} y^{-1} in core RLG1-A

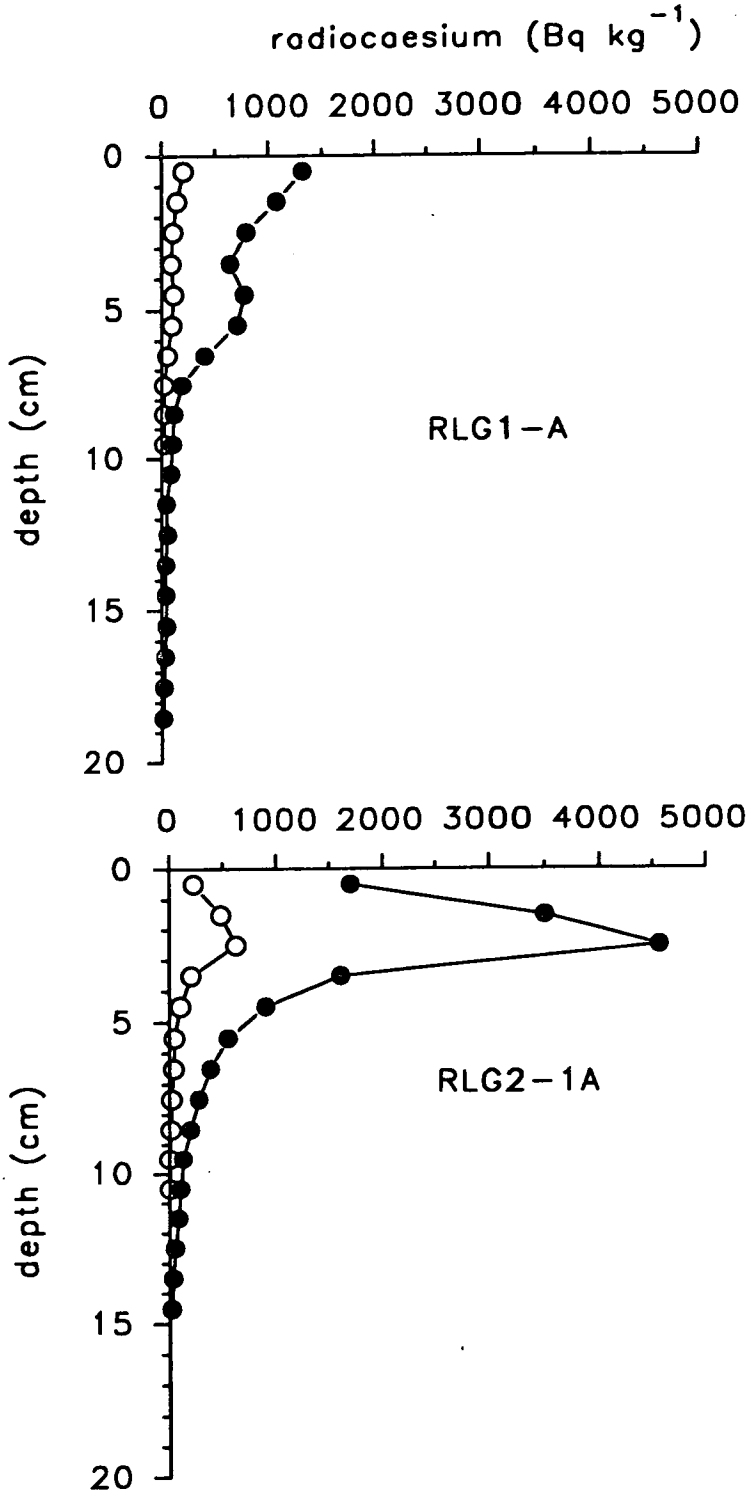

Fig. 3.3 ^{134}Cs (o) and ^{137}Cs (●) concentrations in Round Loch of Glenhead sediment cores RLG1-A and RLG2-1A

Table 3.24 Estimated ^{137}Cs inventories in Round Loch of Glenhead compared with reported deposition values (Clark and Smith, 1988; Baxter *et al.*, 1989; Peirson *et al.*, 1982). Inventories have been corrected for decay since 1.5.86 (Chernobyl fallout) and 1963 (weapons testing fallout).

	Round Loch of Glenhead		reported value
	site 1 (RLG1-A)	site 2 (RLG2-1A)	
Chernobyl ^{137}Cs ($kBq\ m^{-2}$)	4.68 ± 0.03 → 5.13 ± 0.04	7.37 ± 0.12	20-38
weapons testing ^{137}Cs ($kBq\ m^{-2}$)	1.53 ± 0.05	1.20 ± 0.18	2.8

Table 3.25 ^{210}Pb-derived chronology for Round Loch of Glenhead sediment cores RLG2-1A and RLG2-1B*

	RLG2-1A		RLG2-1B	
section depth (cm)	mid-section date	base-section date	mid-section date	base-section date
0-1	1990	1988	1988	1986
1-2	1987	1985	1982	1978
2-3	1981	1977	1974	1970
3-4	1973	1969	1965	1960
4-5	1964	1959	1955	1949
5-6	1955	1950	1944	1939
6-7	1944	1938	1933	1927
7-8	1932	1926	1922	1916
8-9	1920	1914	1910	1905
9-10	1908	1902	1899	1894
10-11	1896	1890	1889	1884
11-12	1882	1874	1878	1872
12-13	1868	1861	1866	1860
13-14	1855	1849	1855	1849
14-15	1844	1838	1842	1835
15-16			1828	1822
16-17			1816	1810
17-18			1804	1798
18-19			1792	1786
19-20			1780	1774
20-21			1768	1761
21-22			1755	1748
22-23			1743	1737

* based on a sedimentation rate of 8 mg $cm^{-2}\ y^{-1}$ in core RLG2-1A

the ^{210}Pb-derived sedimentation rate above). If the lower sedimentation rate of 7.25 mg cm^{-2} y^{-1} is used, the depth is equivalent to 1925.

Radiocaesium inventories at site 1

Below 10 cm ^{134}Cs is not detectable ($\leq$ 15 Bq kg^{-1}), which might be interpreted as indicating that the radiocaesium is all of weapons testing origin, but this cannot be definitively concluded because the ^{137}Cs concentrations are very low in this part of the core. Even if all the radiocaesium was of Chernobyl origin, the limitations of sample size and concentration mean that ^{134}Cs would not be detectable. If it is assumed that all of the ^{137}Cs in the core is due to Chernobyl fallout, an upper limit to the Chernobyl ^{137}Cs inventory of 5.13 kBq m^{-2} (decay-corrected to 1.5.86) is obtained. If Chernobyl ^{137}Cs is assumed to be present only to a depth of 10 cm, then a value of 4.68 kBq m^{-2} is obtained. An upper limit for the weapons testing contribution of 1.53 kBq m^{-2} (decay-corrected to 1963) is calculated assuming that all of the ^{137}Cs below 10 cm and approximately 10% of the ^{137}Cs in the 0-10 cm (based on uncertainty in the ^{134}Cs determination) section is from weapons testing fallout. The ranges of ^{137}Cs inventories for both Chernobyl - and weapons testing fallout are lower than the reported deposition of ^{137}Cs from the two sources in this area (Clark and Smith, 1988; Baxter *et al.*, 1989; Peirson *et al.*, 1982). Table 3.24 compares calculated ^{137}Cs inventories in Round Loch with reported values for weapons testing and Chernobyl fallout to the area and indicates that the difference between the weapons testing inventory and the reported value is not as great as that between the Chernobyl inventory and the estimated deposition value. In addition to the possible underestimation of deposition to this high rainfall area (the value given is a UK average), both the greater duration of weapons testing fallout deposition compared with fallout deposition from Chernobyl, and the possibly less water soluble nature of radiocaesium in fallout from weapons testing (Desmet and Sinnaeve, 1992) could have contributed to a proportionately greater fraction of radiocaesium from weapons fallout, relative to that from Chernobyl, being retained in the lake system. Catchment-derived weapons testing ^{137}Cs may also have been significant over the 30 years since the maximum fallout deposition. The lower estimates of ^{137}Cs compared with those expected on the basis of fallout deposition could be due to either a low efficiency of radiocaesium uptake in the organic sediment or remobilisation from the sediment to the water column after deposition. The latter explanation is supported by penetration of radiocaesium to a depth corresponding to the mid-19th century and an excellent fit to an exponential decrease with depth (r^2=0.955), suggesting diffusive movement of radiocaesium in the sediment porewaters.

The exponential decrease in ^{137}Cs with depth can be characterised mathematically by a diffusion type equation as follows:

$$C = \frac{M}{(\pi Dt)^{1/2}} e^{-x^2/4Dt} \qquad \text{(Crank, 1956)}$$

where: C = concentration of diffusing substance
M = amount of diffusing substance
D = diffusion coefficient
t = time (seconds)
x = depth (cm)

This equation can then be simplified to a linear equation (of the form $y = m x + c$), which is readily solved by regression analyis. However, the process by which the radiocaesium moves downwards in the sediment is complex, involving diffusion, particle mixing, sorption *etc.* and the value obtained from the equation above is a term describing the *net* movement. A value of 7×10^{-12} m^2 s^{-1} is obtained (assuming Chernobyl radiocaesium is restricted to the top 10 cm of the core) with a calculated upper limit of 1.5×10^{-11} m^2 s^{-1} based on the assumption that all the ^{137}Cs in the core is of Chernobyl origin. These values may be compared with the genuine diffusion coefficient (*i.e.* taking adsorption, mixing *etc.* into account) of 10^{-6} m^2 s^{-1} reported by Torgersen and Longmore (1984) for ^{137}Cs in the highly organic sediments of Hidden Lake, Australia. Torgersen and Longmore concluded that the diffusive mechanism had been modified by adsorption or absorption at or near the sediment-water interface, so that the potential for downwards diffusion had not been fully attained.

^{210}Pb and radiocaesium at site 2

The maximum total ^{210}Pb concentration of 1,103 Bq kg^{-1} for sediment from core RLG2-1A (Table 3.11, Fig. 3.4) is found in the section at 1-2 cm, below which concentrations decrease downcore to 10 cm. At greater depths the concentrations remain constant to the maximum sampled depth in the core (14-15 cm). The anomalously low value in the surface (0-1 cm) section could be due to an influx of older material from elsewhere in the loch. As for samples from site 1, ^{226}Ra was not detectable in many of the samples and is only reliably detectable below 7 cm (Table 3.11). The plot of total ^{210}Pb and ^{226}Ra against depth (g cm^{-2}) (Fig. 3.4) shows that below 9 cm the total ^{210}Pb concentrations are constant within error and are equal to the

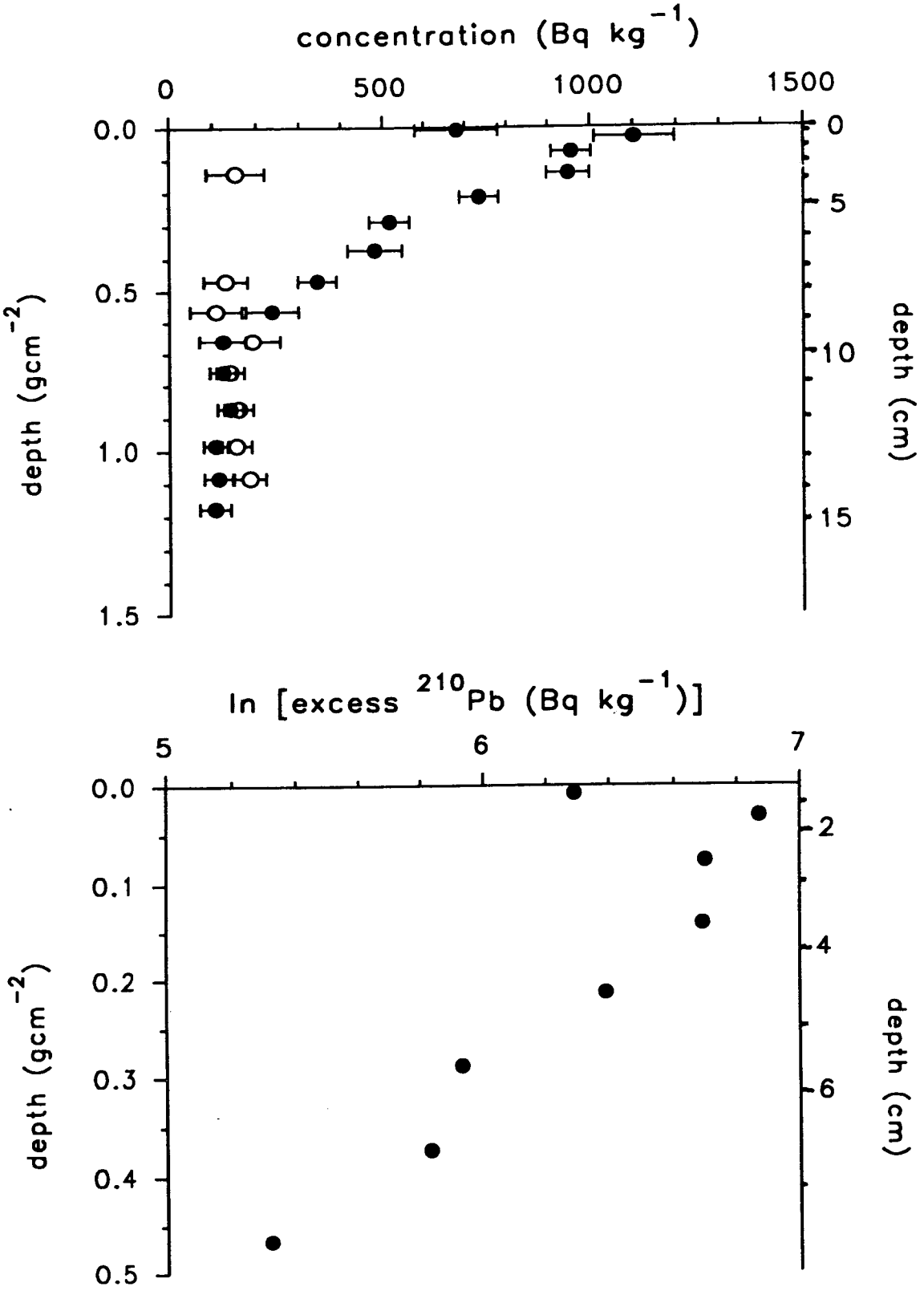

Fig. 3.4 Plots of total ^{210}Pb (●) and ^{226}Ra (○) and ln (excess ^{210}Pb) in Round Loch of Glenhead sediment core RLG2-1A against depth

^{226}Ra concentrations. The supported ^{210}Pb value of 140 ± 30 Bq kg^{-1} was obtained by taking the mean of total ^{210}Pb and ^{226}Ra concentrations between 9 and 15 cm. Excess ^{210}Pb was only reliably detectable to 8 cm and, within error, the values were constant between 1 and 4 cm (*i.e.* excluding the low surface value), implying mixing to 4 cm as found at site 1. A CIC calculation of ln (excess ^{210}Pb) values (Fig. 3.4) from 3-4 cm to 8 cm gives a sedimentation rate of 7.5 ± 0.7 mg cm^{-2} y^{-1} (if values from 1-8 cm are used, a sedimentation rate of 8.5 ± 0.7 mg cm^{-2} y^{-1} is obtained). If steady-state conditions are assumed, the total excess ^{210}Pb inventory of 2.7 kBq m^{-2} can be used to calculate a ^{210}Pb flux of 82.8 Bq m^{-2} y^{-1}, which is similar to the value calculated for site 1. Dividing the ^{210}Pb flux by the highest excess ^{210}Pb concentration in the core of 963 Bq kg^{-1} (taken to be equivalent to the ^{210}Pb concentration of settling particulates), gives an upper limit to the sedimentation rate of 8.6 mg cm^{-2} y^{-1}, in good agreement with the sedimentation rate of 7.5 ± 0.7 mg cm^{-2} y^{-1} calculated by the CIC method. The ^{210}Pb-derived chronology for site 2 (Table 3.2S) was based on a mean of these sedimentation rates, giving a value of 8.0 mg cm^{-2} y^{-1}.

The radiocaesium concentration profile for core RLG2-1A (Table 3.11, Fig.3.3) is different in shape from the profile at site 1 and concentrations are greater than at site 1. A low surface value is observed, as for the ^{210}Pb concentrations, and the maximum concentration of both ^{134}Cs and ^{137}Cs is at a depth of 2-3 cm which, on the basis of the ^{210}Pb chronology, corresponds to dates of 1977-1985 (using upper and lower section limits), the latter date being close to the Chernobyl fallout deposition event in 1986. The $^{134}Cs/^{137}Cs$ activity ratio (compared with the Chernobyl ratio of 0.12 corrected for decay to the sampling date) reveals that all ^{137}Cs to a depth of 4 cm (1969 at the section base) is due to Chernobyl fallout (Appendix 1) and that Chernobyl-derived radiocaesium is detectable to a depth of 9 cm or a date of 1914, which means downward movement of radiocaesium in the sediment has occurred. Weapons testing fallout ^{137}Cs (Appendix 1) is detectable from 4 cm down to the base of the core at a date of 1838 (or 1860 if mixing is taken to occur to 4 cm), with a maximum at a depth of 5-6 cm, corresponding to dates of 1950-1959, close to the fallout maximum in 1963. However, the overall ^{137}Cs concentration profile (Fig.3.3) shows no observable peak at this depth, the signal having been obscured by the Chernobyl fallout ^{137}Cs. If the cumulative weight/area is taken between the mid-sections of the two ^{137}Cs peaks from the different fallout sources (Chernobyl and weapons testing) a time span of 26 years is obtained (using the ^{210}Pb-based sedimentation rate of 8.0 mg cm^{-2} y^{-1}), which agrees well with the actual time span of 23 years between the historical occurrence of the two fallout events.

Site 2 radiocaesium data therefore show downward movement of radiocaesium in the sediment, but to a lesser extent than at site 1, since the radiocaesium results agree well with the ^{210}Pb-derived chronology in terms of a historical record of radiocaesium fallout input to the loch. Calculation of an effective diffusion coefficient at this site is not feasible because of the Chernobyl ^{137}Cs concentrations above the peak at 2 cm, probably due to sediment mixing, and the calculation would require no radiocaesium to occur above the Chernobyl fallout peak.

Radiocaesium inventories at site 2

Estimated inventories of ^{137}Cs from the two fallout sources (Table 3.24), decay-corrected to the time of fallout deposition), again show a lower inventory compared with reported deposition values for Chernobyl fallout ^{137}Cs of 7.66 kBq m^{-2}, slightly higher than the inventory at site 1 (4.7-5.1 kBq m^{-2}). However, the weapons testing inventory of 1.20 kBq m^{-2} is similar to that at site 1. A ^{137}Cs inventory of 2.33 kBq m^{-2} was obtained by Appleby *et al.* (1990) in Round Loch at the time of sampling, prior to the Chernobyl reactor accident. This inventory gives a value of 3.7 kBq m^{-2} if corrected for 20 years of decay.

Comparison of radionuclide data at sites 1 and 2

The greater Chernobyl inventory, higher specific activities and lower Chernobyl ^{137}Cs diffusion at site 2 compared with site 1, despite similar ^{210}Pb fluxes at the two sites, shows that radiocaesium is less mobile within the sediment at site 2 than at site 1. Loss of radiocaesium from the sediment to the water column, reduced efficiency of radiocaesium deposition to the sediment or a combination of these two factors, followed by loss from the loch by hydraulic flushing, could result in lower ^{137}Cs inventories compared with reported deposition values. Differences in the extents of these factors, due to differences in the sediment at the two sites, perhaps due to a higher clay content at site 2 (Appendix 2), may have caused the discrepancies between the inventories at the two sites. Iron concentrations are greater at site 2 than site 1, which suggests a larger clay component in the sediments and therefore more binding sites for ^{137}Cs. Porosity and %C and N concentrations at sites 1 and 2 (Section 3.4.1, Tables 3.4-3.7) show that the sediment is highly porous and organic-rich, but do not clearly reveal differences between the two sites in terms of sediment composition which might result in the observed higher Chernobyl radiocaesium inventory at site 2.

In conclusion, the radionuclide data provide information on the sedimentation processes in Round Loch, despite the fact that radiocaesium is not useful as a dating tool at the sampled sites due to its mobility in the organic-rich sediments, as found

previously in this loch (Appleby *et al.*, 1990). Partial sediment mixing to 4 cm is implied by both the ^{210}Pb and the radiocaesium data, but at site 2 this has not obscured ^{137}Cs concentration peaks attributable to the weapons testing fallout maximum and fallout from Chernobyl. At site 1, low concentrations and small sample sizes, together with downward movement of Chernobyl radiocaesium in the sediment prevent the radiocaesium being conclusively related to either weapons testing or Chernobyl fallout sources. A ^{210}Pb-derived sedimentation rate and chronology was obtained for site 2 and upper and lower limits for sediment accumulation were derived for site 1. These conclusions will be used in the following section to assist in interpretation of the metal data.

3.4.3 Metal data for Round Loch of Glenhead

The metal concentration profiles obtained for sediment cores RLG1-B and RLG2-1B and solution phase results for the two sampled sites will be discussed together. The radionuclide data show that partial mixing occurs at both sites, but that this is not sufficiently intense to have completely obscured radiocaesium signals from the different fallout sources (Chernobyl and weapons testing) and so it is valid to consider the metal concentration trends in terms of ^{210}Pb-derived chronology, shown in Table 3.25 for site 2 and using the upper and lower limits to the sedimentation rate of 7.25-12.3 mg cm^{-2} y^{-1} to establish a core chronology at site 1. (Table 3.23b) Inputs of any pollutant metals to Round Loch will have been largely via atmospheric deposition as this is a loch remote from populated or industrialised areas and there are no heavily used roads in the area.

Lead, zinc, copper, cadmium, cobalt and nickel in HNO_3/HCl acid digested sediment

At site 1 Pb concentrations (Table 3.12, Fig.3.5) increase from a mean of 53 mg kg^{-1} below a depth of 27 cm to a sub-surface zone of enhanced concentrations between 9 and 16 cm (mean = 345 mg kg^{-1}), peaking at 9-10 cm. Above 9 cm the concentration decreases, most sharply from 4 cm, to reach the sediment surface with a concentration of 199 mg kg^{-1}. Using the limits to the sedimentation rate shown above, the onset of increase in concentration can be dated to between 1668 and 1800, with the peak concentration at 1901-1938, decreasing markedly from 1963-1974 (mid-section at 3-4 cm). Concentrations and profile patterns for Pb at site 2 (Table 3.13, Fig. 3.6) are similar to those at site 1, although here the main onset of increase in concentration occurs at around 20 cm, corresponding to a mid-section date of 1780, concentrations increasing above this to a peak of 333 mg kg^{-1} (1910), remaining between 255 and

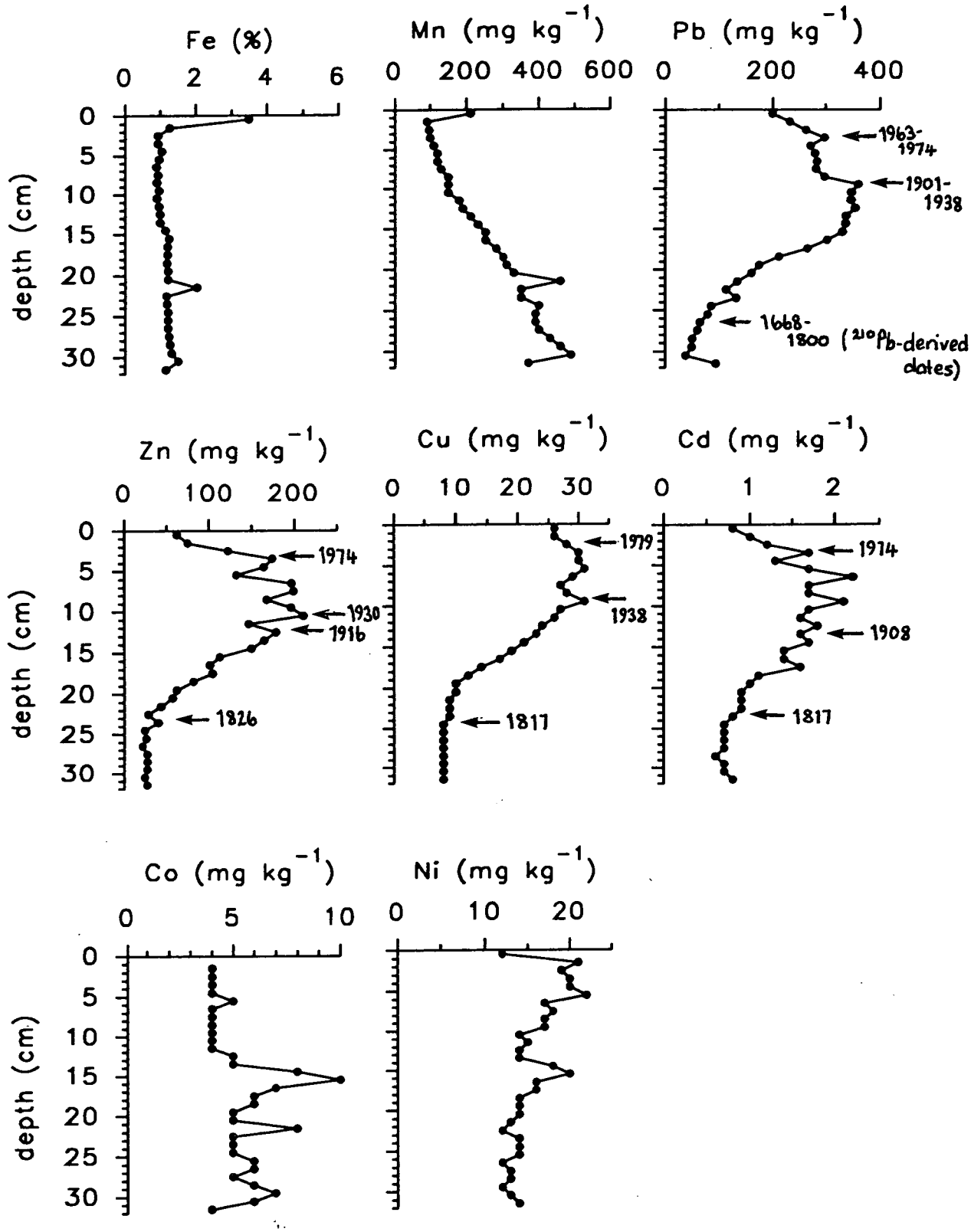

Fig 3.5 Metal concentrations in HNO_3/HCl acid digested Round Loch of Glenhead sediment core RLG1-B

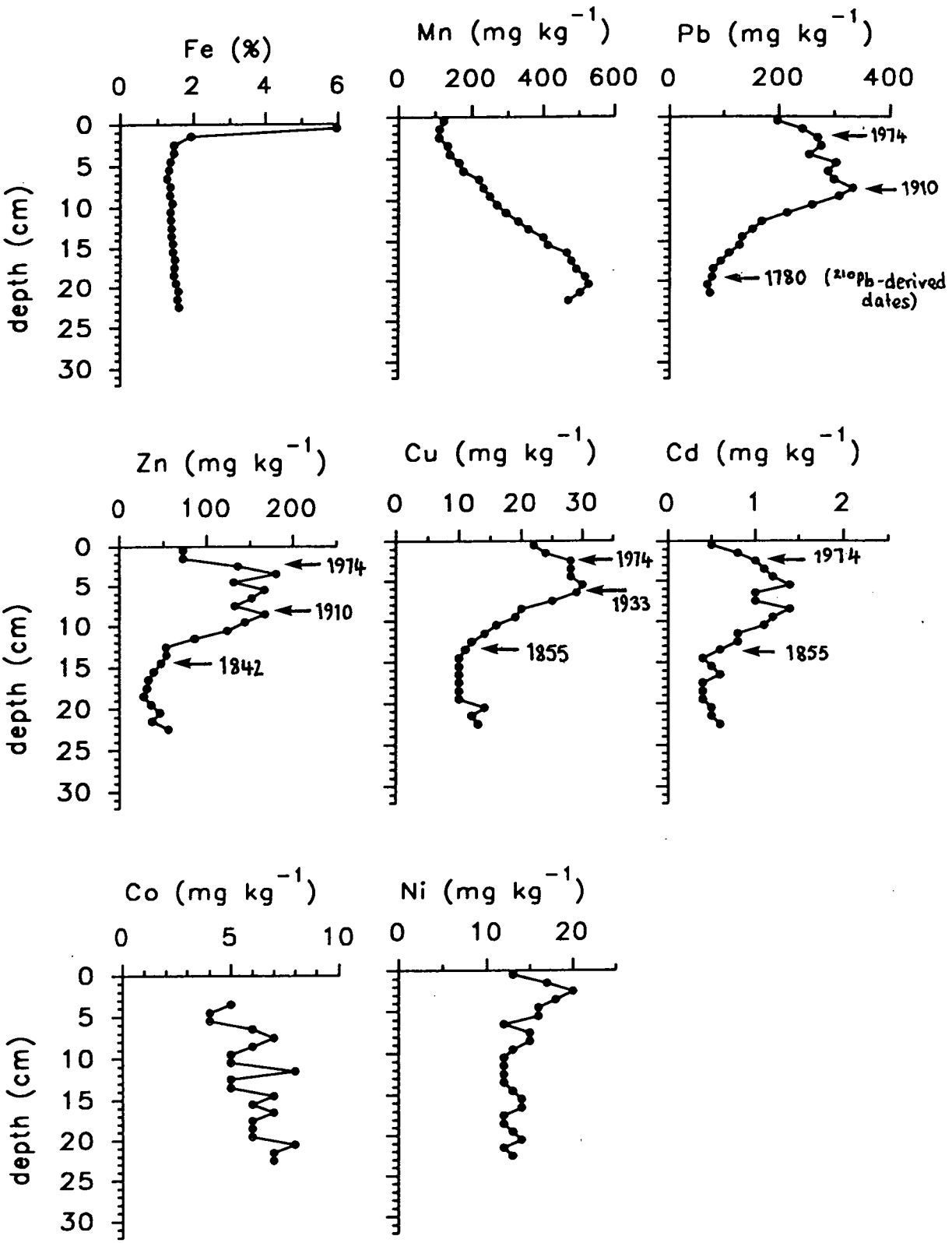

Fig 3.6 Metal concentrations in HNO_3/HCl acid digested Round Loch of Glenhead sediment core RLG2-1B

303 mg kg^{-1} to 2-3 cm (1974) before decreasing towards the surface to 197 mg kg^{-1} in the 0-1 cm section. If the dates at site 1 based on the upper sedimentation rate of 12.3 mg kg-1 are used, then the trends in Pb concentration show close correspondence between the two sites. The concentration profile patterns can be interpreted in terms of changes in the historical atmospheric deposition of pollutant lead, *i.e.* an increase commencing during the Industrial Revolution (around the middle of the 18th century), rising to peak levels at the beginning-middle of this century before a decrease in Pb emissions to the environment in the last 20 years, as a result of a reduction in fossil fuel combustion, heavy industry and leaded petrol. The results are also consistent with published Pb data for this loch (Battarbee *et al.*, 1989; Rippey, 1990). While it has been argued (Ridgway and Price, 1987) that elevated Pb concentrations in the near-surface sediment may be caused by diagenetic remobilisation of Pb, which would also affect the radioactive ^{210}Pb profile, the difference between the shape of the concentration profiles of stable Pb and radioactive ^{210}Pb in these cores provides good evidence that this is not the cause of the enhanced Pb concentrations in the acid digested sediment.

On the basis of the agreement between ^{210}Pb-based dates of changes in the Pb concentration profile at site 2 and site 1 if the upper sedimentation rate limit is used for site 1, this sedimentation rate will be used to date changes in the concentration profiles of the remaining metals at site 1.

Zn concentrations increase at site 1 from 27 mg kg^{-1} below 24 cm (1826), slightly later than the onset of increase in Pb concentration, to enhanced values from 13-3 cm (mean = 177 mg kg^{-1}) corresponding to dates of 1916-1974 and peaking at 210 mg kg^{-1} around 1930 with a much more rapid decrease towards the surface (concentration 62 mg kg^{-1} at 0-1 cm) than for Pb (Table 3.12, Fig. 3.5). Similarly at site 2, Zn concentrations start to increase from a slightly higher background concentration than at site 1 of 38 mg kg^{-1} below 15 cm (1842), with sub-surface enhanced concentrations between 9 and 3 cm (mean = 152 mg kg^{-1}) corresponding to dates of 1910-1974 and then decreasing rapidly to 73 mg kg^{-1} at the surface (0-1 cm) (Table 3.13, Fig. 3.6). Patterns in the Zn concentration profile differ from those found for Pb, although trends in pollutant deposition of the two metals should be broadly similar, since they are often emitted to the atmosphere from the same industrial sources (Nriagu, 1990). The onset of increase in Zn concentration is slightly later than for Pb and while sub-surface enhanced concentrations are observed for both metals, the decrease towards the surface is more pronounced for Zn. Although there has been a reduction in Pb and Zn emission from industrial sources, it has been suggested that low Zn concentrations in the surface sediment of this loch could result from a

combination of reduced atmospheric pollution and processes related to acidification of the loch (Rippey, 1990). This will be discussed further with the partitioning data.

Cd concentrations (Table 3.12, Fig. 3.5) show an increase at site 1 from a mean 0.7 mg kg^{-1} below 24 cm (1826) to higher concentrations (1.3-2.2 mg kg^{-1}) between 14 and 3 cm (1908-1974) and then a sharp decrease to 0.8 mg kg^{-1} at the surface. Patterns at site 2 are broadly similar (Table 3.13, Fig. 3.6), increasing from a mean 0.5 mg kg^{-1} below 14 cm (1855) to a peak at 1.4 mg kg^{-1} and then decreasing from around 3 cm (1974) to 0.5 mg kg^{-1} at the surface. The Cd profile shapes at sites 1 and 2 are similar to those of Zn, which is unsurprising as Cd is geochemically similar to Zn and, partly because of this, is often released to the atmosphere by processes involving Zn emissions, such as smelting/refining and fossil fuel combustion (Nriagu, 1990). The Cd concentration profiles are therefore explicable (as for Zn) in terms of historical variations in pollutant deposition, as well as possible influences from acidification.

Cu concentration profiles are comparable in acid digested sediment from the two sites (Tables 3.12 and 3.13, Figs. 3.5 and 3.6), increasing from a mean background of 8 mg kg-1 (corresponding to a date of 1817) at site 1 and 11 mg kg^{-1} (1855 at site 2), to a mean concentration of 29 mg kg^{-1} between 1938 and 1979 (site 1) and 1933-1974 (site 2), and then decreasing above 3 cm to the surface.

Peaks in Co and Ni concentrations at 15-16 cm at site 1 (Tables 3.12 and 3.13, Figs. 3.5 and 3.6) are similar to those found (acid digested concentrations only) for Fe and Mn. Apart from a slight increase in Ni concentration towards the sediment surface (to 2 cm at site 1 and 3 cm at site 2), there is little change in the concentrations, which were near the detection limit.

'Excess' pollutant metal inventories for Pb, Zn, Cu and Cd at sites 1 and 2 are listed in Table 3.26 and were calculated by subtracting the background (non-anthropogenic) concentration from the total metal concentration for each section, multiplying this value by the corresponding section dry weight and summing over the whole core. The background concentration was the mean value of the constant concentrations below the indicated depths in the core and these were found to be higher at site 2 than site 1.

Various features are noticeable in the concentrations and values of Table 3.26, *e.g.* the background Pb concentration is high compared with background values for Pb in sediments of the other sampled lochs (Chapters 4-6). This is attributable to the high Pb content of the granite bedrock underlying the catchment (Rippey, 1990). Another important point is that while the Chernobyl radiocaesium inventory at site 2 was higher than at site 1, the reverse is true of the pollutant metal inventories. While it might be

Table 3.26 Calculated 'excess' pollutant metal inventories and background concentrations in Round Loch of Glenhead sediment cores RLG1-B and RLG2-1B.

	Pb		Zn		Cu		Cd	
	site 1	site 2	site 1	site 2	site 1	site 2	site 1	site 2
background conc. (mg kg^{-1})	53	74	27	38	8	11	0.7	0.5
depth limit for background conc. (cm)	26	19	24	15	24	14	24	14
'excess' inventory (g m^{-2})	4.34	2.24	1.93	0.95	0.25	0.12	0.014	0.006

argued that this is due to an overestimation in the higher background concentrations of pollutant metals at site 2, if the lower site 1 background concentrations are used to calculate inventories for site 2, this makes little difference to the overall inventories for site 2, *e.g.* the inventories (g m^{-2}) would be 2.65 for Pb and 1.18 for Zn, still considerably lower than at site 1. The reason for this difference, both in the background concentrations and inventories, may be due to a different source of sediment at the two sites. If site 2 has a greater clay content, indicated by the radiocaesium inventories and the higher supported ^{210}Pb concentration, the higher metal background concentrations at this site are consistent with this. The higher sedimentation rate at site 1, despite the proximity of the two basins in which the sampling sites are located, could be due to the bathymetry of the loch (Fig. 3.1), which shows that site 1 is closer to steeper areas than site 2, possibly resulting in an input of sediment from surrounding slopes to site 1 and, therefore, in a higher input of pollutant metals. In this case the lower Chernobyl radiocaesium inventories at site 1 would mean that loss of radiocaesium must outweigh any increased input of radiocaesium at site 1 compared with site 2. This explanation is less convincing for the ^{210}Pb inventory which is only slightly greater at site 1 than at site 2.

Iron and manganese in HNO_3/HCl acid digested sediment

Peak Fe concentrations (Tables 3.12 and 3.13, Figs. 3.5 and 3.6), about three times higher than underlying concentrations, occur in the surface section (0-1 cm) at both sites. The surface maximum is greater at site 2 (5.96% Fe) than at site 1 (3.49% Fe) and in general, Fe concentrations are slightly greater at site 2, but trends of Fe in both cores show a very gradual increase in concentration with depth. In the absence of known recent high inputs of Fe to the loch, the enhanced Fe concentrations in the surface sediment are indicative of redox controlled diagenetic remobilisation of Fe^{2+} in the porewaters of anoxic sediment, followed by reprecipitation in the oxic surface section (Berner, 1980; Davison, 1982).

As Mn is a redox sensitive metal, it might be expected to show similar surface enhancements and this is the case at site 1 (Table 3.12, Fig.3.5), though the enhancement is not as pronounced as for Fe (at 210 mg kg^{-1}, around twice as high as the underlying concentrations). However, there is no observable Mn surface enhancement at site 2 (Table 3.13, Fig.3.6), suggesting that the presence of a Mn surface peak in this loch is a transient feature and that release of Mn to the overlying water can occur. The absence of a Mn peak could mean that the surface sediment is still at a low enough Eh value to prevent oxidation of Mn^{2+} (*i.e.* the surface sediment Eh would be between the Fe^{2+}/Fe^{3+} and Mn^{2+}/Mn^{4+} redox potentials (Chapter 1),

which seems unlikely since Round Loch is well-mixed, probably with high oxygen concentrations throughout the water body. Alternatively, the association of Mn with particulates decreases with decreasing pH and so supply of particulate-associated Mn from the water column to the sediment may be diminished in acidic waters (White and Driscoll, 1986). This is supported by the very similar values obtained for Mn in unfiltered and filtered water column samples (Tables 3.20, 3.21 and 3.23), particularly noticeable in the unfiltered overlying core water samples, which contain relatively high amounts of particulates. The same effect is not noted for Fe. Bendell-Young and Harvey (1992) have suggested that gradual leaching of a surface Mn peak of diagenetic origin to overlying acidified water results in a net export of Mn from the lake system and once this pool of Mn has been exhausted, only trace amounts of Mn are found in surficial sediments. This could account, to some extent, for the lack of Mn peak at site 2 and the less pronounced Mn peak relative to Fe at site 1.

An additional feature of the Mn concentration profiles is the systematic increase in concentration with depth from 91-490 $mgkg^{-1}$ (0-31 cm, site 1) and 110-527 mg kg^{-1} (2-21 cm, site 2). This pattern has been observed in sediment cores of other acidified lakes (Carignan and Nriagu, 1985; Renberg, 1985) and has been interpreted either as post-depositional loss of Mn from the sediments or as a historical record of the pH of the water column at the time of deposition, with Mn concentration positively correlated with inferred pH values of the water column (Steinberg and Högel,1990). Since Mn concentrations increase virtually to the maximum sampled depth in cores from both sites, it is not possible to relate the onset of change in Mn concentration at depth conclusively to historical trends in the water column pH, but there is some evidence, especially at site 2 of the onset being just above the base of the core with concentrations decreasing slightly below 21 cm (site 2) and 31 cm (site 1). These depths correspond to dates of around the mid-18th century, which is slightly earlier than the initial change in water column to lower pH values (about 1800) inferred by changes in the diatom assemblage (Flower *et al.*, 1987). The observed earlier onset could be explained by post-depositional loss of Mn from the sediment.

Iron and manganese partitioning and solution phase data

The sum of Fe concentrations in fractions I-V in sediment from sites 1 and 2 (Tables 3.14 and 3.16, Figs. 3.7 and 3.8) is similar to, or slightly greater than in the HNO_3/HCl acid digested sediment, which may be attributed to cumulative errors in the five step sequential extraction procedure, or non-homogeneity of the wet sediment used for sequential extraction (compared with the dried, ground sediment used for acid

Fig. 3.7 Fe concentrations in sequentially extracted and HNO_3/HCl acid digested Round Loch of Glenhead sediment core RLG1-B, porewater and overlying water samples from core RLG1-C and water column samples from site 1.

Key to fractions:

I exchangeable
II carbonate bound/specifically sorbed
III easily reducible
IV moderately reducible
V organic bound/sulphides

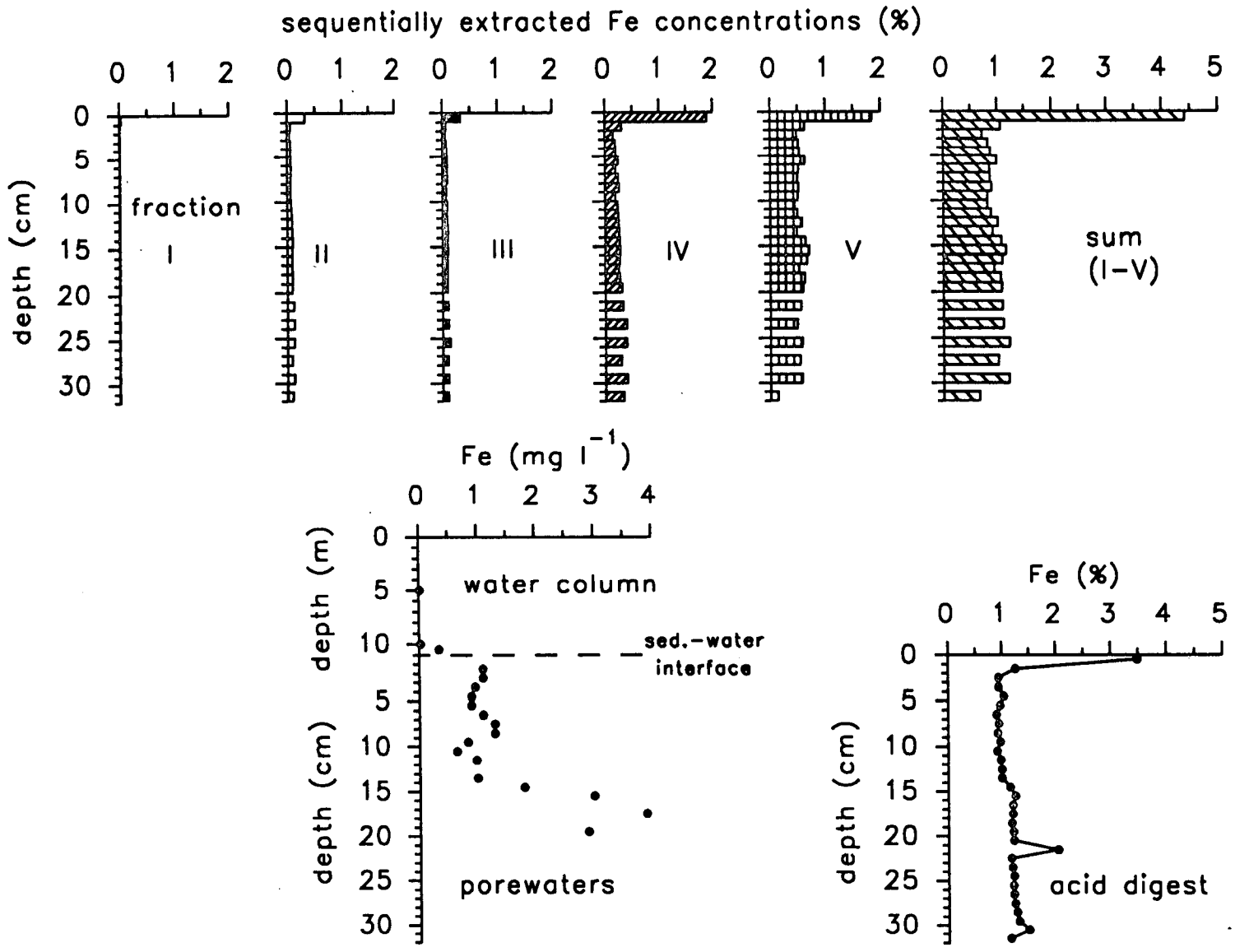
sequentially extracted Fe concentrations (%)
depth (cm)
fraction
I
II
III
IV
V
sum
(I-V)
Fe (mg l^{-1})
water column
sed.-water
interface
depth (m)
depth (cm)
porewaters
Fe (%)
depth (cm)
acid digest

Fig. 3.8 Fe concentrations in sequentially extracted and HNO_3/HCl acid digested Round Loch of Glenhead sediment core RLG2-1B, porewater and overlying water samples from core RLG2-1C and water column samples from site 2.

Key to fractions:

I exchangeable
II carbonate bound/specifically sorbed
III easily reducible
IV moderately reducible
V organic bound/sulphides

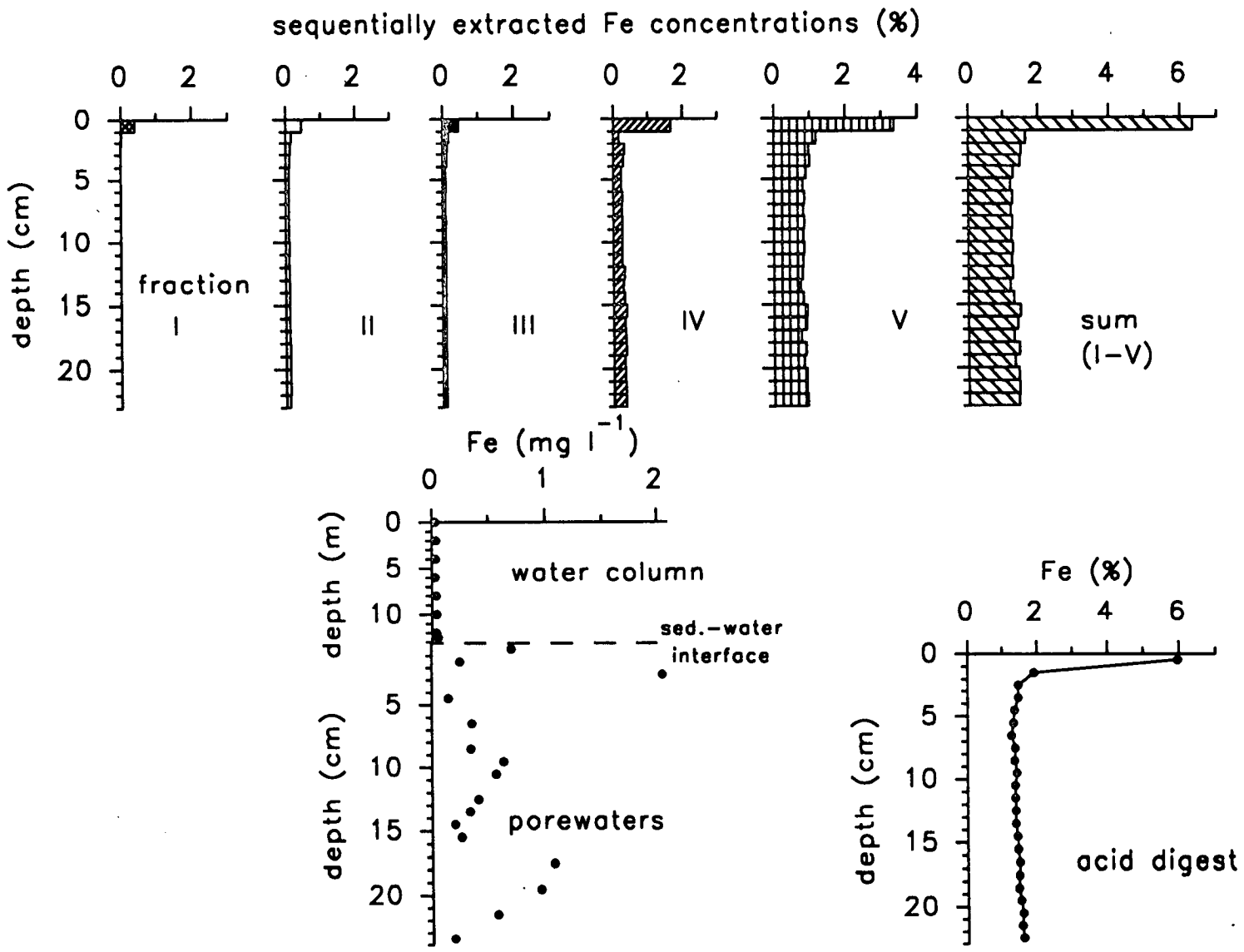
sequentially extracted Fe concentrations (%)
depth (cm)
fraction
I
II
III
IV
V
sum
(I-V)
Fe (mg l^{-1})
water column
sed.-water
interface
depth (m)
depth (cm)
porewaters
Fe (%)
depth (cm)
acid digest

digestion). The similarity of these concentrations indicates that little or no Fe is bound within stable mineral lattices.

Concentrations of Fe are enhanced in all fractions in the surface section (0-1 cm), in which the overall maximum concentration is observed. At both sites patterns in the partitioning data are similar (though with higher concentrations in fractions IV and V at site 2) with Fe predominantly associated with fraction V throughout the core and, once below the surface maximum of 1.84% (site 1) and 3.36% (site 2), remains fairly constant in this fraction. A slight increase in concentration with depth is observed in fraction IV, although this only extends to 19 cm at site 2. Concentrations of Fe in fractions II and III are almost identical, but the surface enhancements are less marked than in fractions IV and V. Fraction I contains little Fe below the surface peak of 0.025% (site 1) and 0.39% (site 2).

The prominence of Fe in fraction IV in the surface sediment, overlying much lower concentrations, provides some evidence for redox cycling since fraction IV is the moderately reducible fraction representing Fe oxides/hydroxides, enhanced at the surface due to reprecipitation of Fe remobilised in the reducing zone at greater depths. An additional, important contributing factor to the surface peak in Fe concentration is Fe in fraction V, the organic/sulphides component, which may be related to acidification. Under acid conditions increased uptake of Fe by humic substances can occur (Tipping, 1981), giving greater amounts of organically bound Fe in the surficial sediments of acid lakes compared with circumneutral lakes (Bendell-Young and Harvey, 1992).

As for Fe, the sum of Mn concentrations (Tables 3.14 and 3.16, Figs. 3.9 and 3.10) is similar to (or slightly greater than) concentrations in the acid digested sediment. The enhancement of Mn in the surface sediment of site 1 is a result of higher Mn concentrations in fractions III (34 mg kg^{-1}), IV (60 mg kg^{-1}) and V (71 mg kg^{-1}). Below 1 cm Mn concentrations in fraction V do not vary much downcore (31-49 mg kg^{-1}) and the overall trend of increasing Mn concentration with depth is attributable to a pronounced increase in fraction I (maximum 256 mg kg^{-1} at 23-24 cm) and, to a lesser extent, fractions II, III and IV (in which Mn was not detectable from 0-5 cm, 1-9 cm and 1-14 cm respectively). At site 2, where there is no surface Mn enhancement, Mn increases downcore in all five fractions, though this is most marked, as at site 1, in fraction I (maximum 239 mg kg^{-1} at 20-21 cm). Mn concentrations also increase with depth in fractions III and IV (slightly in fraction V), though the increase is less pronounced and with lower concentrations than fractions I and II.

The presence of Mn in the more labile fractions I (exchangeable) and II (specifically sorbed), despite the acidic water column, is explicable due to the higher

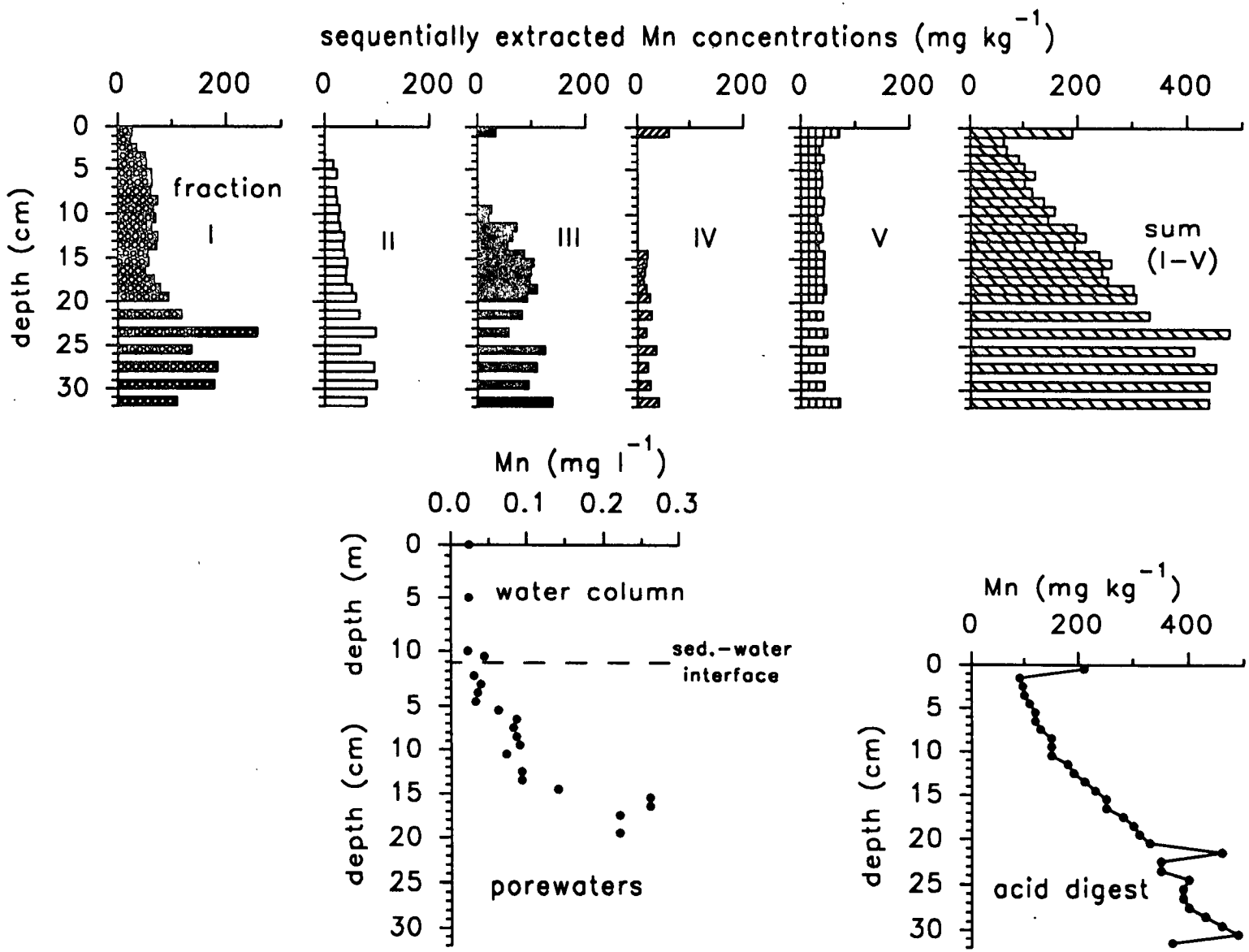
sequentially extracted Mn concentrations (mg kg^{-1})
0 200
0 200
0 200
0 200
0 200
0 200 400
depth (cm)
0
5
10
15
20
25
30
fraction
I
II
III
IV
V
sum
(I–V)
Mn (mg l^{-1})
0.0 0.1 0.2 0.3
depth (m)
depth (cm)
water column
sed.–water
interface
porewaters
Mn (mg kg^{-1})
0 200 400
acid digest

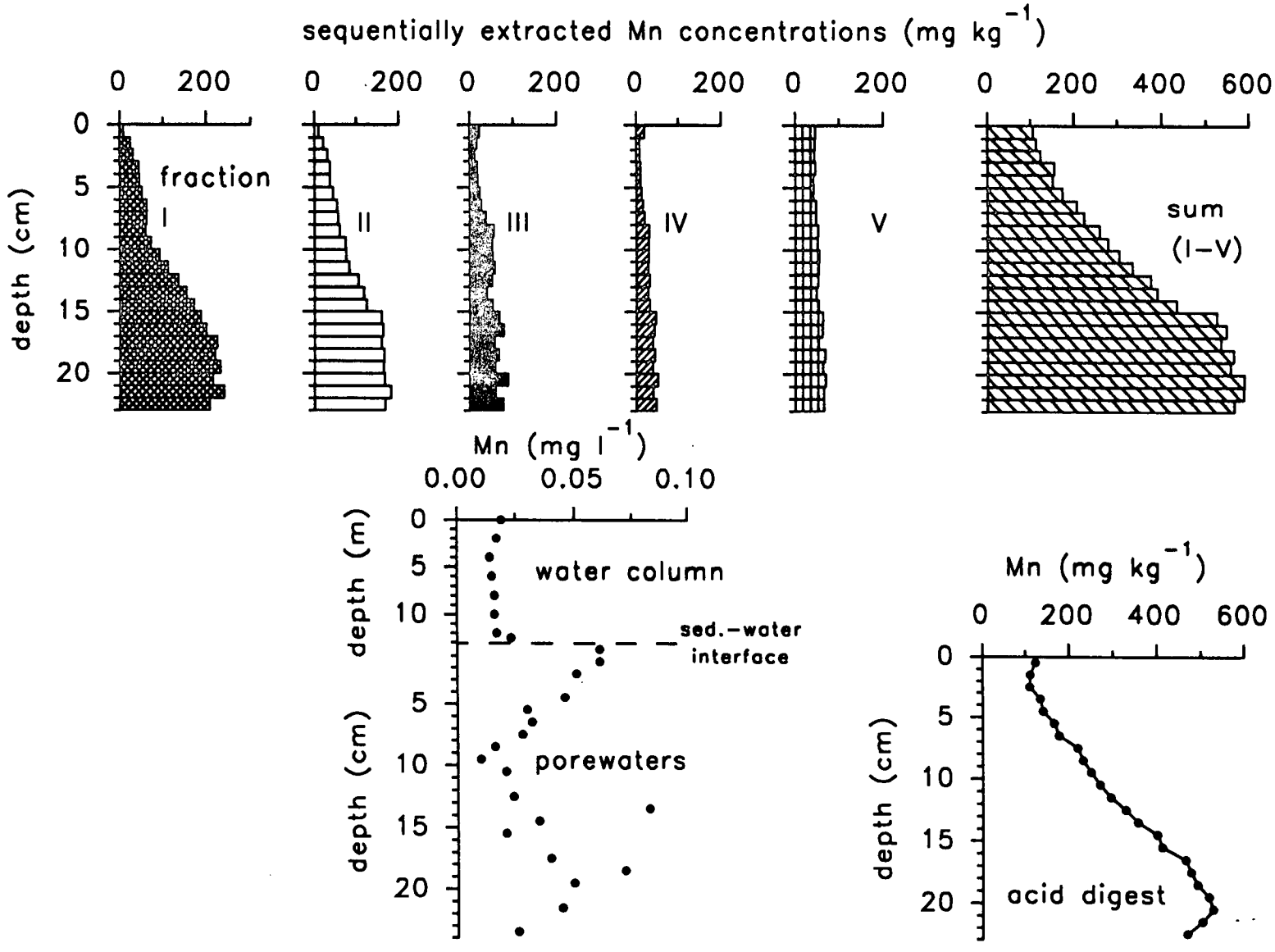
sequentially extracted Mn concentrations (mg kg^{-1})
0 200
0 200
0 200
0 200
0 200
0 200 400 600
depth (cm)
0
5
10
15
20
fraction
I
II
III
IV
V
sum
(I–V)
Mn (mg l^{-1})
0.00 0.05 0.10
depth (m)
depth (cm)
water column
sed.–water
interface
porewaters
Mn (mg kg^{-1})
0 200 400 600
depth (cm)
acid digest

pH values in anoxic sediments as a result of H^+ consumption in the microbially mediated reduction of sulphate and nitrate (denitrification) (Rudd *et al.*, 1986; Norton *et al.*, 1990). The surface Mn enhancement at site 1 is, as for Fe, attributable to redox-cycling as Mn is present in fractions III (easily reducible, Mn oxides) and IV (moderately reducible), the latter probably a reflection of Mn oxides not removed by fraction III extractants. The diagenetic remobilisation of Mn does not appear to be as extensive as, for example, in Loch Lomond (Chapter 4), as Mn in fraction III (Mn oxides) increases downcore.

Concentrations of dissolved Fe at site 1 (Tables 3.19-3.20, Fig. 3.7) show the maximum point of Fe dissolution in the porewaters occuring at 17-18 cm, indicated by the peak concentration at this depth (3.9 mg l^{-1}), above which a decreasing concentration implies upward movement of Fe to 10-11 cm. At depths above 11 cm there is a slight increase to 7-9 cm, with little variation above this. These trends are consistent with release of Fe to the porewaters in reducing sediment, movement upwards to the solid phase surface peak above which solution concentrations decrease. This is also consistent with the formation of sulphides at depth, because the porewater concentration decreases below 18 cm, therefore indicating downward movement and removal of soluble Fe to the solid phase.

The porewater Fe concentration profile for site 2 (core RLG2-1C) (Table 3.19, Fig. 3.8) shows release of Fe occurring (as at site 1), with a peak at 17-18 cm (1.1 mg l^{-1}), below which concentrations decrease to low levels at 23-24 cm, consistent with removal via sulphide formation at depth. Above the porewater peak there is a slight concentration increase to 9-10 cm and fairly constant values above this. The pronounced porewater Fe peak at 2-3 cm (2.0 mg l^{-1}) may well be a sampling artefact, due to the presence of particulate/colloidal matter which could have passed through the membrane filter. Fe concentrations in the additional sediment collected for porewater analysis in May 1992 (RLG2-2A and RLG2-2B) (Table 3.22, Fig. 3.11) are similar to those in sediment from the previously collected sediment core RLG2-1C. The trends are also broadly comparable in the three cores, but results from core RLG2-2A are more regular, and possibly more reliable, than those from core RLG2-2B.

Considering all the data for Fe in Round Loch, it can be concluded that redox-cycling is important in causing the surface enhancement of Fe, indicated by the proportion of Fe in fraction IV (moderately reducible, Fe oxides/hydroxides) in the 0-1 cm section, relative to the low concentrations in this fraction in the depths below. The porewater results support this conclusion, overall indicating release of Fe at depth and upwards diffusion of Fe to precipitate in the surface section where porewater concentrations are low. Downwards diffusion of Fe from the maximum point of

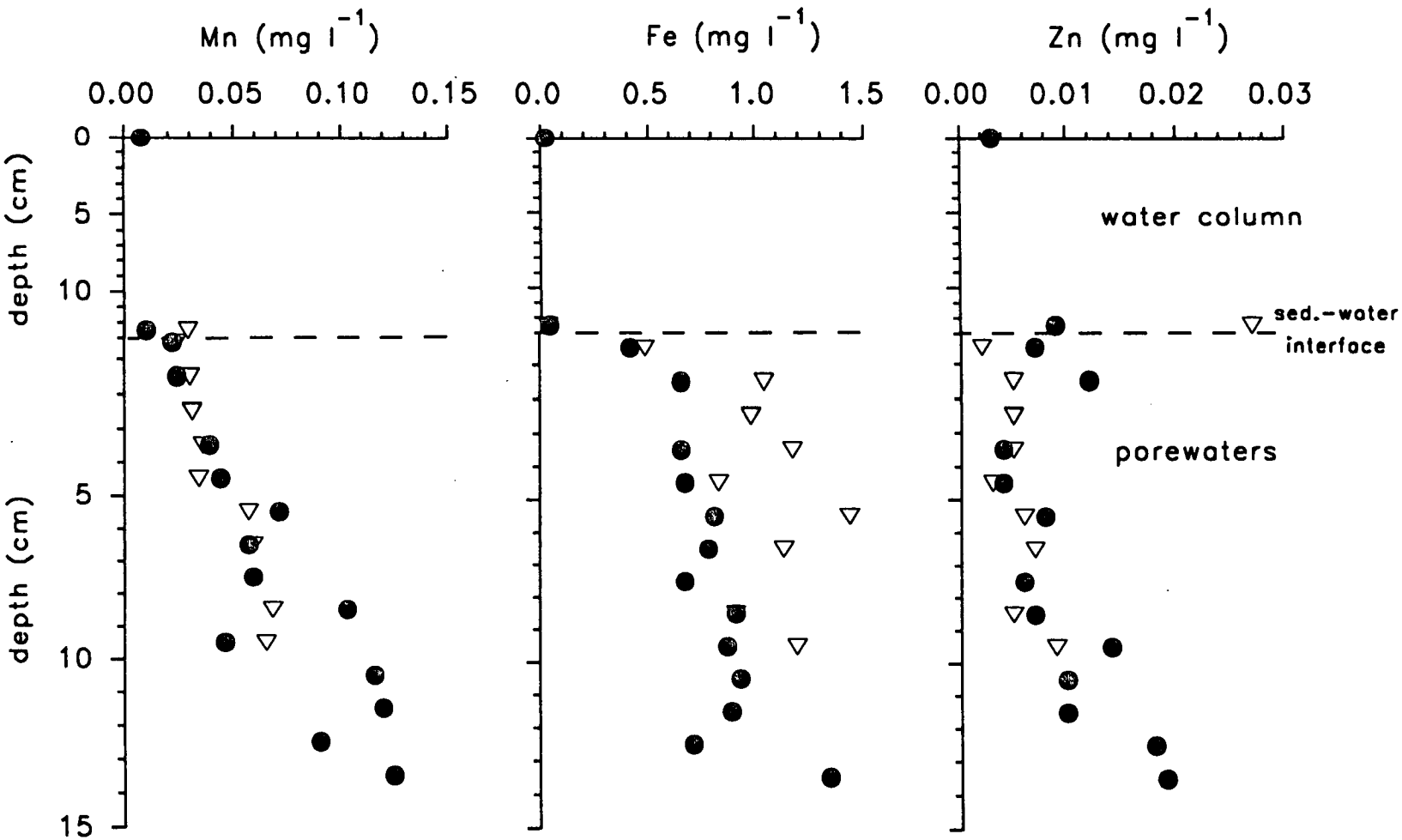

Fig. 3.11 Concentration profiles of Mn, Fe and Zn in the surface water of Round Loch of Glenhead and in porewaters and overlying water from sediment cores RLG2-2A (●) and RLG2-2B (▽)

dissolution, implied by the negative porewater gradient, particularly at site 2, is attributable to the formation of sulphides at depth, for which a slight increase of Fe in fraction V provides further evidence. However, in addition to the redox cycling of Fe, acid-enhanced precipitation of Fe with humic substances is probably also relevant in causing the surface solid phase Fe peak.

As with Fe, Mn porewater concentrations are generally higher at site 1 than site 2, especially at depth (Tables 3.19-3.23; Figs.3.9-3.11). Maximum dissolution of Mn, indicated by peak porewater concentrations, appears to occur at depths of 15-17 cm (0.26 mg l^{-1} RLG1-C) and 13-14 cm (0.083 mg l^{-1} RLG2-1C and 0.12 mg l^{-1} RLG2-2A). This is consistent with the Fe porewater results in terms of redox-cycling, since Mn oxides are more readily reduced than those of Fe and would therefore show dissolution nearer the surface (*i.e.* at higher Eh) (Berner, 1980). The trend of Mn concentrations decreasing upwards in the porewaters to the suface of core RLG1-C at site 1 is attributable to redox-driven release of Mn at depth, upwards diffusion, followed by precipitation of Mn oxides at the sediment surface to give the observed enhanced solid phase concentration. Similarly, Mn concentrations in core RLG2-2B show the same trend and for core RLG2-2A, this pattern is observed above 9 cm, but minima occur at 9-10 cm and 12-13 cm, making interpretation more complex, although it is possible that the measured concentrations at these depths are erroneous. Noticeably Mn concentrations in the porewaters of sediment core RLG2-1C, collected during the initial sampling of site 2, decrease downcore to 10 cm from the sediment surface, where no overall solid phase enhancement was present, but a slight increase in Mn in fractions III and IV is found. This indicates downward diffusion of Mn, but since release of Mn is also implied by the peak at 13-14 cm, this profile is difficult to interpret and is likely to be a result of competing processes (dissolution of Mn in two areas of the core). A further contrast between the Mn porewater concentration profiles at site 1, site 2 (cores RLG2-2A and RLG2-2B) and the porewater profile for core RLG2-1C at site 2 is that for the former three cores, Mn concentrations in the water overlying the sediment are similar to those in the surface sediment (0-1 cm), whereas in core RLG2-1C there is a decrease in Mn porewater concentration between the 0-1 cm section and the overlying water. This implies diffusive loss of Mn from the sediment (as well as movement of Mn downcore) in core RLG2-1C, which could have contributed to the lack of solid phase Mn enhancement in this sediment, but which is not occurring at site 1 where a solid phase surface peak is observed.

In conclusion, the solid and solution phase Mn concentration profiles at site 1, and the porewater profiles of sediment cores RLG2-2A and RLG2-2B for site 2, are interpretable in terms of redox-driven diagenesis, as for Fe. The presence of Mn in

fraction III (easily reducible, Mn oxides) at depth in cores from both sites and the lack of significant solid phase Mn enhancement at site 2, indicate that near-complete recycling of Mn does not occur in Round Loch. This constrasts with, for example, Loch Lomond (Chapter 4), where highly enhanced concentrations of solid phase Mn in the surficial sediment, overlying very low concentrations, were observed. Reasons for the different situation in Round Loch are apparently transient changes in the points of maximum Mn dissolution and loss of Mn to the overlying water, which compete with the redox-driven process of solid phase Mn enhancement at the surface. This transient change may well be a seasonal effect, since the profiles showing evidence of redox-cycling with a surficial Mn enhancement (at site 1 sediment cores and the porewater profiles for cores RLG2-2A and RLG2-2B at site 2) were from cores collected in May and June,whereas the cores RLG2-1C and RLG2-1B, with no marked solid phase surface peak of Mn and a porewater profile indicating Mn dissolution at the surface as well as at depth, were collected in January.

The implications of the Fe and Mn results for the behaviour of the other metals studied, are that redox-driven diagenesis is an operative process in Round Loch, which could result in scavenging by Fe/Mn secondary minerals or remobilisation of other species by release from oxides/hydroxides of Fe/Mn. Additionally, surface water acidification has probably caused increased precipitation of Fe with humic substances and decreased deposition of Mn to the sediments and/or post-depositional loss of Mn from the sediment to the water column.

Lead, zinc and copper partitioning and solution phase data

The sum of Pb concentrations in fractions I-V (Tables 3.15 and 3.17, Figs. 3.12 and 3.13) is, in many of the sections, greater than the corresponding concentrations in acid digested sediment, most noticeably at site 2. Since sediment samples for sequential extraction and acid digestion were taken from the same core, this difference must be due to cumulative errors associated with the five step sequential extraction procedure being greater than the error associated with the acid digestion method. Non-homogeneity of sediment, as mentioned in the discussion of the Fe partitioning data, is unlikely to have a marked effect on so many of the samples as observed for Pb. Nevertheless, the partitioning data (Figs. 3.12 and 3.13) overall show a similar trend in the concentration profile to that obtained by sediment acid digestion. Intersite variations are noticeable for the partitioning data, although concentrations and patterns in the profiles of the sum of fractions I-V are comparable. Pb concentrations are higher in fractions I and II and undetectable in fraction III at site 1, but greater concentrations are found in fractions IV and V at site 2. At site 1, the

sequentially extracted Pb concentrations (mg kg^{-1})
0
200
400
depth (cm)
0
5
10
15
20
25
30
fraction
I
II
III
IV
V
sum
(I–V)

Pb (mg kg^{-1})
0
200
400
depth (cm)
0
5
10
15
20
25
30
acid digest

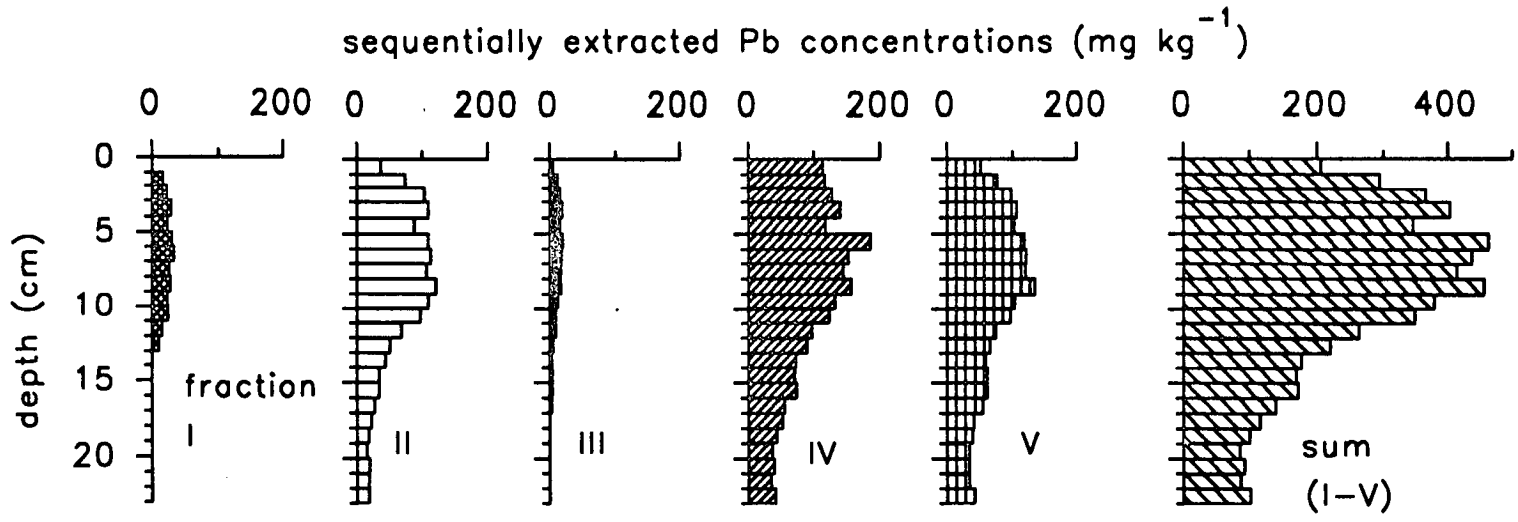
sequentially extracted Pb concentrations (mg kg^{-1})
0
200
0
200
0
200
0
200
0
200
0
200
400
depth (cm)
0
5
10
15
20
fraction
I
II
III
IV
V
sum
(I–V)

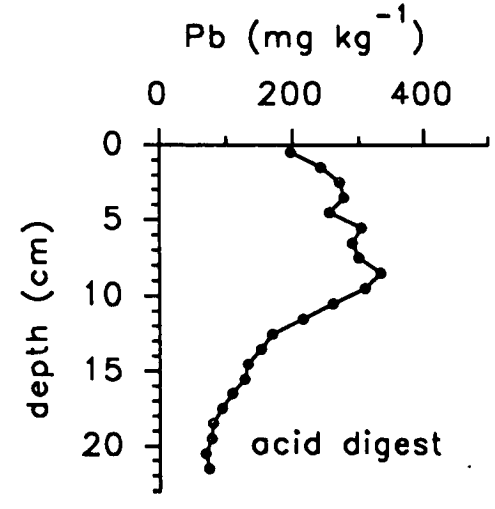
Pb (mg kg^{-1})
0
200
400
depth (cm)
0
5
10
15
20
acid digest

sub-surface zone of enhanced Pb concentrations is mainly due to fraction II, with fractions I and IV showing similar trends, but with lower concentrations. Pb in fraction V varies little with depth to around 18 cm, decreasing slightly below this. In contrast, the zone of enhancement at site 2 is largely a result of higher Pb concentrations in fraction IV, although fractions II and V are also important. Patterns of Pb in fractions I and III show broadly the same trends as fraction IV, but concentrations are much lower. The similarity in trends of Pb concentrations in fractions I, II and IV (site 1) and I-V (site 2) respectively, and the shape of the Pb concentration profile in acid digested sediment, suggests that the partitioning patterns are attributable to changes in the flux of pollutant Pb to the loch, because the lack of change in Pb distribution between the five fractions with depth implies little or no post-depositional Pb mobility.

Pb was below the detection limit of 0.003 mg l^{-1} in all of the water column and most of the porewater samples and the few samples in which Pb was detectable were $\leq$ 0.02 mg l^{-1}. This indicates that there is little or no post-depositional mobility of Pb in the sediment of Round Loch, supported by the solid phase data, interpretable in terms of historical trends in anthropogenic input of Pb to the area. The difference between the profile shape of ^{210}Pb and total Pb (*i.e.* stable Pb and ^{210}Pb) provides further evidence for the lack of Pb mobility, since any influential diagenetic processes would affect both ^{210}Pb and stable Pb, resulting in more similar profile shapes. The immobility of Pb once deposited in the sediment in acidified conditions is consistent with the findings of Davis *et al.* (1982) who found in laboratory experiments that Pb release from sediments did not occur at pH values > 3.

The sum of Zn concentrations in fractions I-V is (as for Pb) also similar to, or greater than, concentrations of Zn in acid digested sediment indicating little or no association of Zn with stable mineral lattices (Tables 3.15 and 3.17, Figs. 3.14 and 3.15). The principal fractions with which Zn is associated for both sites are IV and V, with comparable concentrations at site 1, whereas Zn concentrations are higher in fraction V at site 2. The sub-surface zone of increased Zn concentrations observed in the overall (sum I-V) profiles for both sites is attributable to concentration increases in the following fractions, in order of importance: IV=V>II>III (site 1) and V>IV>III>II>I (site 2).

The Zn partitioning data, when contrasted with the Pb partitioning, in particular the major association of Zn with fractions V (and IV at site 1), suggest a difference in transfer mechanism of Pb and Zn to the sediment. Two of the factors potentially capable of influencing Zn behaviour in this loch are a pH-related decrease in particulate Zn deposition, due to increased solubility of Zn at lower pH, which may decrease

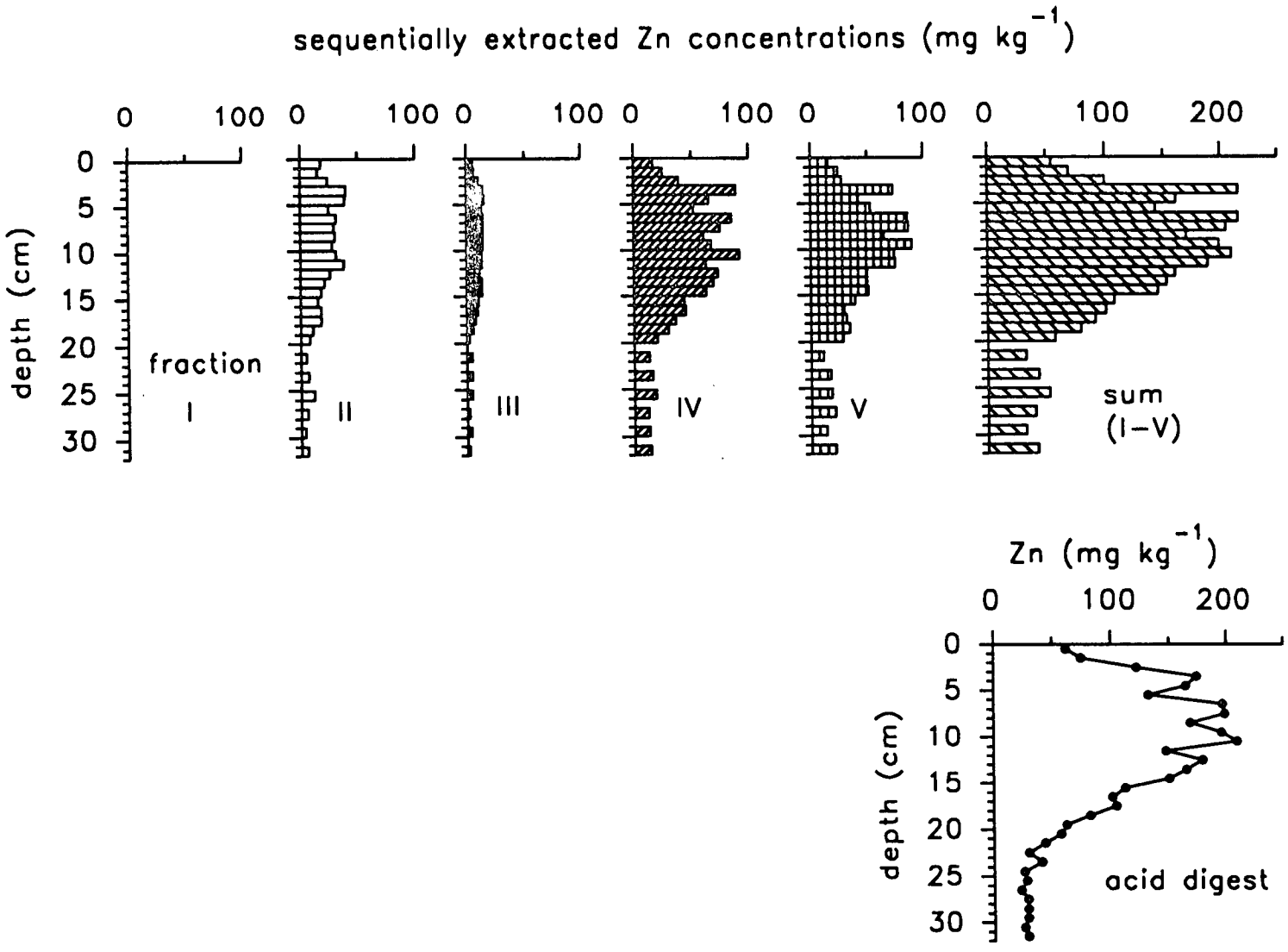
sequentially extracted Zn concentrations (mg kg^{-1})
0
100
0
100
0
100
0
100
0
100
0
100
200
depth (cm)
0
5
10
15
20
25
30
fraction
I
II
III
IV
V
sum
(I–V)
Zn (mg kg^{-1})
0
100
200
depth (cm)
0
5
10
15
20
25
30
acid digest

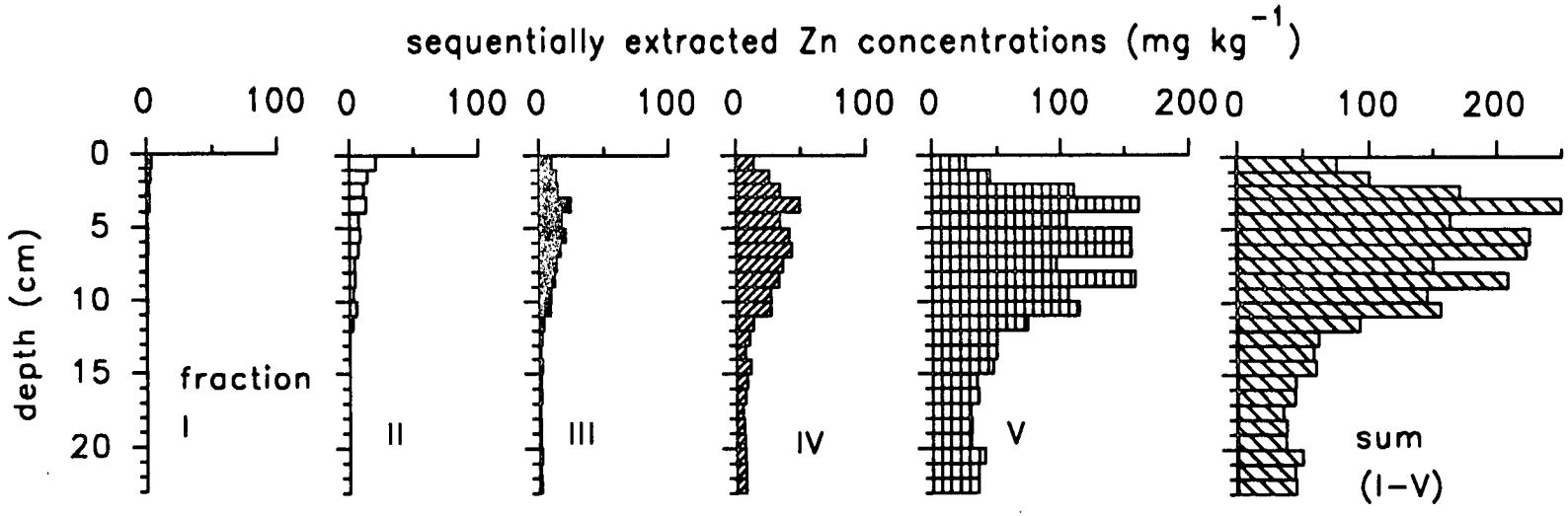
sequentially extracted Zn concentrations (mg kg^{-1})
0
100
0
100
0
100
0
100
0
100
200
0
100
200
depth (cm)
0
5
10
15
20
fraction
I
II
III
IV
V
sum
(I–V)

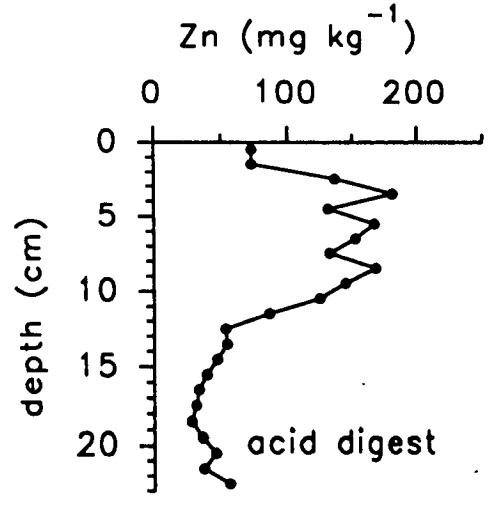
Zn (mg kg^{-1})
0
100
200
depth (cm)
0
5
10
15
20
acid digest

deposition of Zn to the sediment (Tessier *et al.*, 1989), and post-depositional release of Zn from the sediments to the overlying water, evidence for which has been published by Schindler *et al.* (1980) in a study of experimentally acidified lakes. The combination of release of Zn from the surface sediment and decreased particulate deposition of Zn to the sediments would result in the more pronounced decrease of Zn concentrations towards the sediment surface, compared with concentrations of the apparently immobile Pb. This may also account for the rapid decrease in Cd concentrations towards the sediment surface, indicating it too has been influenced by acidification, as described for Zn. Similar concentration profiles of Zn and Cd were found in the acidified Swedish Lake Gårdsjön by Renberg (1985), who explained the pronounced decrease in concentrations towards the sediment surface as being due to acidification effects, probably by a pH-related decrease in deposition of Zn (and Cd) to the sediment.

An alternative mechanism causing enhanced concentrations of Zn in the sub-surface sediment of acid lakes has been reported by Carignan and Tessier (1985), involving diffusion of Zn from the water column to the porewater, followed by precipitation of ZnS at depth. The observed increased concentrations of Zn in fraction V (organic/sulphides) between 3 and 13 cm (site 1) and 3 and 9 cm (site 2), corresponds with the zone of enhanced Zn in the acid digested sediment and suggests that diffusion-precipitation may be a process operating in Round Loch. High Zn concentrations in the porewater blanks meant that the only reliable Zn porewater profiles were from cores RLG2-2A and RLG2-2B. In these cores the Zn solution phase profile (Tables 3.22 and 3.23; Fig. 3.11) does show that concentrations were higher in the overlying water compared with the value in the 0-1 cm sediment section, indicating downward movement of Zn from the water column to the sediment. Below this depth however, concentrations do not continue to decrease, as would be expected if ZnS formation were occurring, but instead, despite some irregularities, show similar trends to those observed in the Mn porewater profiles in the corresponding cores.

In conclusion, the solid phase Zn data (from the acid digestion and sequential extraction) indicate an enhancement of Zn in the sub-surface sediments, which, on the basis of the ^{210}Pb chronology at both sites, can in part be attributed to changes in the atmospheric input of pollutant Zn to the loch. Additionally, however, the sharp decrease in Zn concentration above the enhanced zone and the difference in the transfer mechanism of Zn to the sediment compared with Pb (implied by the different distribution of Pb and Zn between the five sequential extraction fractions) shows that Zn is also influenced by surface water acidification. Interpretation of the Zn solution phase data is not straightforward, but perhaps does indicate some diffusive movement

of Zn from the water column to the sediment. The porewater profiles cannot be interpreted solely on this basis, however, since the trends are not entirely consistent with downward movement of soluble Zn and precipitation of ZnS at depth (for which patterns of Zn in fraction V provide evidence). It is likely that a combination of processes is affecting the Zn behaviour in the studied sites in Round Loch, involving some diffusive movement of Zn into the sediment, as well as decreased deposition of Zn to the sediment due to a lower surface water pH, caused by the deposition of acid precipitation to the loch. The same processes are probably also influencing the shape of the Cd profile, but for this metal no partitioning data are available and porewater concentrations were all similar to the blank concentration of 5×10^{-4} mg l^{-1}.

Cu is heavily associated with, and only detectable in, fraction V (organic/sulphides), comprising 86% of the Cu concentration in acid digested sediment at site 1 and 88% at site 2 (Table 3.18, Fig. 3.16). The similarity in the concentration profile patterns between fraction V and the acid digest concentration profile, combined with the lack of significant Cu concentrations in the solution phase (all ≤ 0.02 mg l^{-1}, mostly ≤ 0.003 mg l^{-1}) strongly suggests that Cu is not remobilised once deposited in the sediment.

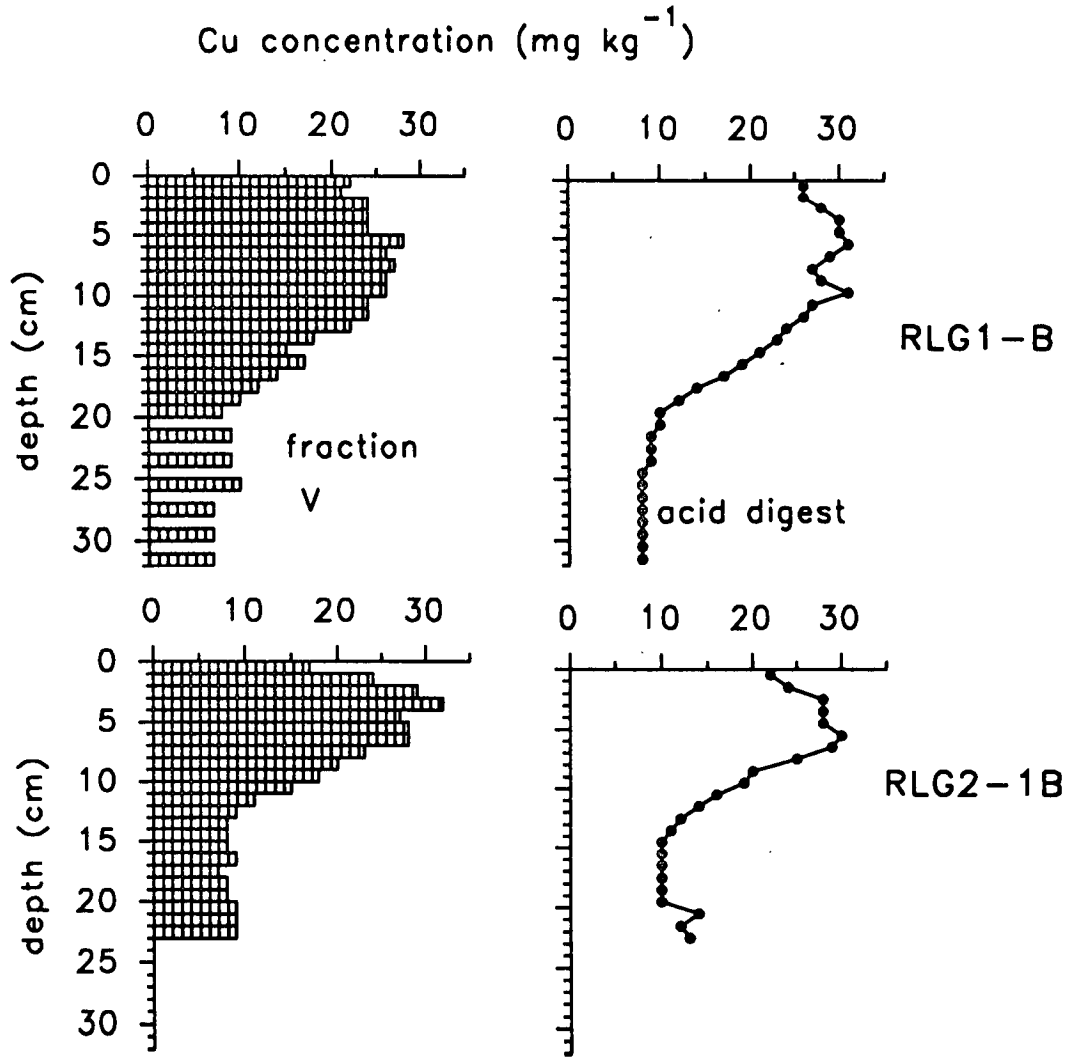
Cu concentration (mg kg^{-1})
0 10 20 30
depth (cm)
0
5
10
15
20
25
30
fraction
V
acid digest
RLG1-B
RLG2-1B

3.5 Conclusions

1. The ^{210}Pb and radiocaesium data provide information on the sedimentation processes operative at the sampled sites in Round Loch of Glenhead, indicating partial sediment mixing to 4 cm at both sites. A ^{210}Pb-derived sedimentation rate of 8.0 mg cm^{-2} y^{-1} was obtained at site 2, while at site 1 a range of 7.2-12.3 mg cm^{-2} y^{-1} was calculated. On the basis of subsequent interpretation of the pollutant metal data for the two sites, the upper limit to the sedimentation rate at site 1 of 12.3 mg cm^{-2} y^{-1} , which is in close agreement with published data, was thought to be the more appropriate value.

2. Radiocaesium appears to be mobile within the sediment at both sites, though less at site 2, where separate ^{137}Cs peaks due to fallout from Chernobyl and weapons testing are discernible. The mobility of radiocaesium at both sites is indicated by penetration of ^{137}Cs from the two different fallout sources to depths dated by ^{210}Pb to periods long before fallout deposition to the area, even if downward smearing effects due to mixing are taken into account.

3. Estimated inventories of ^{137}Cs in the sediment from Chernobyl fallout are considerably lower than reported deposition values of ^{137}Cs to the area, indicating post-depositional loss of radiocaesium from the sediment or low efficiency of radiocaesium deposition to the sediment, both followed by loss from the loch via hydraulic flushing. The difference between the Round Loch inventory for weapons testing derived ^{137}Cs and the UK average for the deposition of weapons testing fallout to the area is not as marked as with the Chernobyl inventories. This is attributed to the greater duration of weapons testing fallout deposition and the less water soluble nature of radiocaesium in fallout from weapons testing, compared with that from Chernobyl. The higher estimated Chernobyl fallout inventory and less mobility of radiocaesium at site 2, compared with site 1, implies a higher sediment clay content at site 2.[x] This is also evident in the higher metal 'background' (non-anthropogenic) concentrations of pollutant metals at site 2.

4. Pb and Cu results are interpretable in terms of historical trends in the atmospheric input of these pollutant metals to the area and there is no evidence of post-depositional mobility, on the basis of no significant detectable porewater Pb and Cu concentrations, and observed trends in the partitioning data. Trends in the concentration profiles of Pb and Cu in sequentially extracted fractions largely mirror patterns observed in the profiles of acid digested sediment and show little variation in the relative contributions of each fraction to the sum of concentrations in all fractions with depth. Cu is

[x] See Corrigenda, page 365

significantly associated with fraction V (organic/sulphides), while the important fractions for Pb are I, II and IV (site 1) and II, IV and V (site 2).

5. Sub-surface enhancements in the concentrations of Zn and Cd in acid digested sediment are broadly explicable by historical pollution trends, as for Pb and Cu. In addition, sharply decreasing concentrations of Zn and Cd towards the surface of the core and, for Zn, patterns in the partitioning data (with a significant association of Zn with fractions IV and V, contrasting with the Pb partitioning data) and porewater concentrations, suggest an influence of acidification on Zn and, by implication, on Cd. This influence is thought to involve a pH-related decrease in the efficiency of Zn (and Cd) deposition to the sediment and also, perhaps, downward diffusion of Zn from the water column to the sediment to form ZnS in the zone of enhanced concentrations. The importance of Zn in fraction V (organic/sulphides) in the zone of enhanced Zn concentrations provides some evidence for the sub-surface formation of ZnS.

6. Calcuated 'excess' inventories for the pollutant metals have values of (g m^{-2}) 4.34 (Pb), 1.93 (Zn), 0.25 (Cu) and 0.014 (Cd) at site 1 and at site 2, 2.24 (Pb), 0.95 (Zn), 0.12 (Cu) and 0.006 (Cd). The higher inventories for each metal at site 1, compared with site 2, are possibly a result of the proximity of site 1 to steeper areas in the loch and, as a result, a higher input of sediment (reflected in the higher sedimentation rate at site 1) and pollutant metals from the slopes to site 1.

7. Redox-cycling has influenced the behaviour of both Fe and, to a lesser extent, Mn in this loch, as evidenced by both the solid and solution phase data. However, acidification effects are also important, the solid phase surface peaks for Fe being attributable to both redox-driven diagenesis and a pH-related increase in the precipitation of Fe humic substances in the surficial sediment. An increase in the solid phase Mn concentration below 1 cm in the sediment is attributed to surface water acidification, specifically a pH-related decrease in the efficiency of Mn deposition, but also some loss of Mn from the sediment to the water column, both processes resulting in loss of Mn from the loch by hydraulic flushing. Mn enhancements at the sediment surface appear to be transient and may be a seasonal effect.

Chapter 4 Loch Lomond

4.1 Study Area

Loch Lomond, the largest freshwater body in Britain, is situated 30 km north-west of Glasgow. The loch occupies a narrow glacial valley, which lies across the major Highland Boundary fault, marked by a series of islands extending from Balmaha to Arden (Fig. 4.1). The surrounding catchment consists of agricultural land to the south, with mountainous terrain, overlain by peaty moorland, in the north.

In the past, there were several minor industries in the area, such as iron smelters and tanneries (17th century), printing and dyeing (19th and early 20th century) and mining of lead and zinc ores (in the mineralised area of Tyndrum to the north of the loch). Today, although the loch is an important drinking water reservoir and is used for recreational purposes, the area remains relatively unpopulated, with the major loch town of Balloch having a population of only 1,500.

Geology

The Highland Boundary fault (marked by a band of serpentine) essentially divides Loch Lomond into two geologically different sections. The northern 'highland' section of 18 km length lies in a steep-sided trough of metamorphosed Dalradian mica schists, has a maximum water depth of almost 200 m and is broken up by a number of small islands (Slack, 1954). South of this, between Inverberg and Rowardennan, there is an outcrop of resistant grit (water depth 15 m) which isolates the northern 'upper loch' from a short (3 km length) section (max. water depth 66 m) overlying mica schists and schistose grits, and spreading out over Carboniferous and Devonian sedimentary rocks and alluvial deposits in the lower loch (max. depth 31 m) (Lovell, 1985). Loch Lomond was below sea level during the late Devensian and sediment cores collected from the southern basin have shown evidence of a further marine transgression which lasted from around 5,450 to 6,900 y B.P. (Dickson *et al.*, 1978). This transgression resulted in marine sediment layers lying between freshwater sediments and has been useful for studying long-term migration of elements, for modelling migration of radioactive waste from a repository (MacKenzie *et al.*, 1983).

Viewed in profile (Fig.4.2), Loch Lomond is composed of four separate basins (Maitland, 1981) which have been characterised by Slack (1954) on the basis of geological, physical and chemical data into the 'upper' and 'lower' loch with a possible distinction of a further 'intermediate' central loch (basin C).

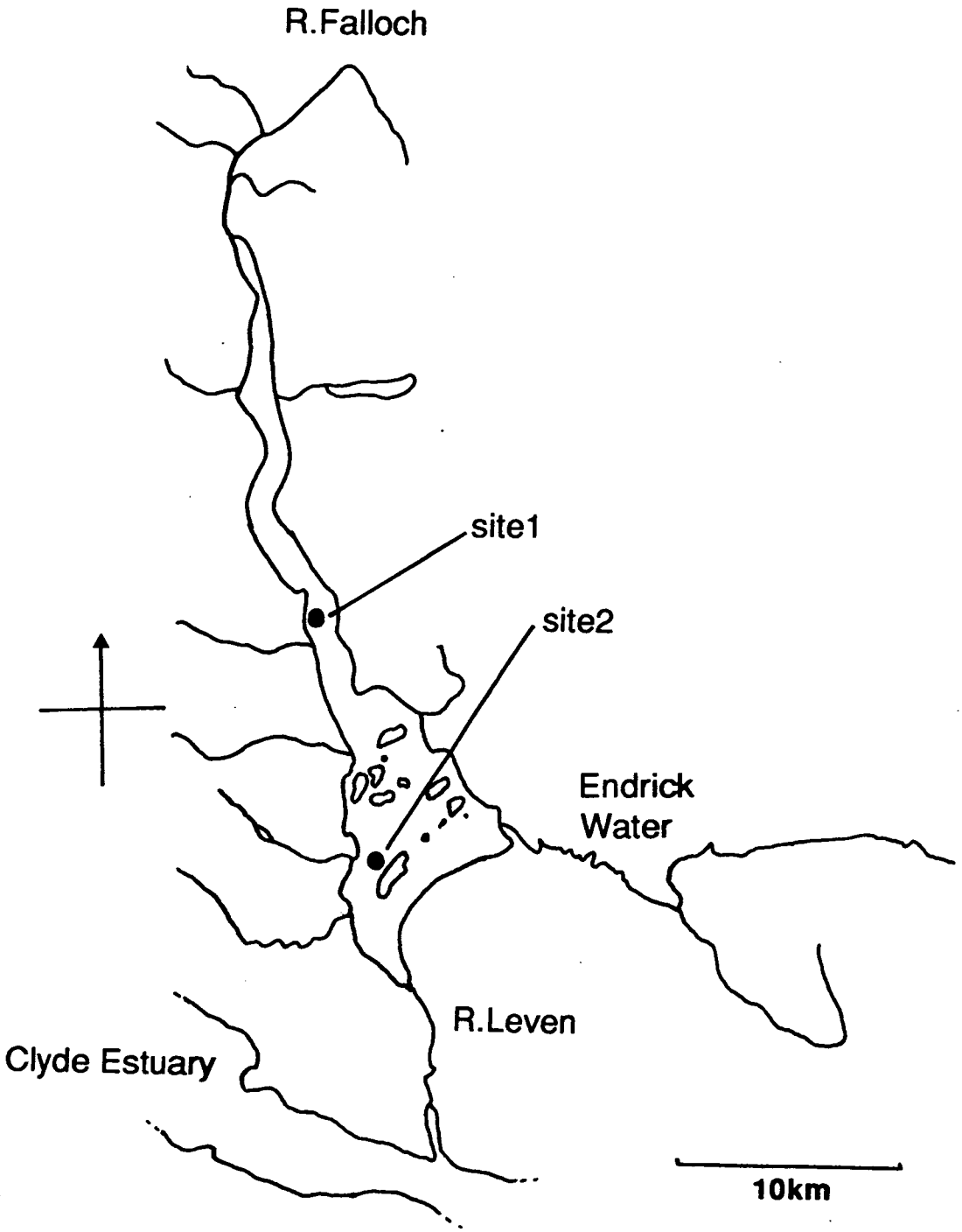

Fig. 4.1 Loch Lomond showing sampling sites 1 and 2 (•)

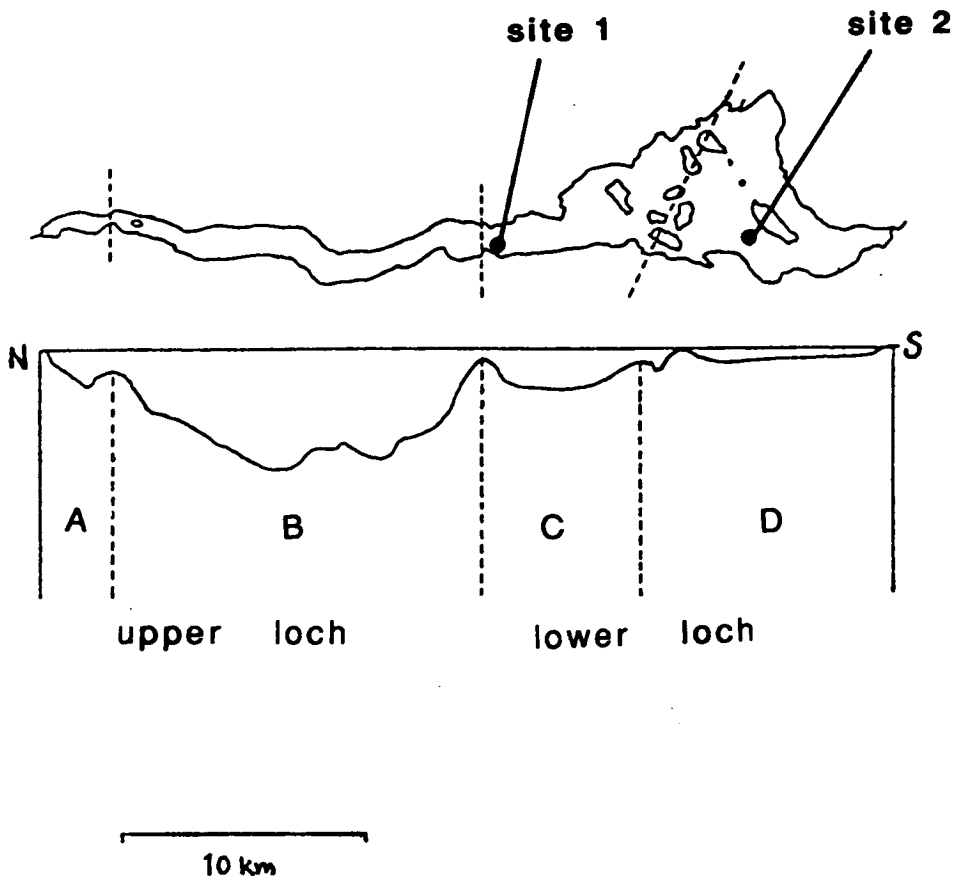

Fig. 4.2 Depth profile of Loch Lomond, showing the 4 basins A, B, C and D, North to South (Maitland, 1981) and sampling sites 1 and 2 (●)

Hydrology

The major rivers influencing Loch Lomond are the Falloch, Endrick, Luss (inflows) and Leven (outflow). The river Falloch drains a catchment (80 km^2) of metamorphic rocks, overlain by peat and poor in available nutrients. In contrast, the river Endrick drains 220 km^2 of productive farmland on beds of boulder clay and glacial marine deposits. Nutrient input is usually greatest in the south due to the Endrick, but the loch water is, on the whole, low in the major nutrients, nitrate, phosphate and silicate, for most of the year (Maulood and Boney, 1980). Trends in nutrient concentration tend to follow expected seasonal cycling patterns, with relatively high levels in the winter (lowest productivity) and low levels in the summer (highest productivity). An additional effect of the different drainage basins is the difference in water chemistry between the north and south basins. Slack (1954) found a pH of 6.6 in the upper loch and 7.6 in the south.

The upper loch (basin B) develops a stable thermocline from May-January, the central basin C from May-November and the southern basin only from June-August, because of turbulence and more rapid mixing in the shallower waters. The annual mean temperature is higher in the south (14°C at the surface) than in the north (11.7°C) and, even during stratification, Maulood and Boney (1980) found oxygen saturation was generally high and never fell below 72% in the north or 78% in the rest of the loch.

Sedimentology

According to Slack (1954), the bottom deposits of Loch Lomond fall into two main categories. In the south are brown muds with a thin, near-surface rust-red layer; to the north are black micaceous oozes, overlain by thin dark-brown unconsolidated material. Porosities are high: 80-98% (north) and 90-99% (south) over the top 20 cm (Farmer and Lovell, 1986). Surficial organic carbon content is greater in the north (10-20%) than in the south (5-10%) (Slack, 1954; Farmer and Lovell, 1986) and decreases more slowly with depth in the northern basin, due to increasing acidity and lower temperature of the bottom waters in the north. Additionally there is a greater proportion of peaty, allochthonous material, more resistant to microbial degradation, in the north, compared with more autochthonous planktonic debris in the south (indicated by the slightly greater C/N ratio of 18 in the upper loch, compared with 15 in the lower loch).

Mineralogical analysis of a sediment core collected in the southern basin (MacKenzie *et al.*, 1983) showed a relatively uniform clay mineral content (about 80%) throughout the length (443 cm) of the core. From 0-72 cm the component clay

minerals were mica, kaolinite, chlorite and smectite and the non-clays (approximately 20% of the sediment) were quartz and feldspars.

Biology

Loch Lomond is generally described as oligotrophic, tending to mesotrophic in the south. It has an abundant and varied fauna owing to its habitat diversity. There are zoological differences between the upper and lower lochs with 62 invertebrate taxa identified by Smith (in Maitland, 1981) in the northern loch. Fish species include trout, powan and perch, which are common throughout the loch, while pike and roach are usually restricted to the southern loch (Lovell, 1985).

4.2 Sampling and analysis

All samples were collected from the Glasgow University catamaran based at Rowardennan, where glovebox core sectioning was carried out in the laboratory of the Glasgow University Field Station.

4.2.1 Site 1 (central basin)

Sampling of the loch was initially carried out on 25.4.90 in the central basin (Fig.4.1 and basin C in Fig. 4.2) at a water depth of 45 m. Water column samples (surface, 3 m, 15 m and 30 m) were collected with a van Dorn sampler (Chapter 2) and pH, conductivity and $\%O_2$ were measured (Table 4.1).

Two sediment cores (Lo1-A and Lo1-B, Table 4.2) were collected at a site near to where the water column was sampled, at a depth of 13 m, using a Mini-Mackereth corer (Chapter 2). The water column sampling site was found to be unsuitable for coring because of steep slopes. The cores had an unconsolidated layer of 2-5 mm, followed by a red-brown layer of approximately 2 cm, below which the sediment was grey-brown. Core lengths were 82 cm (Lo1-A) and 83 cm (Lo1-B). Water overlying the sediment in the core tube was removed by syringe, filtered via 0.45 µm filters, treated and stored as porewater samples (see Chapter 2 for details). Core Lo1-A was sectioned on shore at 1 cm vertical intervals and used for γ-spectrometric analysis. Core Lo1-B was sectioned at 1 cm vertical intervals to 20 cm, 2 cm intervals to 40 cm, followed by 5 cm intervals to the base of the core. This core was used for acid digestion (HNO_3/HCl) of all sediment sections and sequential extraction of sections 0-40 cm, as described in Chapter 2. However, fraction V was not obtained because of experimental problems involving sample loss. Sample solutions were then analysed for metals.

4.2.2 Site 2 (southern basin)

Water column samples (surface, 5 m and 10 m) were collected on 26.4.90 from site 2 in the southern basin (Fig.4.1 and 4.2) using the van Dorn sampler (Chapter 2). Sub-samples were filtered via 0.45 µm filters and all samples were acidified and stored as described in Chapter 2.

Two sediment cores (Table 4.2) were collected at a water depth of 13 m using the Mini-Mackereth corer (Chapter 2). Core Lo2-1A, used for γ-spectrometry, was 91 cm in length with a surface 1 cm brown layer, followed by 0.5 cm of dark brown

Table 4.1 Water column characteristics in Loch Lomond

	site 1 (25.4.90)		site 2 (26.4.90)	
secchi disc (m)	8.5		6	
OS grid ref.	NS 347 995		NS 372 881	
	water depth (m)	pH	water depth (m)	pH
	surface (0)	7.04	0	7.04
	3	6.94	5	7.12
	15	6.98	10	7.18
	30	6.95		

	site 1			site 2		
water depth (m)	T. (°C)	cond. (µS)	O_2 (%)	T. (°C)	cond. (µS)	O_2 (%)
0	8.7	34.7	100	7.9	41.4	94
1	8.6	34.6	100	7.9	41.3	94
2	8.4	33.0	100	7.8	41.2	95
3	7.0	28.7	96	7.8	41.2	95
4	6.7	27.5	94	7.8	41.2	96
5	6.6	27.4	94	7.8	41.2	96
6	6.6	27.4	94	7.8	41.2	96
7	6.6	27.3	94	7.8	41.2	96
8	6.6	27.3	94	7.8	41.1	95
9	6.6	27.2	92	7.8	41.1	95
10	6.6	27.2	92	7.8	41.1	95
11	...	...	...	7.8	41.1	95
12	6.6	27.1	92	7.7	41.0	94
14	6.6	27.2	92			
16	6.5	27.2	92			
18	6.5	27.2	90			
20	6.5	27.0	90			
22	6.5	27.1	90			

Table 4.2 Core codes, sampling dates, type of corer and purpose of core collection from Loch Lomond

core code	location	sampling date	type of corer	core purpose
Lo1-A	site 1	25.4.90	Mini-Mackereth	γ-spectrometry
Lo1-B	"	"	"	chemical digestion
Lo2-1A	site 2	26.4.90	"	γ-spectrometry
Lo2-1B	"	"	"	chemical digestion
Lo2-1C	"	"	Jenkin	porewater analysis
Lo2-2C	"	26.11.91	"	porewater analysis

sediment, less compacted sediment to a depth of 10 cm, a dark grey compacted layer to 14 cm, mid-grey brown to 23 cm and light grey brown below this. The core was sectioned at 1 cm vertical intervals. Core Lo2-1B was 90 cm in length and sediment from this core was sequentially extracted and acid digested (Chapter 2). In this core (Lo2-1B) the less compacted sediment to 14 cm had a surface 1.5 cm of brown sediment, followed by dark brown sediment 1 cm thick. The more compacted dark grey sediment reached 17 cm, mid-grey brown to 25 cm and was light grey below this. The core was sectioned at 1 cm vertical intervals to 20 cm, at 2 cm intervals to 40 cm and 5 cm intervals below this. As at site 1, sequential extraction (all five fractions) was carried out on samples to 40 cm and HNO_3/HCl digestions on all sample depths, followed by metal analyses (Chapter 2).

A Jenkin corer (Chapter 2) was used to collect sediment core Lo2-1C at the same site for porewater sampling using the syringe method (Chapter 2) with a stainless steel needle and neoprene syringe stopper. The porewater was extracted by hand-forced filtration through a 0.45 μm filter and the filtered samples were stored in 20 ml self-sealing glass vials. Samples were acidified prior to analysis, upon removal of vial tops.

Further sediment (core Lo2-2C, Table 4.2) was collected with a Jenkin sampler on 26.11.91 for porewater samples. Sediment was sectioned at 1 cm vertical intervals in a nitrogen-purged glovebox (Chapter 2), centrifuged and the porewater was passed via 0.1 μm filters (syringes used for filtration had teflon stoppers). The filtered porewater samples were acidified and stored in 30 ml Nalgene plastic 'low metal' bottles, before metal analysis (Chapter 2). Residual sediment was collected from the filters and digested by HNO_3/HCl for analyis of the solid phase metal concentrations. Water overlying the sediment in the core tube was collected by syringe and passed through a 0.1 μm filter, treated and stored as for porewaters.

Water chemistry results for sites 1 and 2 are shown in Table 4.2 and methods used for measurements are described in Chapter 2.

4.3 Results

Data are listed in Tables 4.3-4.20. Figures based on the data are presented in Section 4.4 (Discussion).

1. Tables 4.3-4.6 contain wet and dry sediment section weights, mid-section cumulative weights (g cm^{-2}), porosities and, where measured, carbon content and C/N ratios. Porosities were calculated assuming solid sediment densities of 2.48 g cm^{-3} (site 1) and 2.46 g cm^{-3} (site 2).

2. Total ^{210}Pb, excess ^{210}Pb and depths (as cm and mid-section cumulative weights) are listed in Tables 4.7 and 4.8. At site 1, ^{226}Ra concentrations were found to be higher than the constant total ^{210}Pb concentrations at depths below 10 cm. A value of 35 ± 10 Bq kg^{-1} was therefore obtained by taking the mean of total ^{210}Pb concentrations below 10 cm. At site 2, ^{226}Ra was undetectable in many of the samples and total ^{210}Pb values did not clearly indicate a supported ^{210}Pb component at the maximum depth to which the sediment was counted. For this reason it was assumed that the supported ^{210}Pb value at site 2 was equal to that at site 1.

3. Radiocaesium concentrations and $^{134}Cs/^{137}Cs$ activity ratios are presented in Tables 4.9 and 4.10. Mean ^{134}Cs concentrations (x ^{134}Cs) represent the mean value of concentrations using the 605 keV and 796 keV γ lines. Where ^{134}Cs was detectable at 605 keV, but not at 796 keV, the former value was used to calculate the $^{134}Cs/^{137}Cs$ activity ratio.

4. Tables 4.11-20 contain metal data for sediment acid digestions, sequential extractions and solution phase (porewater and water column from sites 1 and 2). Column headings for metal concentrations in sequentially extracted sediment refer to the following:

I 1M ammonium acetate, pH7, 20°C (exchangeable fraction)

II 1M sodium acetate, pH5 with acetic acid, 20°C ("carbonate bound"/specifically sorbed)

III 0.1M hydroxylammonium chloride/0.01M nitric acid, 20°C (easily reducible)

IV 1M hydroxylammonium chloride/4.4M acetic acid, 20°C (moderately reducible)

V 30% w/v hydrogen peroxide, pH2, 85+/-2°C; 3.2M ammonium acetate in 3.2M nitric acid (organic fraction/sulphides)

Sum I-V refers to the sum of metal concentrations in all fractions.

5. Cd was not detectable ($\leq 1x10^{-4}$ mg l^{-1}) in any of the porewater or water column samples. Cu was below detection limit (≤ 0.01 mg l^{-1}) in porewaters of core Lo2-2C at site 2 and in all water column samples.

6. (BDL) is entered where samples were below detection limit, and (...) where a result was not available.

Table 4.3 Some physical characteristics, carbon content and carbon/nitrogen ratios of Loch Lomond sediment core Lo2-1A.

section depth (cm)	wet section weight (g)	dry section weight (g)	mid-section cumulative weight (g cm^{-2})	porosity (%)	carbon content (%)	C/N ratio
0-1	20.211	2.463	0.037	94.6	5.69	11.6
1-2	37.532	4.752	0.146	94.4	4.12	12.1
2-3	35.289	5.714	0.304	92.7	4.25	13.3
3-4	28.422	5.198	0.468	91.7	4.52	11.6
4-5	27.216	4.734	0.618	92.1	4.51	9.8
5-6	36.119	7.557	0.803	90.3	4.39	10.7
6-7	37.929	8.602	1.046	89.3	4.09	13.2
7-8	34.655	8.344	1.302	88.6	3.86	11.7
8-9	35.310	8.361	1.553	88.8	4.10	14.6
9-10	33.946	8.064	1.801	88.8	3.73	14.3
10-11	31.725	7.702	2.038	88.5	...	...
11-12	36.514	10.144	2.308	86.5	...	...
12-13	38.538	11.843	2.639	84.7	...	...
13-14	37.992	12.841	3.011	82.8	...	...
14-15	41.076	14.967	3.430	81.1	...	...
15-16	41.921	15.308	3.886	81.0	...	...

core cross-section area = 33.18 cm^2

Table 4.4 Some physical characteristics of Loch Lomond sediment core Lo2-1B.

section depth (cm)	wet section weight (g)	dry section weight (g)	mid-section cumulative weight (g cm^{-2})	porosity (%)
0-1	18.914	2.340	0.035	95.1
1-2	43.423	6.023	0.161	93.8
2-3	29.040	4.558	0.321	93.0
3-4	29.259	4.524	0.458	93.1
4-5	28.569	4.834	0.599	92.4
5-6	29.818	5.518	0.755	91.5
6-7	28.232	6.071	0.929	90.0
7-8	29.870	6.745	1.122	89.4
8-9	32.681	7.220	1.333	89.7
9-10	31.249	6.853	1.545	89.8
10-11	28.319	6.419	1.745	89.4
11-12	30.451	7.183	1.950	88.8
12-13	28.735	7.215	2.167	88.0
13-14	32.343	9.886	2.424	84.8
14-15	32.296	10.527	2.732	83.6
15-16	35.176	12.457	3.078	81.8
16-17	37.643	13.545	3.470	81.3
17-18	36.789	13.633	3.880	80.7
18-19	36.980	13.809	4.293	80.5
19-20	41.524	16.065	4.744	79.6
20-22	82.088	31.983	5.468	79.4
22-24	74.156	26.893	6.355	81.2
24-26	68.713	23.276	7.111	82.8
26-28	75.389	26.070	7.854	82.3
28-30	75.706	28.794	8.681	80.0
30-32	77.576	31.984	9.597	77.8
32-34	83.894	35.962	10.621	76.6
34-36	77.946	32.605	11.654	77.4
36-38	81.945	34.000	12.658	77.6
38-40	77.495	32.075	13.654	77.7
40-45	197.950	83.470	15.395	77.1
45-50	196.402	84.232	17.922	76.6
50-55	209.442	89.542	20.541	76.7
55-60	207.579	89.849	23.244	76.3
60-65	201.761	80.081	25.805	78.9
65-70	202.122	80.892	28.230	78.7
70-75	201.930	81.120	30.672	78.6
75-80	202.214	87.574	33.214	76.3

core cross-section area = 33.18 cm^2

Table 4.5 Some physical characteristics and carbon content of Loch Lomond sediment core Lo1-A

section depth (cm)	wet section weight (g)	dry section weight (g)	mid-section cumulative weight (g cm^{-2})	porosity (%)	carbon content (%)*
0-1	20.762	4.741	0.071	89.3	2.40
1-2	41.578	10.334	0.299	88.2	2.34
2-3	38.760	11.597	0.629	85.3	1.79
3-4	36.544	12.287	0.989	83.0	1.83
4-5	41.733	16.045	1.416	79.9	1.60
5-6	38.801	15.553	1.892	78.8	1.74
6-7	43.342	18.204	2.401	77.4	1.64
7-8	43.957	19.379	2.967	75.9	1.23
8-9	41.430	18.898	3.544	74.7	1.45
9-10	39.383	18.602	4.109	73.5	1.36
10-11	40.622	18.858	4.674	74.1	...
11-12	51.018	24.243	5.323	73.2	...
12-13	47.328	22.285	6.024	73.6	...
13-14	40.574	18.609	6.640	74.5	...
14-15	38.241	16.627	7.171	76.3	...
15-16	39.314	16.174	7.666	78.0	...

core cross-section area = 33.18 cm^2

* nitrogen was not detectable in this core.

Table 4.6 Some physical characteristics of Loch Lomond sediment core Lo1-B

section depth (cm)	wet section weight (g)	dry section weight (g)	mid-section cumulative weight ($g\ cm^{-2}$)	porosity (%)
0-1	24.211	5.812	0.088	88.7
1-2	33.464	9.742	0.322	85.8
2-3	35.676	11.665	0.644	83.6
3-4	44.290	15.419	1.053	82.3
4-5	39.611	15.641	1.521	79.2
5-6	36.478	14.988	1.982	78.0
6-7	40.085	18.563	2.488	74.2
7-8	43.804	18.571	3.047	77.1
8-9	45.869	20.089	3.630	76.1
9-10	52.223	24.701	4.305	73.4
10-11	45.574	21.003	4.994	74.4
11-12	43.804	19.235	5.600	76.0
12-13	41.468	19.029	6.177	74.5
13-14	38.525	19.524	6.758	70.7
14-15	43.572	24.700	7.424	65.4
15-16	48.015	26.689	8.198	66.5
16-17	45.854	25.492	8.985	66.4
17-18	49.155	25.208	9.749	70.2
18-19	45.998	23.457	10.482	70.4
19-20	43.633	21.176	11.155	72.4
20-22	86.866	42.479	12.114	72.2
22-24	85.310	43.873	13.415	70.1
24-26	88.762	45.532	14.762	70.2
26-28	82.330	44.793	16.124	67.5
28-30	77.043	39.700	17.397	70.0
30-32	83.345	38.935	18.582	73.9
32-34	85.115	40.680	19.782	73.0
34-36	83.353	41.233	21.016	71.7
36-38	91.670	45.578	22.324	71.5
38-40	88.639	34.869	23.536	79.3
40-45	223.593	117.363	25.830	69.2
45-50	231.119	121.619	28.486	69.1
50-55	232.056	131.706	33.249	65.4
55-60	237.262	137.802	37.310	64.2
60-65	229.436	122.516	41.233	68.4
65-70	227.412	115.092	44.814	70.8

core cross-section area = 33.18 cm^2

Table 4.7 ^{210}Pb and ^{226}Ra data for Loch Lomond sediment core Lo2-1A (26.4.90)

section depth (cm)	mid-section cumul. wt. ($g\ cm^{-2}$)	total ^{210}Pb ($Bq\ kg^{-1}$)	^{226}Ra ($Bq\ kg^{-1}$)	excess ^{210}Pb ($Bq\ kg^{-1}$)	ln (excess ^{210}Pb)
0-1	0.037	449 ± 68	BDL	414 ± 69	6.02
1-2	0.146	370 ± 32	BDL	335 ± 34	5.81
2-3	0.304	316 ± 30	BDL	281 ± 32	5.64
3-4	0.468	334 ± 23	BDL	299 ± 25	5.70
4-5	0.618	346 ± 39	100 ± 51	311 ± 40	5.74
5-6	0.803	364 ± 26	95 ± 46	329 ± 28	5.80
6-7	1.046	243 ± 22	BDL	208 ± 24	5.34
7-8	1.302	185 ± 27	84 ± 32	150 ± 29	5.01
8-9	1.553	196 ± 24	73 ± 32	161 ± 26	5.08
9-10	1.801	137 ± 23	BDL	102 ± 25	4.62
10-11	2.038	...	...	...	...
11-12	2.308	99 ± 24	BDL	64 ± 26	4.16
12-13	2.639	93 ± 22	82 ± 30	58 ± 24	4.06
13-14	3.011	...	...	...	
14-15	3.430	64 ± 28	BDL	BDL	
15-16	3.886	BDL	BDL	BDL	

Table 4.8 ^{210}Pb and ^{226}Ra data for Loch Lomond sediment core Lo1-A (25.4.90)

section depth (cm)	mid-section cumul. wt. ($g\ cm^{-2}$)	total ^{210}Pb ($Bq\ kg^{-1}$)	^{226}Ra ($Bq\ kg^{-1}$)	excess ^{210}Pb ($Bq\ kg^{-1}$)	ln (excess ^{210}Pb)
0-1	0.071	119 ± 40	BDL	84 ± 41	4.43
1-2	0.299	160 ± 30	50 ± 16	125 ± 32	4.83
2-3	0.629	125 ± 18	57 ± 23	90 ± 20	4.50
3-4	0.989	101 ± 13	64 ± 19	66 ± 16	4.19
4-5	1.416	44 ± 12	BDL	BDL	
5-6	1.892	95 ± 12	56 ± 13	60 ± 16	4.09
6-7	2.401	97 ± 12	58 ± 10	62 ± 16	4.13
7-8	2.967	95 ± 10	58 ± 12	60 ± 14	4.09
8-9	3.544	68 ± 11	54 ± 12	33 ± 15	3.50
9-10	4.109	55 ± 13	72 ± 15	BDL	
10-11	4.674	31 ± 8	60 ± 10		
11-12	5.323	28 ± 10	60 ± 10		
12-13	6.024	55 ± 8	62 ± 9		
13-14	6.640	30 ± 9	30 ± 11		
14-15	7.171	34 ± 8	63 ± 9		
15-16	7.666	31 ± 10	60 ± 11		

Table 4.9 Radiocaesium concentrations and $^{134}Cs/^{137}Cs$ activity ratios for Loch Lomond sediment core Lo2-1A (26.4.90).

section depth (cm)	^{137}Cs 661 keV (Bq kg^{-1})	^{134}Cs 605 keV (Bq kg^{-1})	^{134}Cs 796 keV (Bq kg^{-1})	X^{134}Cs (Bq kg^{-1})	$^{134}Cs/^{137}Cs$
0-1	943 ± 13	144 ± 14	152 ± 23	148 ± 13	0.157 ± 0.014
1-2	1,366 ± 8	221 ± 6	231 ± 11	226 ± 6	0.165 ± 0.005
2-3	1,482 ± 8	231 ± 6	232 ± 10	231 ± 6	0.156 ± 0.004
3-4	790 ± 5	95 ± 4	100 ± 6	98 ± 4	0.124 ± 0.004
4-5	622 ± 8	6 ± 3	BDL		0.010 ± 0.005
5-6	931 ± 6	BDL	"		
6-7	869 ± 5	"	"		
7-8	503 ± 4	"	"		
8-9	224 ± 4	"	"		
9-10	100 ± 3	"	"		
10-11	37 ± 2	"	"		
11-12	18 ± 3	"	"		
12-13	10 ± 3	"	"		
13-14	5 ± 2	"	"		
14-15	7 ± 3	"	"		

Table 4.10 Radiocaesium concentrations and $^{134}Cs/^{137}Cs$ activity ratios for Loch Lomond sediment core Lo1-A (25.4.90).

section depth (cm)	^{137}Cs 661 keV (Bq kg^{-1})	^{134}Cs 605 keV (Bq kg^{-1})	^{134}Cs 796 keV (Bq kg^{-1})	X^{134}Cs (Bq kg^{-1})	$^{134}Cs/^{137}Cs$
0-1	407 ± 6	49 ± 6	52 ± 12	50 ± 6	0.123 ± 0.016
1-2	368 ± 2	48 ± 2	51 ± 4	50 ± 2	0.136 ± 0.006
2-3	255 ± 3	27 ± 3	29 ± 3	29 ± 3	0.115 ± 0.012
3-4	161 ± 2	13 ± 2	13 ± 5	13 ± 3	0.079 ± 0.016
4-5	127 ± 2	BDL	BDL		
5-6	201 ± 2	"	"		
6-7	221 ± 1	"	"		
7-8	180 ± 2	"	"		
8-9	100 ± 2	"	"		
9-10	32 ± 1	"	"		
10-11	13 ± 1	"	"		
11-12	6 ± 1	"	"		
12-13	2 ± 1	"	"		

Table 4.11 Fe, Mn, Pb, Zn, Cu, Cd, Co and Ni concentrations in HNO_3/HCl digested Loch Lomond sediment core Lo2-1B

depth (cm)	Fe %	Mn %	Pb mg kg^{-1}	Zn mg kg^{-1}	Cu mg kg^{-1}	Cd mg kg^{-1}	Co mg kg^{-1}	Ni mg kg^{-1}
0-1	5.0	3.2	60	312	37	1.6	28	61
1-2	5.7	3.2	59	289	32	1.1	30	57
2-3	7.2	1.8	76	358	32	1.3	33	61
3-4	7.6	1.1	95	421	35	2.0	32	64
4-5	6.8	0.88	114	530	38	1.9	29	63
5-6	6.3	0.70	124	530	39	1.4	31	66
6-7	6.2	0.58	121	496	39	1.9	32	61
7-8	6.1	0.52	117	475	38	1.7	32	62
8-9	6.0	0.51	119	459	38	1.5	34	65
9-10	...	0.51	129	477	40	1.4	34	65
10-11	6.7	0.49	120	403	36	1.2	30	59
11-12	6.8	0.48	130	408	37	1.3	31	61
12-13	6.4	0.45	126	376	36	1.2	31	62
13-14	5.8	0.36	119	329	35	0.8	30	58
14-15	5.4	0.32	107	290	36	0.8	28	58
15-16	5.3	0.30	93	239	37	0.7	29	55
16-17	5.3	0.28	82	206	37	0.8	30	54
17-18	5.1	0.28	82	195	38	0.6	29	55
18-19	5.3	0.26	81	175	37	0.6	30	54
19-20	5.3	0.27	73	163	36	0.5	29	52
20-22	5.1	0.26	67	145	35	0.4	27	54
22-24	5.8	0.32	82	145	31	0.5	29	56
24-26	6.2	0.33	92	134	31	0.4	28	59
26-28	6.1	0.31	62	124	29	0.4	31	60
28-30	6.0	0.28	42	108	30	0.4	28	58
30-32	5.8	0.25	37	105	32	0.4	28	60
32-34	5.9	0.24	29	104	31	0.4	26	55
34-36	6.0	0.26	32	105	30	0.4	26	55
36-38	6.1	0.28	31	100	32	BDL	27	54
38-40	6.3	0.27	30	121	31	0.3	27	58
40-45	6.0	0.26	31	124	30	0.3	28	53
45-50	6.1	0.25	27	100	31	0.4	28	55
50-55	6.2	0.26	26	..89	30	BDL	29	57
55-60	6.3	0.26	24	101	30	"	28	53
60-65	6.7	0.29	22	108	28	"	28	56
65-70	6.7	0.29	23	104	28	"	30	58
70-75	6.4	0.28	22	111	28	"	28	52
75-80	6.1	0.24	24	113	28	"	26	51

Table 4.12 Fe, Mn, Pb, Zn, Cu, Cd, Co and Ni concentrations in HNO_3/HCl digested Loch Lomond sediment core Lo1-B

depth (cm)	Fe %	Mn mg kg^{-1}	Pb mg kg^{-1}	Zn mg kg^{-1}	Cu mg kg^{-1}	Cd mg kg^{-1}	Co mg kg^{-1}	Ni mg kg^{-1}
0-1	3.70	1,980	35	129	25	0.8	21	34
1-2	4.12	7,820	39	139	27	0.7	28	38
2-3	3.89	3,570	37	133	24	0.5	24	33
3-4	4.47	3,330	36	143	24	0.5	24	34
4-5	4.15	1,020	38	138	25	0.7	21	34
5-6	3.74	840	41	148	25	0.9	20	35
6-7	3.44	790	40	138	25	0.5	19	34
7-8	4.40	870	33	120	23	BDL	21	31
8-9	4.85	910	36	96	22	"	20	30
9-10	4.84	820	40	87	21	"	18	30
10-11	3.96	732	32	87	20	"	16	28
11-12	5.25	800	34	80	22	"	20	30
12-13	4.09	750	22	83	23	"	20	32
13-14	3.78	658	14	74	20	"	16	26
14-15	3.12	495	9	58	15	"	15	24
15-16	3.00	460	8	62	15	"	15	22
16-17	3.10	495	12	68	16	"	16	27
17-18	3.07	511	12	64	16	"	15	28
18-19	2.81	493	10	64	15	"	15	26
19-20	2.88	493	8	65	15	"	15	26
20-22	2.65	488	12	64	16	"	16	24
22-24	2.47	440	10	61	14	"	18	24
24-26	2.88	492	9	66	16	"	18	25
26-28	3.38	472	8	69	15	"	18	24
28-30	3.22	464	10	68	16	"	17	25
30-32	3.00	492	11	70	16	"	17	28
32-34	2.80	511	9	64	15	"	15	27
34-36	2.97	552	6	64	15	"	19	28
36-38	3.74	576	8	69	17	"	24	28
38-40	3.94	534	11	69	17	"	20	27
40-45	4.68	651	...	...	21	"	21	31
45-50	3.76	616	14	86	21	"	24	36
50-55	5.41	653	13	92	22	"	21	34
55-60	3.59	523	17	98	23	"	19	35
60-65	3.46	558	18	104	26	"	22	40
65-70	3.58	...	16	90	24	0.3	28	40

Table 4.13 Fe and Mn concentrations in sequentially extracted Loch Lomond sediment core Lo2-1B

	Fe (%) fractions						Mn (%) fractions					
depth (cm)	I	II	III	IV	V	sum I-V	I	II	III	IV	V	sum I-V
0-1	0.023	0.049	0.34	1.17	1.31	2.89	0.009	0.034	3.62	0.22	0.021	3.90
1-2	0.018	0.039	0.29	1.32	1.40	3.06	0.009	0.041	3.85	0.35	0.039	4.29
2-3	0.006	0.12	0.23	1.70	1.72	3.78	0.140	0.103	1.45	0.19	0.055	1.94
3-4	0.005	0.23	0.22	1.46	2.18	4.10	0.378	0.204	0.31	0.13	0.076	1.10
4-5	0.011	0.27	0.22	1.54	2.20	4.24	0.490	0.209	0.15	0.090	0.064	1.00
5-6	0.005	0.24	0.22	1.50	1.76	3.72	0.414	0.140	0.10	0.067	0.052	0.77
6-7	0.006	0.23	0.20	1.22	1.61	3.26	0.323	0.108	0.072	0.047	0.046	0.60
7-8	0.002	0.20	0.19	1.12	1.33	2.84	0.294	0.093	0.059	0.043	0.042	0.53
8-9	0.007	0.20	0.25	1.20	1.23	2.89	0.312	0.079	0.052	0.040	0.043	0.53
9-10	0.002	0.28	0.26	1.34	1.28	3.16	0.316	0.065	0.026	0.036	0.037	0.48
10-11	0.004	0.26	0.29	1.98	1.35	3.89	0.339	0.075	0.042	0.052	0.033	0.54
11-12	0.002	0.22	0.22	1.36	1.10	2.90	0.298	0.083	0.044	0.043	0.037	0.50
12-13	0.004	0.29	0.27	1.53	1.21	3.30	0.298	0.093	0.042	0.036	0.032	0.50
13-14	0.002	0.24	0.20	1.23	1.26	2.93	0.222	0.078	0.051	0.028	0.030	0.41
14-15	BDL	0.21	0.19	0.76	1.16	2.33	0.181	0.036	0.035	0.019	0.027	0.30
15-16	"	0.20	0.17	0.83	1.00	2.21	0.154	0.044	0.034	0.020	0.026	0.28
16-17	0.001	0.17	0.16	0.77	0.97	2.07	0.141	0.056	0.043	0.020	0.026	0.29
17-18	0.001	0.20	0.17	0.60	1.01	1.98	0.149	0.037	0.037	0.014	0.025	0.26
18-19	0.002	0.19	0.18	0.64	1.12	2.13	0.159	0.045	0.021	0.020	0.027	0.27
19-20	BDL	0.12	0.13	0.60	0.98	1.83	0.136	0.046	0.020	0.012	0.026	0.24
20-22	0.001	0.17	0.13	0.54	0.93	1.77	0.138	0.046	0.016	0.013	0.026	0.24
22-24	0.001	0.15	0.19	0.70	1.12	2.16	0.164	0.043	0.019	0.016	0.031	0.27
24-26	0.001	0.38	0.21	0.87	1.05	2.51	0.187	0.064	0.016	0.018	0.028	0.31
26-28	0.001	0.32	0.25	0.86	1.04	2.47	0.174	0.055	0.024	0.017	0.028	0.30
28-30	0.001	0.27	0.29	0.80	1.18	2.54	0.161	0.050	0.024	0.016	0.031	0.28
30-32	0.003	0.39	0.18	0.64	1.05	2.27	0.143	0.050	0.012	0.012	0.028	0.24
32-34	0.002	0.34	0.17	0.54	1.05	2.10	0.138	0.048	0.010	0.010	0.027	0.23
34-36	...	...	...	...	...	...	...	...	...	...	...	...
36-38	0.003	0.26	0.18	0.66	0.87	1.97	0.126	0.044	0.015	0.013	0.026	0.22
38-40	0.003	0.42	0.16	0.52	1.10	2.20	0.136	0.067	0.011	0.010	0.030	0.25

Table 4.14 Pb and Zn concentrations in sequentially extracted Loch Lomond sediment core Lo2-1B

	Pb (mg kg^{-1}) fractions						Zn (mg kg^{-1}) fractions					
depth (cm)	I	II	III	IV	V	sum I-V	I	II	III	IV	V	sum I-V
0-1	BDL	BDL	BDL	38	BDL	38	BDL	109	120	59	59	347
1-2	"	"	"	44	...	44	3	66	96	70	50	285
2-3	"	"	"	48	...	48	15	73	58	85	88	319
3-4	"	15	"	77	16	108	21	120	61	125	135	462
4-5	"	23	"	82	15	120	43	134	72	153	136	538
5-6	"	30	"	84	15	129	43	115	78	148	134	518
6-7	"	36	"	72	14	122	37	136	63	128	128	492
7-8	"	31	"	71	14	116	34	120	70	124	91	439
8-9	"	29	"	78	13	120	38	114	78	125	92	447
9-10	"	37	"	73	BDL	110	39	120	62	103	77	401
10-11	"	31	"	90	12	133	33	112	74	136	79	434
11-12	"	31	"	80	18	129	27	98	55	103	81	364
12-13	"	35	"	75	15	125	23	110	59	96	67	355
13-14	"	34	"	78	13	125	22	95	49	90	68	324
14-15	"	33	"	56	13	102	19	78	38	58	56	249
15-16	"	23	"	53	9	85	8	48	25	46	46	173
16-17	"	21	"	52	6	79	6	39	23	41	41	150
17-18	"	23	"	42	BDL	65	6	45	20	29	40	140
18-19	"	23	"	46	10	79	4	33	20	31	39	127
19-20	"	17	"	48	8	73	3	22	17	33	37	112
20-22	"	21	"	38	8	67	3	27	12	24	33	99
22-24	"	18	"	46	8	72	1	18	15	26	37	97
24-26	"	24	"	47	9	80	0.8	22	8	15	27	73
26-28	"	11	"	27	4	42	BDL	16	8	15	24	63
28-30	"	9	"	21	BDL	30	"	13	10	11	29	63
30-32	"	7	"	19	"	26	"	14	4	8	26	52
32-34	"	6	"	14	"	20	"	10	3	8	25	46
34-36	...	...	...	...	...	...	...	...	...	...	...	...
36-38	"	4	"	13	"	17	"	8	3	6	20	37
38-40	"	7	"	10	"	17	"	10	2	7	24	43

Table 4.15 Cu concentrations in sequentially extracted* Loch Lomond cores Lo1-B and Lo2-1B

depth (cm)	Lo1-B (mg kg^{-1}) fraction IV	Lo2-1B (mg kg^{-1}) fractions IV	V	sum IV + V
0-1	1.3	9	20	29
1-2	0.9	6	23	29
2-3	0.8	8	14	22
3-4	0.6	8	18	26
4-5	0.9	10	21	31
5-6	0.8	8	23	31
6-7	0.7	7	22	29
7-8	1.2	7	21	28
8-9	0.9	7	17	24
9-10	0.8	7	18	25
10-11	0.9	7	17	24
11-12	1.2	8	18	26
12-13	1.3	8	18	26
13-14	1.5	7	16	23
14-15	1.1	6	16	22
15-16	0.8	7	17	24
16-17	0.5	6	22	28
17-18	0.3	6	18	24
18-19	0.5	6	18	24
19-20	0.5	5	17	22
20-22	0.5	4	14	28
22-24	0.4	5	20	25
24-26	0.5	4	15	19
26-28	1.4	5	12	17
28-30	1.0	5	14	19
30-32	0.7	4	14	18
32-34	0.4	6	13	19
34-36	0.8	3	12	15
36-38	0.6	4	11	15
38-40	0.9	4	14	18

* Copper was not detectable in fractions I-III

Table 4.16 Fe and Mn concentrations in sequentially extracted Loch Lomond sediment core Lo1-B

	Fe (%) fractions					Mn (mg kg^{-1}) fractions				
depth (cm)	I	II	III	IV	sum I-IV	I	II	III	IV	sum I-IV
0-1	0.0002	0.016	0.11	0.36	0.49	0.8	59	2,300	760	3,120
1-2	0.0002	0.004	0.095	0.27	0.37	0.4	46	4,700	2,400	7,146
2-3	0.0002	0.003	0.065	0.26	0.33	0.5	49	3,200	2,200	5,450
3-4	0.0003	0.004	0.042	0.18	0.23	1.2	64	2,000	760	2,825
4-5	BDL	0.010	0.049	0.18	0.24	37	204	400	210	851
5-6	0.0001	0.008	0.061	0.17	0.24	109	256	130	80	575
6-7	0.0001	0.014	0.061	0.18	0.26	109	248	120	70	547
7-8	0.0001	0.018	0.059	0.26	0.34	147	264	150	100	661
8-9	0.0001	0.019	0.056	0.31	0.38	116	266	140	100	622
9-10	0.0001	0.016	0.071	0.33	0.42	86	241	120	70	517
10-11	0.0001	0.053	0.084	0.28	0.42	99	244	120	70	533
11-12	0.0002	0.037	0.10	0.31	0.45	147	236	120	80	583
12-13	0.0004	0.037	0.085	0.28	0.40	121	229	120	80	550
13-14	0.0003	0.039	0.083	0.24	0.36	98	197	80	50	425
14-15	0.0002	0.028	0.063	0.23	0.32	73	160	70	40	343
15-16	0.0002	0.041	0.075	0.17	0.29	64	139	60	30	293
16-17	0.0001	0.020	0.056	0.15	0.23	75	112	40	30	257
17-18	0.0001	0.021	0.056	0.14	0.22	68	126	60	40	294
18-19	0.0002	0.030	0.072	0.15	0.25	84	134	50	30	298
19-20	0.0002	0.025	0.061	0.18	0.27	92	146	50	40	328
20-22	0.0002	0.019	0.060	0.18	0.26	87	126	50	40	303
22-24	0.0002	0.028	0.068	0.18	0.28	68	102	40	30	240
24-26	0.0002	0.034	0.078	0.19	0.30	58	101	40	30	229
26-28	0.0002	0.091	0.13	0.37	0.59	43	92	30	30	195
28-30	0.0003	0.065	0.11	0.35	0.52	49	96	40	30	215
30-32	0.0003	0.048	0.098	0.24	0.39	64	107	40	20	231
32-34	0.0002	0.039	0.079	0.22	0.34	65	119	50	40	274
34-36	0.0003	0.11	0.19	0.51	0.81	64	157	90	70	381
36-38	0.0004	0.13	0.12	0.79	1.04	56	133	80	60	329
38-40	0.0004	0.18	0.18	0.70	1.06	53	140	60	40	293

Table 4.17 Pb and Zn concentrations in sequentially extracted Loch Lomond sediment core Lo1-B.

	Pb (mg kg^{-1}) fractions					Zn (mg kg^{-1}) fractions				
depth (cm)	I	II	III	IV	sum I-IV	I	II	III	IV	sum I-IV
0-1	BDL	3.1	3.6	36	43	BDL	16	16	34	66
1-2	"	BDL	3.1	28	31	"	6.3	19	36	61
2-3	"	1.2	1.7	27	30	"	5.0	12	29	46
3-4	"	1.2	0.7	20	22	"	3.5	6.4	29	39
4-5	"	4.2	1.9	23	29	"	2.4	4.1	33	40
5-6	"	11	2.1	26	39	"	3.1	4.3	39	46
6-7	"	6.8	1.0	22	30	"	4.5	4.7	19	28
7-8	"	2.2	BDL	18	20	"	5.2	4.7	24	34
8-9	"	1.2	0.5	13	15	"	3.7	3.5	18	25
9-10	"	1.3	BDL	14	15	"	2.0	2.2	14	18
10-11	"	3.5	"	20	24	"	1.2	1.2	10	12
11-12	"	4.6	1.2	21	27	"	0.89	1.5	14	16
12-13	"	3.0	0.8	14	18	"	1.1	1.2	10	12
13-14	"	3.3	BDL	12	15	"	1.3	1.3	8	11
14-15	"	2.7	"	10	13	"	0.96	0.90	7	8.9
15-16	"	3.0	0.6	9	13	"	0.86	0.75	5	6.6
16-17	"	2.9	BDL	9	12	"	0.12	0.41	6	6.5
17-18	"	2.5	0.6	8	11	"	0.23	0.36	4	4.6
18-19	"	4.5	BDL	10	14	"	0.22	0.38	8	8.6
19-20	"	4.7	"	11	16	"	BDL	0.56	12	13
20-22	"	3.8	"	10	14	"	0.33	1.4	14	16
22-24	"	4.3	"	9	13	"	1.5	2.0	15	18
24-26	"	3.2	"	10	13	"	1.2	1.3	11	14
26-28	"	2.9	"	11	14	"	1.1	1.7	7	9.8
28-30	"	2.6	"	10	13	"	0.54	1.0	..7	8.5
30-32	"	3.5	"	10	14	"	0.52	1.0	8	9.5
32-34	"	2.9	"	9	12	"	1.2	1.7	17	20
34-36	"	2.1	"	10	12	"	2.2	2.9	16	21
36-38	"	1.2	"	8	9	"	0.61	1.6	14	16
38-40	"	2.6	"	8	11	"	0.65	2.4	10	13

Table 4.18 Fe, Mn, Pb, Zn and Cu concentrations in the water column and in porewaters from Loch Lomond sediment core Lo2-1C

water column depth (m)	Fe ($mg\ l^{-1}$)	Mn ($mg\ l^{-1}$)	Pb ($mg\ l^{-1}$)	Zn ($mg\ l^{-1}$)	Cu ($mg\ l^{-1}$)
surface (0)	...	BDL (0.005)	BDL (0.005)	≤blank	BDL (")
5	...	BDL (0.009)	BDL (0.01)	0.003(0.004)	BDL (")
10	...	BDL (0.006)	BDL (0.006)	≤blank	BDL (")
core water	...	BDL (0.026)	BDL (0.01)	0.006(0.009)	BDL (")
porewater depth (cm)					
0-1	...	...	...	...	...
1-2	5.2	...	BDL	0.105	0.018
2-3	7.4	...	0.005	0.082	0.025
3-4	11	18	0.008	0.095	0.025
4-5	...	...	...	...	...
5-6	9.8	16	0.009	0.078	0.035
6-7	19	26	0.005	0.024	0.015
7-8	10	19	0.005	0.045	0.019
8-9	...	...	0.011	0.030	0.092
9-10	...	...	...	...	...
10-11	16	16	0.014	0.088	0.035
11-12	...	15	0.019	0.110	0.039
detection limit		0.002	0.003	blank=0.006	0.01

Table 4.19 Fe, Mn, Pb and Zn concentrations in the water column and in porewaters from Loch Lomond sediment core Lo2-2C

porewater depth (cm)	Fe ($mg\ l^{-1}$)	Mn ($mg\ l^{-1}$)	Pb ($mg\ l^{-1}$)	Zn ($mg\ l^{-1}$)
0-1	0.27	3.7	BDL	0.103
1-2	0.13	22	"	...
2-3	1.29	22	"	0.087
3-4	1.53	21	"	0.047
4-5	0.30	24	"	0.033
5-6	2.01	21	0.012	0.021
6-7	2.39	26	0.004	0.027
7-8	2.49	24	BDL	...
8-9	...	34	BDL	0.026
9-10	21	...	0.010	0.021
10-11	34	31	0.029	0.058
11-12	26	23	0.019	0.025
12-13	...	18	BDL	0.030
13-14	12	19	0.054	0.085
detection limit		0.002	0.003	blank=0.006

unfiltered water concentrations in brackets ()

Table 4.20 Fe, Mn, Pb and Zn concentrations in HNO_3/HCl digested sediment from Loch Lomond porewater core Lo2-2C

section depth (cm)	Fe (%)	Mn (%)	Pb (mg kg^{-1})	Zn (mg kg^{-1})
0-1	4.4	3.9	59	294
1-2	6.0	1.5	67	313
2-3	5.6	0.71	66	306
3-4	7.5	0.90	100	477
4-5	6.2	0.64	125	558
5-6	5.2	0.48	139	573
6-7	5.6	0.45	124	486
7-8	5.4	0.41	118	440
8-9	5.8	0.47	135	450
9-10	6.4	0.50	146	481
10-11	6.5	0.46	143	453
11-12	5.5	0.33	142	419
12-13	5.2	0.27	105	296
13-14	4.9	0.25	85	239

4.4 Discussion

As data are more complete for site 2, results from this site will be discussed first, followed by site 1, with some comparisons between the two sites.

4.4.1 Sediment core characteristics: sites 1 and 2

Physical characteristics of the sediment cores Lo2-1A, Lo2-1B, Lo1-A and Lo1-B are listed in Tables 4.3-4.6. Porosities at site 2 were higher than at site 1, at corresponding depths, ranging at site 2 from 95% at the surface to 76% at 75-80 cm and showing a steady downcore decrease. At site 1 the maximum porosity occurred in the surface section (0-1 cm) at 89% and decreased below this to 74% at 8-9 cm, below which there was no obvious trend, porosities ranging from 64-78%. The difference in porosities between the two sites is a reflection of the finer-grained sediment at site 2 and the sandier sediment at site 1. Mineralogical analysis of a southern basin sediment core by MacKenzie *et al.* (1983) showed no evidence of carbonates in the sediment and so the carbon contents (total) for cores Lo2-1A and Lo1-A can reliably be taken as organic carbon contents. Again, %C contents illustrate the difference between the two sampled sites, with higher values at the more biologically productive site 2 (5.69%C at 0-1 cm), compared with site 1 (2.4%C at 0-1cm). The general trend of downcore increase in C/N ratio at site 2 shows the influence of preferential decomposition of planktonic organic matter (relatively high in N) over the allochthonous (catchment-derived) organic matter (low in N).

4.4.2 Radionuclide data for site 2

^{210}Pb data

Excess ^{210}Pb concentrations (Table 4.7, Fig. 4.3) decrease from a surface maximum of 414 Bq kg^{-1} (0-1 cm) to 281 Bq kg^{-1} at 2-3 cm and remain constant (within error) to 6 cm. Below this there is an exponential decrease with depth to non-detectable levels below 13 cm. This indicates mixing to 6 cm and, using a CIC calculation for values fom 5-6 cm downwards, gives a sedimentation rate of 32 ± 4 mg cm^{-2} y^{-1}, which is slightly greater than the value of 22 ± 2 mg cm^{-2} y^{-1} obtained for a core near this site (Baxter *et al.*, 1981). If steady state conditions prevail, a sedimentation rate of 37 ± 2 mg cm^{-2} y^{-1} is obtained (^{210}Pb flux/settling particulate ^{210}Pb concentration), using an implied ^{210}Pb flux (excess ^{210}Pb inventory x λ) of

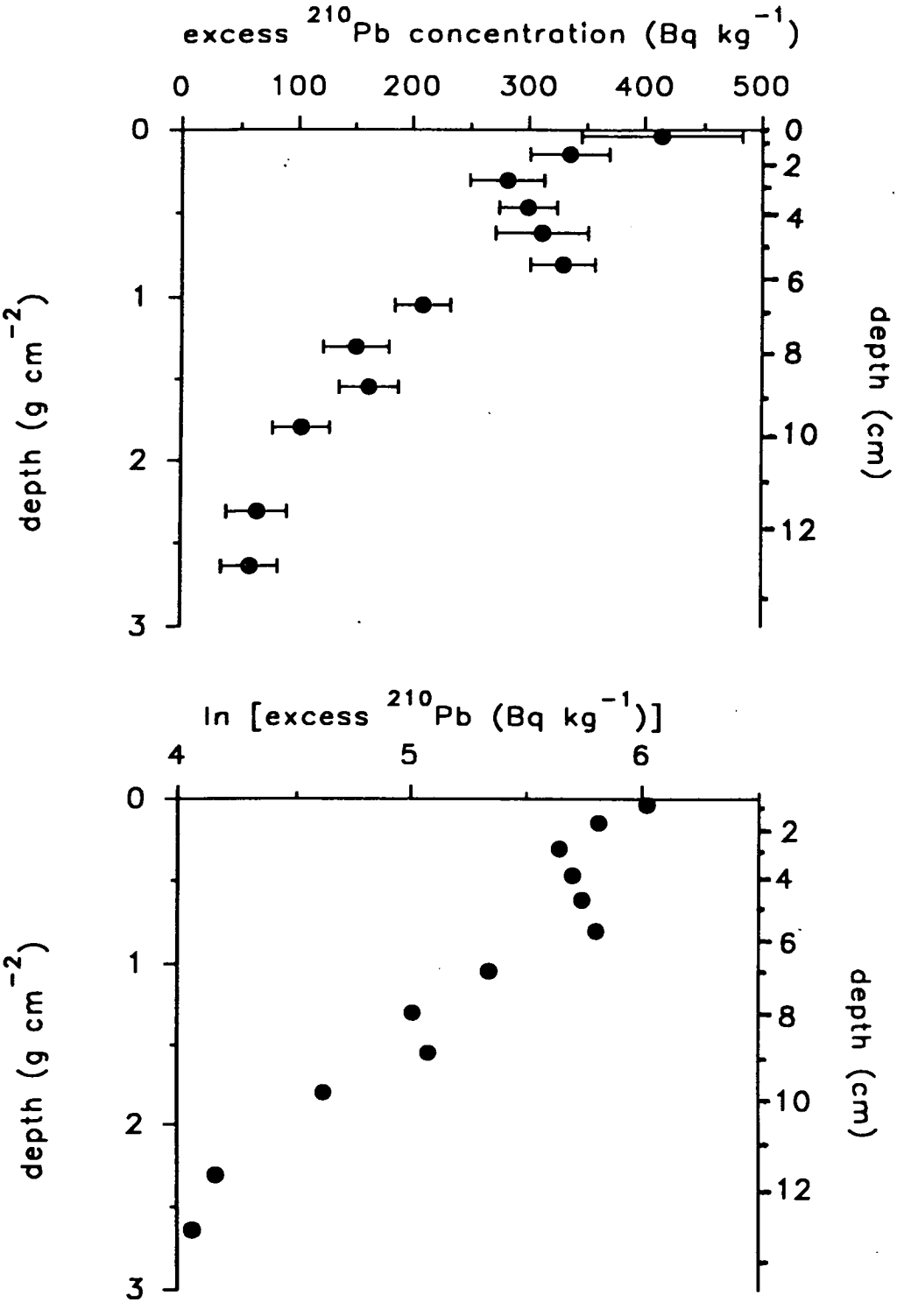

Fig 4.3. Excess ^{210}Pb and ln (excess ^{210}Pb) against depth (weight/area) in Loch Lomond sediment core Lo2-1A

152 Bq m^{-2} y^{-1} and assuming that settling particulates have an unsupported ^{210}Pb activity of 414 Bq kg^{-1} (equivalent to the maximum in the sediment). Since settling particulates would probably have a higher ^{210}Pb concentration, this sedimentation rate represents an upper limit. The 32 ± 4 mg cm^{-2} y^{-1} sedimentation rate was used to obtain a core chronology for core Lo2-1A and the adjacent core Lo2-1B (Table 4.21).

Radiocaesium data

In the ^{137}Cs profile (Table 4.9, Fig. 4.4), two sub-surface peaks are apparent, the larger of which (1,482 Bq kg^{-1}) is at 2-3 cm and the smaller (931 Bq kg^{-1}) at 5-6 cm. The maximum depth of ^{137}Cs penetration is 14-15 cm, while ^{134}Cs is detectable to 3-4 cm, indicating sediment mixing to 4 cm, consistent with the implications of the ^{210}Pb data. Using the $^{134}Cs/^{137}Cs$ ratios (Table 4.9) to separate the ^{137}Cs into its component sources (Fig. 4.4, Appendix 1), the ^{137}Cs maximum due to weapons testing is at a depth of 5-6 cm, which corresponds to dates of 1961 to 1968 on the basis of the ^{210}Pb-derived sedimentation rate of 32 mg cm^{-2} y^{-1}. These dates are in good agreement with the historical fallout pattern, *i.e.* maximum weapons testing fallout input to the area in 1963. The maximum ^{137}Cs concentration of Chernobyl origin occurs at 2-3 cm, with upper and lower limits to the section dates of 1983 and 1978 respectively, the former being closer to the fallout maximum in 1986. The base of the deepest section in which ^{137}Cs was detectable (14-15 cm) corresponds to a date of 1876, long before the onset of nuclear technology and indicating that, although the profile pattern is generally consistent with historical inputs of ^{137}Cs, some mixing/diffusion must have occurred, but not sufficiently intense to totally obscure the historical record of radiocaesium fallout input.

Sediment chronology at site 2

Both the ^{210}Pb and radiocaesium concentration profiles indicate partial, rapid mixing to a depth of around 6 cm. The mixing has not however, been sufficiently intense to obscure the historical record of ^{137}Cs fallout input from weapons testing and Chernobyl to the area. The ^{210}Pb-derived sedimentation rate of 32 mg cm^{-2} y^{-1} is consistent with the radiocaesium data, *i.e.* the ^{137}Cs peaks, separated into weapons testing and Chernobyl fallout components, reflect the historical maxima in fallout input to the area, if the ^{210}Pb chronology is used.

The chronology can therefore be used to interpret the metal concentration profiles, because historical trends in pollutant inputs should be reflected in the

Table 4.21 ^{210}Pb-derived chronology for Loch Lomond sediment cores Lo2-1A and Lo2-1B*

	Lo2-1A		Lo2-1B	
section depth (cm)	mid-section date	base-section date	mid-section date	base-section date
0-1	1989	1987	1989	1988
1-2	1985	1983	1985	1982
2-3	1980	1978	1980	1978
3-4	1975	1973	1976	1973
4-5	1971	1968	1971	1969
5-6	1965	1961	1966	1964
6-7	1957	1953	1961	1958
7-8	1949	1945	1955	1952
8-9	1941	1937	1948	1945
9-10	1934	1930	1942	1938
10-11	1926	1922	1935	1932
11-12	1918	1913	1929	1926
12-13	1907	1902	1922	1919
13-14	1896	1890	1914	1909
14-15	1883	1876	1904	1899
15-16	1868	1861	1894	1888
16-17			1881	1875
17-18			1869	1862
18-19			1856	1849
19-20			1842	1834
20-22			1819	1804
22-24			1791	1779
24-26			1768	1757
26-28			1735	1732
28-30			1719	1705
30-32			1690	1675
32-34			1658	1641
34-36			1626	1610
36-38			1563	1578
38-40			1509	1548

* based on a sedimentation rate of 32 ± 4 mg cm^{-2} y^{-1} in core Lo2-1A

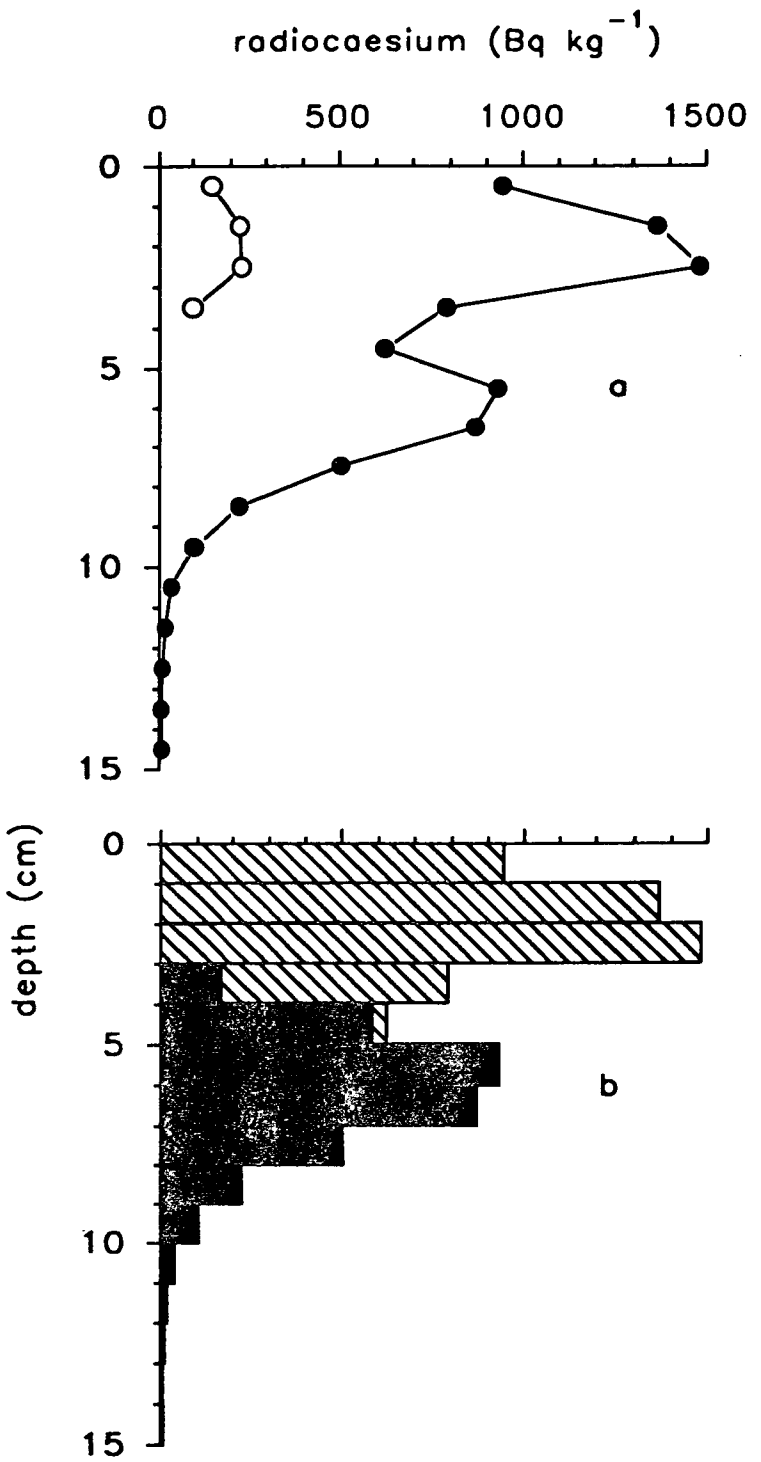

Fig. 4.4 Profiles of ^{134}Cs (o) and ^{137}Cs (•) concentrations (a) and ^{137}Cs concentrations showing the calculated component sources of fallout from weapons testing (■) and Chernobyl (▨) (b) in Loch Lomond sediment core Lo2–1A.

sediment (providing chemical remobilisation has not occurred), with a slight damping of any peaks and downward smearing due to partial mixing.

4.4.3 Metal data for site 2

Historical interpretation

Interpretation of the pollutant metal data for HNO_3/HCl acid digested sediment (Table 4.11, Fig. 4.5) in terms of historical input to the loch will be considered for Pb, Zn, Cu and Cd.

The onset of increase in Pb concentration in HNO_3/HCl acid digested sediment is around 32 cm, below which Pb has a mean concentration of 27 mg kg^{-1}. Apart from a peak of 92 mg kg^{-1} in the 24-26 cm section, Pb increases steadily to 11-12 cm, before decreasing towards the surface (60 mg kg^{-1}) over the top 6 cm. The corresponding dates for the changes in Pb concentration are 1690 for the onset of increase, 1929 (11-12 cm) for maximum concentrations and 1966, after which the Pb concentration decreases.

If the Zn data are considered similarly, the concentration starts to increase above 28 cm (1719) with a mean background concentration below this of 106 mg kg^{-1}. The concentrations increase to a maximum of 530 mg kg^{-1} between 4 and 6 cm (around 1970) and then decrease towards the surface to about 300 mg kg^{-1}.

Cu concentrations are relatively constant below 22 cm (mean = 30 mg kg^{-1}), corresponding to 1820. Above this section, the concentration gradually increases to a relatively constant concentration (35-39 mg kg^{-1}), before decreasing above 5 cm (1971) to 1-2 cm. In the surface sediment (0-1 cm) a slightly higher value of 37 mg kg^{-1} is observed.

Cd concentrations increase above 20 cm (1842) to 5 cm (1971), similar to Zn, then decrease to 1-2 cm (1.1 mg kg^{-1}), with a slight surface enhancement of 1.6 mg
kg^{-1} (0-1 cm). Below 20 cm the mean concentration to a depth of 60 cm is 0.4 mg kg^{-1}. Cd was undetectable below 60 cm ($\leq$ 0.2 mg kg^{-1}).

The onset of increase in concentrations of Pb and Zn is before that of Cu and Cd, and earlier than the generally observed pattern of increase during the Industrial Revolution, around the mid-18th century. However, due to the partial mixing of the surface sediment, downward smearing of inputs will have occurred, so the true onset of pollutant metal increase is probably at later dates than those indicated above. The downward smearing effect can be quantified by calculating dates for the onset of pollutant metal inputs, assuming mixing to the base of 6 cm, and subtracting the

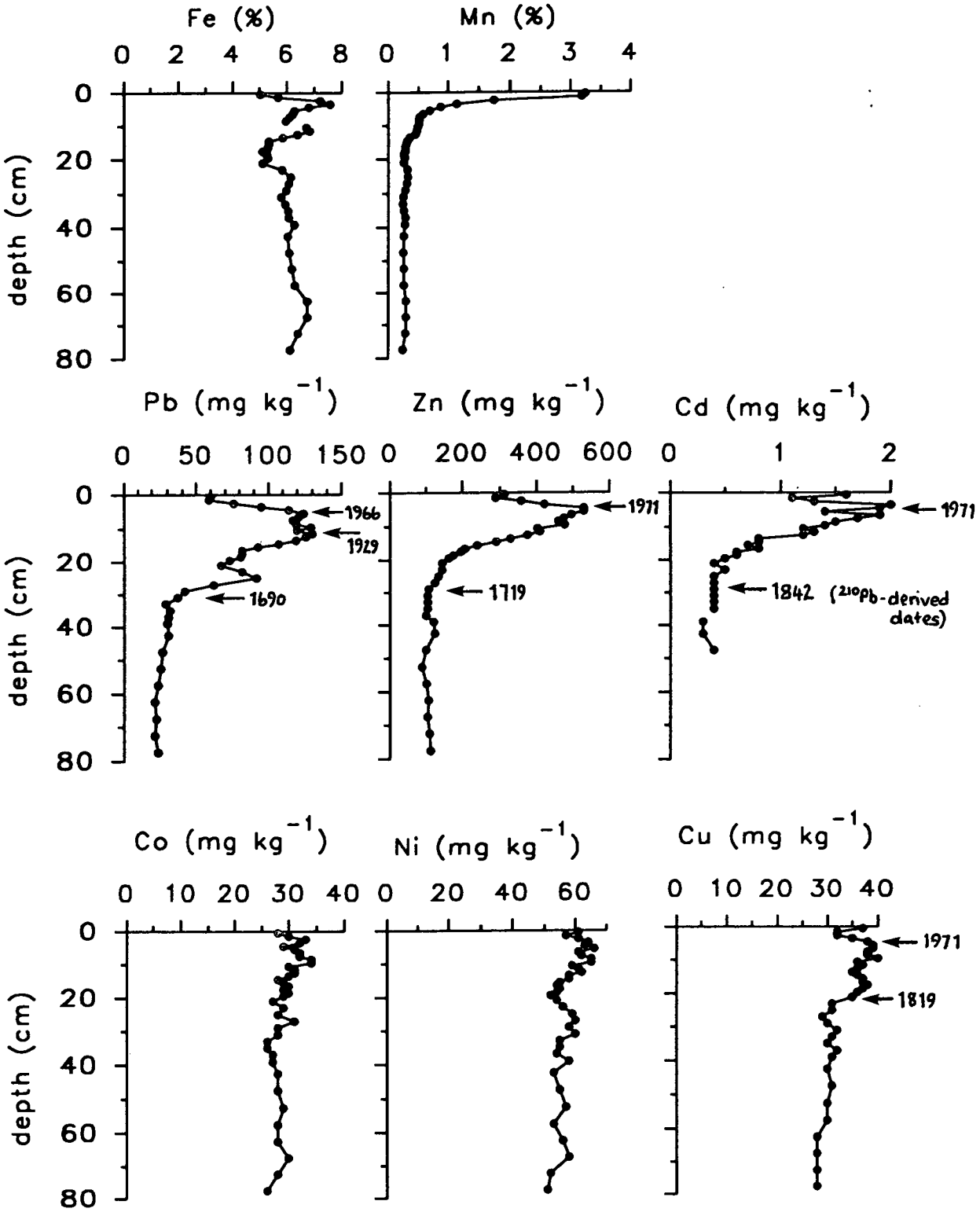

Fig 4.5 Metal concentrations in HNO_3/HCl acid digested Loch Lomond sediment core Lo2-1B

cumulative weight to this depth from the cumulative weight at the depth to be dated, before dividing by the sedimentation rate, to give the time elapsed since the onset of increase in pollutant metal concentrations. This gives dates of 1716 (Pb), 1745 (Zn) and 1845 (Cu) and 1865 (Cd), which are in broad agreement with the rapid industrialisation (and increased atmospheric pollutant input) of the Clyde area during the 17th century, which continued until early this century (Oakley, 1975).

In a core collected near this site in the southern basin (Farmer *et al.*, 1980), observed trends in Pb, Zn, Cu and Cd profiles were attributed to historical changes in atmospheric deposition of these metals. 'Excess' (anthropogenic) fluxes of the metals to the surface sediment were calculated ('excess' metal concentration x sedimentation rate) and agreed well with the atmospheric deposition data reported for dates shortly before the core was collected. 'Excess' inventories of pollutant metals (Pb, Zn, Cu and Cd) were calculated for core Lo2-1B by subtracting the background concentrations (mean of the relatively constant concentrations at depth, Table 4.22) for each section, multiplying by the section dry weight and summing the values. 'Excess' inventories of pollutant metals (Table 4.22) are in reasonably good agreement with those obtained by Farmer *et al.* (1980) in 1976 for Pb, Cu and Cd, but for Zn the inventory is more than twice as high in core Lo2-1B.

Bearing in mind the effects of partial mixing in this sediment core, that is, peak pollutant concentrations being at a correct date, though damped, and a downwards smearing of pollutant metals to a greater depth (and date) than in the absence of sediment mixing, temporal trends in pollutant metal fluxes have been nonetheless calculated (Table 4.23) as it was thought to be a useful comparison with similar data from other studies.

Temporal trends in pollutant Pb fluxes in this core agree well with those calculated by Sugden *et al.* (1991a) for a sediment core collected nearby in the southern basin, where peak fluxes of almost 40 mg m^{-2} y^{-1} were obtained at ^{210}Pb-derived dates of around 1920 and 1946 and decreased from 1920 to 9 mg m^{-2} y^{-1} by around mid-19th century. In the present study, peak fluxes of 32 mg m^{-2} y^{-1} at (mid-section) dates of 1942 and 1929 occurred (Table 4.23), slightly lower than the value quoted above due to the damping effects of mixing, and fluxes decreasing from 14 cm downwards to a minimum of 3 mg m^{-2} y^{-1} at a date of 1716 (taking mixing into account, as described above).

Despite the effects of partial mixing in sediment at site 2 and while the flux data from core Lo2-1B cannot be directly compared on an exact date basis (due to mixing effects) with reported values, there is good agreement between pollutant metal fluxes at a mid-section date of 1976 (Table 4.23) of (mg m^{-2} y^{-1}) 21 (Pb), 101

Table 4.22 Background concentrations and 'excess' inventories of pollutant metals for Loch Lomond sediment core Lo2-1B and 'excess' inventories for metals in a core from a nearby site in the southern basin (Farmer *et al.*, 1980).

	Pb	Zn	Cu	Cd
'Background' concentration (mg kg^{-1})	27	106	30	0.4
'Excess' inventory (g m^{-2})	5.4	11.5	0.38	0.03
'Excess' inventory to 1976 (g m^{-2}) (Farmer *et al.*, 1980)	3.62	5.02	0.44	0.02

Table 4.23 Temporal trends in pollutant metal fluxes in Loch Lomond sediment core Lo2-1B.

depth (cm)	mid-section date	fluxes (mg m^{-2} y^{-1}) Pb	Zn	Cu	Cd
0-1	1989	10	66	2.2	0.4
1-2	1985	10	58	0.6	0.2
2-3	1980	15	81	0.6	0.3
3-4	1976	21	101	1.6	0.5
4-5	1971	27	136	2.6	0.5
5-6	1966	30	136	2.9	0.3
6-7	1961	30	125	2.9	0.5
7-8	1955	28	118	2.6	0.4
8-9	1948	29	113	2.6	0.4
9-10	1942	32	119	3.2	0.3
10-11	1935	29	95	1.9	0.2
11-12	1929	32	96	2.2	0.3
12-13	1922	31	87	1.9	0.3
13-14	1914	29	71	1.6	0.1
14-15	1904	25	59	1.9	0.1
15-16	1894	21	43	2.2	0.1
16-17	1881	17	32	2.2	0.1
17-18	1869	17	28	2.6	0.06
18-19	1856	17	22	2.2	0.06
19-20	1842	14	18	1.9	0.03
20-22	1819	12	12	1.6	
22-24	1791	17	12		
24-26	1768	20	9		
26-28	1735	11	6		
28-30	1719	5			
30-32	1690	3			

(Zn) and 0.5 (Cd), and fluxes in 1976 obtained by Farmer *et al.* (1980) of (mg m^{-2} y^{-1}) 25.1 (Pb), 88.4 (Zn) and 0.25 (Cd) and atmospheric deposition fluxes for the Clyde sea area 1972-1973 of (mg m^{-2} y^{-1}) 29.5 (Pb), 103 (Zn) and 0.57 (Cd) (Cambray *et al.*, 1975). This agreement, together with the trends in concentrations of Pb, Zn, Cu and Cd in the profiles of HNO_3/HCl acid digested sediment of core Lo2-1B, provides strong support for the historical interpretation of the results. However, the partitioning data, porewater and water column metal concentrations must be examined, to establish whether other processes may be affecting the distribution of metals amongst the different fractions and the metal behaviour in this particular system, in which much evidence has been found for the redox-driven remobilisation of Fe, Mn and As (*e.g.* Farmer and Lovell, 1986), which, as outlined in Chapter 1, could potentially influence other metals.

Nickel and cobalt in HNO_3/HCl acid digested sediment

Ni concentrations range from 51-66 mg kg^{-1} with no distinct pattern throughout the core. The Co profile is similar to that of Ni with concentrations ranging from 26-34 mg kg^{-1}. (Table 4.11, Fig. 4.5).

Iron and manganese in HNO_3/HCl acid digested sediment

The Fe concentration profile in HNO_3/HCl acid digested sediment (Table 4.11, Fig. 4.5) shows a subsurface maximum of 7.6% Fe at 3-4 cm, with a secondary peak of 6.8% at 11-12 cm. Concentrations below this decrease to a sub-surface minimum between 15 and 22 cm (mean concentration = 5.2%) and then rise to a mean 6.2% below 22 cm. The Mn concentration profile (Table 4.11, Fig.4.5) exhibits a surface enhancement of 3.2% in the depth range 0-2 cm, below which a decrease to a relatively constant 0.3% below 13 cm is apparent. The 'dip' in Fe concentrations between 15 and 22 cm also occurs with Mn, but to a much lesser extent. The Ni profile also shows lower concentrations in this depth range and in the Pb profile it could be argued that a change in the sediment has occurred between 15 and 22 cm to give slightly depleted concentrations, despite the overall historical trend of Pb concentrations increasing towards 5-6 cm. There is no pronounced change in porosity between 15 and 22 cm (Table 4.4, Section 4.4.1), so no evidence of a change in sediment type. Subtracting the cumulative weight of sediment to the base of 6 cm from the mid-section depth at 14-15 cm and 20-22 cm and dividing by the sedimentation rate of 32 mg cm^{-2} y^{-1}, gives a date of 1846 for the initial change to lower concentrations. In a core collected from a nearby site in the southern basin, MacKenzie *et al.* (1983) also found concentration minima at similar depths (in an

area of similar sedimentation rate) for numerous elements: Rb, Cs, Ba, Sc, Cr, Fe, Co, Hf, Ta, Ce, Sm, Eu, Tb and Th, which were attributed to a change in sediment input, *e.g.* due to catchment erosion, implied by old ^{14}C dates at comparable depths (Dickson *et al.*, 1978). Processes such as road building or afforestation could disturb the catchment, causing an input of older material, relatively low in the elements listed above. During this time, atmospheric deposition of pollutant metals (Cu, Cd, Zn, Pb *etc.*) would have continued and explains why for these elements the minima are, if at all, only slightly apparent.

The 10-fold enhancement of Mn in the surface sediment and the uppermost Fe maximum (less well-defined than for Mn) are characteristic of redox-driven diagenetic remobilisation and reprecipitation (Davison, 1984), which has been well-established in this loch (Farmer and Lovell, 1984 and 1986). The upwards displacement of the Mn peak, relative to that of Fe, is consistent with both the earlier reduction of Mn and the eventual re-precipitation of authigenic Mn oxides at a higher Eh (more oxic, or less reducing, conditions) than for Fe (Berner, 1980; Farmer and Lovell, 1984) (Chapter 1).

Partitioning data for Mn, Fe, Pb, Zn and Cu for sediment core Lo2-1B have, for clarity, been plotted (Figs. 4.6, 4.9, 4.11, 4.13 and 4.15) with each fraction on the same scale (*i.e.* depth and concentration). Sequential extraction of sediment was only carried out to 40 cm depth, but acid digestions to 80 cm, so the sum of concentrations in fractions I-V has additionally been plotted separately (Figs. 4.7, 4.10, 4.12, 4.14 and 4.16) on a depth scale of 0-80 cm, for comparison with the acid digest concentration profiles. Similarly, because porewater data were collected to 12 cm, these have been plotted (Figs. 4.7, 4.8, 4.10, 4.12, 4.14 and 4.16) with metal concentrations from the acid digestions on a 0-15 cm depth scale.

Manganese partitioning data

Trends of Mn in the concentration profile of fraction I (Table 4.13, Fig. 4.6) show low concentrations in the 0-2 cm sections (0.009% Mn), followed by higher concentrations between 2 and 14 cm (maximum 0.49%) and relatively constant concentrations below this (0.126-0.187%). The fraction II concentration profile shape is similar, though with lower concentrations. Mn concentrations in fraction III show a very similar pattern to the HNO_3/HCl acid digest Mn concentration profile, in which Mn concentrations are lower at 0-2 cm (Fig. 4.7), probably due to the non-homogeneity of the wet sediment sample used for the sequential extraction, compared with the dried, ground sample used for the acid digestion. Below 2 cm,

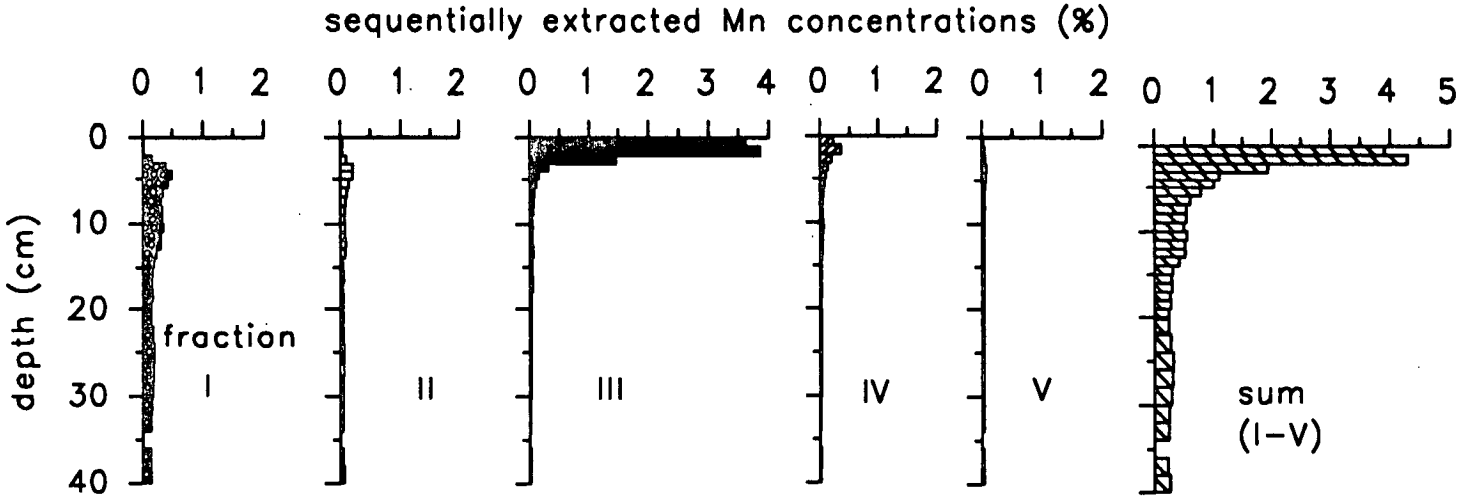
sequentially extracted Mn concentrations (%)
depth (cm)
0
10
20
30
40
0 1 2
0 1 2
0 1 2 3 4
0 1 2
0 1 2
0 1 2 3 4 5
fraction
I
II
III
IV
V
sum
(I–V)

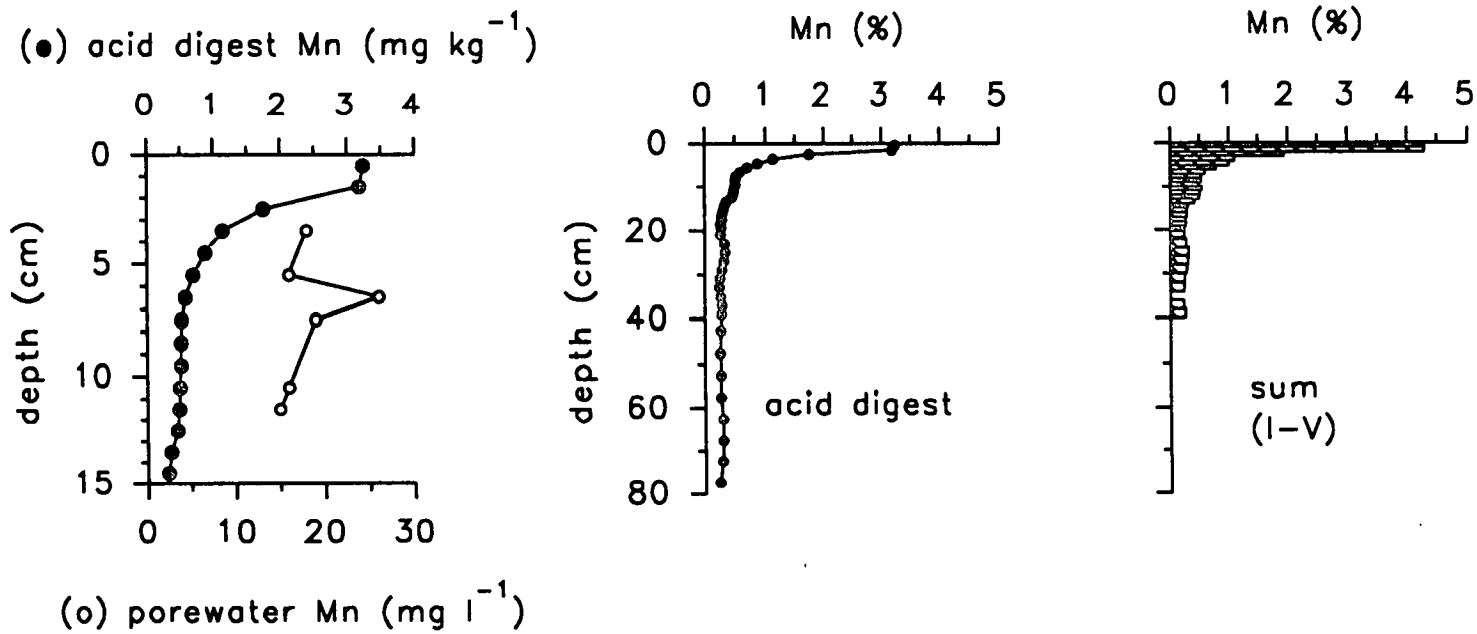
(●) acid digest Mn (mg kg^{-1})
0 1 2 3 4
0
5
10
15
depth (cm)
0 10 20 30
(o) porewater Mn (mg l^{-1})
Mn (%)
0 1 2 3 4 5
0
20
40
60
80
depth (cm)
acid digest
Mn (%)
0 1 2 3 4 5
sum
(I–V)

Mn in fraction III decreases rapidly to 4-5 cm (0.15%) and then, at much lower concentrations, decreases gradually downcore (minimum 0.01% at 32-34cm). Although there is little Mn in fraction IV, the trend is similar to that in fraction III. Finally, fraction V is low in Mn and concentrations do not vary much downcore.

Mn in fraction III comprises 93% of the sum of concentrations in fractions I-V in the 0-1cm section but below 5 cm, the contribution is only 9%, whereas Mn in fraction I, although much lower in concentration, shows the reverse trend and indicates that Mn remains relatively labile throughout the core below 2 cm. The Mn partitioning results are consistent with redox-controlled cycling involving dissolution of Mn (fraction III) below 2 cm, followed by diffusion and reprecipitation (Chapter 1) leading to the surface enhancements of Mn in fraction III observed in Figs. 4.5 and 4.6.

Solution phase manganese

Concentrations of porewater Mn (Tables 4.18 and 4.19, Figs. 4.7 and 4.8) are enhanced by factors of at least 1,850-17,000 relative to water column concentrations, which were $\leq$ 0.002 mg l^{-1} in all filtered water samples. Porewater Mn concentrations are similar in both cores (Lo2-1C and Lo2-2C) (3.7-34 mg l^{-1}) and solid phase concentrations for cores Lo2-1B and Lo2-2C are also comparable (Tables 4.11 and 4.20). However, as porewater data for core Lo2-2C are more complete, trends can be more readily observed in this core (Fig. 4.8). The porewater Mn concentrations confirm patterns due to diagenetic remobilisation, that is, dissolution of Mn oxide, release of Mn^{2+} to solution (maximum dissolution coinciding with the maximum concentration at 8-9 cm), upward diffusion of Mn^{2+} in the reduction zone, followed by a drop in concentration due to oxidation/precipitation in the oxidation zone (shown in core Lo2-2C at 0-1 cm, where the solid phase Mn enrichment is observed).

Iron partitioning data

For Fe, the picture in the partitioning results (Table 4.13, Fig. 4.9) is not so clear as for Mn. If the sum of Fe concentrations in fractions I-V is divided by the concentration obtained by HNO_3/HCl acid digestion of sediment for each section, then a mean ratio of 0.6 at the surface (0-1 cm) decreases to 0.3 by 38-40 cm, showing that at least 50% of the $Fe^{acid\ digested}_{V}$ is not released by reagents used for sequential extraction and that, with depth, Fe becomes associated with more stable fractions. The structure in the acid digest concentration profile (Fig. 4.10) and that of the sum of fractions I-V is strongly related to the structures seen in the two

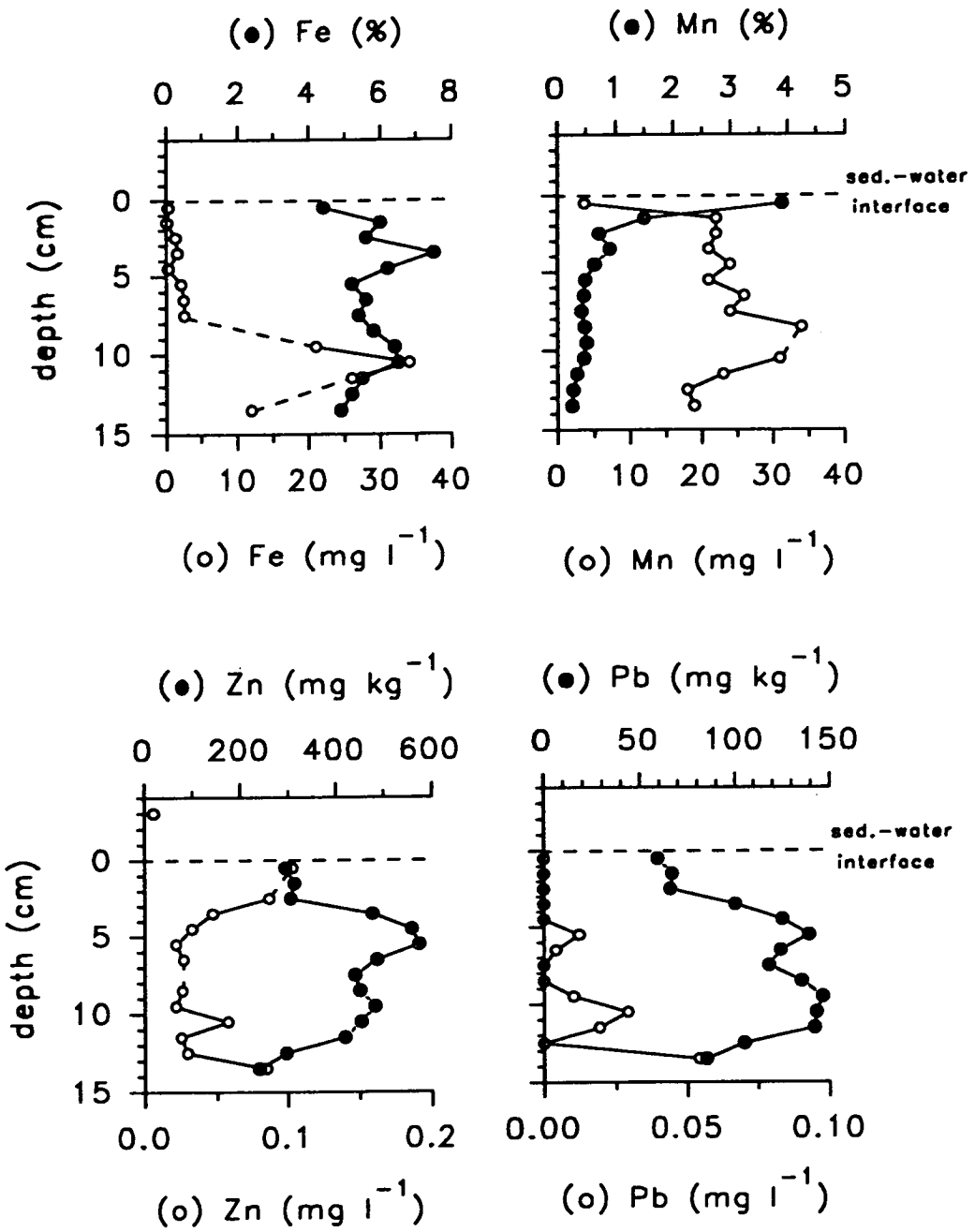

Fig. 4.8 Metal concentrations in solid (●) and solution (o) phases of Loch Lomond sediment core Lo2–2C

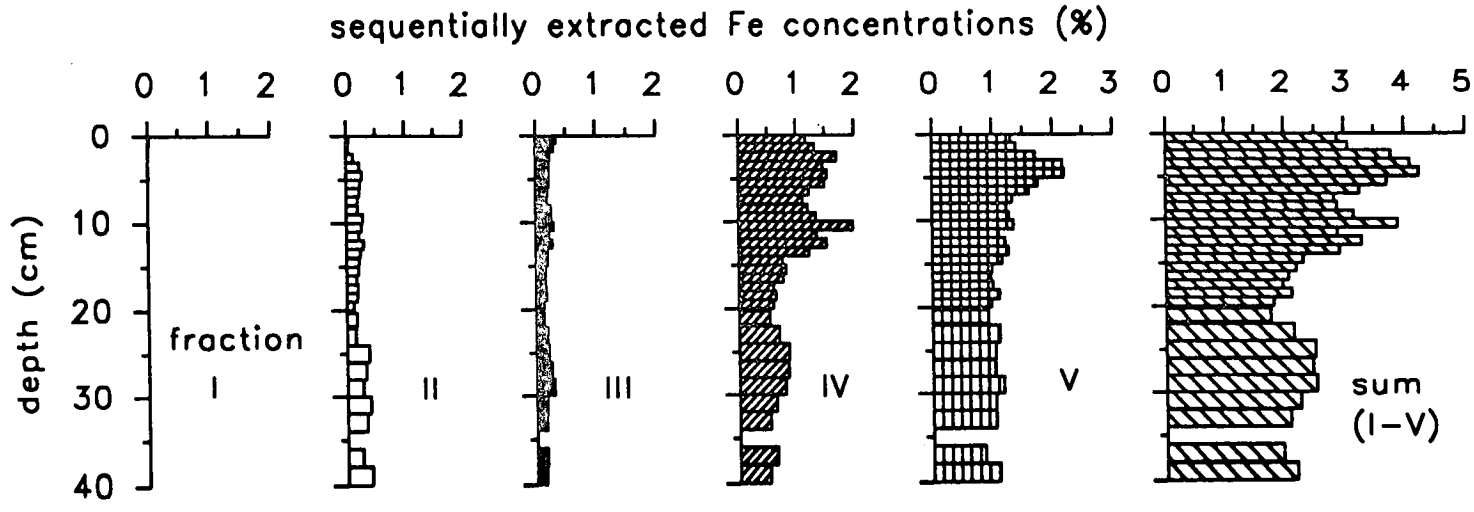
sequentially extracted Fe concentrations (%)
depth (cm)
0
10
20
30
40
0 1 2
0 1 2
0 1 2
0 1 2
0 1 2 3
0 1 2 3 4 5
fraction
I
II
III
IV
V
sum
(I–V)

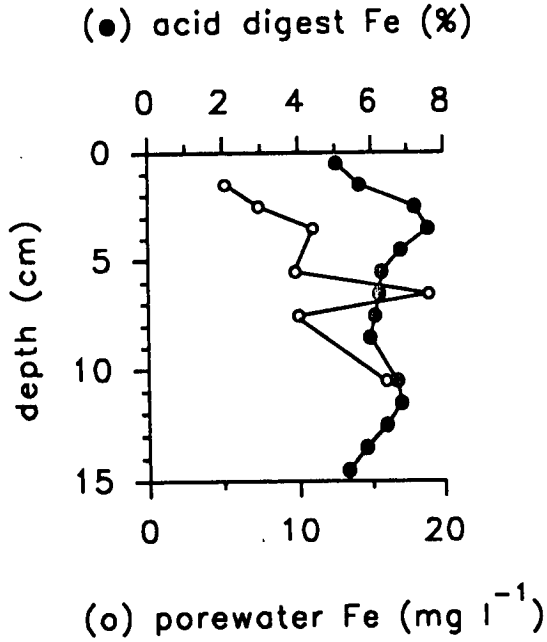
(●) acid digest Fe (%)
0 2 4 6 8
0
5
10
15
depth (cm)
0 10 20
(o) porewater Fe (mg l^{-1})

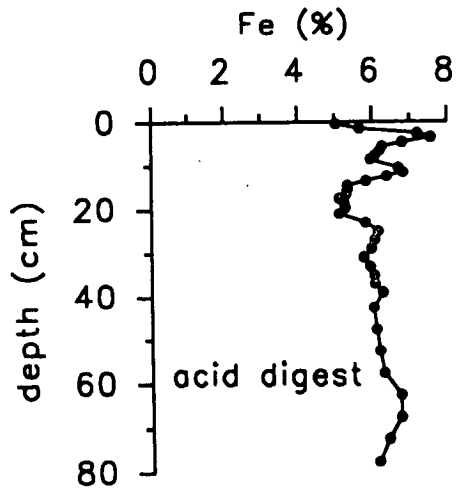
Fe (%)
0 2 4 6 8
0
20
40
60
80
depth (cm)
acid digest

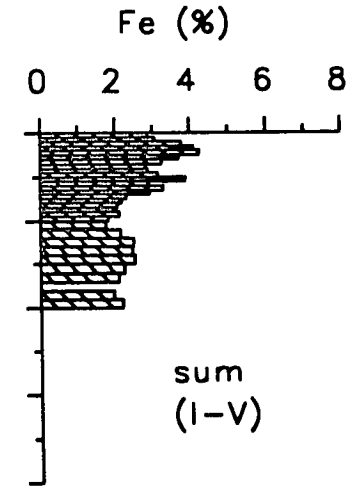
Fe (%)
0 2 4 6 8
sum
(I–V)

predominant fractions IV (moderately reducible) and V (organic/sulphides), excluding the residual fraction mentioned above. The sub-surface low concentrations between 15 and 22 cm are clearly seen in the Fe concentration trend in fraction IV, and, to a much lesser extent, also in fractions II, III and V.

Fe concentrations in fraction IV decrease much more with depth than in fraction V, to 0.52% Fe (38-40 cm), about one-third of the near-surface peak value of 1.70% (2-3 cm). The sub-surface Fe maximum in fraction V between 3 and 5 cm (mean concentration = 2.19%) is a characteristic pattern of redox-driven diagenesis, suggesting that this feature could be due to Fe left behind in a more readily extractable form, following the previous extraction in step IV, rather than due to changes in the association of Fe with organics/ sulphide. The highest Fe concentration of 1.98% in fraction IV occurs at 10-11 cm and this sub-surface peak is also seen both in the concentration profile of the sum of fractions I-V and the HNO_3/HCl acid digest concentration profile (Fig. 4.10). Whether or not this feature is of diagenetic origin might be clarified by the porewater data.

Solution phase iron

Porewater Fe profiles (Tables 4.18 and 4.19, Figs. 4.8 and 4.10) are not similar in the two cores collected (Lo2-1C and Lo2-2C) and although the overall pattern indicates upward diffusion (from a concentration maximum at depth), the sudden drop in concentration indicates a change in redox conditions at a depth of about 8 cm for Lo2-2A and 6 cm for Lo2-1C (for which the drop in concentration is not so pronounced).

Since data are more complete for core Lo2-2C and the glovebox method of porewater collection, which gave more reliable results (Chapters 6 and 7), was used for this core, it seems sensible to base the interpretations on porewater results from sediment core Lo2-2C (Fig. 4.8). The concentrations and trends in the solid phase (HNO_3/HCl acid digestion, Table 4.20) of core Lo2-2C are comparable with those in core Lo2-1B, though the peaks are more marked. Core Lo2-2C has sub-surface solid phase Fe peaks in the sections 3-4 cm (7.5% Fe) and 10-11 cm (6.5% Fe). Evidence for the control of the porewater profile by redox-cycling lies in the peak in porewater Fe and the drop to low concentrations at a slightly greater depth than the corresponding features in the Mn profile. The solid phase Fe peak at 10-11 cm, not observed in the Mn profile, cannot be explained in terms of redox cycling at the time of sampling, since the porewater data show the maximum point of Fe dissolution to be also at 10-11 cm. However, it is possible that the solid phase peak is a relict feature of past diagenetic redox cycling, which has not been obscured due to the

rates of reaction involved in dissolving Fe. Since Fe was extracted in fraction IV throughout the core, this provides evidence that the reducing conditions are not sufficient to completely reduce the Fe oxides/hydroxides. This would be consistent with the lack of a similar solid phase peak in the Mn profile, because dissolution of Mn oxides is a much more rapid reaction than the reduction of Fe oxides and this is reflected in the very low concentrations of Mn extracted in fraction III below the surface enhancement.

Lead partitioning and solution phase data

Pb was undetectable in fractions I and III throughout the core (Table 4.14, Fig. 4.11), with concentrations all ≤ 12 mg kg^{-1} and mostly ≤ 5 mg kg^{-1} in fraction I and ≤ 20 mg kg^{-1}, mostly ≤ 10 mg kg^{-1} in fraction III. Pb is associated largely with fraction IV (moderately reducible) and all detectable Pb to 3 cm is in this fraction. The shape of the concentration profilesof the sum of fractions I-V and the HNO_3/HCl acid digest profile are dominated by the concentration trends in fraction IV, in which enhanced Pb concentrations occur between 3 and 14 cm (mean concentration = 78 mg kg^{-1}), below which the concentration decreases to 10 mg kg^{-1} at 38-40 cm. Pb in fraction II shows a similar pattern to the one previously described, but with lower concentrations - mean concentration between 5 and 15 cm = 33 mg kg^{-1}, decreasing to 4 mg kg^{-1} at 36-38 cm. In fraction V, Pb was only detectable between 3 and 28 cm, and again, concentrations were enhanced in sub-surface sections 3 to 15 cm (mean = 14 mg kg^{-1}). Although Pb is predominantly associated with fraction IV, the moderately reducible fraction generally associated with Fe oxides/hydroxides, there is no evidence to suggest remobilisation of Pb associated with redox-driven Fe cycling, since there is no significant Pb enrichment in the depths between 3 and 5 cm, where the Fe enhancement is observed.

Concentrations of Pb in HNO_3/HCl acid digested sediment are similar to the sum of concentrations in fractions I-V, indicating that little or no Pb is bound to fractions more resistant to the extractants used in the sequential leaching scheme (Fig. 4.12). For some of the sections (*e.g.* 10-11 cm) the concentrations in the sum of fractions I-V were higher than HNO_3/HCl digested concentrations, probably due to cumulative errors in the five step extraction procedure and/or the non-homogeneity of the wet sediment used in the sequential extraction (Chapter 2).

Pb was not detectable (≤0.003 mg l^{-1}) in the filtered water column samples (Table 4.18), but in both porewater cores (Lo2-1C and Lo2-2C), Pb was detectable in some samples (Tables 4.18 and 4.19, Figs. 4.12 and 4.8): below 2 cm (Lo2-1C)

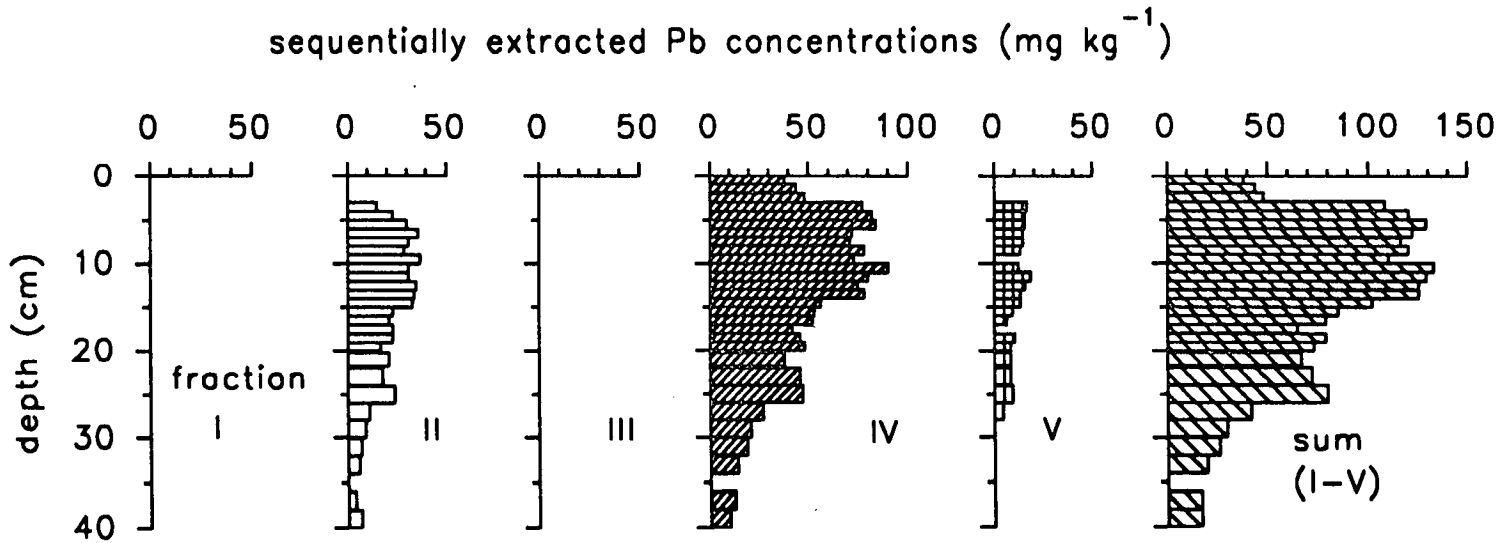
sequentially extracted Pb concentrations (mg kg^{-1})
0 50
0 50
0 50
0 50 100
0 50
0 50 100 150
depth (cm)
0
10
20
30
40
fraction
I
II
III
IV
V
sum
(I–V)

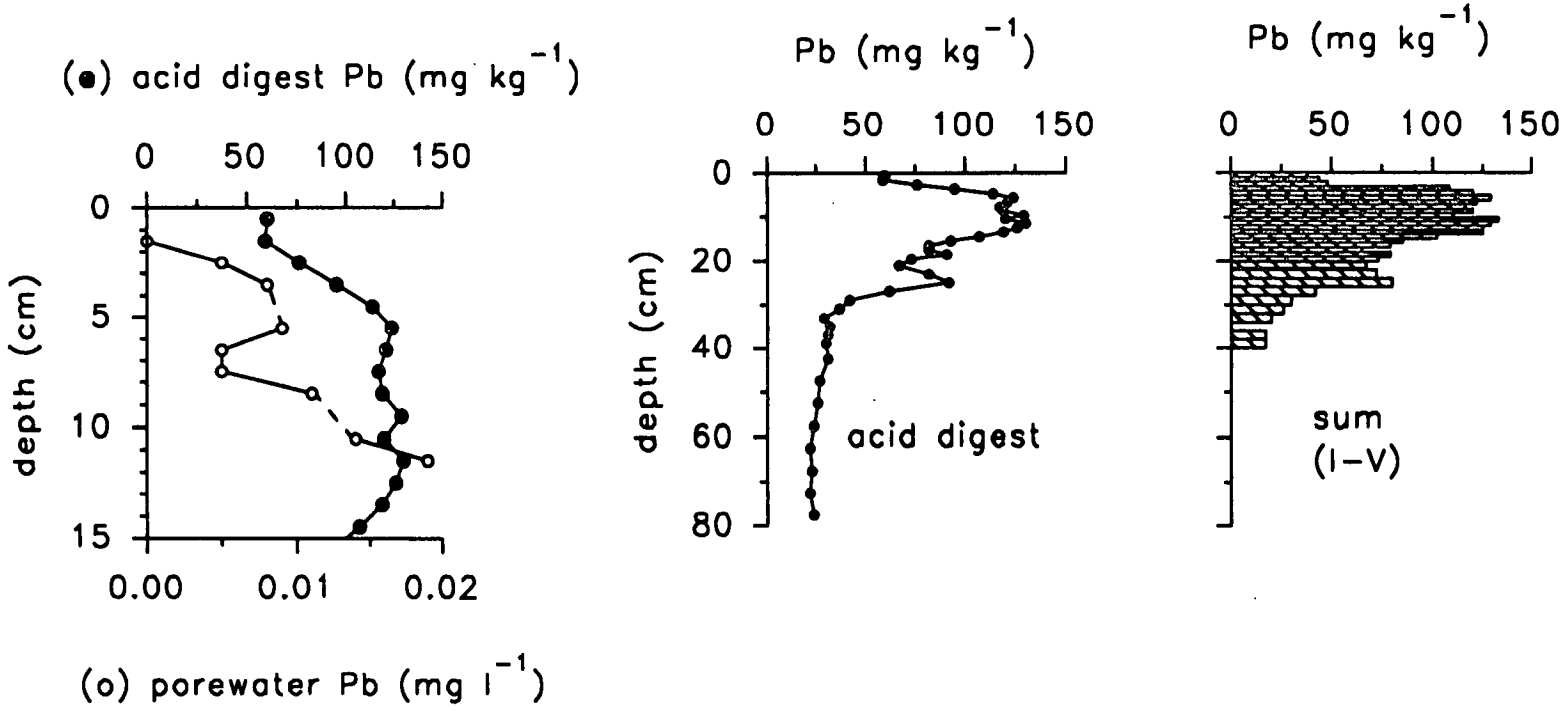
(●) acid digest Pb (mg kg^{-1})
0 50 100 150
0
5
10
15
depth (cm)
0.00 0.01 0.02
(o) porewater Pb (mg l^{-1})
Pb (mg kg^{-1})
0 50 100 150
0
20
40
60
80
depth (cm)
acid digest
Pb (mg kg^{-1})
0 50 100 150
sum
(I–V)

and 5 cm (Lo2-2C). However, porewater Pb concentrations are low (0.004 -0.054 mg l^{-1}) and although in core Lo2-2C there is a Pb peak at 10-11 cm, mirroring the porewater Fe peak in the same core, the decrease in Pb concentration above and below this section, to non-detectable levels within 2 cm, indicates that vertical mobility of Pb, if occurring at all, is only over a short distance (no more than 2 cm), involving very low concentrations. Similarly, the other peaks in core Lo2-2C at 5-6 cm and 13-14 cm do not suggest significant mobility of Pb, but rather rapid readsorption to the solid phase. The downcore increase in porewater Pb concentrations in core Lo2-1C (Fig. 4.12) parallels the acid digest solid phase Pb concentrations to a depth of 8-9 cm and this pattern, with no sharp concentration gradients, together with extremely low porewater concentrations, implies that Pb release to solution is controlled by equilibrium with the solid phase.

The significant association of Pb with fraction IV throughout the core, the decrease in solid phase Pb concentration towards the surface (in contrast to the near-surface enhancement for Fe) and the lack of Pb mobility, indicated by the porewater data, taken together, strongly suggest that the Pb distribution and solid phase concentration patterns are attributable to changes in historical input from anthropogenic sources. This has been found for other cores, both at this site, on the basis of $^{206}Pb/^{207}Pb$ trends associated with varying inputs of Pb from sources of different isotopic signature (Sugden *et al.*, 1991a), and at a nearby site in the southern basin (Farmer *et al.*, 1980).

Zinc partitioning and solution phase data

Zn was detectable in all five fractions (Table 4.14, Fig. 4.13) and in all sections, except for 0-1 cm and below 26 cm in fraction I. Additionally, all fractions showed sub-surface enhancements of Zn, as reflected in the concentration profile of Zn in acid digested sediment. For fraction I, this enhancement occurred between 4 and 11 cm (mean concentration = 38 mg kg^{-1}), fraction II 3-10 cm (mean concentration = 123 mg kg-1), fraction III 3-11 cm (mean = 70 mg kg^{-1}), fraction IV 3-11 cm (mean = 130 mg kg^{-1}) and fraction V 3-7 cm (mean = 133 mg kg^{-1}). In sections immediately above and below these sub-surface enhancements, concentrations decrease. However, enhanced concentrations also occur in the surface sediment of fractions II (0-1 cm) and, notably, fraction III (0-2 cm), which is the dominant fraction with which Zn is associated in the 0-2 cm depth range. The significance of Zn in fraction III in the top 2 cm (as for Mn), followed by a smaller proportion of Zn in fraction III (relative to the sum of fractions I-V) at depths greater

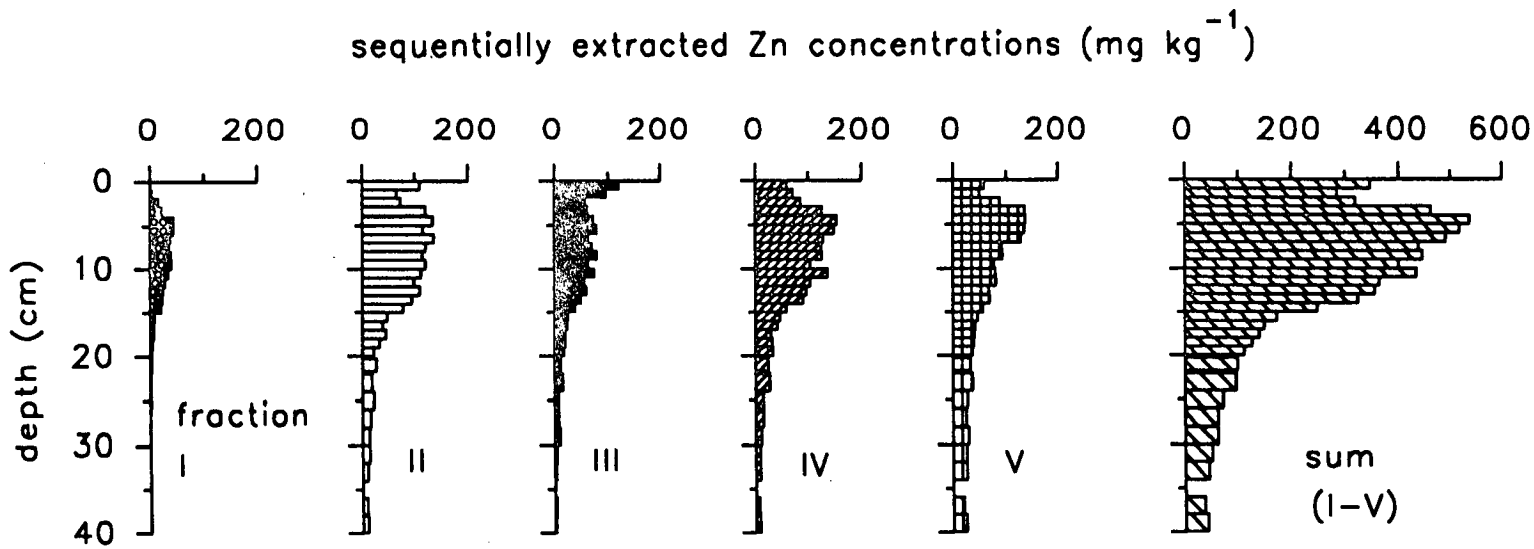
sequentially extracted Zn concentrations (mg kg^{-1})
0 200
0 200
0 200
0 200
0 200
0 200 400 600
depth (cm)
0
10
20
30
40
fraction
I
II
III
IV
V
sum
(I–V)

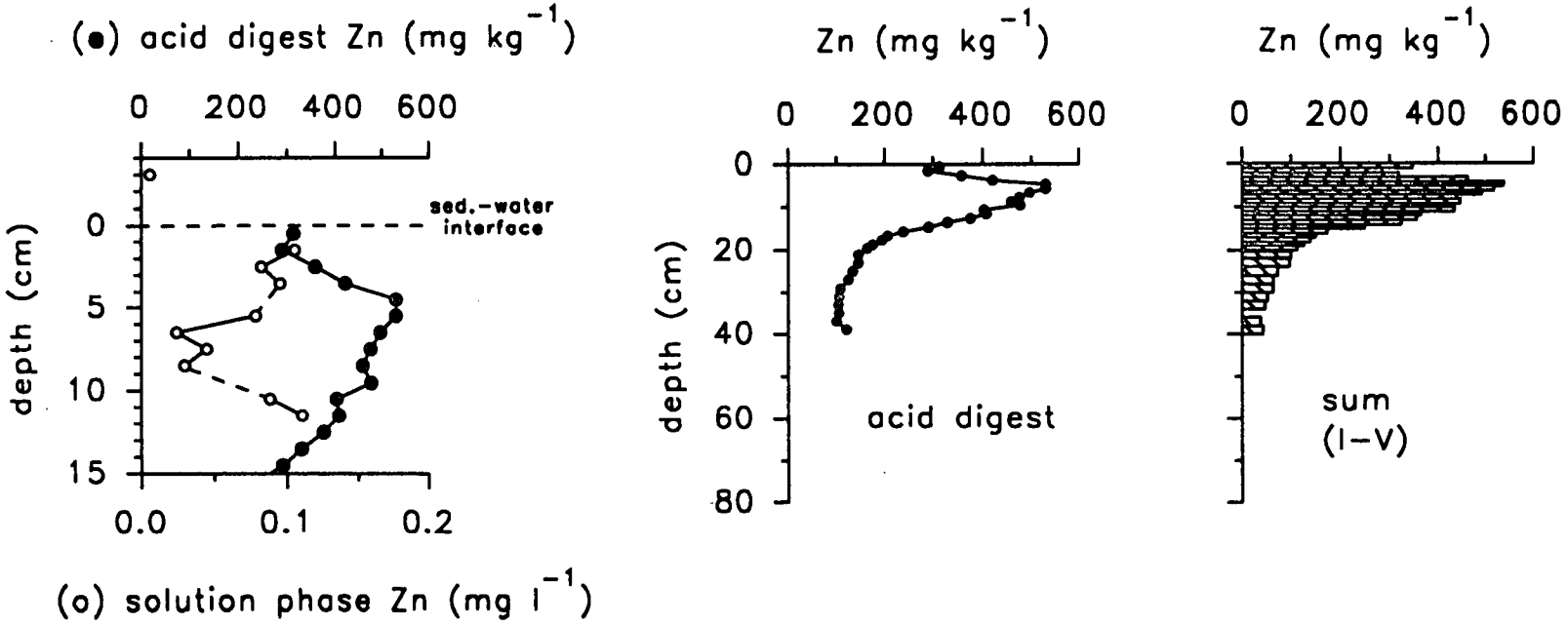
(●) acid digest Zn (mg kg^{-1})
0 200 400 600
sed.–water interface
depth (cm)
0
5
10
15
0.0 0.1 0.2
(o) solution phase Zn (mg l^{-1})
Zn (mg kg^{-1})
0 200 400 600
0
20
40
60
80
depth (cm)
acid digest
Zn (mg kg^{-1})
0 200 400 600
sum
(I–V)

than 2 cm, combined with an increase in Zn lability, indicated by higher Zn concentrations in fraction I between 1 and 26 cm (also similar to the Mn partitioning), suggests a relationship between Zn behaviour and that of Mn at this site. In contrast, patterns in the Zn porewater data (Tables 4.18 and 4.19, Figs. 4.8 and 4.14) are different from the Mn solution phase data. Zn concentrations (similar in the two cores) decrease from the surface downcore to fairly constant values between 5 and 10 cm (Lo2-2C) and 6 and 9 cm (Lo2-1C), followed by an increase towards the base of the core with an additional peak in core Lo2-2C at 10-11 cm (the section in which the Fe porewater maximum is observed). On the basis of the porewater data, maximum release of Zn to the porewaters occurs at 0-1 cm and in the deepest sampled section (13-14 cm in core Lo2-2C or 11-12 cm in core Lo2-1C). These porewater results and the sub-surface solid phase Zn enhancements are not explicable in terms of an association of Zn with the diagenetic redox-cycling of Mn.

The increasing contribution of Zn in fraction V to the sum of fractions I-V with depth is probably a result of sulphide formation, as conditions for this become more favourable with increasing depth. The ratio of sum concentrations I-V/acid digest concentrations to 15 cm is approximately 1 (where greater than 1, due to factors previously explained for Pb), but then decreases to 0.4 (by 40 cm) showing that with depth Zn is forming more resistant associations.

In conclusion, Zn is more labile in the sediment at this site than Pb, but mobility is limited and does not appear to have significantly altered the historical record of trends in anthropogenic input of Zn to the loch.

Copper partitioning and solution phase data

Cu was not detectable in fractions I, II or III, all samples were ≤ 5 mg kg^{-1} and below 3 cm, were ≤ 2 mg kg^{-1}. The ratios of the sum of fractions I-V /acid digest concentrations ranged from 0.5-0.9 (mean = 0.68), with no obvious trend (Table 4.15, Fig. 4.15). Cu in fraction V comprises a mean 72% of the total Cu removed by the sequential extraction, and concentrations (ranging from 11 to 23 mg kg^{-1}) show an overall decreasing trend downcore. The same trend also appears for Cu in fraction IV (3-10 mg kg^{-1}).

Cu was only detectable in the porewaters from core Lo2-1C (0.015-0.092 mg l^{-1}) (Table 4.18, Fig. 4.16) and was below the detection limit of 0.01 mg l^{-1} in porewater core Lo2-2C and in all water column samples. The peak in porewater Cu at 8-9 cm could be a sampling artefact, since above and below this depth there is no evidence of a trend towards this maximum value, but if real, the low concentrations in the rest of the core do not imply significant mobility of Cu. The results show that

once deposited, Cu is associated mainly with organic matter, and possibly CuS at depth, and is not remobilised, so that interpretation of the concentration profile trends in terms of historical Cu deposition is justified.

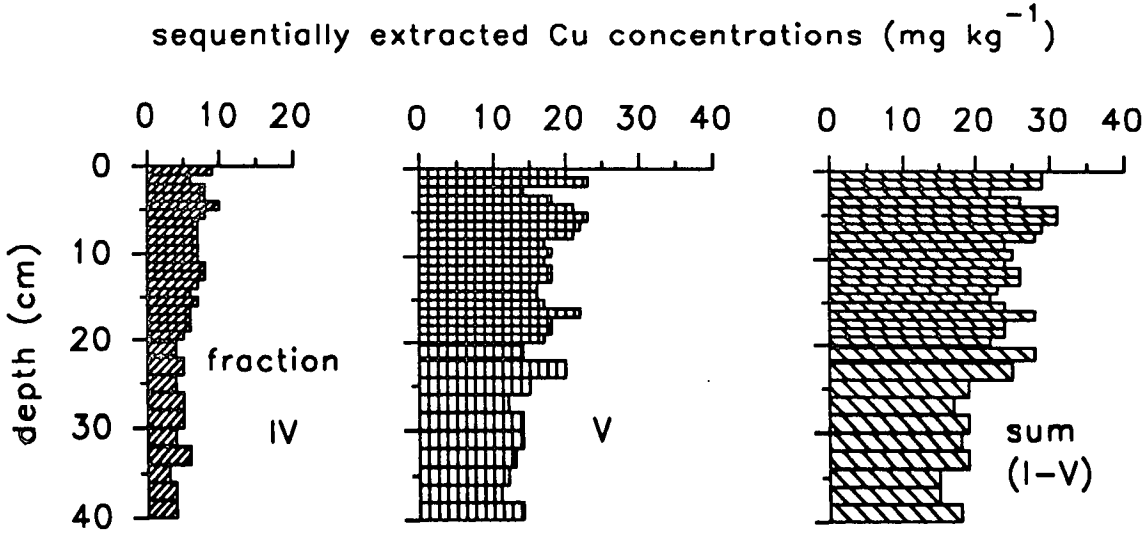
sequentially extracted Cu concentrations (mg kg^{-1})
depth (cm)
0
10
20
30
40
0 10 20
0 10 20 30 40
0 10 20 30 40
fraction
IV
V
sum
(I–V)

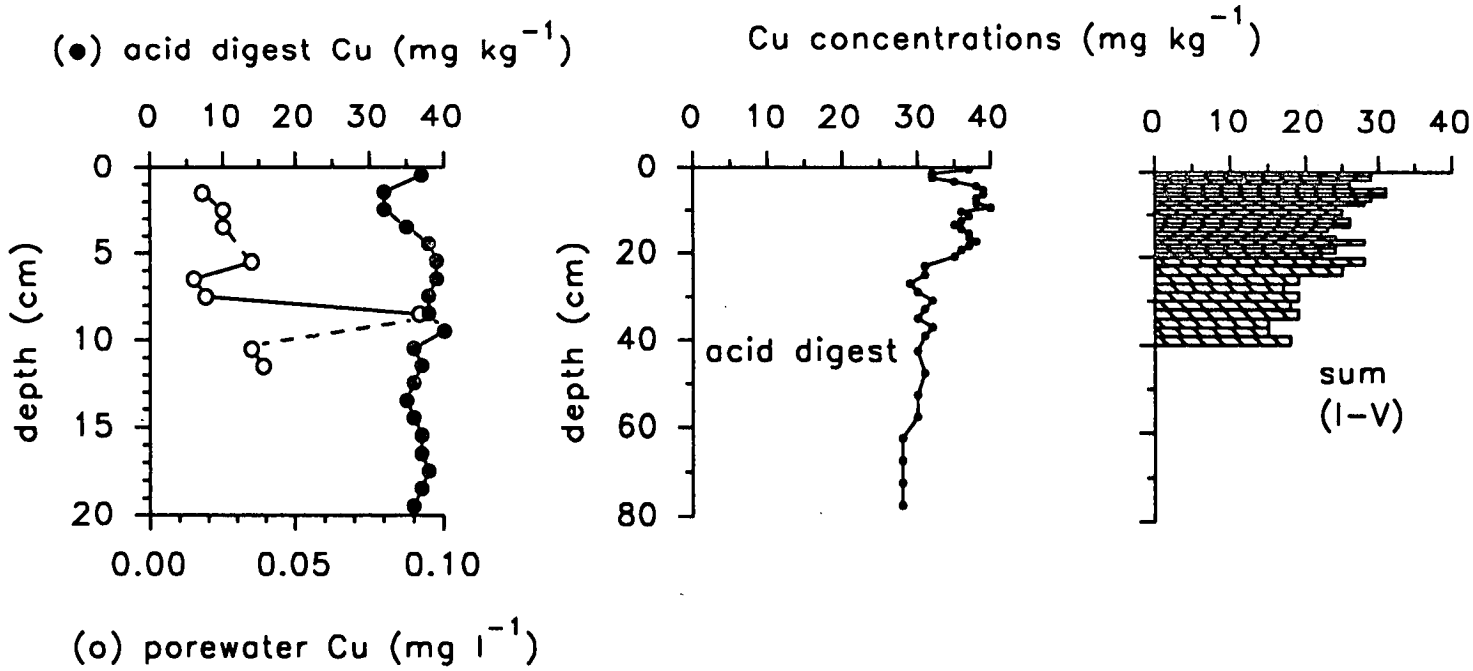
(●) acid digest Cu (mg kg^{-1})
0 10 20 30 40
0
5
10
15
20
depth (cm)
0.00 0.05 0.10
(o) porewater Cu (mg l^{-1})
Cu concentrations (mg kg^{-1})
0 10 20 30 40
0
20
40
60
80
depth (cm)
acid digest
0 10 20 30 40
sum
(I–V)

4.4.4 Radionuclide data for site 1

^{210}Pb data

The peak excess ^{210}Pb concentration (Table 4.8, Fig.4.17) of 125 Bq kg^{-1} occurs in the 1-2 cm section, but apart from this slightly increased value, the ^{210}Pb concentrations are constant, within the limits of experimental error, from 0-8 cm. ^{210}Pb then drops to a minimum of 33 Bq kg^{-1} (8-9 cm) and was not detectable below 9 cm. The ^{210}Pb concentration profile pattern, with an abrupt decrease to non-detectable levels below 9 cm, strongly suggests that the sediment is well-mixed to at least 8 cm (by bioturbation or physical means), or that sediment slumping or very rapid accumulation has occurred. If steady state conditions prevail, then an excess ^{210}Pb flux of 72 Bq m^{-2} y^{-1} is implied (inventory x λ). The ^{210}Pb results are not suitable for deriving a core chronology.

Radiocaesium data

^{137}Cs concentrations (Table 4.10, Fig. 4.18) decrease from a maximum of 407 Bq kg^{-1} at the surface (0-1 cm) to 4-5 cm and then rise to a sub-surface peak at 6-7 cm (221 Bq kg^{-1}), below which concentrations decrease to the base of the core. ^{134}Cs concentrations decrease from 49 Bq kg^{-1} (0-1 cm) to non-detectable levels by 4-5 cm, indicating a maximum depth of Chernobyl radiocaesium penetration of 4 cm. This implies sediment mixing to a depth of 4 cm since deposition of Chernobyl fallout, four years prior to the sampling, and rules out the possibility of sediment slumping or rapid accumulation, suggested on the basis of the ^{210}Pb data alone. The radiocaesium specific activities are much lower than at site 2, where the sediment was less sandy and had a higher porosity. The higher activities at site 2 are probably due to finer-grained sediment having a greater scavenging capacity than sediment at site 1.

On the basis of the $^{134}Cs/^{137}Cs$ activity ratios (Table 4.10), weapons testing fallout ^{137}Cs extends from the surface to a depth of 13 cm, with a sub-surface maximum at 6-7 cm (Fig.4.18, Appendix 1). The persistence of weapons testing fallout ^{137}Cs in the surface layers and the sub-surface maximum at 6-7 cm suggests sediment accumulation together with strong mixing. The sediment mixing is apparently more intense than at site 2, so extreme caution must be applied in interpretation of the metal profiles. If the weapons testing peak (Fig. 4.18) is taken to be at a date of 1963 and the cumulative weight between this section and the section containing the maximum Chernobyl-derived ^{137}Cs concentration (1-2 cm) (Fig. 4.18, Appendix 1) is divided by 23 years, this gives a sedimentation rate of 91

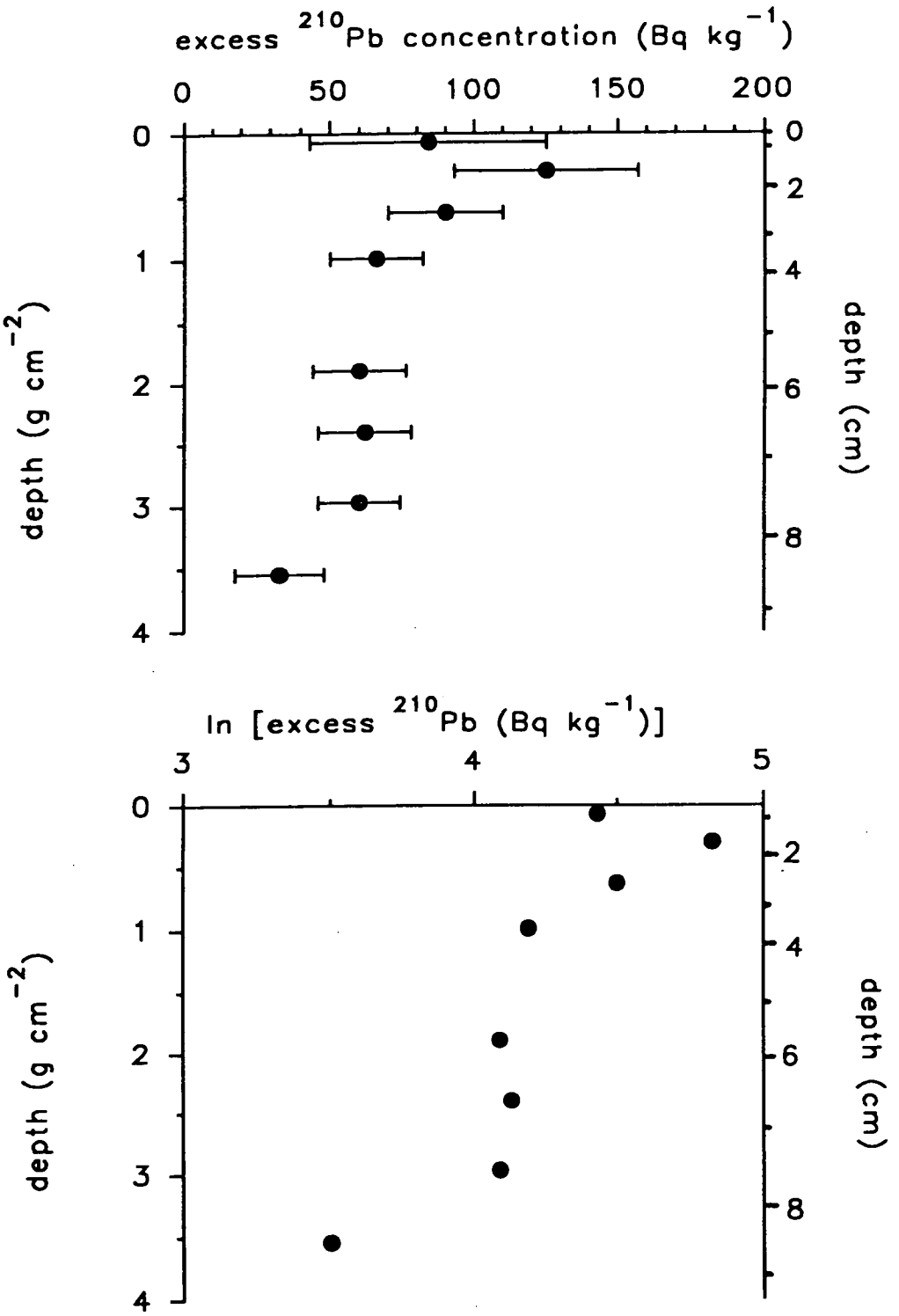

Fig 4.17 Excess ^{210}Pb and ln (excess ^{210}Pb) against depth (weight/area) in Loch Lomond sediment core Lo1–A

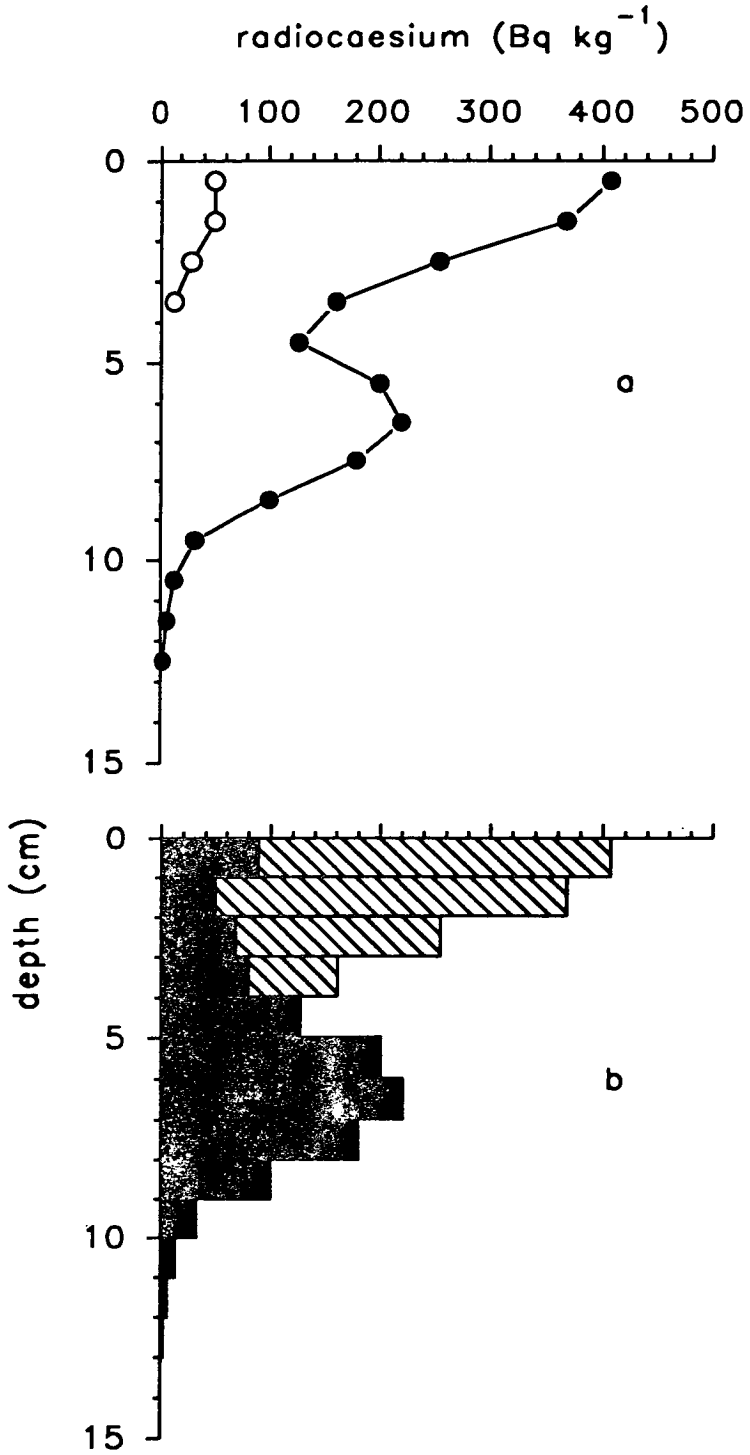

Fig. 4.18 Profiles of ^{134}Cs (o) and ^{137}Cs (•) concentrations (a) and ^{137}Cs concentrations showing the calculated component sources of fallout from weapons testing (■) and Chernobyl (▨) (b) in Loch Lomond sediment core Lo1–A.

mg cm^{-2} y^{-1}. While a good chronology cannot be obtained for this core, this value gives an indication of the accumulation rate.

Radiocaesium inventories at sites 1 and 2

Table 4.24 shows estimated contributions to ^{137}Cs inventories from Chernobyl and weapons testing fallout (decay-corrected to fallout deposition dates), which have been calculated using the $^{134}Cs/^{137}Cs$ activity ratios. The agreement between the estimated deposition values and the recorded fallout values is reasonably good, although the estimated Loch Lomond deposition values are slightly higher than the recorded deposition values, which could be due to catchment weathering or some sediment focusing. Generally however, there appears to be little or no loss of radiocaesium from the sediment and the distinction of separate weapons testing/Chernobyl peaks in the sediment at both sites shows that radiocaesium is efficiently scavenged in the clay-rich sediment.

4.4.5 Metal data for site 1

Lead, zinc, copper and cadmium in HNO_3/HCl acid digested sediment

Since a reliable core chronology for this site could not be established, due to the sediment mixing, discussed in the previous section, an historical interpretation of the Pb, Zn, Cu and Cd data, as at site 2, is not really justified. However, the approximate sedimentation rate of 91 mg cm^{-2} y^{-1} will be used to date changes in the metal concentration profiles, for comparison with trends at site 2.

Low concentrations of Pb, Zn, Cu and also Co, Ni, Fe and Mn are observed between depths of around 13-14 cm and 34-40 cm. This is similar to patterns in the HNO_3/HCl digested metal concentration profiles for site 2. Using the sedimentation rate of 91 mg cm^{-2} y^{-1}, and the cumulative weight/area for the sections 34-40 cm, the onset of low concentrations dates to between 1768 (38-40 cm) and 1809 (32-34 cm), if mixing to the base of 8 cm is taken into account (as described for site 2). These dates are earlier than the corresponding date for site 2 (1846), but since the sedimentation rate for site 1 is an approximation, this difference may not be significant and it seems probable that the low metal concentrations at the two sites are a result of the same input of older material, indicated by Dickson *et al.* (1978). Additionally this dilution of metal concentrations by an input of older material could explain the apparent increase in concentrations (Fe, Pb, Zn, Cu, Co, Ni) below 40 cm.

Table 4.24 ^{137}Cs inventories in Loch Lomond sediment cores Lo2-1A (site 2, southern basin) and Lo1-A (site 1, intermediate, central basin), compared with reported deposition values (Clark and Smith, 1988; Peirson *et al.*, 1982). Sediment inventories have been corrected for decay since 1.5.86 (Chernobyl fallout) and 1963 (weapons testing fallout).

	Loch Lomond		
	Lo2-1A	Lo1-A	reported deposition
Chernobyl ^{137}Cs (k Bq m^{-2})	6.85 ± 0.05	2.64 ± 0.13	1-5
weapons testing ^{137}Cs (k Bq m^{-2})	14.41 ± 0.10	10.22 ± 0.22	6-8

Table 4.25 Radionuclide and anthropogenic Pb and Zn inventories at sites 1 and 2 in Loch Lomond.

radionuclide data (Lo1-A & Lo2-1A) (kBq m^{-2})	site 1	site 2	ratio site 1/site 2
Chernobyl ^{137}Cs	2.64	6.85	0.38
weapons testing ^{137}Cs	10.22	14.41	0.71
excess ^{210}Pb	2.32	4.90	0.47
metal data (Lo1-B & Lo2-1B) (g m^{-2})			
excess Pb	1.59	5.3	0.30
excess Zn	3.10	11.5	0.27

Pb concentrations (Table 4.12, Fig. 4.19) increase from around 13-14 cm (14 mg kg^{-1}) to enhanced values between 10 cm and the sediment surface (mean concentration = 38 mg kg^{-1}). Concentrations from 14 cm downward are a mean 11 mg kg^{-1}. Concentrations are lower than the corresponding values at site 2. The peak concentration (41 mg kg^{-1}) at 5-6 cm corresponds to a radiocaesium-derived date of 1968, which agrees well with the onset of a sub-surface decrease in Pb concentration at site 2, dated to the mid-1960's.

The HNO_3/HCl digested Zn concentration profile (Table 4.12, Fig. 4.19) shows a similar trend to Pb, increasing from 15 cm to a maximum concentration of 148 mg kg^{-1} at 5-6 cm, as for Pb *i.e.* at a date of 1968, similar to the Zn concentration peak at site 2, dated to 1970. Above 5 cm, the concentration generally decreases to the surface (0-1 cm), where the concentration is 129 mg kg^{-1}. Concentrations below 15 cm are fairly constant to 40 cm (mean = 65 mg kg^{-1}), below which a gradual increase occurs to 104 mg kg^{-1} in the 60-65 cm section. Again, the onset of increase in concentration is further up the core than at site 2 and concentrations are lower at this site.

The Cu concentration profile (Table 4.12, Fig. 4.19) is very similar in shape to those of Pb and Zn. A maximum of 27 mg kg^{-1} is observed in the 1-2 cm section, below which concentrations decrease slightly to 20 mg kg^{-1} at 13-14 cm. Concentrations remain at a fairly constant 16 mg kg^{-1} from 14-40 cm, increasing again to the base of the core, reaching as high as 26 mg kg^{-1} in the 60-65 cm section.

Cd was undetectable below 7 cm, with the exception of a value of 0.3 mg kg^{-1} in the 65-70 cm section (Table 4.12). A surface peak at 0-1 cm (0.8 mg kg^{-1}), decreasing to 0.5 mg kg^{-1} by 3 cm, and a sub-surface maximum of 0.9 mg kg^{-1} occurs at 5-6 cm, as for Zn and Pb.

While the radiocaesium-derived dates for peak concentrations of Pb, Zn and Cd agree well with the dates at site 2 for the onset of declining concentrations of these metals towards the sediment surface, the depths at which pollutant metals increase at site 1 is clearly later than at site 2. A combination of the intense sediment mixing and different sediment type at site 1 may have resulted in a more distorted historical record of pollutant metal input to the loch at this site, compared with site 2.

Cobalt and nickel in HNO_3/HCl digested sediment

Concentration profiles of both Co and Ni in HNO_3/HCl digested sediment (Table 4.12, Fig. 4.19) show similar trends, with peaks more defined for Co than Ni. The lower concentrations between 15 and 38 cm (Co 16 mg kg^{-1}) and 16-40 cm (Ni 26 mg kg^{-1}) are apparent, as in the Fe, Mn, Pb, Zn and Cu concentration profiles.

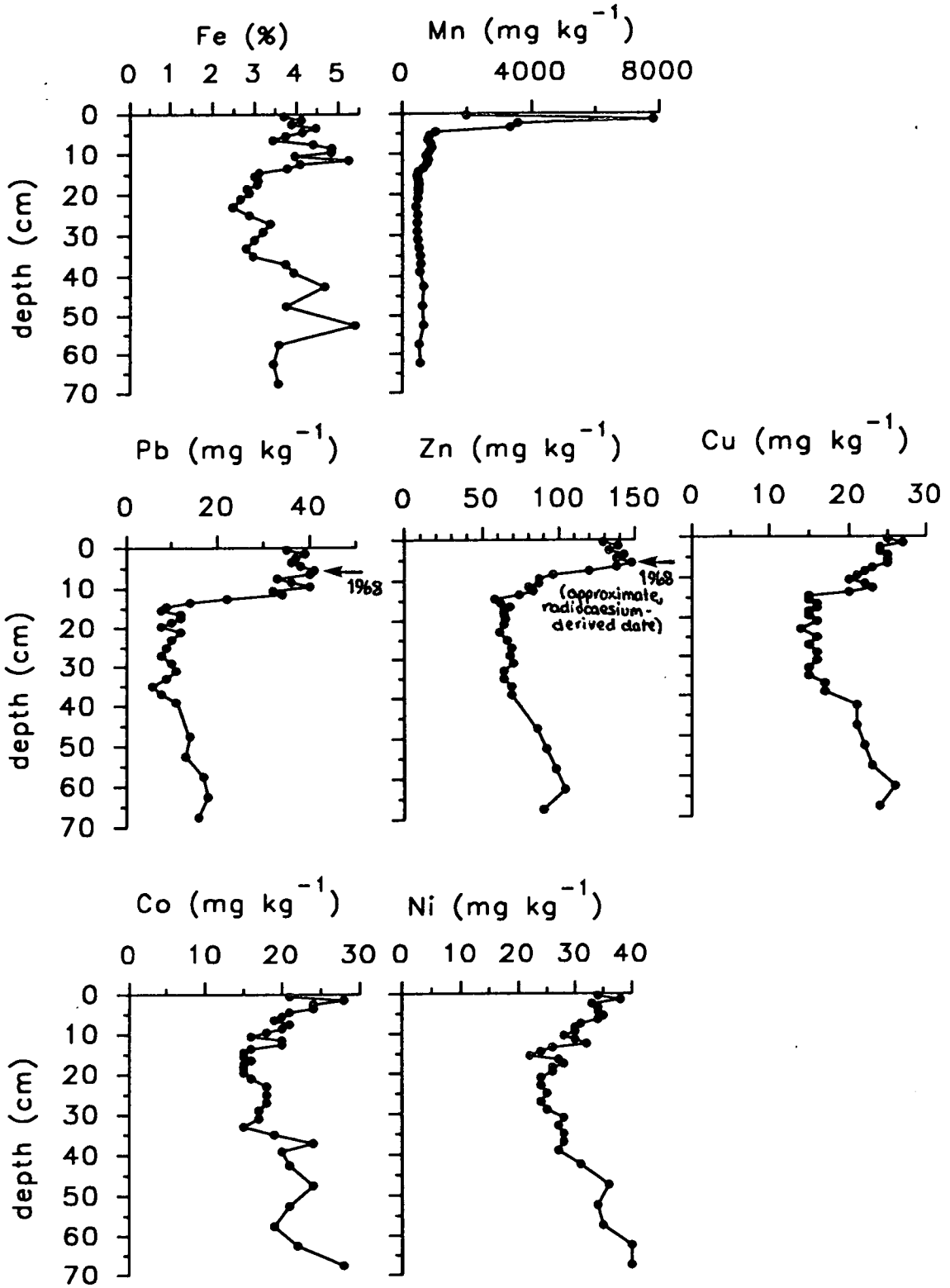

Fig 4.19 Metal concentrations in HNO_3/HCl acid digested Loch Lomond sediment core Lo1–B

Above this depth, concentrations generally rise to sub-surface (1-2 cm) enhancements of 28 mg kg^{-1} (Co) and 38 mg kg^{-1} (Ni).

Iron and manganese in HNO_3/HCl digested sediment

Concentrations of Fe in HNO_3/HCl acid digested sediment at site 1 (Table 4.12, Fig. 4.19) range from peaks of 5.4% at 50-55 cm and 5.2% at 11-12 cm to a minimum concentration of 2.5% at 22-24 cm. The zone of low concentrations extends from 15-36 cm (mean = 3.0%).

The Mn profile (Table 4.12, Fig. 4.19) has a sub-surface maximum of 7,820 mg kg^{-1} at 1-2 cm, slightly deeper than the Mn peak position at site 2. Below this peak, the concentration decreases to 840 mg kg^{-1} by 6 cm and the mean concentration below this is 605 mg kg^{-1}. The values between 15 and 40 cm are slightly depressed (mean = 498 mg kg^{-1}), as for Fe.

The sub-surface maximum in Mn and the less pronounced enhancement of Fe in the sediment above 12 cm are explicable, as at site 2, in terms of redox-driven diagenesis.

Manganese partitioning data

The profile of sum concentrations in fractions I-IV (Table 4.13, Fig. 4.20) shows a similar pattern to concentrations in acid digested sediment, and the ratio of sum concentrations I-IV/acid digest concentrations is >0.8 above 5 cm and below this an average of 0.6. In the enhanced zone of 0-4 cm, fraction III is most significant, comprising a mean 72% of the sum I-IV concentrations. Fraction IV is also important, particularly in the 1-3 cm depth range (37%), contrasting with site 2 where fraction IV is not significant. This may be an artefact of the extraction procedure in which some of the Mn oxides/hydroxides were not removed by fraction III, but in fraction IV. As the sum I-IV/acid digests ratio decreases to 0.6 below 5 cm and in the absence of fraction V, it is more useful to compare actual concentration changes in the fractions (rather than % contributions). Similar to the situation at site 2, there is an increase in labile Mn below the enhancement zone, indicated by an increase of Mn in fraction I from a mean 0.7 mg kg^{-1} to 109 mg kg^{-1} by 6 cm, which is coincident with the drop in concentration in fractions III and IV, consistent with redox-driven diagenesis.

Iron partitioning data

The ratios of sum of fractions I-IV/acid digest for Fe are low (0.05-0.28), so that much of the Fe must be associated with fraction V (organic matter/sulphides) or,

more probably, with stable (HNO_3/HCl digestible) mineral lattices. Despite this, Table 4.13 and Fig. 4.21 show that more Fe is removed in fraction IV than in fractions II and III (concentrations of 0.14-0.79%). Fe was not detectable in fraction I.

Lead, zinc and copper partitioning data

Pb and Zn show similar trends to Fe (Table 4.14, Figs.4.22 and 4.23), with fraction IV a major component of the total extracted concentrations, and non-detectable levels in the exchangeable fraction I. There is little downcore change in the distribution of Pb and Zn amongst the fractions, indicating little or no mobility of these metals. The ratios of sum concentrations II-IV/acid digest are higher for Pb (mean = 1.1 than for Zn (0.07-0.59), indicating that much of the Zn must be associated with fraction V or be extractable only by acid digestion. Values above 1 could be due to cumulative errors in the partitioning results, or non-homogeneity of the wet sediment sample).

Cu was only detectable in fraction IV (Table 4.15) and showed little variation downcore.

4.4.6 Comparison between sites 1 and 2

Concentrations of radiocaesium, ^{210}Pb and all metals in acid digested sediment were higher at site 2 than site 1. This might be attributed to a higher sedimentation rate at site 1, so in order to compare the two sites, inventories were calculated (Table 4.25) for radiocaesium (both sources), excess ^{210}Pb and 'excess' (anthropogenic) Pb and Zn. A comparison of inventories including non-anthropogenic metal components (*i.e.* total metal inventories) would not be useful since a depth limit would have to be set and, in cores with different sedimentation rates, this would correspond to deposition over a different time period.

'Excess' Pb and Zn, Chernobyl ^{137}Cs and excess ^{210}Pb inventories are around three times higher at site 2 than site 1 (Table 4.25). The weapons testing ^{137}Cs inventory is only 1.4 times higher, which could be due to higher catchment inputs of weapons testing radiocaesium at site 1. The higher inventories of radionuclides and metals are probably due to greater scavenging capacity of finer-grained, less sandy particulates at site 2 than site 1.

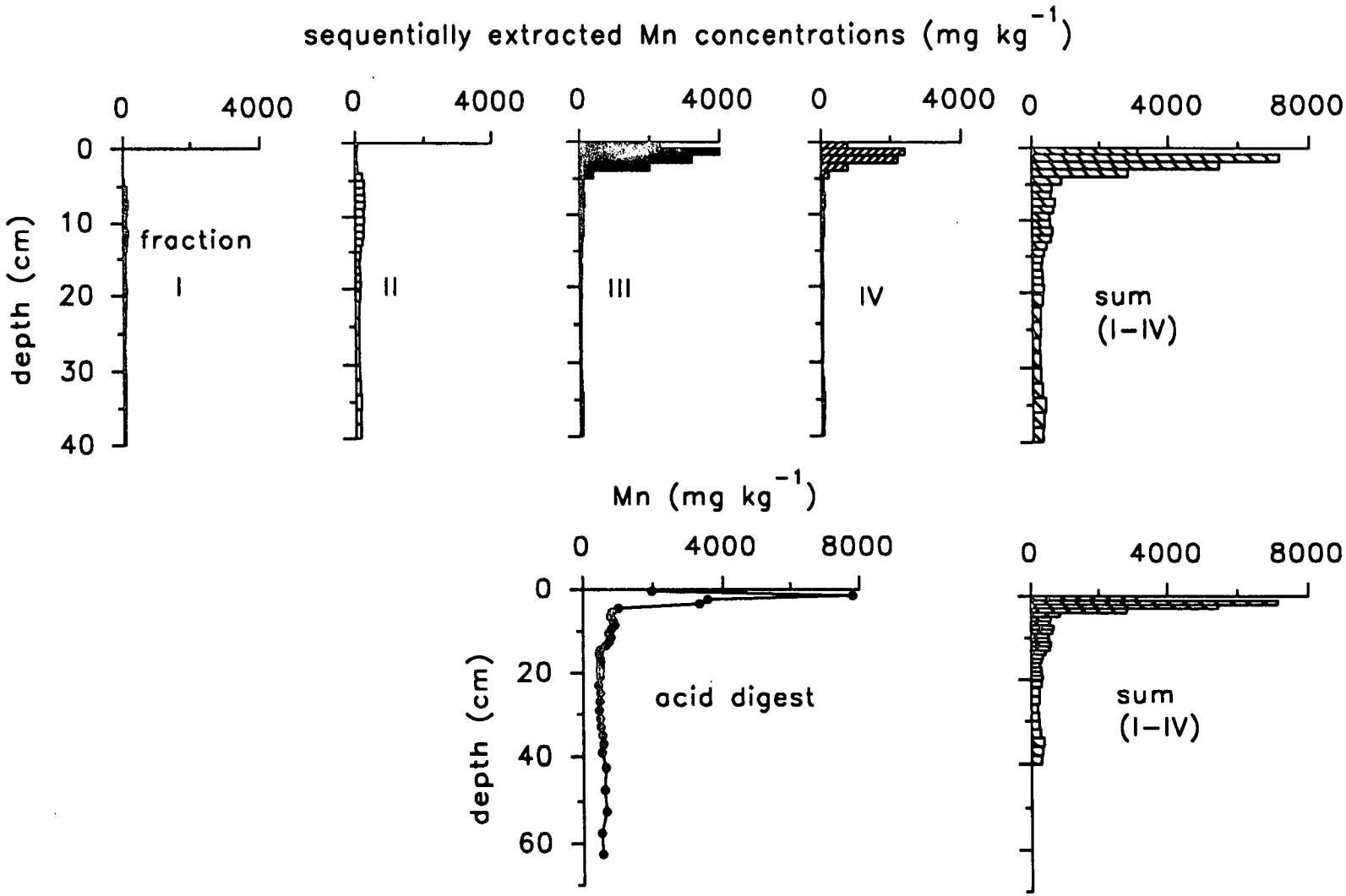
sequentially extracted Mn concentrations (mg kg^{-1})
0
4000
8000
depth (cm)
0
10
20
30
40
fraction
I
II
III
IV
sum
(I–IV)
Mn (mg kg^{-1})
60
acid digest

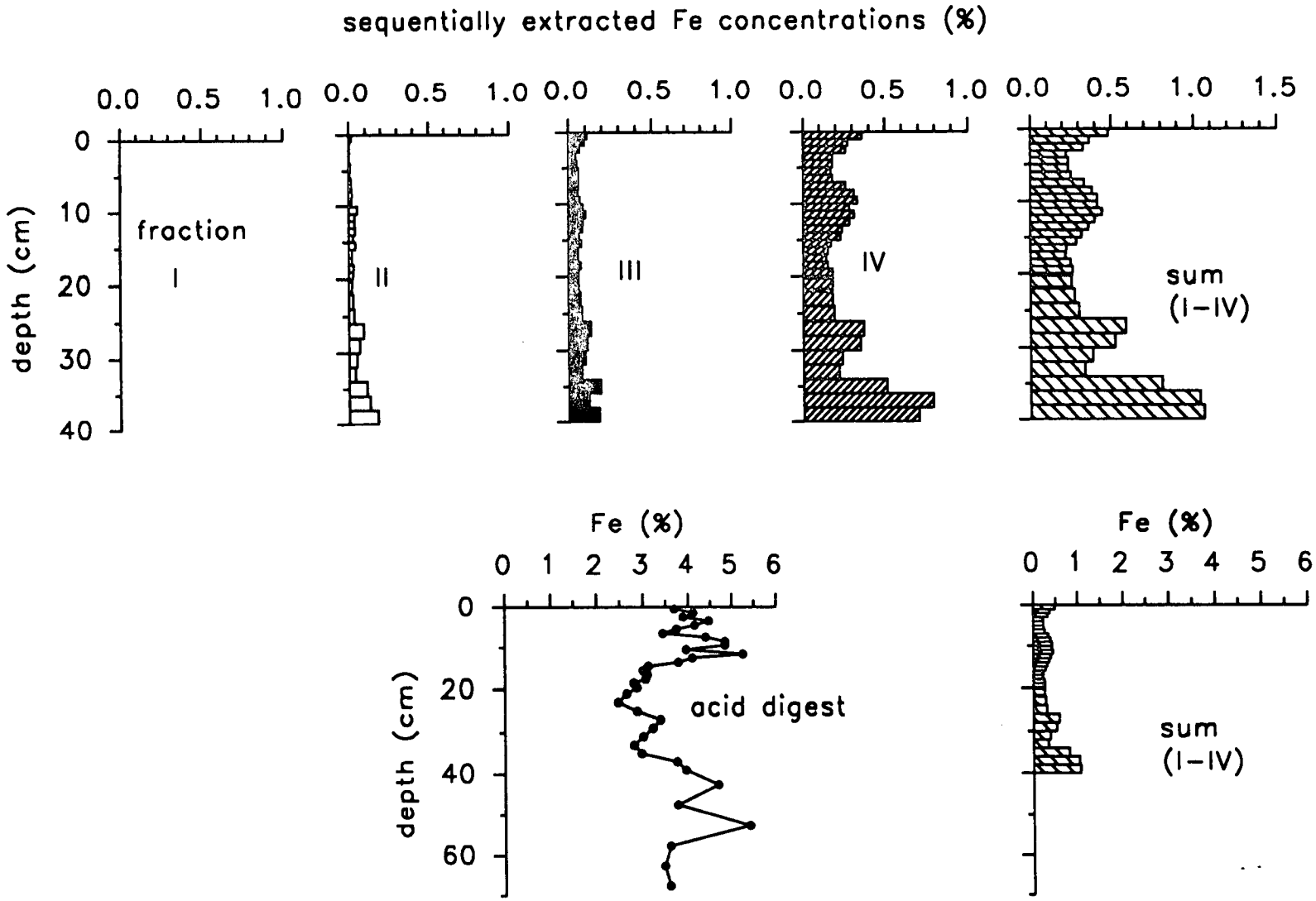
sequentially extracted Fe concentrations (%)
0.0 0.5 1.0
0.0 0.5 1.0
0.0 0.5 1.0
0.0 0.5 1.0
0.0 0.5 1.0 1.5
depth (cm)
0
10
20
30
40
fraction
I
II
III
IV
sum
(I–IV)
Fe (%)
0 1 2 3 4 5 6
Fe (%)
0 1 2 3 4 5 6
depth (cm)
0
20
40
60
acid digest
sum
(I–IV)

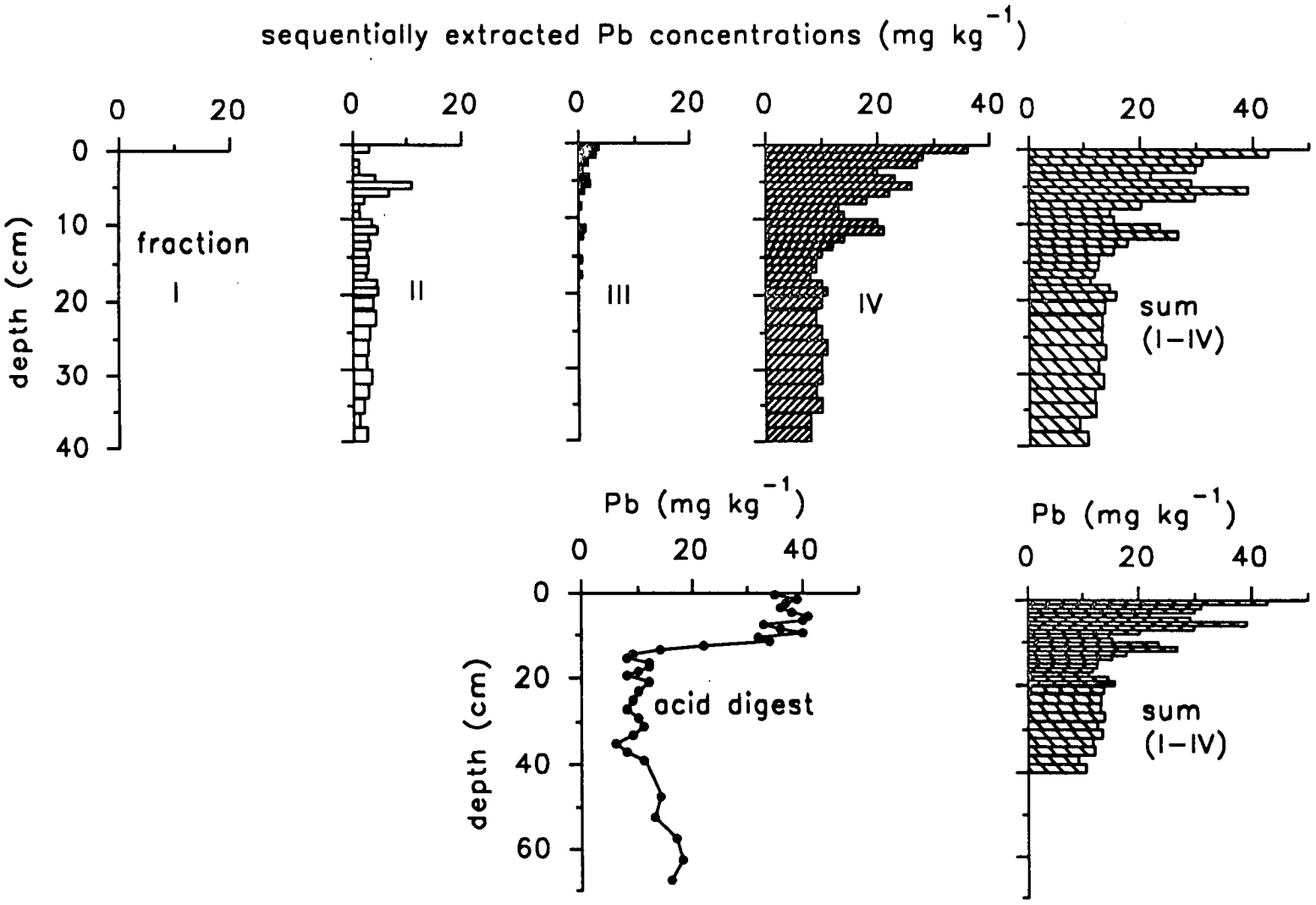
sequentially extracted Pb concentrations (mg kg^{-1})
depth (cm)
fraction
I
II
III
IV
sum
(I–IV)
Pb (mg kg^{-1})
acid digest
sum
(I–IV)

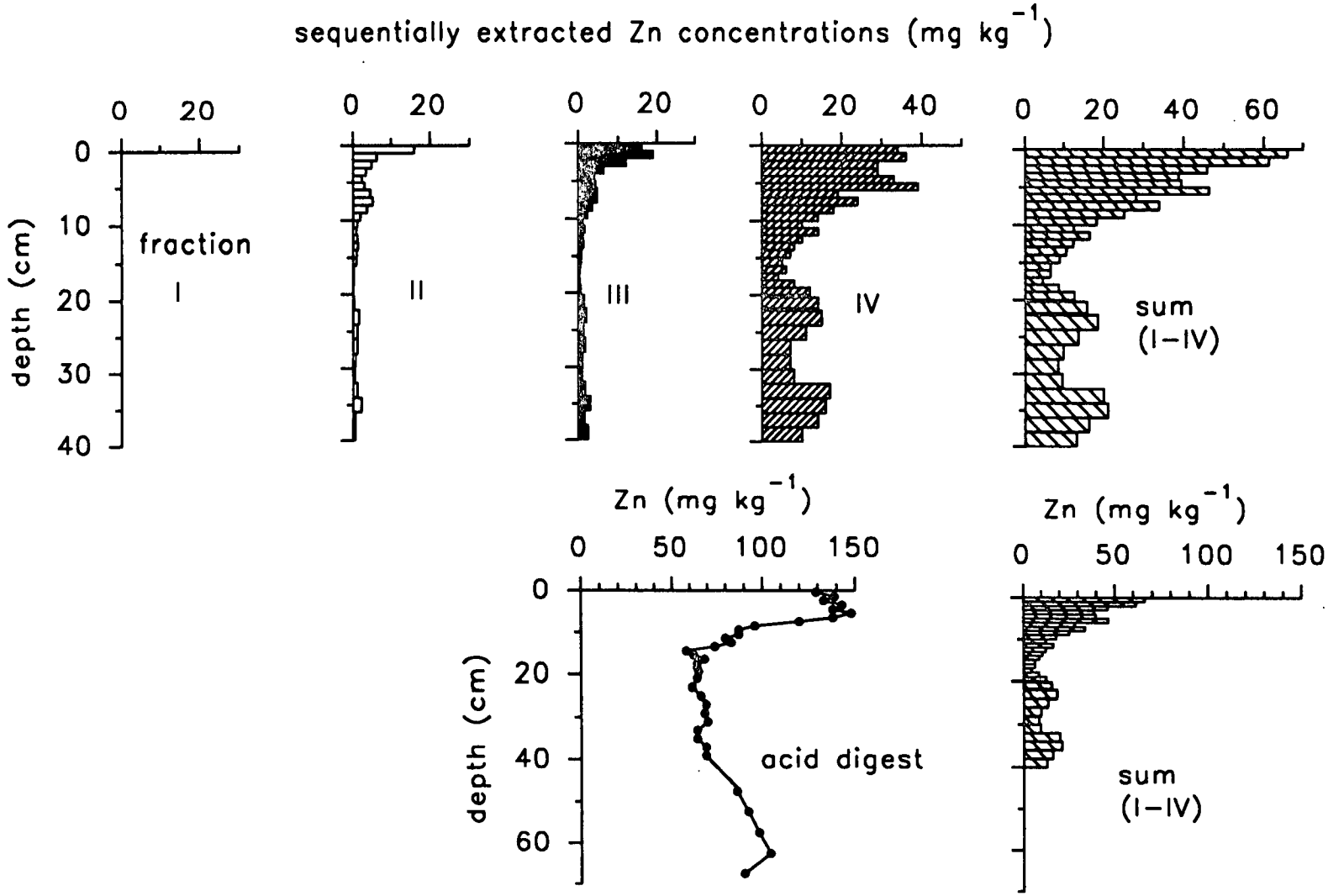
sequentially extracted Zn concentrations (mg kg^{-1})
depth (cm)
fraction
I
II
III
IV
sum
(I–IV)
Zn (mg kg^{-1})
acid digest
sum
(I–IV)

4.5 Conclusions

1. ^{210}Pb and radiocaesium data at site 2 (southern basin) indicate partial mixing of surface sediment to a depth of 6 cm. A sedimentation rate of 32 ± 4 mg cm^{-2} y^{-1} was obtained using the ^{210}Pb data below the mixed zone and this value was used to establish a chronology for the core to interpret the metal data in terms of historical trends.

At site 1 (intermediate, central basin), a high degree of sediment mixing to a depth of 8 cm was found, so that establishing a ^{210}Pb-based chronology is not possible at this site.

2. The radiocaesium profile trends at site 2 are in good agreement with historical fallout inputs. At site 1, although radiocaesium peaks due to weapons testing and Chernobyl fallout cannot be dated by ^{210}Pb chronology, the separation of the radiocaesium into the two source components is nevertheless clear and the positions of the fallout peaks were used to derive an indication of the sedimentation rate, of 91 mg cm^{-2} y^{-1}. Inventories for Chernobyl and weapons testing fallout ^{137}Cs for both sites are similar to, or greater than, values recorded for atmospheric fallout deposition. Results therefore show that radiocaesium is efficiently scavenged in Loch Lomond in the clay-rich sediment.

3. At site 2, acid digest concentration profiles of the pollutant metals Pb, Zn, Cu and Cd are consistent with historical trends in deposition, if sediment mixing is taken into account. Increases in anthropogenic metals commenced around the start of the 18th century for Pb, mid-18th century for Zn and mid-19th century for Cu and Cd. Calculated fluxes and total core inventories of 'excess' metals are in reasonably good agreement with data from other studies in the area.

4. Partitioning data for site 2 show the importance of organic matter associations (fraction V) for Cu, while Pb is predominantly associated with fraction IV, and Zn with fractions II, IV and V. There is no evidence to suggest post-depositional mobility of Pb, Cu or Cd in the core and although the partitioning data imply some Zn mobility associated with Mn redox cycling, this is not supported by the porewater data. It is therefore reasonable to conclude that, despite partial mixing of the surface sediment, the pollutant metal profiles in the southern basin reflect historical trends in atmospheric deposition of these metals to Loch Lomond.

5. At site 1 the maximum Pb, Zn and Cd concentrations in acid digested sediment were dated to the mid-1960's, which agreed well with the dates at site 2 of onset of the decline in metal concentrations towards the sediment surface. There is no

evidence from the acid digest or sequential extraction data to suggest post-depositional mobility of Pb, Zn, Cd or Cu at site 1.

6. Metal concentration profiles at sites 1 and 2 indicate a period of change in sediment composition, which is in agreeement with other work on Loch Lomond and is attributed to changes in the sediment source, due to catchment disturbance, resulting in an input of older sediment material depleted in various elements, notably in this study, Fe, Mn, Ni and Pb (both sites) and Zn, Cu and Co (site 1). At site 2 the onset of lower concentrations was dated to the mid-19th century and at site 1, where the derived sedimentation rate was less reliable, to the late 18th/early 19th centuries.

7. The behaviour of Fe and Mn at both sites is dominated by redox-driven diagenetic remobilisation and reprecipitation, as shown by the data from acid digestion, sequential extraction and, at site 2, solution phases. This agrees with previous work carried out on the loch.

8. Inventories of radionuclides and 'excess' Pb and Zn are higher at site 2 than site 1, which is probably a reflection of the finer-grained sediment, with greater scavenging capacity, at site 2.

Chapter 5 Loch Leven

5.1 Study Area

Loch Leven lies approximately 35 km north of Edinburgh (OS grid ref. NO 150 010) (Fig. 5.1). The loch occupies the central part of a natural bedrock depression overlying Upper Old Red Sandstone, which was much less resistant to erosion than surrounding lithologies during the Aberdeen-Lammermuir Readvance glaciation (15,000-17,000 BP). Loch Leven is a drift basin, formed in sand and gravel deposits, which overlie boulder clay, and is surrounded by the Lomond Hills to the east, Benarty Hill to the south and the Ochil Hills to the north and north-west, all consisting of relatively resistant igneous rocks. The larger islands in the loch today are upstanding masses of glaciofluvial sand, while the major deeps are dead ice hollows. The loch form resembles a dish, with a shallow rim around the edge of a central deeper area of water. The morphology of Loch Leven has only been affected by one major event: the partial drainage of the loch during 1829-1831 for land reclamation and water storage for industries. This resulted in a lowering of the water level by approximately 1.4 m, reduction of the loch area by a quarter, an increase in size of four existing islands and emergence of three new islands, so that a total of seven islands currently exist (Fig. 5.1). (Kirby, 1974).

In the shallow water areas of the loch the sediments are medium to very fine-grained sands, whilst silty clays predominate in the deeps (Fig. 5.2). Calvert, 1974 The largest area of more or less uniform sediment type is the north-eastern shelf, with mainly sands occurring. The finest sediment occurs to the south and east of Castle Island and Reed Bower, where the median grain size is <4 μm. To summarise, the most common sediment types are:

1. Silty clay - confined to the deeper areas of the loch, where the amounts of clay are >50% by weight.
2. Medium-grained sand - representing the coarsest sediment, found in shallower waters.
3. Fine-grained sand - intermediate between sediment types 1 and 2, occuring in intermediate water depths.

Combinations of sediment types 1 and 3, and 2 and 3, are common, whereas mixing between 1 and 2 is rare. Surface sediment organic carbon contents (0.05-8.89% by weight) are highly correlated with the amounts of both clay and silt in the sediments. The transition from organic-rich sediments in deep water areas of fine-grained

Islands in Loch Leven

I. St. Serf's Island
II. Castle Island
III. Reed Bower
IV. Roy's Folly
V. Alice's Bower
VI. Scart Island
VII. Unnamed

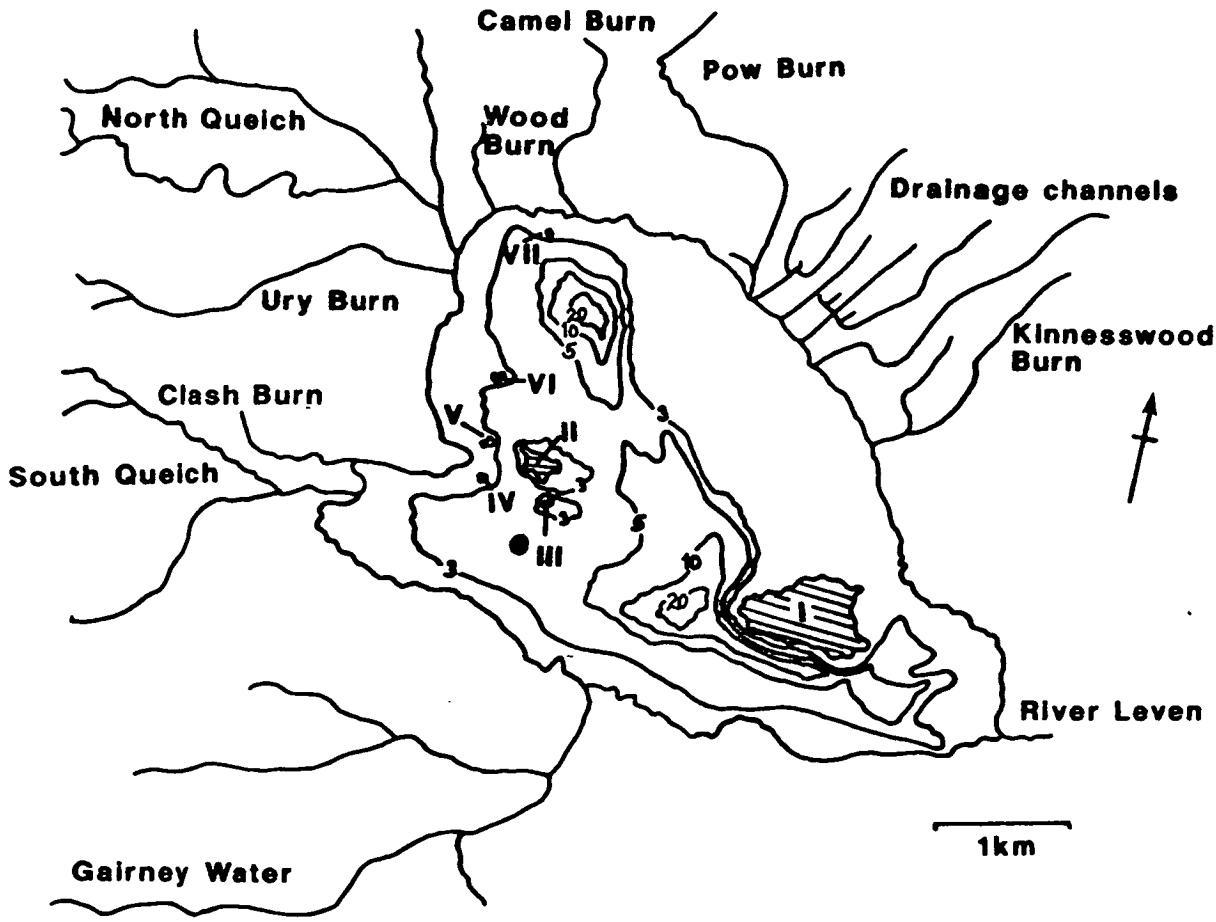

Fig. 5.1 Loch Leven showing depth contours (m) and sampling site (●).

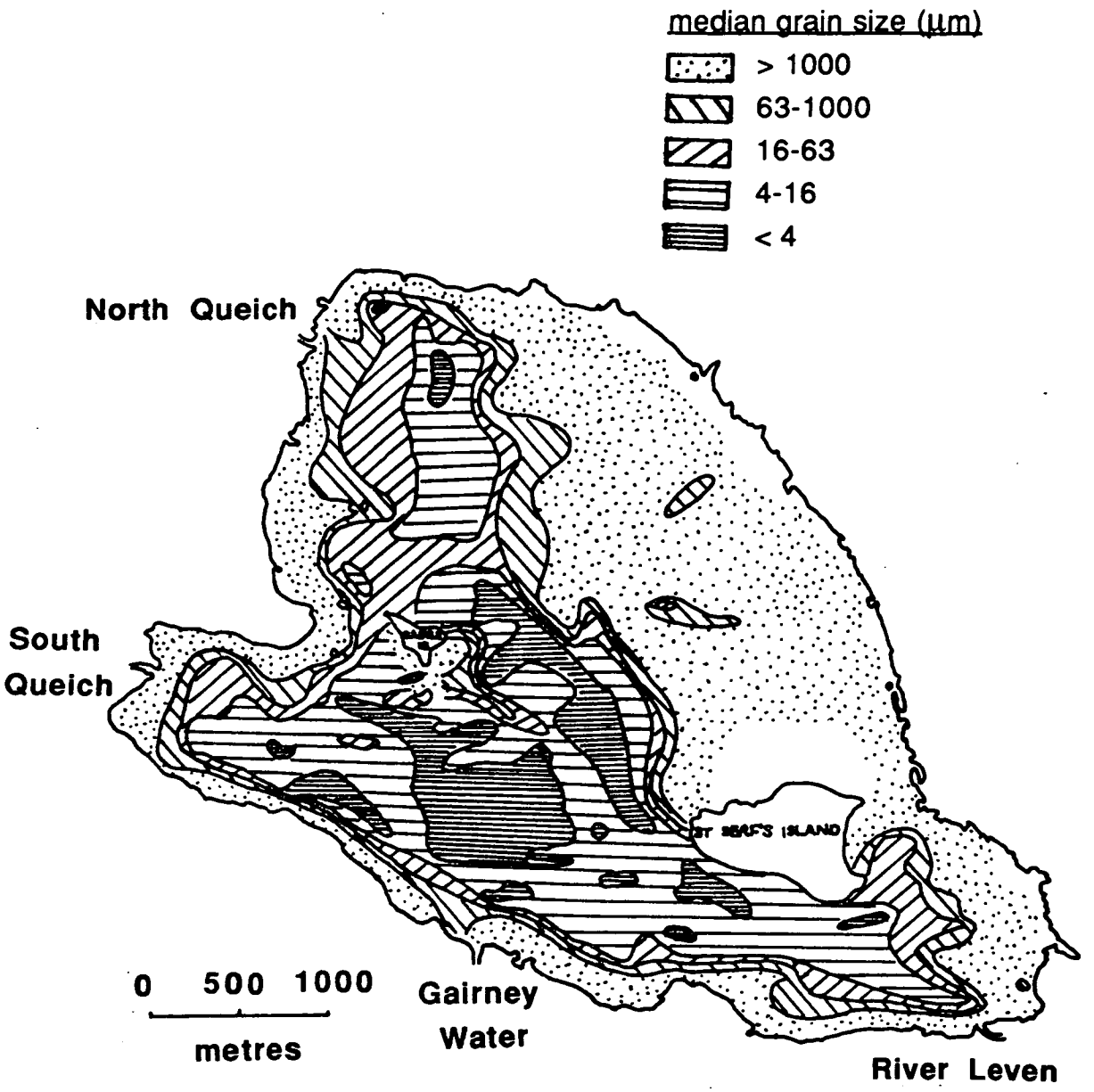

Fig. 5.2 Median grain size of the bottom sediments of Loch Leven (from Calvert, 1974).

sediment to the nearshore sandy areas of low organic carbon content is very abrupt. (Calvert 1974).

The climate of the area is predominantly maritime with a small temperature range and rain and wind at any time of the year, ensuring that the loch is well-mixed and unstratified throughout most of the year. Stratification only occurs in the deeper areas of the loch during occasional continental climatic conditions of warm, calm periods or when the water surface is frozen. If stratification does occur it is more common in the northern than southern deep, but the hypoliminion is generally poorly defined, forming in depths below 10 m. This weak, intermittent stratification is likely to be insignificant, as only 6.2% of the total loch area and 10.3% of the volume occurs below this depth. Diurnal water temperature fluctuations tend to be small, as the incoming radiation and nocturnal heat loss are usually restricted by the frequent cloud cover, particularly during autumn and winter. Loch Leven is therefore typically isothermal with an oxygen concentration approaching saturation (Smith, 1974).

Primary production is mainly due to phytoplankton, with macrophytes occurring sparsely and forming a negligible part of the total primary production. Phytoplankton populations are generally dense and even winter crops can be considerable. Zooplankton are species poor and *Cyclops strenuus abyssorum* predominates. Benthic invertebrates of the shallow, sandy zones are mainly Oligochaeta, Chironomidae, Nematoda, snails *Pisidium* and *Anodonta* and, in the deeper mud, Tubificidae and Chironomidae. In the deep mud zones 90% of the Chironomidae occur in the top 5 cm of sediment and of these, 85-90% are small larvae (1-4 mm), but larger larvae can penetrate to 20 cm and up to 50% of the biomass in the sediment can be in the depth zone 15-20 cm. Loch Leven is famous as an angling fishery, which started around 1850, with a large population of brown trout (*Salmo trutta* L.). Other fish found in the loch are perch (*Perca fluviatilis* L.) and pike (*Esox lucius* L.). Loch Leven also supports populations of wildfowl, some of which occur seasonally (Morgan, 1972).

Morgan and McLusky (1972/73) have noted that a major feature of the Loch Leven ecosystem is its variability from year to year, and the quantity and quality of the flora and fauna are variable. Some of the changes appear to be long-term/permanent, *e.g.* the increase in phytoplankton density, whereas others are cyclical, such as year to year fluctuations in the composition of dominant phytoplankton. Possible causes of these variations include increasing nutrient levels (eutrophication) in the loch and the shallowness and exposure of Loch Leven, which make it particularly susceptible to rapid changes, such as storm events.

The loch is a shallow, eutrophic system and recently has become the focus of concern due to changes in the water quality associated with eutrophication, *e.g.* the nature and density of phytoplankton have meant that the water is unsuitable for potable supplies and, intermittently, for recreational purposes. The limiting factor for algal bloom maximum densities is apparently phosphorus (Bailey-Watts, 1983) and the main phosphorus loadings have been identified as sewage effluents and industrial waste (from a woollen mill) with additional, smaller contributions from roosting wildfowl, rain and runoff from the catchment (mainly agricultural land-use) (Bailey-Watts and Kirika, 1987). Although phosphorus inputs to Loch Leven have been considerably reduced, the algal blooms are a continuing problem, largely because while much of the phosphorus is bound in the sediments for most of the time, it can be released to the water column when conditions become favourable (often coinciding with conditions favourable for algal growth). The main features of Loch Leven and its catchment are listed in Table 5.1.

Table 5.1 Characteristics of Loch Leven and its catchment (Holden, 1974; Smith, 1974)*

Catchment	
area (km^2)	145
ratio catchment:loch area	11:1
Loch	
length (km)	5.9
width (km)	2.3
length of shoreline (km)	18.5
volume ($m^3 x 10^6$)	52.4
mean depth (m)	3.9
maximum depth (m)	25.5
mean renewal time of water	5.2 months
pH	7.2-9.3
alkalinity (mg l^{-1} $CaCO_3$)	30-70
total phosphorus (mg l^{-1})	0.04-0.15
SO_4^{2-} (mg l^{-1})	*ca.* 25

* chemistry reported in 1974

5.2 Sampling and analysis

Sediment cores were collected on three occasions from the same sampling site in Loch Leven, in an area of fine-grained sediment (< 16 μm) (Fig. 5.1), at a water depth of 4 m, using a Jenkin Surface-Mud Sampler (Chapter 2). Reasons for a return to the same sampling site are outlined below. Table 5.2 shows core codes, sampling dates and purpose of core collection. Unsectioned core lengths were 17-20 cm and all cores were sectioned on shore in air at 1 cm intervals (Chapter 2).

Sediment samples from cores LL1-B, LL2-B and LL3-B were acid digested using HNO_3/HCl and LL3-B core sections were also sequentially extracted (Chapter 2). Samples from core LL2-A were used for γ-spectrometric analysis. Water column measurements (Table 5.3) were made in situ on 25.7.90, using the Windermere Profiler 2 (Chapter 2).

The initial sampling in 1989 provided material which enabled experience to be gained in digestion by HNO_3/HCl and metal analysis. This sampling trip was followed by collection of sediment cores in January 1990 and a repeat of the HNO_3/HCl digestion, permitting a comparison with results from core LL1-B. Furthermore, it was important to collect a core for γ-spectrometric analysis with the aim of describing the sedimentation processes at this site. The final sampling of Loch Leven was carried out during an algal bloom in the summer of 1990 as it was felt that a comparison between the HNO_3/HCl acid digest results obtained in the autumn/winter and the summer (especially during an algal bloom) would be of value. Porewater samples were not collected successfully at this site, due to problems encountered with the filter holders during filtration of sediment from the July 1990 sampling.

Table 5.2 Core codes, sampling dates and purpose of core collection from Loch Leven

core code	sampling date	core purpose
LL1-B	22.10.89	chemical digestion
LL2-A	28.1.90	γ-spectrometry
LL2-B	"	chemical digestion
LL3-B	25.7.90	"

Table 5.3 Water column measurements in Loch Leven (25.7.90)

water depth (m)	T. (°C)	O_2 (%)	cond. (µS)	pH
0.2	21.4	118	209	9.7
0.7	19.6	127	211	9.7
1.0	19.3	125	211	9.7
1.5	18.7	110	211	9.6
2.1	18.6	110	211	9.6
2.5	18.6	105	211	9.5
3.1	18.4	105	213	9.5
3.4	18.2	100	214	9.4

5.3 Results

Data for Loch Leven samples are listed in Tables 5.4-5.14. Figures illustrating some of this information are presented in the Discussion (Section 5.4).

1. Tables 5.4-5.7 contain wet and dry sediment section weights, mid-section cumulative weights (g cm^{-2}) and porosities (using an assumed solid sediment density of 2.43 g cm^{-3}) for cores LL1-B, LL2-A, LL2-B and LL3-B. Total carbon content and C/N ratios were measured in core LL1-B (Table 5.4).

2. Total ^{210}Pb, ^{226}Ra and excess ^{210}Pb concentrations are listed in Table 5.8 with mid-section cumulative weights for core LL2-A. ^{226}Ra was not detectable in many of the samples, because of small sample sizes and associated high analytical errors. A value for supported ^{210}Pb of 39 ± 9 $Bqkg^{-1}$ was obtained by taking the mean value from total ^{210}Pb and ^{226}Ra concentrations between 9 and 15 cm.

3. Radiocaesium concentrations (at the time of sampling) and $^{134}Cs/^{137}Cs$ ratios in core LL2-A are presented in Table 5.9.

4. Tables 5.10-5.15 contain metal concentrations from sediment acid digestions (cores LL1-B, LL2-B and LL3-B) and sequential extractions (core LL3-B), for which column headings I-V refer to the following fractions and extractants:

I 1M ammonium acetate, pH7, 20°C (exchangeable fraction)

II 1M sodium acetate, pH5 with acetic acid, 20°C ("carbonate bound"/specifically sorbed)

III 0.1M hydroxylammonium chloride/0.01M nitric acid, 20°C (easily reducible)

IV 1M hydroxylammonium chloride/4.4M acetic acid, 20°C (moderately reducible)

V 30% w/v hydrogen peroxide, pH2, 85+/-2°C; 3.2M ammonium acetate in 3.2M nitric acid (organic fraction/sulphides)

Sum I-V refers to the sum of metal concentrations in all fractions.

5. (BDL) is entered where samples were below detection limit, and (...) where a result was not available.

Table 5.4 Some physical characteristics, carbon content and carbon/nitrogen ratios of Loch Leven sediment core LL1-B. [1]

section depth (cm)	wet section weight (g)	dry section weight (g)	mid-section cumulative weight ($g\ cm^{-2}$)	porosity (%)	carbon content (%)	C/N ratio
0-1	39.99	5.88	0.079	93.4	...	...
1-2	39.00	3.98	0.210	95.5	8.57	8.4
2-3	39.16	5.70	0.340	93.5	7.23	8.9
3-4	36.55	6.14	0.498	92.3	6.32	10.2
4-5	40.98	7.65	0.683	91.4	6.11	9.4
5-6	42.93	8.46	0.898	90.8	5.65	9.9
6-7	45.77	9.66	1.140	90.1	5.18	10.4
7-8	39.61	8.79	1.387	89.5	5.71	11.4
8-9	43.36	9.31	1.629	89.9	5.72	11.9
9-10	41.51	9.34	1.878	89.3	5.58	10.7
10-11	42.33	9.34	2.128	89.6	5.77	9.8
11-12	38.24	8.02	2.360	90.2	6.23	10.6
12-13	40.63	8.23	2.578	90.5	6.87	10.7
13-14	43.73	9.12	2.810	90.2	6.65	8.4
14-15	43.64	9.08	3.053	90.2	6.41	8.4
15-16	41.68	8.34	3.286	90.7	6.79	8.2
16-17	29.43	6.04	...	90.4	6.52	9.7

Table 5.5 Some physical characteristics of Loch Leven sediment core LL2-A[2]

section depth (cm)	wet section weight (g)	dry section weight (g)	mid-section cumulative weight ($g\ cm^{-2}$)	porosity (%)
0-1	37.328	2.992	0.040	96.5
1-2	41.199	4.747	0.144	94.9
2-3	45.441	5.821	0.285	94.3
3-4	45.197	6.704	0.452	93.3
4-5	45.647	7.806	0.646	92.2
5-6	48.771	8.948	0.870	91.5
6-7	49.344	9.177	1.113	91.4
7-8	44.644	8.566	1.350	91.1
8-9	48.247	9.625	1.593	90.7
9-10	52.150	10.597	1.864	90.5
10-11	49.056	10.085	2.140	90.4
11-12	49.676	10.174	2.411	90.4
12-13	48.654	10.123	2.683	90.2
13-14	45.414	10.125	2.953	89.4
14-15	46.714	10.163	3.225	89.7
15-16	25.684	5.321	...	90.3

core cross-section area = 37.39 cm^2

1 incomplete section at 16-17 cm

2 incomplete section at 15-16 cm

Table 5.6 Some physical characteristics of Loch Leven sediment core LL2-B [3]

section depth (cm)	wet section weight (g)	dry section weight (g)	mid-section cumulative weight ($g\ cm^{-2}$)	porosity (%)
0-1	35.536	3.047	0.041	96.3
1-2	40.299	4.690	0.144	94.8
2-3	42.866	4.819	0.271	95.0
3-4	55.784	7.558	0.437	93.9
4-5	45.820	7.169	0.634	92.9
5-6	49.665	8.594	0.845	92.1
6-7	44.448	8.210	1.069	91.5
7-8	45.843	8.857	1.298	91.0
8-9	45.787	8.894	1.535	91.0
9-10	43.334	8.468	1.767	90.9
10-11	51.426	10.412	2.020	90.5
11-12	41.420	8.866	2.277	89.9
12-13	53.400	12.183	2.559	89.2
13-14	49.601	11.252	2.872	89.2
14-15	49.033	10.569	3.164	89.8
15-16	35.112	7.641	...	89.7

Table 5.7 Some physical characteristics of Loch Leven sediment core LL3-B[4]

section depth (cm)	wet section weight (g)	dry section weight (g)	mid-section cumulative weight ($g\ cm^{-2}$)	porosity (%)
0-1	47.815	4.192	0.056	96.2
1-2	39.194	4.617	0.174	94.8
2-3	42.620	6.137	0.318	93.5
3-4	39.413	5.693	0.476	93.5
4-5	39.531	6.492	0.639	92.5
5-6	42.115	8.254	0.836	90.9
6-7	41.624	8.730	1.063	90.2
7-8	36.735	7.983	1.287	89.7
8-9	43.659	9.598	1.522	89.6
9-10	37.509	8.402	1.762	89.4
10-11	44.532	10.430	2.014	88.8
11-12	35.675	8.343	2.265	88.8
12-13	38.456	9.217	2.500	88.5
13-14	34.084	8.587	2.738	87.8
14-15	40.393	9.787	2.984	88.4
15-16	30.668	7.044	...	89.1

core cross-section area = 37.39 cm^2

[3] incomplete section at 15-16 cm

[4] incomplete section at 15-16 cm

Table 5.8 ^{226}Ra and ^{210}Pb data for Loch Leven sediment core LL-2A (28.1.90).

section depth (cm)	mid-section cumulative weight ($g\ cm^{-2}$)	total ^{210}Pb ($Bq\ kg^{-1}$)	^{226}Ra ($Bq\ kg^{-1}$)	excess ^{210}Pb ($Bq\ kg^{-1}$)
0-1	0.040	74 ± 57	BDL	BDL
1-2	0.144	138 ± 26	"	99 ± 27
2-3	0.285	145 ± 31	"	106 ± 32
3-4	0.452	83 ± 18	"	44 ± 20
4-5	0.646	88 ± 32	"	49 ± 33
5-6	0.870	...	...	...
6-7	1.113	65 ± 27	BDL	BDL
7-8	1.350	73 ± 24	"	"
8-9	1.593	51 ± 21	"	"
9-10	1.864	47 ± 12	46 ± 6	"
10-11	2.140	51 ± 12	48 ± 15	"
11-12	2.411	41 ± 11	41 ± 14	"
12-13	2.683	33 ± 12	43 ± 15	"
13-14	2.953	26 ± 11	38 ± 15	"
14-15	3.225	25 ± 13	30 ± 16	"
15-16	...	BDL	BDL	"

Table 5.9 Radiocaesium concentrations and $^{134}Cs/^{137}Cs$ activity ratios in Loch Leven sediment core LL2-A (28.1.90).

section depth (cm)	^{137}Cs ($Bq\ kg^{-1}$)	^{134}Cs 605keV ($Bq\ kg^{-1}$)	$^{134}Cs/^{137}Cs$
0-1	56 ± 6	16 ± 7	0.28 ± 0.14
1-2	88 ± 3	15 ± 3	0.17 ± 0.04
2-3	113 ± 4	18 ± 3	0.16 ± 0.03
3-4	86 ± 2	11 ± 2	0.12 ± 0.02
4-5	69 ± 3	8 ± 4	0.11 ± 0.05
5-6	...	...	...
6-7	50 ± 3	BDL	
7-8	50 ± 3	"	
8-9	46 ± 3	"	
9-10	36 ± 2	4 ± 1	0.10 ± 0.03
10-11	34 ± 1	4 ± 1	0.12 ± 0.04
11-12	26 ± 1	3 ± 1	0.12 ± 0.04
12-13	20 ± 2	BDL	
13-14	12 ± 1	"	
14-15	17 ± 1	"	
15-16	8 ± 2	"	

Table 5.10 Fe, Mn, Pb, Zn, Cu and Cd concentrations in HNO_3/HCl digested Loch Leven sediment core LL1-B.

depth (cm)	Fe %	Mn mg kg^{-1}	Pb mg kg^{-1}	Zn mg kg^{-1}	Cu mg kg^{-1}	Cd mg kg^{-1}
0-1	4.10	4,190	48	212	32	0.9
1-2	3.82	2,430	48	153	35	0.5
2-3	3.55	1,560	51	169	33	0.6
3-4	2.90	880	43	138	24	0.6
4-5	3.20	910	42	172	29	0.6
5-6	3.42	900	42	144	29	0.5
6-7	3.43	840	33	136	27	0.5
7-8	3.47	850	29	131	27	0.6
8-9	3.80	880	30	144	27	0.5
9-10	3.43	750	24	109	26	0.6
10-11	2.62	830	18	105	23	0.5
11-12	2.82	520	18	109	22	0.5
12-13	3.54	770	18	118	25	0.5
13-14	3.69	760	18	116	22	0.5
14-15	2.81	530	12	83	20	0.2
15-16	3.43	710	14	113	23	0.8
16-17	3.33	570	11	110	23	0.5

Table 5.11 Fe, Mn, Pb, Zn, Cu and Cd concentrations in HNO_3/HCl digested Loch Leven sediment core LL2-B.

depth (cm)	Fe %	Mn mg kg^{-1}	Pb mg kg^{-1}	Zn mg kg^{-1}	Cu mg kg^{-1}	Cd mg kg^{-1}
0-1	3.80	4,100	53	166	35	0.6
1-2	3.70	2,300	49	155	30	0.5
2-3	3.58	1,490	52	154	33	0.7
3-4	3.40	1,080	48	133	31	0.6
4-5	3.43	940	50	138	30	0.6
5-6	3.36	890	40	141	29	0.5
6-7	3.38	870	39	128	25	0.5
7-8	3.57	900	35	120	26	0.4
8-9	3.65	910	32	114	23	0.3
9-10	3.76	930	25	107	23	0.4
10-11	3.82	1,000	24	110	23	0.4
11-12	3.32	830	25	97	26	0.4
12-13	3.31	850	25	94	23	0.3
13-14	3.43	950	20	95	24	0.3
14-15	3.30	760	18	95	24	0.2
15-16	3.33	790	19	98	25	0.4

Table 5.12 Fe, Mn, Pb, Zn, Cu, Cd, Co and Ni concentrations in HNO_3/HCl digested Loch Leven sediment core LL3-B.

depth (cm)	Fe %	Mn mg kg^{-1}	Pb mg kg^{-1}	Zn mg kg^{-1}	Cu mg kg^{-1}	Cd mg kg^{-1}	Co mg kg^{-1}	Ni mg kg^{-1}
0-1	3.68	6,000	53	140	35	0.6	18	42
1-2	3.57	2,500	50	140	33	0.5	18	42
2-3	3.45	1,230	47	128	30	0.5	17	39
3-4	3.51	1,220	55	138	34	0.5	18	38
4-5	3.39	1,000	54	147	33	0.5	18	39
5-6	3.43	950	41	119	29	0.4	17	41
6-7	3.36	860	35	103	25	0.3	17	38
7-8	3.49	840	33	98	25	0.4	18	40
8-9	3.37	860	30	93	25	0.3	17	41
9-10	3.43	910	31	90	25	0.3	18	39
10-11	3.27	820	21	80	23	BDL	18	41
11-12	3.49	890	22	81	25	0.3	19	41
12-13	3.32	820	17	86	25	0.3	17	39
13-14	3.08	690	20	91	24	0.3	16	38
14-15	3.12	750	20	81	24	BDL	17	39
15-16	3.09	780	19	79	23	0.3	18	40

Table 5.13 Fe and Mn concentrations in sequentially extracted Loch Leven sediment core LL3-B.

	Fe (%) fractions						Mn (mg kg^{-1}) fractions					
depth (cm)	I	II	III	IV	V	sum I-V	I	II	III	IV	V	sum I-V
0-1	0.006	0.034	0.077	0.687	1.70	2.50	13	276	4,660	1,170	346	6,460
1-2	0.009	0.078	0.083	1.07	1.17	2.41	6	170	1,770	554	214	2,710
2-3	0.002	0.075	0.074	0.970	1.33	2.45	24	81	676	251	142	1,170
3-4	0.002	0.088	0.084	1.01	1.33	2.51	19	80	617	227	145	1,090
4-5	0.006	0.118	0.094	0.859	0.992	2.07	8	57	522	159	110	856
5-6	0.001	0.100	0.084	0.826	1.05	2.06	4	42	428	155	104	733
6-7	0.003	0.103	0.098	0.987	1.34	2.53	BDL	44	455	166	126	791
7-8	0.006	0.096	0.081	0.823	1.40	2.41	"	56	502	206	136	900
8-9	0.001	0.113	0.105	0.992	1.02	2.23	4	56	504	171	98	833
9-10	0.015	0.121	0.107	0.692	1.19	2.02	5	61	460	137	111	774
10-11	0.005	0.114	0.117	0.932	1.11	2.28	6	57	438	153	121	775
11-12	0.016	0.160	0.126	0.993	1.12	2.42	12	62	470	135	113	792
12-13	0.010	0.156	0.133	1.07	...	...	18	61	422	124	75	700
13-14	BDL	0.151	0.121	0.850	0.945	2.07	12	41	273	81	89	496
14-15	"	0.149	0.113	0.989	0.965	2.22	86	75	374	109	96	740
15-16	"	0.192	0.162	0.888	0.892	2.13	132	89	405	103	86	815

Table 5.14 Pb and Zn concentrations in sequentially extracted Loch Leven sediment core LL3-B

depth (cm)	Pb (mg kg^{-1}) fractions I	II	III	IV	V	sum I-V	Zn (mg kg^{-1}) fractions I	II	III	IV	V	sum I-V
0-1	BDL	BDL	BDL	32	16	48	4.2	25	13	30	67	139
1-2	"	"	"	35	23	58	5.8	23	12	31	57	129
2-3	"	"	"	29	11	40	7.6	22	9	28	58	125
3-4	"	"	"	32	14	46	7.3	22	10	29	64	132
4-5	"	"	"	30	BDL	30	9.1	23	9	30	53	124
5-6	"	"	"	25	"	25	4.9	17	7	28	49	106
6-7	"	"	"	21	"	21	2.5	12	6	28	51	100
7-8	"	"	"	19	"	19	1.8	12	6	27	55	102
8-9	"	"	"	18	"	18	2.6	12	6	26	40	87
9-10	"	"	"	10	"	10	2.2	10	4	17	40	73
10-11	"	"	"	12	"	12	1.5	9	5	18	44	78
11-12	"	"	"	10	"	10	3.8	12	5	19	31	71
12-13	"	"	"	10	"	10	2.2	10	5	17	46	80
13-14	"	"	"	11	"	11	3.8	12	6	18	37	77
14-15	"	"	"	10	"	10	4.9	11	9	15	46	86
15-16	"	"	"	BDL	"	BDL	5.1	10	7	11	40	73

Table 5.15 Cu concentrations in sequentially extracted Loch Leven sediment core LL3-B

depth (cm)	Cu (mg kg^{-1}) fractions I	II	III	IV	V	sum
0-1	BDL	BDL	BDL	3	24	27
1-2	"	"	"	5	24	29
2-3	"	"	"	4	18	22
3-4	"	"	"	6	25	31
4-5	"	"	"	6	18	24
5-6	"	"	"	3	18	21
6-7	"	"	"	3	18	21
7-8	"	"	"	3	17	20
8-9	"	"	"	4	16	20
9-10	"	"	"	BDL	18	18
10-11	"	"	"	3	17	20
11-12	"	"	"	4	16	20
12-13	"	"	"	3	15	18
13-14	"	"	"	BDL	16	16
14-15	"	"	"	"	16	16
15-16	"	"	"	"	15	15

5.4 Discussion

5.4.1 Sediment core characteristics

Porosities (Tables 5.4-5.7) are similar and fairly high in the sediment of all four cores collected from Loch Leven, ranging from a maximum of 96.5 % at the surface (0-1 cm) of sediment core LL2-A to a minimum of 87.8 % in the 13-14 cm section of core LL3-B. An overall decrease downcore is observed in all four cores, but in core LL1-B, slightly lower porosities beween 7 and 11 cm are coincident with an increase in total % C (7-8 cm). Maximum total % C content (8.57 %) (Table 5.4) occurs in the 1-2 cm section (no result available for the surface section) and decreases to the minimum value of 5.18 % at 6-7 cm, below which the C content ranges between 5.58 and 6.87 %, as described above. The C/N ratios vary between 8.2 and 11.9, showing no definite trend.

5.4.2 Radionuclide data

^{210}Pb and ^{226}Ra data

Total ^{210}Pb concentrations (Table 5.8) ranged from 145 Bq kg^{-1} (2-3 cm) to 25 Bq kg^{-1} (14-15 cm) and ^{210}Pb was below the detection limit (25 Bq kg^{-1}) in the 15-16 cm section. ^{226}Ra (Table 5.8) was detectable between 9 and 15 cm, but was below the detection limit of 30 Bq kg^{-1} above 9 cm (due to the small sample sizes and consequently greater analytical errors) and at 15-16 cm. The value of 39 ± 8 Bq kg^{-1} used as supported ^{210}Pb, was obtained by taking the mean value of the ^{226}Ra concentrations and total ^{210}Pb concentrations between 9 and 15 cm, because the ^{210}Pb values here were similar to ^{226}Ra concentrations, so that if secular equilibrium between ^{210}Pb and ^{226}Ra is assumed, the total ^{210}Pb values at these depths represent supported ^{210}Pb. As a result of the combined errors for total ^{210}Pb and supported ^{210}Pb, the excess ^{210}Pb was detectable between 1 and 5 cm only, with the maximum value of 106 Bq kg^{-1} at 2-3 cm and so the ^{210}Pb data are clearly unsuitable for deriving a sedimentation rate and core chronology. The total excess ^{210}Pb inventory for core LL2-B is 0.472 Bq m^{-2} and, assuming steady-state conditions prevail, a ^{210}Pb flux of 14.6 kBq m^{-2} is calculated (λ x inventory), which is low compared with a flux of 49 Bq m^{-2} y^{-1} for nearby Balgavies Loch (Chapter 6). The low ^{210}Pb flux for Loch Leven may be due to an overestimation of the supported ^{210}Pb component and/or many of the samples being below the detection limit.

The excess ^{210}Pb concentrations are all constant, within error, and the results do not fit any reasonable accumulation model, implying that sediment mixing occurs at this site to a depth of at least 5 cm. Since excess ^{210}Pb is undetectable below 5 cm, the radiocaesium data should be examined for information on sedimentation processes in this part of the core.

Radiocaesium data

^{137}Cs was detectable to 16 cm, the maximum depth in the core (Table 5.9, Fig. 5.3), with concentrations ranging from 8 Bq kg^{-1} (15-16 cm) to a maximum of 113 Bq kg^{-1} in the sediment section at 2-3 cm. From the sediment surface, the ^{137}Cs concentration increases downcore to a sub-surface peak in the 2-3 cm section, followed by a steady decrease below this depth. The maximum ^{134}Cs concentration (Table 5.9, Fig. 5.3) also occurs in the 2-3 cm section (18 Bq kg^{-1}) and ^{134}Cs penetrates to a depth of 12 cm, below which it is not detectable. Between depths of 6 and 9 cm ^{134}Cs was not detected, probably because the counted sample sizes here were smaller than those below 9 cm. Comparison of the $^{134}Cs/^{137}Cs$ activity ratios in the core (Table 5.9) with the characteristic Chernobyl-emitted ratio of 0.17 (corrected for decay since 1.5.86) shows that, within error, all the radiocaesium to 3 cm is due to Chernobyl and indicates a maximum depth of Chernobyl radiocaesium penetration of 12 cm (Appendix 1). Since radiocaesium from Chernobyl fallout (a single input) is detectable to 12 cm, it is highly unlikely that the observed profile is attributable to the effects of sediment accumulation only, because if the maximum depth of Chernobyl radiocaesium penetration (12 cm) corresponds to a date of 1986, this would give a sedimentation rate of 728 mg cm^{-2} y^{-1},which is unreasonably high. The presence of detectable levels of ^{137}Cs of weapons testing origin (Fig. 5.3) from 3 cm downwards and the penetration of Chernobyl radiocaesium to 12 cm, provide good evidence that the radiocaesium concentration profile shape is due to accumulation and intense sediment mixing in this core. The exponential decrease in ^{137}Cs of Chernobyl origin below 3 cm indicates diffusive movement of radiocaesium may also occur, but this alone would be insufficient to account for the movement of radiocaesium to 12 cm over a period of 3.5 years (*i.e.* since deposition of Chernobyl fallout to the area) in sediment containing > 50 % by weight of clay (Calvert, 1974). Weapons testing fallout ^{137}Cs is detectable over the depth range 3-15 cm (Fig. 5.3, Appendix 1), with no clear maximum, again indicating significant downward movement of radiocaesium by mixing and, additionally, perhaps diffusion. The presence of radiocaesium of weapons testing origin from 3-15 cm, with no clear peak, and of Chernobyl-derived

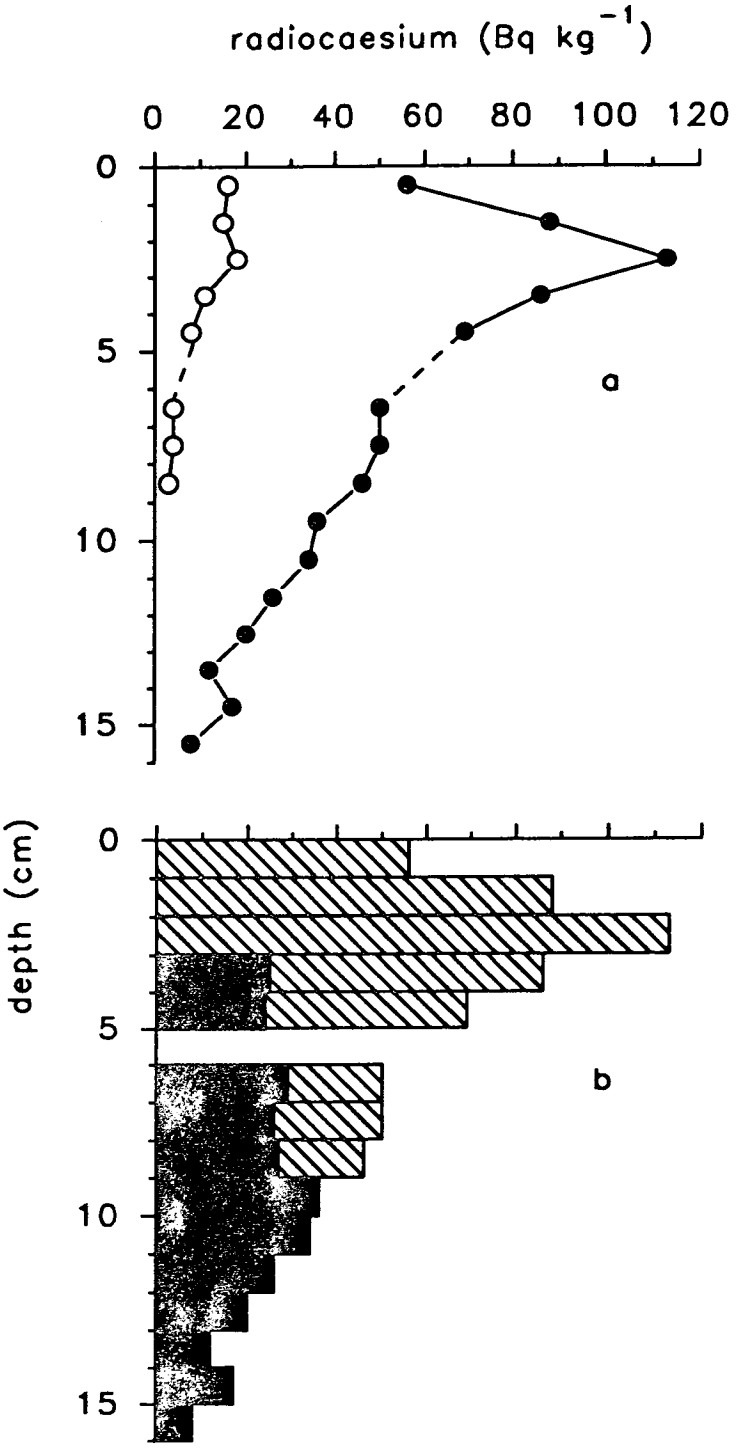

Fig. 5.3 Profiles of ^{134}Cs (o) and ^{137}Cs (•) concentrations (a) and ^{137}Cs concentrations showing the calculated component sources of fallout from weapons testing (▩) and Chernobyl (▨) (b) in Loch Leven sediment core LL2-1A.

radiocaesium to 12 cm, preclude the estimation of a sedimentation rate, based on the difference between maximum ^{137}Cs concentrations from the two fallout sources.

Using the $^{134}Cs/^{137}Cs$ activity ratios, the inventories for fallout from Chernobyl and weapons testing can be estimated and compared with recorded deposition values for the area (Table 5.16). The Chernobyl-derived ^{137}Cs inventory of 0.78 kBq m^{-2} is within the range of recorded deposition for this area. The estimated weapons testing fallout inventory of 1.46 kBq m^{-2} is slightly lower than the recorded deposition value of 2.8 kBq m^{-2} (Peirson *et al.*, 1982), perhaps because not all the weapons testing fallout at this site has been detected by the maximum core depth of 16 cm or the estimated deposition value (a UK average) is not sufficiently accurate for this area.

In summary, a core chronology cannot be obtained at this site using either the ^{210}Pb data or the radiocaesium results. The ^{210}Pb data imply mixing to at least 5 cm. The radiocaesium in Loch Leven is apparently efficiently deposited from the water column to the sediment, as indicated by the agreement between the estimated Chernobyl fallout deposition and reported deposition values in the area. However, downward movement of radiocaesium in the core, probably due to sediment mixing, has obscured the historical record of fallout deposition maxima and so the data are not useful for dating purposes.

5.4.3 Metal data

The Fe and Mn data will be discussed initially, with the aim of deriving conclusions about the redox regime in the sediment. Since a core chronology has not been calculated at this site, a discussion of the metal profiles in terms of historical changes is not possible, similar to the situation in Balgavies Loch (Chapter 6). A comparison of the results from cores collected from the same sampling site at different times of the year will be considered.

Iron and manganese concentrations in HNO_3/HCl acid digested sediment

Fe concentration ranges in the three cores are similar (Tables 5.10-5.12, Figs. 5.4-5.6): 2.62-4.1% (LL1-B), 3.30-3.80% (LL2-B) and 3.1-3.7% (LL3-B). The overall concentration profile trends for cores LL2-B and LL3-B are much more alike, showing a slight decrease in concentration with depth from the surface, compared with the more erratic pattern in core LL1-B, which is likely to be due to experimental technique. Duration of the HNO_3/HCl acid digestion can be important and give rise to variations if not kept constant, especially for a major element such as Fe, a significant

Table 5.16 Estimated Chernobyl and weapons testing fallout ^{137}Cs inventories in Loch Leven sediment core LL2-A[1] compared with recorded deposition values (Clark and Smith, 1988; Peirson *et al.*, 1982)

	Loch Leven (kBq m^{-2})	recorded deposition (kBq m^{-2})
Chernobyl fallout	0.78 ± 0.06	0.1-1
weapons testing fallout	1.46 ± 0.12	2.8

[1]corrected for decay since fallout deposition maxima (1.5.86 and 1963 respectively)

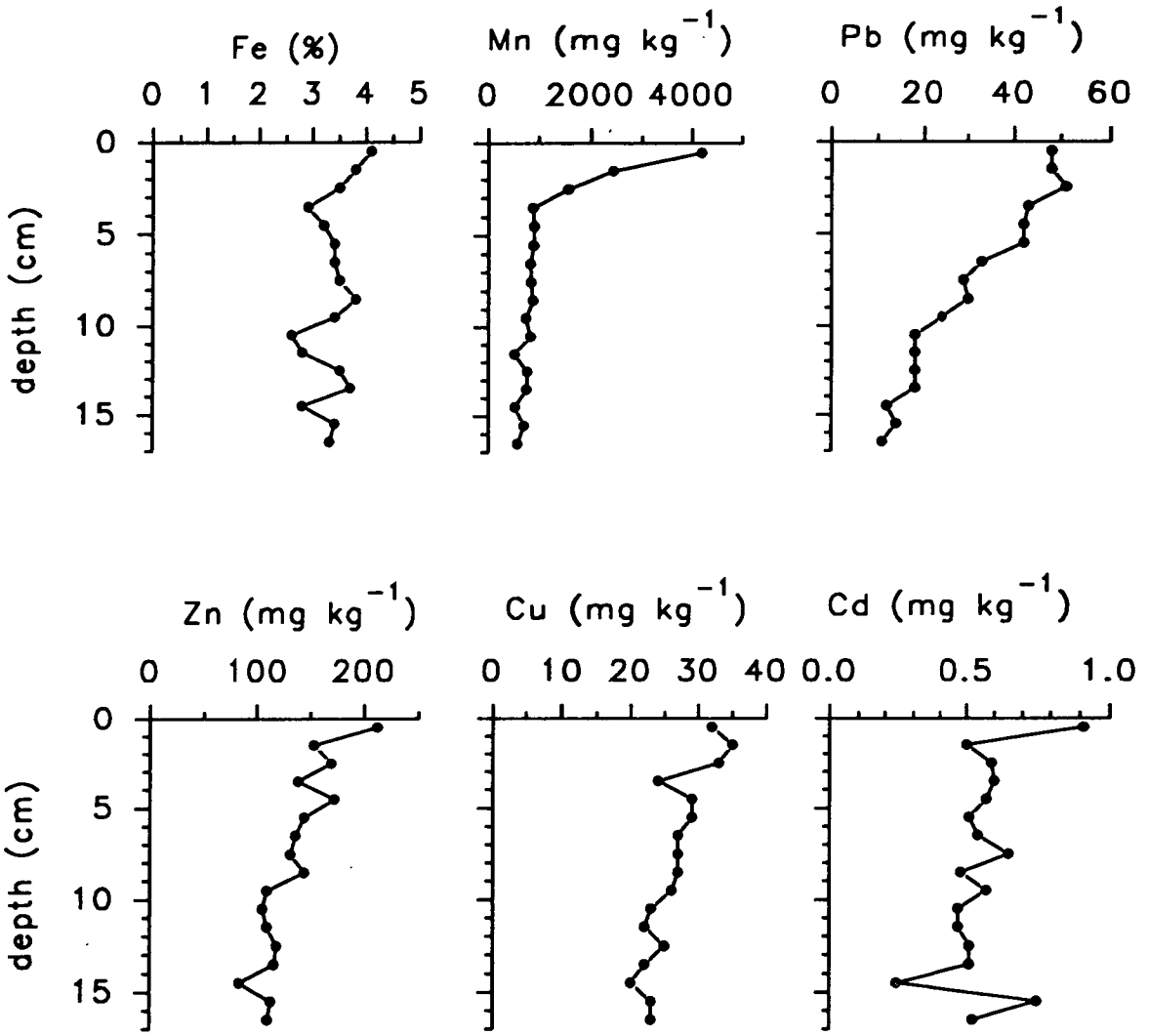

Fig 5.4 Metal concentrations in HNO_3\HCl acid digested Loch Leven sediment core LL1-B

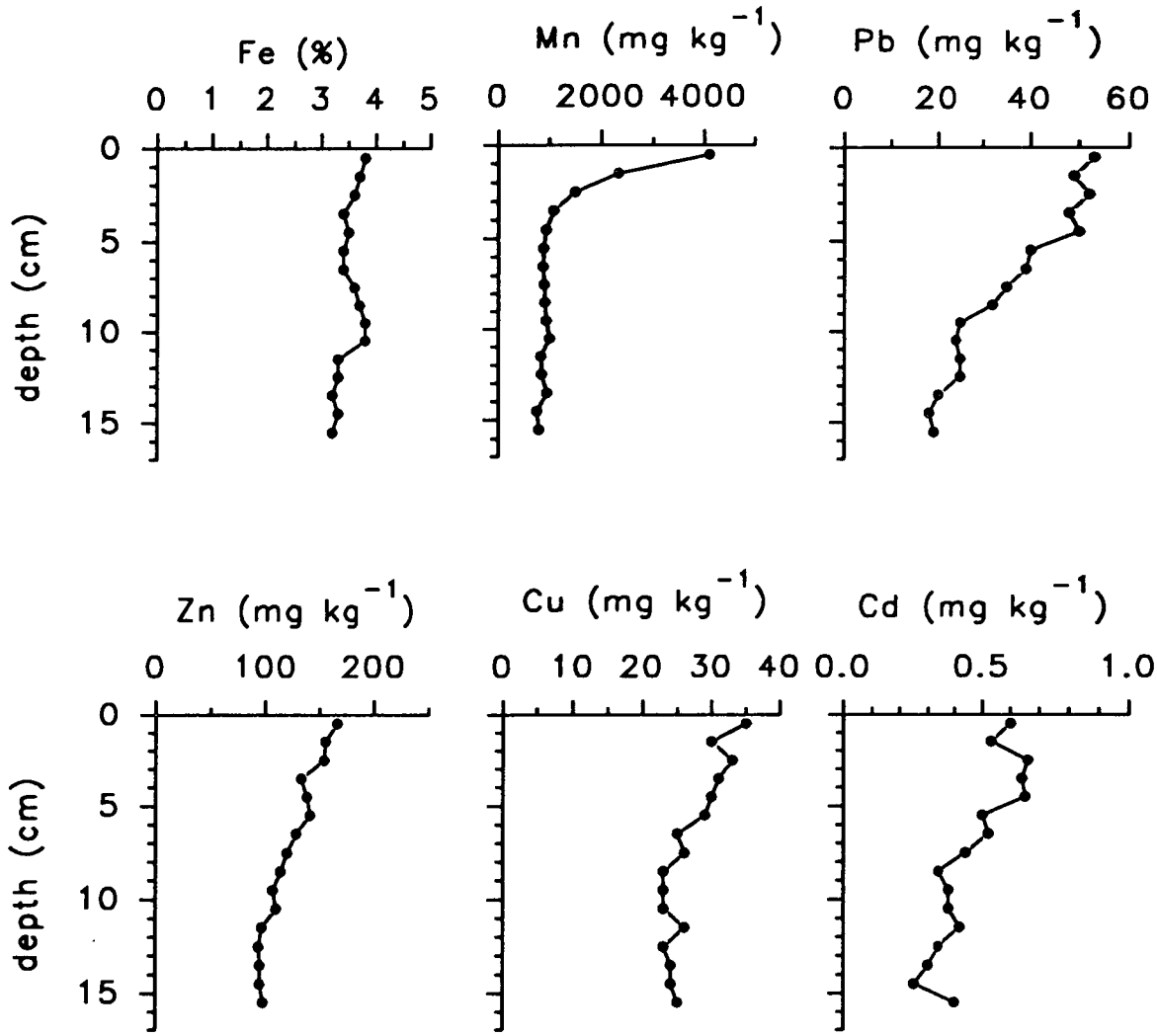

Fig 5.5 Metal concentrations in HNO_3\HCl acid digested Loch Leven sediment core LL2-B

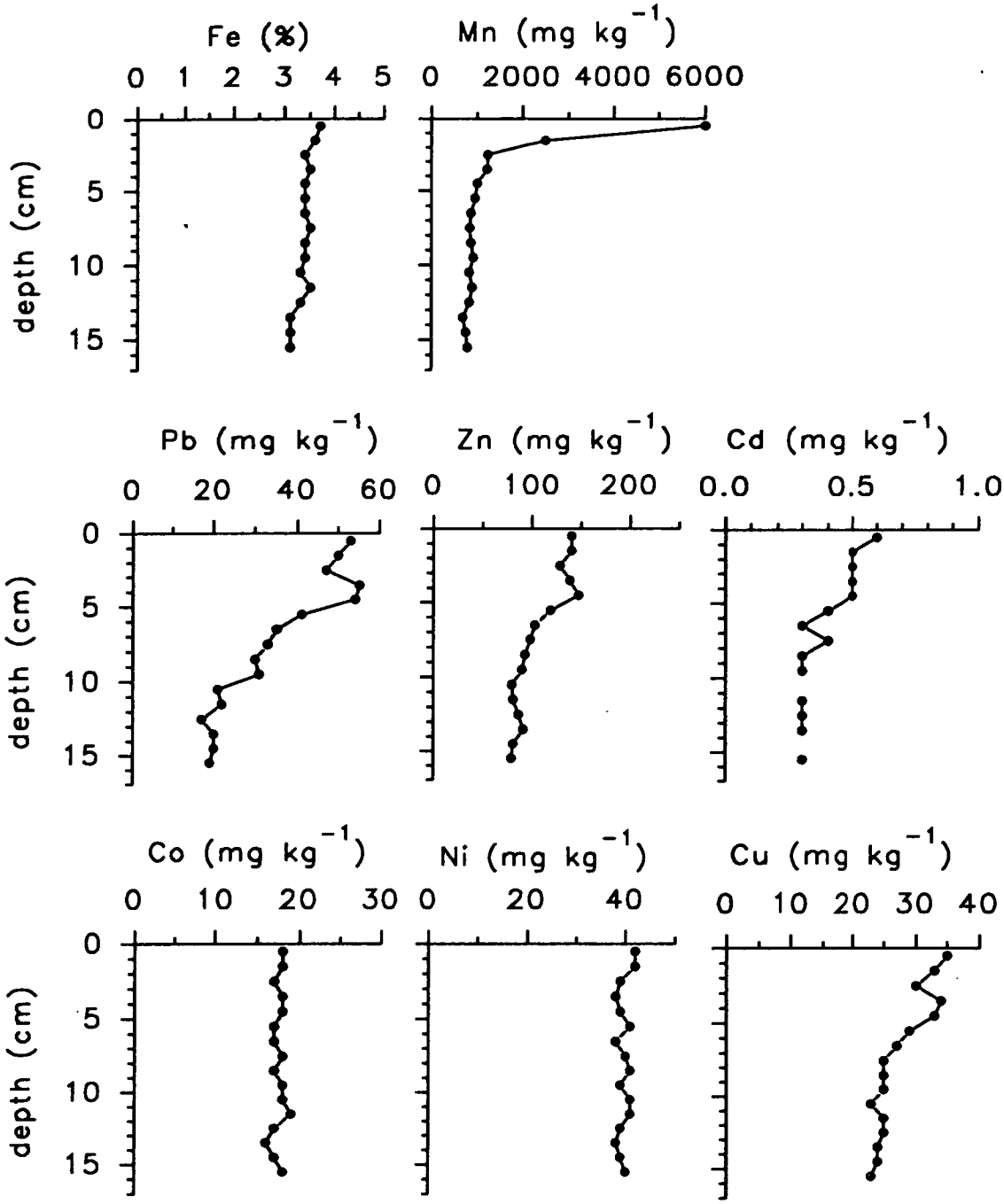

Fig 5.6 Metal concentrations in HNO_3\HCl acid digested Loch Leven sediment core LL3–B.

proportion of which may be bound within mineral lattices and only removed by vigorous chemical digestion. This contrasts with the 'pollutant' metals Pb, Zn, Cu and Cd, which are largely associated with less resistant fractions, so that increasing the duration of the acid digestion would probably not give rise to higher measured concentrations. Slightly higher concentrations of Fe are observed in the surface sediment of core LL1-B and, to a lesser extent, LL2-B compared with core LL3-B, collected in the summer, which shows no increase at the surface.

Peak Mn concentrations occur in the surface (0-1 cm) sections of all three cores (Tables 5.10-5.12, Figs. 5.4-5.6) and below this the concentration decreases to relatively constant values of 764 ± 136 mg kg^{-1} (core LL1-B below 3 cm), 885 ± 69 mg kg^{-1} (core LL2-B below 4 cm) and 848 ± 85 mg kg^{-1} (core LL3-B below 4 cm). Although these concentrations are similar, the peak concentrations (0-1 cm) differ between the two cores collected in the autumn and winter (LL1-B and LL2-B), with peaks of 4,190 mg kg^{-1} and 4,100 mg kg^{-1} respectively, and core LL3-B, collected during an algal bloom, which has a greater and more pronounced surface maximum of 6,000 mg kg^{-1}. The patterns for all three cores of high concentrations in the near-surface sediments overlying much lower, relatively constant values are characteristic of redox-driven diagenetic remobilisation of Mn followed by upward movement and precipitation of Mn in the surface sediment. To determine whether there is a genuine difference between the Mn profiles of cores LL1-B and LL2-B, and LL3-B, or whether the patterns observed are simply a sampling artefact (*e.g.* sectioning of the initial section at slightly different depths between cores, so that the high surface concentration of Mn in core LL3-B may be more 'spread out' in the other two cores), Mn inventories have been calculated above the depths where the constant concentrations commence. The inventory values of (g m^{-2}) 9.2 (LL1-B), 10.3 (LL2-B) and 13.7 (LL3-B) indicate that there *is* a greater amount of Mn in the summer core and the sequential extraction results must be studied to establish a possible cause for this. Unless uptake of Mn by algae followed by deposition to the sediment occurs (which seems unlikely *during* an algal bloom, when most of the algal biomass is still in the water column), a lower Mn inventory might have been expected in the summer due to more reducing conditions (higher water temperatures enhancing bacterial degradation of organic matter and calmer water column conditions) and consequently greater dissolution of the solid phase Mn.

Iron and manganese partitioning data

Fe was detectable in all five fractions in core LL3-B (Table 5.13, Fig. 5.7), but is associated largely with fractions IV (mean concentration = 0.915 %) and V (mean

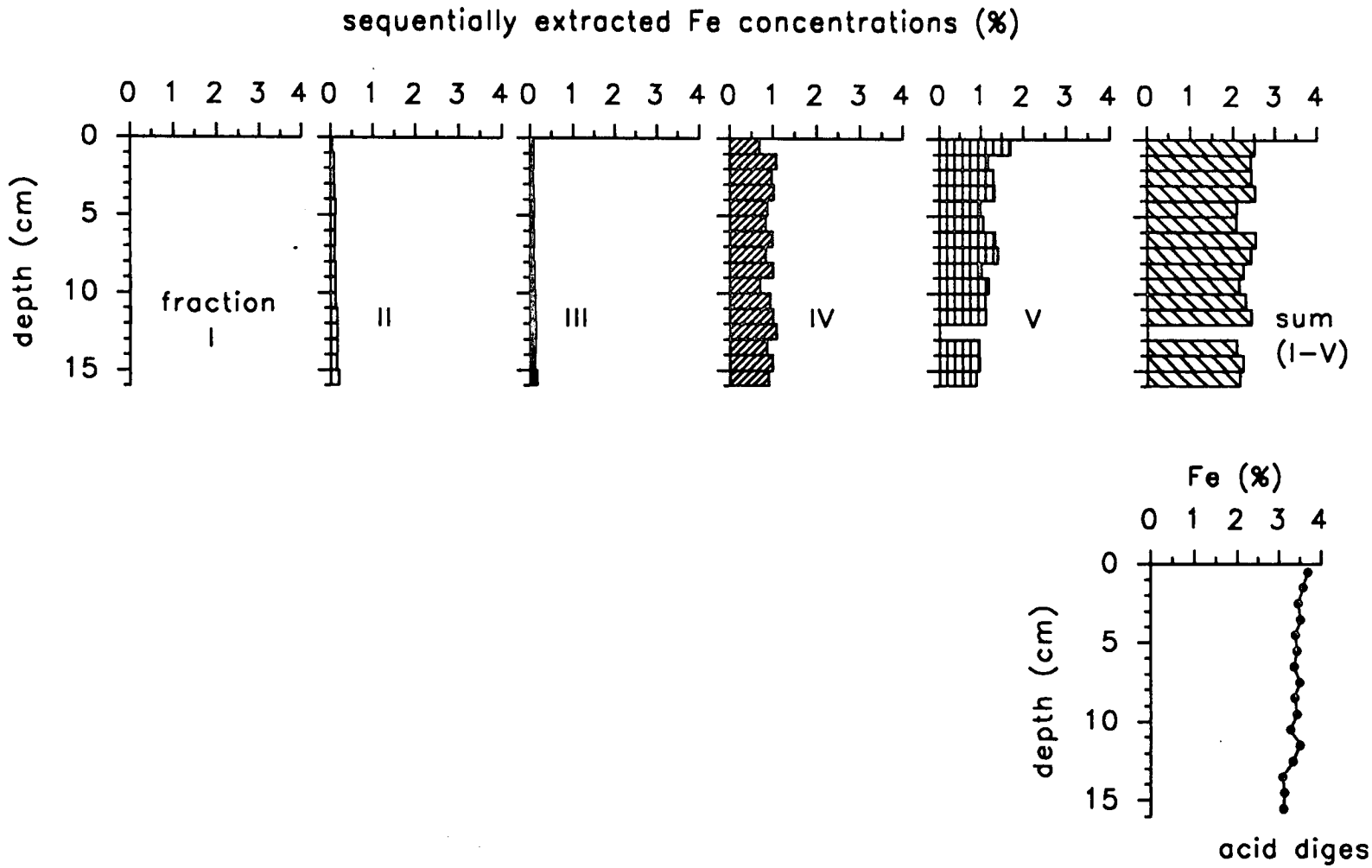
sequentially extracted Fe concentrations (%)
0 1 2 3 4
depth (cm)
0
5
10
15
fraction I
II
III
IV
V
sum (I–V)
Fe (%)
acid digest

concentration = 1.17 %), consistent with Fe being present mainly as oxides, sulphides and/or associated with organic matter. A slightly higher concentration of Fe in the surface (0-1 cm) section of fraction V suggests some Fe is released from organic matter when this is degraded downcore (implied by the decreasing carbon content with depth in core LL1-B (Table 5.4, Section 5.4.1) and becomes rapidly reassociated with fractions II and III, in which Fe concentrations gradually increase downcore, while there is a corresponding decrease in Fe concentrations in fraction V. Fe concentrations remain fairly constant in fraction IV.

The sum of Fe concentrations in all fractions (mean = 2.29 %) is lower than the corresponding concentrations in the acid digested sediment (mean = 3.38%), indicating that around 30% of the acid digested Fe concentration is associated with minerals more resistant to the sequential extractants.

Mn is associated largely with fraction III (Table 5.13, Fig. 5.8) and this contributes most to the peak found in the surface sediment (0-1 cm), with a concentration of 4,660 mg kg^{-1} comprising 72 % of the sum of Mn in all fractions. The concentration profile pattern for fraction III is the same as in the acid digested concentration profile, with high concentrations (0-2 cm) overlying lower concentrations (mean 467 mg kg^{-1} below 2 cm). A similar pattern is also seen for fraction IV, but concentrations here are lower and the surface enhancement is less marked: 1,170 mg kg^{-1} at 0-1 cm, overlying gradually decreasing concentrations (251 mg kg^{-1} at 2-3 cm to 103 mg kg^{-1} at 15-16 cm). The Mn concentration in fraction II also decreases from 276 mg kg^{-1} (0-1 cm) to a mean 62 mg kg^{-1} below 2 cm. These patterns in fractions II, III and IV are consistent with redox cycling involving reduction of Mn oxides (fraction III) followed by upward movement of solubilised Mn and oxidation in the surface sediment to give the observed surface peak. The presence of Mn in fractions II and IV showing less pronounced, but similar, trends to the fraction III concentrations may be due to non-selectivity of the extractants (Chapter 1) *i.e.* to some Mn oxides being reduced during the earlier extraction of fraction II (although $MnCO_3$ may also exist in the sediment) and the later extraction of fraction IV. In fraction V Mn decreases gradually downcore from 346 mg kg^{-1} (0-1 cm) to 86 mg kg^{-1} (15-16 cm). The sum of Mn concentrations in all fractions is similar to, or greater than, the HNO_3/HCl acid digested concentrations, showing that Mn is not significantly associated with more resistant minerals, which may be extracted during the acid digest. Where concentrations are higher in the sum of all fractions (*e.g* at 0-1 cm), this is probably due to combined errors in the five step extraction being greater than the error associated with the acid digestion.

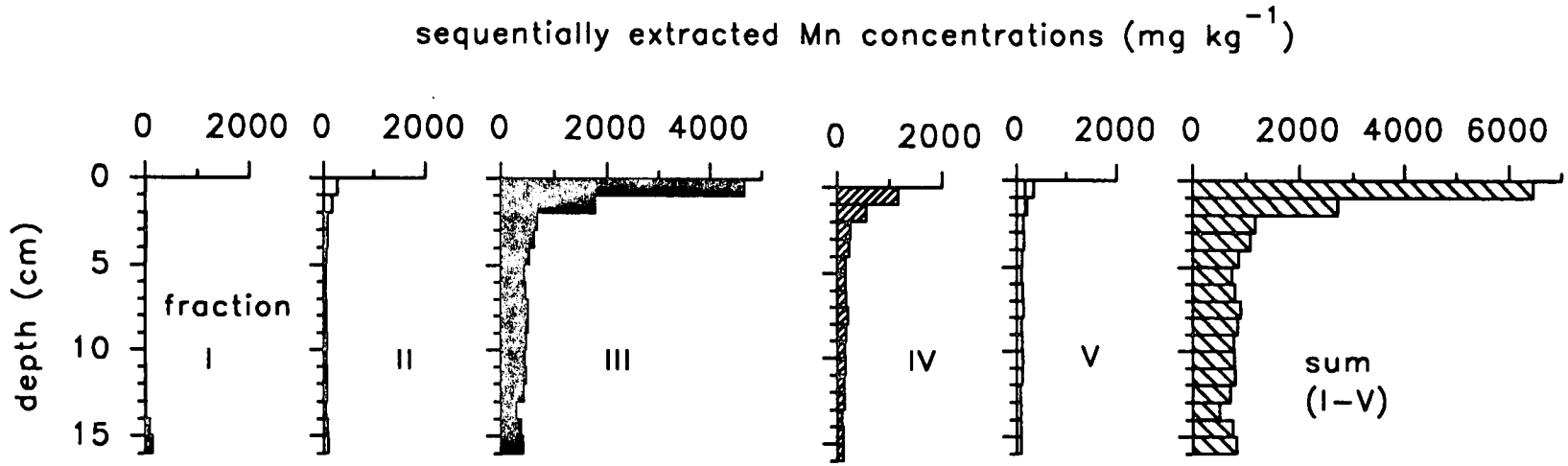
sequentially extracted Mn concentrations (mg kg^{-1})
0 2000
0 2000
0 2000 4000
0 2000
0 2000
0 2000 4000 6000
depth (cm)
0
5
10
15
fraction
I
II
III
IV
V
sum
(I–V)

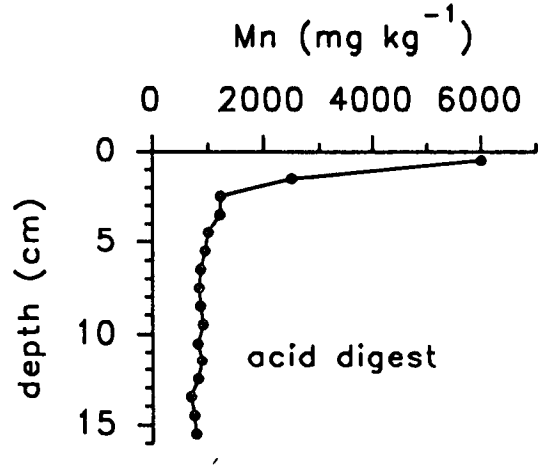
Mn (mg kg^{-1})
0 2000 4000 6000
depth (cm)
0
5
10
15
acid digest

As to the reason for the greater and more pronounced Mn peak from sediment sampled during the summer algal bloom compared with the autumn and winter acid digest concentration profiles of cores LL1-B and LL2-B, two possibilities arise. Firstly, the algal bloom could result in increased uptake of Mn by particulates (*i.e.* phytoplankton), which would increase the flux of Mn to the surface sediment. As previously mentioned, this seems unlikely during an algal bloom, and the sequential extraction results of core LL3-B do not provide supporting evidence, showing no peak of Mn associated with fraction V (organic matter). For the observed Mn associations to occur, there would have to be a rapid release of Mn on degradation of the organic matter, followed by formation of Mn oxides (fraction III) in the 0-1 cm section. This process would need to be rapid and would not account for the lower Mn inventories in autumn and winter cores, so release of Mn from the sediment must occur sometime during the summer (assuming these patterns are observed from year to year at this site). The second, and more plausible, explanation is an indirect effect of the algal bloom, involving an increase in the pH of the water column and high dissolved O_2 concentrations (due to uptake of CO_2 and release of O_2 during primary production), causing enhanced oxidation of Mn (since Mn oxidation is more favourable under higher pH conditions) and an increase in the flux of Mn to the sediment. During the summer sampling, conditions were found to be favourable for Mn oxidation with a high pH and temperature in the water column, which was well oxygenated (Table 5.3). These two hypotheses have been suggested as possible causes of Mn nodule formation in freshwater, eutrophic Lake Oneida, New York (Dean and Greeson, 1979; Dean *et al.*, 1981). In seasonally stratified Lake Windermere, enhanced fluxes of Mn to sediment traps during June and July accounted for 55% of the total Mn deposited in a year (Hamilton-Taylor, 1984). This was attributed to redox-driven remobilisation, involving recycling of Mn from the sediment to the water column, followed by reprecipitation, rather than deposition of Mn associated with algae, giving rise to a high annual trap:sediment flux ratio.

The cycling of phosphorus in Loch Leven is well-established (Bailey-Watts and Kirika, 1987; Bailey-Watts *et al.*, 1991), with reductive release of P from the sediments during calm, warm conditions providing an enhanced nutrient supply to the water column, an important factor in the development of algal blooms. In a study of phosphorus in the sediments of Loch Leven, surface enhancements of reductant-soluble Fe were found in sediment collected during a January 1990 sampling (Scott, 1990), implying that the cycling of Fe and P in the loch is controlled by redox processes. To some extent, this is supported by the slightly higher Fe concentrations observed in the surface sediment of cores LL1-B and LL2-B. Consistent with the

release of Fe to the water column from the sediments in the summer, there is no increase in Fe concentrations in either the acid digested sediment or fraction IV from core LL3-B. The most likely explanation for the greater Mn enhancement during the summer relative to the autumn and winter cores, then, seems to be a redox-controlled release of Mn (and Fe) from the surface sediment to the water column, but rapid precipitation of dissolved Mn in the water column, favourable under the high pH conditions of the water column during the algal bloom, ensures that proportionately more of the Mn enrichment is found in the top 1 cm of the sediment relative to the situation in the surface sediment in autumn and winter. The lower Mn inventories and less pronounced Mn peaks in autumn and winter sediment can be accounted for by redox-driven release of Mn from the sediment to the water column after the end of the algal bloom, due to enhanced degradation of organic matter (*i.e.* freshly deposited plankton remains) and lower pH, dissolved oxygen and temperature conditions.

The lack of Fe enhancement during the summer is unsurprising, with release of Fe from the sediment to the water column outweighing any precipitation/deposition of Fe from the water column to the sediment, since Fe oxidation is not so sensitive to pH changes as Mn precipitation. Further reasons for no clearly distinct Fe peaks (even during the autumn and winter) could be that the redox conditions at depth in the sediment may not be sufficiently reducing for significant Fe dissolution, consistent with the high degree of sediment mixing, but conflicting with dissolution of Fe from the sediment to the water column during the summer. Additionally, a high proportion of Fe is usually associated with resistant mineral phases and is not available for remobilisation, which is supported by the lower sum of Fe concentrations in fractions I-V relative to the acid digest concentrations from core LL3-B.

The more abrupt change in Mn concentration with depth in the near-surface sediment of core LL3-B, compared with the other cores, is probably due to a sharper redox gradient during the summer months as the water temperature increases, causing more rapid microbial decomposition of organic matter.

In the seasonally anoxic hypolimnion of eutrophic, hard water Rostherne Mere, Davison and Woof (1984) reported a maximum hypolimnetic dissolved Mn concentration of 2.7 mg l^{-1} in October, following a high flux of algae to the sediment. They suggested that a fresh supply of actively decomposing organic matter was necessary to generate high concentrations of porewater Mn, facilitating rapid release to the overlying water. Results were quoted from a sediment core collected from the mere in July, with a clear surface enhancement of Mn (but not of Fe), said to be typical for a situation where Mn is being rapidly reduced and released to the overlying water (Davison *et al.*, 1982).

While these findings are consistent with the seasonal variations in Mn observed in Loch Leven, it should be borne in mind that the sediment sectioning for all cores was carried out in air and dissolved Mn at the time of sampling may have undergone precipitation following exposure to the air. Hypothetically, if all the Mn in the surface section (0-1 cm) of core LL3-B were in solution, a concentration in the porewater of 576 mg l^{-1} would be observed, which is 17 times higher than the maximum porewater concentration obtained in this study in the southern basin of Loch Lomond (Chapter 4) and approximately 100 times greater than concentrations measured in Balgavies Loch (Chapter 6), Rostherne Mere (Davison and Woof, 1984) and Greifensee in Switzerland (Emerson, 1986). On this basis, it seems reasonable to conclude that the solid phase enhancements observed are largely representative of in-situ conditions.

Lead, zinc, copper, cadmium, cobalt and nickel in HNO_3/HCl acid digested sediment

Concentrations of Pb, Zn, Cu and Cd in acid digested sediment cores LL1-B, LL2-B and LL3-B (Tables 5.13-5.15) are presented graphically in Figs. 5.4-5.6, using the same scale for each metal respectively in the three different cores, to simplify a comparison of concentration profiles in cores collected at the same sampling site.

Concentration ranges of Pb in the three cores are similar: 11-51 mg kg^{-1} (LL1-B), 18-53 mg kg^{-1} (LL2-B) and 19-55 mg kg^{-1} (LL3-B). The concentration profiles all show an irregular, but systematic, decrease in concentration with depth to between 10 and 14 cm (although a slight sub-surface peak between depths of 3 and 5 cm of core LL3-B is observed), below which concentrations remain constant. These relatively constant values have been used to obtain background (non-anthropogenic) concentrations (Table 5.17).

Zn concentrations vary more than those of Pb between the three cores, with the highest concentration of 212 mg kg^{-1} occurring in the 0-1 cm section of core LL1-B (minimum 83 mg kg^{-1} at 14-15 cm), compared with a range of 94 mg kg^{-1} (12-13 cm) to 165 mg kg^{-1} (0-1 cm) in core LL2-B and 79 mg kg^{-1} (15-16 cm) to 147 mg kg^{-1} (4-5 cm) in core LL3-B. The Zn profile patterns show a less marked downcore decrease in concentration than do the Pb profiles. In core LL1-B there is a slight surface Zn peak (0-1 cm) underlain by a decrease to 9 cm, below which the concentration remains constant at about 108 mg kg^{-1}. The situation in core LL2-B is similar, the concentration gradually decreasing downcore to 11 cm, below which concentrations are constant at about 96 mg kg^{-1}. Apart from the trend in Zn concentrations being very similar in core LL3-B to that described for LL2-B (with relatively constant concentrations of 83 mg kg^{-1} below 10 cm), there is a slight sub-surface enhancement

between 3 and 5 cm, in the same sediment sections as the more pronounced sub-surface Pb enhancement. Since core LL3-B has also been sequentially extracted, discussion of this sub-surface feature will be considered later with the partitioning data.

Cu concentrations do not vary greatly within and between each core, ranging from minimum values of 20-23 mg kg^{-1} to the maximum 35 mg kg^{-1} observed in all three cores. Although the concentrations do not change dramatically within the cores, there is an overall trend of decreasing concentration with depth.

Cd was near detection limit in many of the samples and the gaps in the Cd concentration profile in Fig. 5.6 represent depths at which Cd was below the detection limit. As the detection limit for these samples was ≤ 0.3 mg kg^{-1}, it was thought better to omit these points from the graph than to distort the profile by plotting them at zero concentration. In core LL1-B a maximum Cd concentration of 0.91 mg kg^{-1} occurs in the surface section (0-1 cm) below which there is no definite trend in the concentration, many of the samples containing around 0.5 mg kg^{-1} Cd. The erratic peaks and minima (*e.g.* at 14-15 cm and 15-16 cm) and possibly the surface peak (although this is also observed in the Zn profile) are probably due more to analyte solution concentrations being near to the detection limit than to genuine changes in the sediment concentrations. Trends and concentrations in the Cd profiles of cores LL1-B and LL2-B are similar, decreasing downcore although, again, there are irregularities in the profiles.

Co and Ni were measured in sediment from core LL3-B only and concentrations vary little with depth in the sediment, ranging from 16-19 mg kg^{-1} (Co) and 38-42 mg kg^{-1} (Ni).

The Pb and Zn concentration profiles differ from those observed, for example, in Round Loch of Glenhead and Loch Lomond (Chapters 3 and 4), where concentrations increased upcore to peak concentrations in the sub-surface sediment, but then declined towards the sediment surface, attributable largely to changes in pollutant metal deposition to the lochs. In contrast, concentrations of Pb and Zn, as well as Cu and Cd, in Loch Leven sediments generally increase to the surface, despite the intense mixing, showing a probable influence of metal pollution input, which appears to differ from the previously mentioned lochs.

Table 5.17 shows the background (non-anthropogenic) Pb, Zn and Cu concentrations in the three acid digested sediment cores - these concentrations were obtained by taking the mean of concentrations below the depth at which concentrations remained constant. The values were then subtracted from concentrations above the depths shown in Table 5.17 and, using the sediment section weights (Tables 5.4, 5.6

Table 5.17 Background (non-anthropogenic) Pb, Zn and Cu concentrations in HNO_3/HCl acid digested Loch Leven sediment cores LL1-B, LL2-B and LL3-B

	Pb		Zn		Cu	
	mg kg^{-1}	depth limit[2]	mg kg^{-1}	depth limit	mg kg^{-1}	depth limit
LL1-B	12	14 cm	108	9 cm	22	10 cm
LL2-B	19	13 cm	96	11 cm	24	8 cm
LL3-B	20	10 cm	83	10 cm	24	7 cm
mean (3 cores)	17 ± 4		96 ± 12		23 ± 1	

Table 5.18 Estimated inventories of anthropogenic Pb, Zn and Cu in HNO_3/HCl acid digested Loch Leven sediment cores LL1-B, LL2-B and LL3-B

	Pb	Zn	Cu
	g m^{-2}	g m^{-2}	g m^{-2}
LL1-B	0.56	0.78	0.13
LL2-B	0.45	0.70	0.072
LL3-B	0.39	0.60	0.082
mean (3 cores)	0.47 ± 0.09	0.69 ± 0.09	0.095 ± 0.031

[2]depth limit refers to depth below which mean value taken

and 5.7) and core cross-section areas, pollutant metal inventories were calculated (Table 5.18). Pollutant Cd inventories could not be calculated, because the non-anthropogenic component was not clearly definable. Mean background levels of Pb, Zn and Cu respectively in the three cores are fairly similar (Table 5.17). Whilst the concentrations and trends in the near-surface sediment might vary seasonally and therefore show different results between cores collected in October, January and July, the non-anthropogenic levels would be expected to be comparable in cores from the same site. The background metal values (Table 5.17) therefore give some confidence in the use of duplicate cores. However, other coring locations may be less uniform over a smaller area. The anthropogenic metal inventories (Table 5.18) for the three cores are in reasonable agreement. Overall, the pollutant inventories increase Cu<Pb<Zn and are close to values in Balgavies Loch (Chapter 6), which is only 60 km north of Loch Leven and is therefore likely to receive similar atmospheric pollutant input.

Lead, zinc and copper partitioning data

Pb, below the detection limit in fractions I, II and III, is primarily associated with fraction IV (Table 5.14, Fig. 5.9), indicating that it is bound to oxides of Fe. Pb concentrations in fraction IV are relatively constant downcore to a depth of 5 cm (mean = 32 mg kg^{-1}) followed by a decrease to 9 cm, below which concentrations remain at a constant mean value of 10 mg kg^{-1} (excluding the 15-16 cm section in which Pb was not detectable). This pattern is similar to the acid digest concentration profile and is likely to have been influenced by mixing and changes in pollutant Pb deposition. Fraction V contained Pb to 4 cm (mean = 16 mg kg^{-1}). The acid digested Pb concentrations are similar to the sum of Pb in all fractions to a depth of 4 cm, below which acid digested Pb concentrations are higher, perhaps due to an increasing importance downcore of non-anthropogenic Pb (in more resistant fractions), compared with pollutant Pb. There is no obvious explanation for the sub-surface enhancement of Pb in the acid digested concentration profile between 3 and 5 cm; perhaps a variation in Pb input has caused this minor feature, which is not seen in the sum of concentrations in all fractions. The porosities (Table 5.7, Section 5.4.1) decrease steadily downcore and do not indicate a change in sediment type at this depth (*e.g.* to sediment which could contain Pb in a more resistant fraction), although this is a general guide.

Zn was detectable in all fractions (Table 5.14, Fig. 5.10), but is associated mainly with fraction V, in which concentrations decrease downcore (67 mg kg^{-1} at 0-1 cm to 31 mg kg^{-1} at 11-12 cm). Fraction V Zn concentrations comprise around 50% of the sequentially extracted Zn. Concentrations in fraction IV remain constant (mean

= 28 mg kg^{-1}) to around 9 cm and below this fall to a mean 16 mg kg^{-1}. In fraction II Zn concentrations are constant to 5 cm (mean = 23 mg kg^{-1}), decreasing to a mean 11 mg kg^{-1} below 6 cm. As with Pb, there is no obvious cause of the subsurface enhancement between 3 and 5 cm in the acid digested sediment. Concentrations of Zn in the sum of all fractions are similar to the acid digest concentrations, staying relatively constant to 5 cm (mean = 130 mg kg^{-1}), decreasing to 8 cm and then remaining constant (mean = 78 mg kg^{-1}). These trends are analogous to those in the sum of Pb concentrations in all fractions and again, are probably dominated by the effects of sediment mixing combined with historical changes in pollutant Zn deposition to the loch.

Cu was only detectable in fractions IV and V (Table 5.14, Fig. 5.11) with most Cu in fraction V, in which concentrations range from 15 mg kg^{-1} (15-16 cm) to 25 mg kg^{-1} (3-4 cm) and overall, the concentration decreases with depth. The results indicate that Cu is mainly associated with organic matter and/or present as sulphides. Cu concentrations in the sum of all fractions are slightly lower than the acid digest Cu concentrations, indicating that some Cu must occur in more resistant fractions.

In summary, the presence of significant amounts of Zn and Cu in fraction V suggests the importance of organic matter associations, which could mean that Zn and Cu cycling is influenced by phytoplankton growth and decay. Reynolds and Hamilton-Taylor (1992) investigated the influence of algal cycling on dissolved Zn and Cu concentrations in Windermere and concluded that phytoplankton were involved in the transfer of Zn to the sediments, but had little effect on the cycling of Cu.

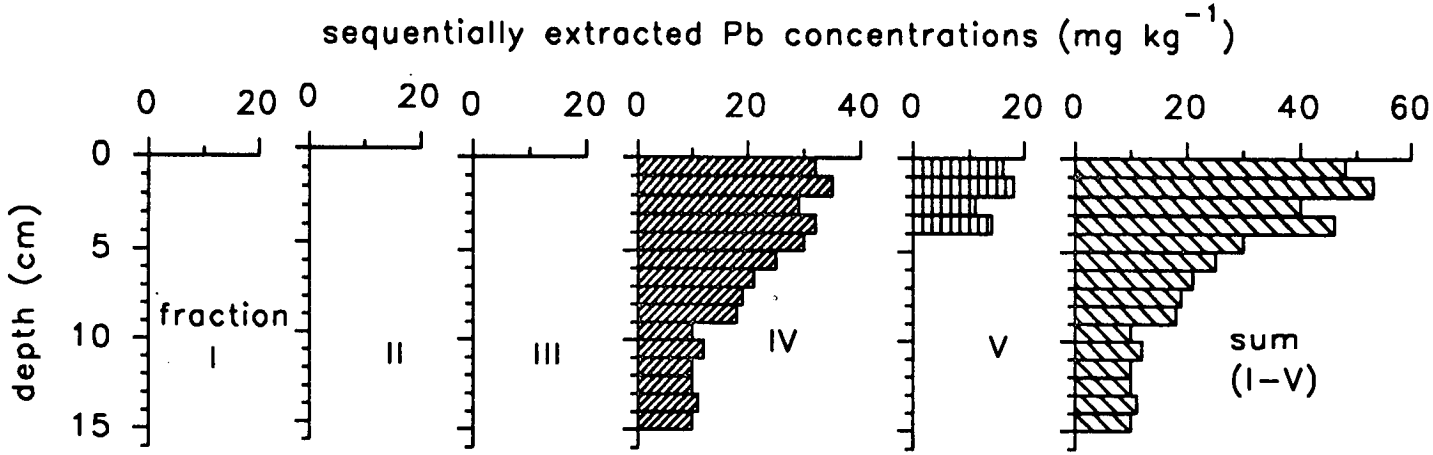
sequentially extracted Pb concentrations (mg kg^{-1})
0 20
0 20
0 20
0 20 40
0 20
0 20 40 60
depth (cm)
0
5
10
15
fraction
I
II
III
IV
V
sum
(I–V)

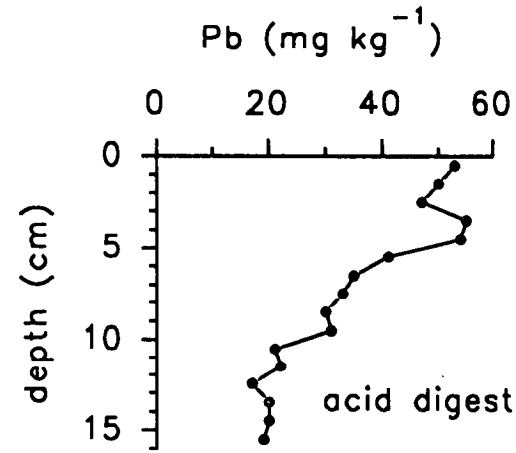
Pb (mg kg^{-1})
0 20 40 60
depth (cm)
0
5
10
15
acid digest

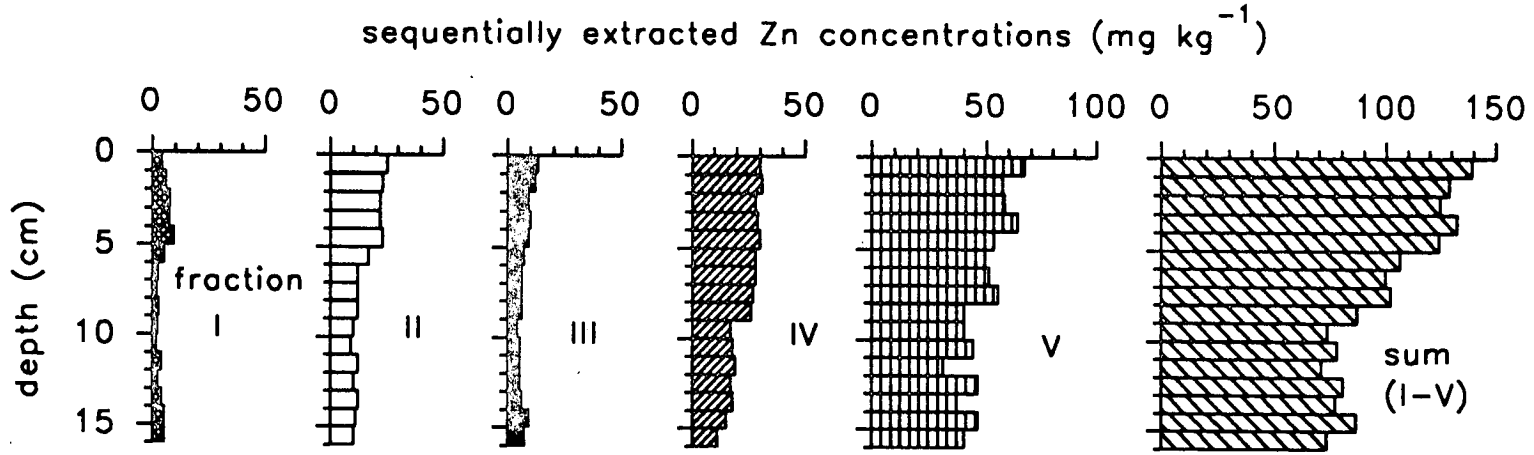
sequentially extracted Zn concentrations (mg kg^{-1})
0 50
0 50
0 50
0 50
0 50 100
0 50 100 150
depth (cm)
0
5
10
15
fraction
I
II
III
IV
V
sum
(I–V)

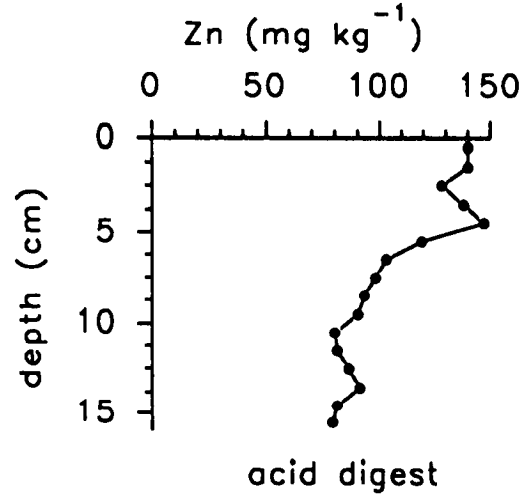
Zn (mg kg^{-1})
0 50 100 150
depth (cm)
0
5
10
15
acid digest

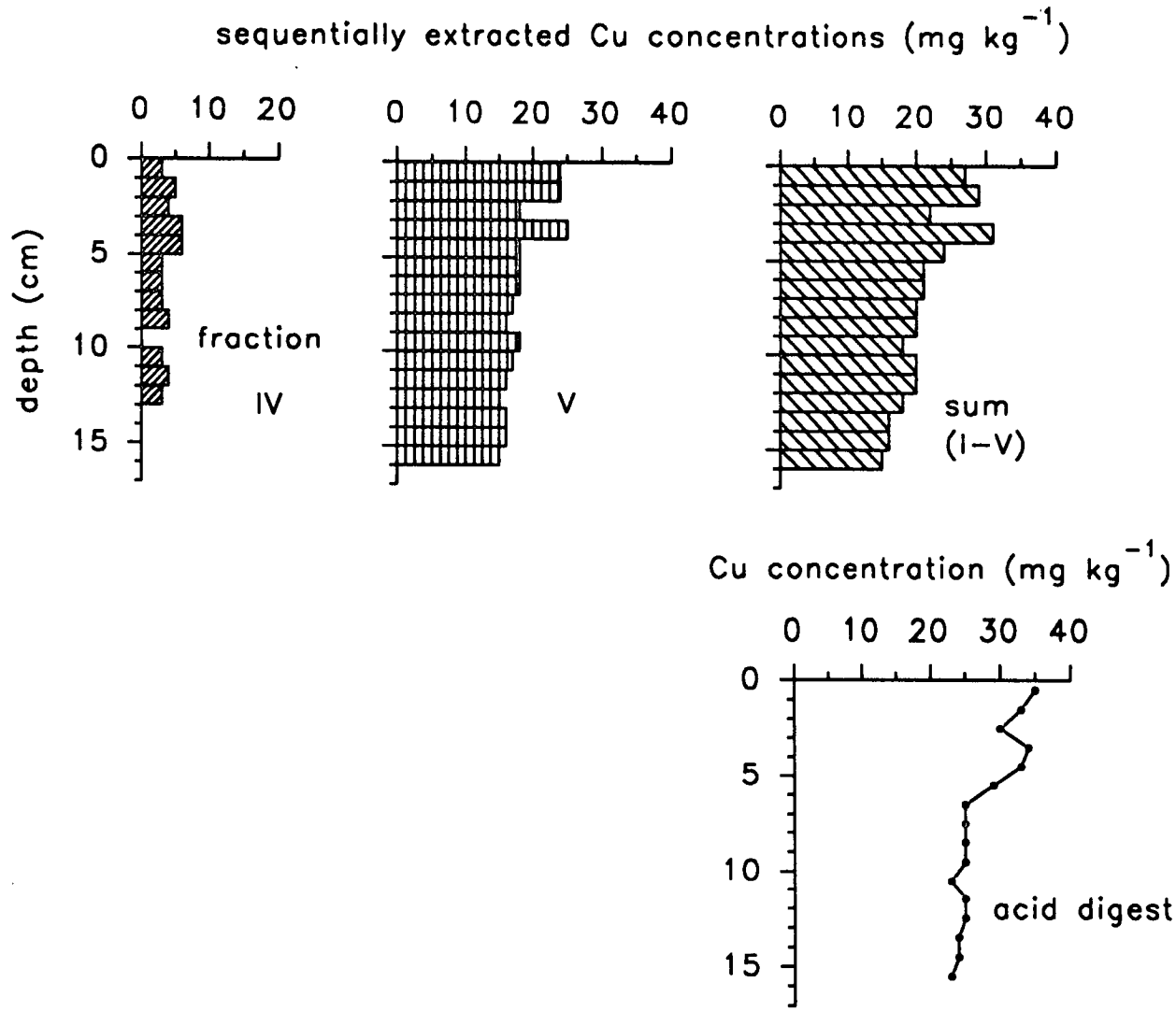
sequentially extracted Cu concentrations (mg kg^{-1})
0 10 20
0 10 20 30 40
0 10 20 30 40
depth (cm)
0
5
10
15
fraction
IV
V
sum
(I–V)
Cu concentration (mg kg^{-1})
0 10 20 30 40
0
5
10
15
acid digest

5.5 Conclusions

1. ^{210}Pb data indicated mixing of the surface sediment to at least 5 cm and the data are unsuitable for calculating a sedimentation rate and core chronology.
2. Radiocaesium results indicate a high degree of movement attributable largely to mixing of the sediment. The radiocaesium movement has obscured patterns expected on the basis of weapons testing and Chernobyl fallout ^{137}Cs maxima, so the use of radiocaesium for dating purposes is not feasible. Efficient deposition of radiocaesium from the water column to the relatively clay-rich sediment occurs, since the estimated inventory from Chernobyl fallout ^{137}Cs is within range of the reported fallout deposition for this area. The slightly low estimated ^{137}Cs inventory from weapons testing fallout is attributed to incomplete attainment of the total inventory by the maximum depth of the sampled core and/or inaccuracy in the reported value for fallout deposition for this area.
3. Mn and, to a lesser extent, Fe show evidence of redox-cycling with peak concentrations in the acid digested surface sediment of all three cores for Mn and the autumn and winter cores in the case of Fe. The greater surface enhancement of Mn in sediment from the summer sampling, compared with sediment collected in autumn and winter, was attributed to seasonal changes in the water column. During the summer, redox-related release of Mn (Fe and P) from the sediment to the water column occurred, followed and outweighed by rapid precipitation and deposition of Mn to the sediment surface, enhanced during higher pH conditions during an algal bloom and higher water temperatures. The less pronounced Mn peaks in the surface sediment of the autumn and winter cores can be explained by dissolution of Mn from the sediment to the water column after the algal bloom has dissipated, when freshly deposited organic matter maintains reducing conditions in the sediment.
4. The slight Fe enhancements in autumn and winter sediment and the lack of enhancement during the summer are consistent with the Mn interpretation, with the less readily reduced Fe oxyhydroxides not being significantly redeposited during the summer and perhaps less redox-driven diagenesis (relative to Mn) all year at depth in the sediment.
5. Pb, Zn, Cu and Cd acid digest concentration profile trends, increasing towards the sediment surface, appear to be influenced by historical changes in the deposition of pollutant metals and, additionally, by the sediment mixing deduced from the radionuclide data. However, since a sedimentation rate could not be determined at this site, changes in concentrations could not be dated. Inventories of pollutant Zn, Cu and Pb, similar to those in nearby Balgavies Loch, show that total deposition of

pollutant metals to the sediment decreased in the sequence Zn>Pb>Cu. Non-anthropogenic concentrations of Pb, Zn and Cu respectively, in the three cores collected at the same site at different times of the year, were similar.

6. The algal bloom exerts no obvious influence on the cycling of Pb, Zn, Cu and Cd, although the partitioning data for Zn and Cu do show the importance of the association of these metals with organic matter.

Chapter 6 Balgavies Loch

6.1 Study Area

Balgavies Loch (OS grid ref. NO 523 516) (Fig. 6.1) lies in central Scotland on the course of Lunan Water, approximately 10 km east of Forfar in the Angus District, between Turin Hill to the north and Dunnichen Hill to the south. The loch was formed over depressions and kettleholes left by the last glaciation. Catchment soils are derived from worked glacial deposits overlying Lower Old Red Sandstone. These soils are basic, nutrient rich and intensively farmed. Catchment land use is predominantly arable, with some woodland and grassland (Harper and Stewart 1987).

At water depths greater than 2 m, black silt sediments are found (Harper and Stewart 1987). Significant nutrient enrichment of the loch has occurred, due to runoff of nitrogen (nitrates/nitrites and ammonia) and phosphorus from the catchment, which is fertilised for agricultural purposes. The enrichment of Balgavies Loch is characterised by various algal blooms during summer months and the loch is classified by Harper and Stewart (1987) as eutrophic with a mean pH of 8.3. Balgavies Loch supports a varied aquatic flora and fauna, with a range of uncommon stoneflies and caddisflies, including some very local species typical of nutrient rich conditions. Unusually high $CaCO_3$ concentrations are found - water concentrations of Ca^{2+} and CO_3^{2-} are 2.2 meq l^{-1} and 1.8 meq l^{-1} respectively (Harper and Stewart 1987), and this is reflected by a rich mollusc fauna with several species of gastropod and bivalve, including those characteristic of hard water.

Physical characteristics of Balgavies Loch and the catchment are listed in Table 6.1.

The western basin of Balgavies Loch has restricted water circulation and, as a consequence, stratification of the water column may develop during the summer. At the beginning of July 1991, the bottom waters of this basin were anoxic at a depth of 4.5 m (A.Kirika, pers. comm.).

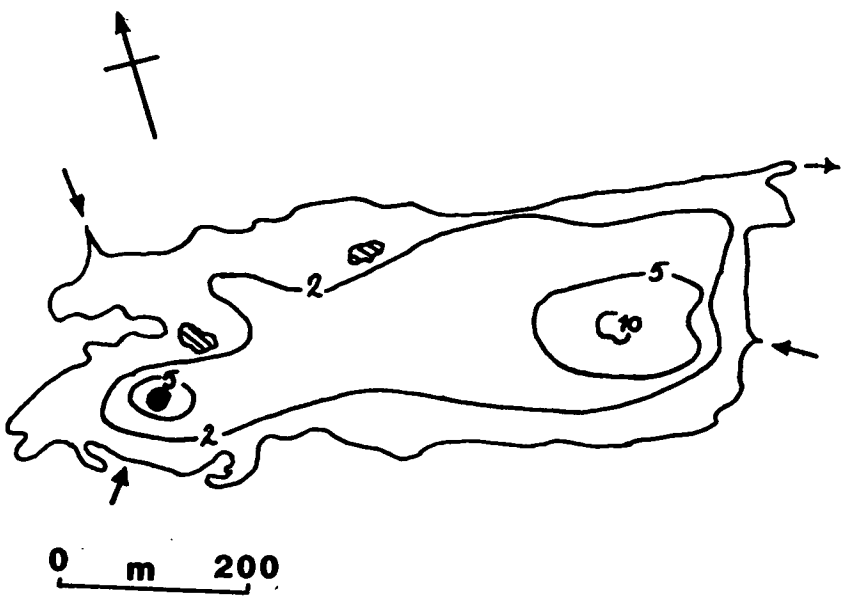

Fig. 6.1 Balgavies Loch bathymetry showing sampling site (•). Depth contours in metres.

Table 6.1 Physical characteristics of Balgavies Loch basin and catchment (Harper and Stewart 1987).

<u>catchment</u>	
area (km^2)	24
ratio catchment:loch area	114:1
<u>loch basin</u>	
length (km)	0.8
width (km)	0.25
area (km^2)	0.2
volume ($m^3 x 10^6$)	0.6
mean depth (m)	3
maximum depth (m)	10

Table 6.2 Core codes, sampling dates and purpose of core collection from Balgavies Loch.

core code	sampling date	core purpose
Ba-A	16.8.91	γ-spectrometry
Ba-B	16.8.91	chemical digestion
Ba-C	15.8.91	porewater analysis
Ba-D	16.8.91	"

6.2 Sampling and analysis

Four sediment cores were collected over two days (15-16.8.91) from the western basin of Balgavies Loch (Fig. 6.1) using a Jenkin Surface-Mud Sampler (Chapter 2) at a water depth of 5.5 m. Table 6.2 shows core codes and purpose of core collection. Unsectioned core lengths were 21-22 cm. Core Ba-B (used for chemical digestion) had a 3 cm unconsolidated layer, followed by dark brown/black sediment to 17 cm, below which sediment was light brown. Sediment cores Ba-C and Ba-D, collected for porewater analysis, respectively had 4 cm and 2 cm mobile layers, dark brown/black sediment to 14 cm (17 cm) and light brown below this. Sediment colour changes in core Ba-A were similar to the other cores.

Core Ba-A was sectioned on shore in air (Chapter 2) at 1 cm vertical intervals for γ-spectrometry. The remaining 3 cores were sectioned in a N_2-purged glovebox (Chapter 2) positioned on shore. Core Ba-B was sectioned at 1 cm intervals in the glovebox and the sediment sealed tightly into polythene bags, which were placed into 125 ml plastic tubs with lids further sealed by insulating tape. After removal from the glovebox, the tubs were kept at 4°C until opened for sediment extraction, which, for fractions I-IV, was carried out under N_2 (Chapter 2).

Porewater samples were collected by sectioning cores Ba-C and Ba-D at 1 cm vertical intervals and, using syringes with teflon stoppers, passing porewaters via 0.45 µm filters (Chapter 2). Filtered porewaters were stored in 30 ml plastic Nalgene 'low metal' bottles and acidified as described in Chapter 2. Water overlying sediment in the core tube (referred to as 'overlying water') from cores Ba-B, Ba-C and Ba-D was collected with a syringe (with teflon stopper) and sub-samples filtered via 0.45 µm filters. All samples were acidified.

Water column samples were collected at 1 m intervals (0-5 m inclusive) using a Friedinger sampler and stored in acid-washed, sample-rinsed bottles. Sub-samples were filtered via 0.45 µm filters. Filtered and unfiltered samples were acidified as in Chapter 2. Water column measurements (Table 6.3) were made by lowering the Windermere Profiler 2 probes to required depths.

Table 6.3 Water column characteristics in Balgavies Loch (16.8.91).

water depth (m)	T. (°C)	O_2 (%)	cond. (µS)	pH
0.25	17.14	70.4	387.1	7.3
0.5	17.15	70.3	386.7	7.3
1.0	17.16	70.0	386.5	7.3
1.5	17.16	69.0	386.4	7.3
2.0	17.16	68.2	386.4	7.3
2.5	17.07	60.4	386.6	7.2
3.0	16.91	57.3	386.6	7.2
3.5	16.88	56.2	386.8	7.2
4.0	16.82	50.9	388.0	7.1
4.5	16.65	28.5	401.5	7.0
5.0	16.26	2.3	437.0	6.9

6.3 Results

Results are listed in Tables 6.4-6.13. Figures containing these data are presented in the Discussion (Section 6.4).

1. Tables 6.4 and 6.5 contain wet and dry sediment section weights, mid-section cumulative weights (g cm^{-2}), porosities and, where measured, carbon content and C/N ratios.

2. ^{226}Ra was not detectable in samples from sediment core Ba-A and, since total ^{210}Pb did not decrease to constant concentrations at depth, a value for supported ^{210}Pb could not be obtained. Total ^{210}Pb concentrations and depths (as cm and mid-section cumulative weights) are listed in Table 6.6.

3. Radiocaesium concentrations and $^{134}Cs/^{137}Cs$ ratios are presented in Table 6.7.

4. Tables 6.8-6.13 contain metal concentration data for sediment acid digestions, sequential extractions and porewater and water column samples. Column headings for metal concentrations in sequentially extracted sediment refer to the following fractions and extractants:

I 1M ammonium acetate, pH7, 20°C (exchangeable fraction)

II 1M sodium acetate, pH5 with acetic acid, 20°C ("carbonate bound"/specifically sorbed)

III 0.1M hydroxylammonium chloride/0.01M nitric acid, 20°C (easily reducible)

IV 1M hydroxylammonium chloride/4.4M acetic acid, 20°C (moderately reducible)

V 30% w/v hydrogen peroxide, pH2, 85+/-2°C; 3.2M ammonium acetate in 3.2M nitric acid (organic fraction/sulphides)

Sum I-V refers to the sum of metal concentrations in all fractions.

5. (BDL) is entered where samples were below detection limit and (...) where no result was available. For porewater Zn concentrations (≤ blank) refers to samples with concentrations less than, or equal to the blank concentration.

Table 6.4 Some physical characteristics, carbon content and carbon/nitrogen ratios of Balgavies Loch sediment core Ba-A.

section depth (cm)	wet section weight (g)	dry section weight (g)	mid-section cumulative weight (g cm^{-2})	porosity (%)	carbon content (%)	C/N ratio
0-1	33.491	1.755	0.023	97.6	15.0	8.8
1-2	31.418	2.118	0.075	97.0	15.5	9.2
2-3	30.910	2.229	0.133	96.7	15.3	9.1
3-4	31.844	2.417	0.196	96.6	15.4	9.3
4-5	30.445	2.291	0.258	96.6	15.0	8.7
5-6	32.223	2.495	0.322	96.5	15.3	8.6
6-7	31.943	2.583	0.390	96.3	15.0	9.1
7-8	27.825	2.293	0.456	96.2	14.9	9.4
8-9	31.503	2.668	0.522	96.1	14.6	9.0
9-10	31.322	2.718	0.594	96.0	14.5	9.0
10-11	29.301	2.661	0.666	95.8		
11-12	29.848	2.700	0.738	95.8		
12-13	30.244	2.765	0.811	95.8		
13-14	34.466	3.465	0.894	95.4		
14-15	34.844	3.655	0.989	95.2		
15-16	29.738	3.126	1.080	95.1		

Table 6.5 Some physical characteristics of Balgavies Loch sediment core Ba-B.

section depth (cm)	wet section weight (g)	dry section weight (g)	mid-section cumulative weight (g cm^{-2})	porosity (%)
0-1	26.362	1.163	0.016	98.0
1-2	20.081	1.390	0.050	96.9
2-3	31.277	2.435	0.101	96.4
3-4	29.928	2.448	0.166	96.3
4-5	32.904	2.611	0.234	96.4
5-6	31.794	2.489	0.302	96.4
6-7	35.261	3.147	0.377	95.9
7-8	39.454	3.841	0.471	95.5
8-9	36.266	3.809	0.573	95.1
9-10	32.034	3.428	0.670	95.0
10-11	38.250	4.207	0.772	94.9
11-12	25.790	2.908	0.867	94.8
12-13	35.929	4.090	0.961	94.7
13-14	36.684	4.334	1.073	94.5
14-15	37.963	4.693	1.194	94.2
15-16	30.830	3.776	1.307	94.3

core cross-section area = 37.39 cm^2

Table 6.6 ^{210}Pb concentrations in Balgavies Loch sediment core Ba-A (16.8.91).

section depth (cm)	mid-section cumulativeweight ($g\ cm^{-2}$)	total ^{210}Pb ($Bq\ kg^{-1}$)
0-1	0.023	148 ± 36
1-2	0.075	150 ± 44
2-3	0.133	118 ± 58
3-4	0.196	...
4-5	0.258	...
5-6	0.322	126 ± 48
6-7	0.390	116 ± 34
7-8	0.456	129 ± 53
8-9	0.522	...
9-10	0.594	197 ± 58
10-11	0.666	166 ± 82
11-12	0.738	104 ± 51
12-13	0.811	100 ± 47
13-14	0.894	174 ± 75
14-15	0.989	184 ± 54
15-16	1.080	109 ± 54

Table 6.7 Radiocaesium concentrations and $^{134}Cs/^{137}Cs$ activity ratios in Balgavies Loch sediment core Ba-A (16.8.91).

section depth (cm)	^{137}Cs ($Bq\ kg^{-1}$)	^{134}Cs 605keV ($Bq\ kg^{-1}$)	$^{134}Cs/^{137}Cs$
0-1	185 ± 7	28 ± 8	0.152 ± 0.042
1-2	221 ± 6	22 ± 4	0.101 ± 0.020
2-3	213 ± 8	...	...
3-4	219 ± 8	26 ± 7	0.117 ± 0.031
4-5	227 ± 6	17 ± 4	0.077 ± 0.020
5-6	246 ± 8	27 ± 6	0.108 ± 0.024
6-7	282 ± 5	28 ± 3	0.097 ± 0.012
7-8	321 ± 9	30 ± 5	0.094 ± 0.015
8-9	299 ± 7	19 ± 5	0.064 ± 0.017
9-10	279 ± 8	30 ± 6	0.107 ± 0.023
10-11	253 ± 6	24 ± 4	0.097 ± 0.016
11-12	200 ± 7	23 ± 4	0.115 ± 0.022
12-13	186 ± 5	15 ± 4	0.083 ± 0.024
13-14	175 ± 8	24 ± 10	0.140 ± 0.055
14-15	155 ± 8	...	...
15-16	144 ± 7	15 ± 4	0.102 ± 0.054

core cross section area = 37.39 cm^2

Table 6.8 Fe, Mn, Pb, Zn, Cu, Cd, Co and Ni concentrations in HNO_3/HCl digested Balgavies Loch sediment core Ba-B

depth (cm)	Fe %	Mn mg kg^{-1}	Pb mg kg^{-1}	Zn mg kg^{-1}	Cu mg kg^{-1}	Cd mg kg^{-1}	Co mg kg^{-1}	Ni mg kg^{-1}
0-1	3.16	1,540	47	140	34	BDL	14	44
1-2	2.92	830	48	165	35	0.8	14	44
2-3	2.86	700	49	152	34	0.7	14	38
3-4	2.77	590	45	137	32	0.8	12	38
4-5	2.75	500	43	140	30	0.8	14	39
5-6	3.11	520	41	144	32	0.7	13	38
6-7	2.85	500	48	158	36	0.9	14	42
7-8	2.78	460	50	158	35	0.8	15	43
8-9	2.89	430	52	160	38	0.8	14	42
9-10	2.98	390	52	159	36	0.8	14	41
10-11	2.93	390	52	161	38	0.9	15	41
11-12	2.96	370	56	163	39	0.9	14	44
12-13	2.95	350	56	165	38	0.9	15	43
13-14	3.10	340	56	163	38	1.0	15	41
14-15	3.01	340	57	164	38	1.0	14	42
15-16	2.94	340	56	166	38	1.0	13	38

Table 6.9 Fe and Mn concentrations in sequentially extracted Balgavies Loch sediment core Ba-B

	Fe (%) fractions						Mn (mg kg^{-1}) fractions					
depth (cm)	I	II	III	IV	V	sum I-V	I	II	III	IV	V	sum I-V
0-1	0.042	0.444	0.105	0.618	1.38	2.59	747	420	84	59	107	1,417
1-2	0.018	0.221	0.090	0.470	1.59	2.39	304	262	50	46	128	790
2-3	0.029	0.493	0.084	0.295	1.47	2.37	273	163	28	25	115	604
3-4	0.057	0.552	0.088	0.271	1.25	2.22	208	114	22	19	100	463
4-5	0.071	0.750	0.105	0.293	1.23	2.45	194	98	18	17	96	423
5-6	0.110	0.934	0.137	0.318	1.37	2.87	196	98	16	16	108	434
6-7	0.030	0.504	0.080	0.256	1.32	2.19	149	88	14	15	108	374
7-8	0.028	0.411	0.069	0.244	1.43	2.18	124	92	16	16	118	366
8-9	0.049	0.475	0.075	0.254	1.41	2.26	128	78	12	13	104	335
9-10	0.046	0.480	0.085	0.263	1.57	2.44	121	72	12	13	111	329
10-11	0.039	0.343	0.065	0.222	1.65	2.32	106	69	10	13	112	310
11-12	0.021	0.215	0.062	0.211	1.92	2.43	104	69	14	13	117	317
12-13	0.014	0.170	0.046	0.171	1.79	2.19	77	69	11	12	102	271
13-14	0.012	0.095	0.030	0.135	2.17	2.44	67	71	12	13	112	275
14-15	0.008	0.061	0.030	0.124	2.19	2.40	55	77	12	13	105	262
15-16	0.007	0.053	0.021	0.106	2.10	2.29	55	73	11	13	102	254

Table 6.10 Pb and Zn concentrations in sequentially extracted Balgavies Loch sediment core Ba-B.

depth (cm)	Pb (mg kg^{-1}) fractions I	II	III	IV	V	sum I-V	Zn (mg kg^{-1}) fractions I	II	III	IV	V	sum I-V
0-1	BDL	11	BDL	30	13	54	BDL	20	7.5	48	57	132
1-2	"	14	"	30	19	63	"	21	8.6	48	66	144
2-3	"	11	"	31	20	62	"	13	5.5	52	77	148
3-4	"	BDL	"	31	20	51	"	7.3	3.4	47	72	130
4-5	"	"	"	31	24	55	"	7.4	3.3	51	75	137
5-6	"	"	"	35	17	52	"	7.4	3.4	52	78	141
6-7	"	12	"	33	19	64	"	11	3.8	50	72	137
7-8	"	11	"	35	19	65	"	9.5	3.0	54	76	142
8-9	"	11	"	35	16	62	"	8.0	3.1	54	85	150
9-10	"	12	"	35	17	64	"	9.2	5.2	52	82	148
10-11	"	11	"	35	12	58	"	8.1	3.9	53	81	146
11-12	"	13	"	32	12	57	"	13	7.0	51	86	157
12-13	"	13	"	33	14	60	"	14	8.8	53	73	149
13-14	"	12	"	34	18	64	"	12	6.0	54	84	156
14-15	"	14	"	32	14	60	"	16	6.3	51	78	151
15-16	"	13	"	35	13	61	"	9.0	4.3	56	78	147

Table 6.11 Cu concentrations in sequentially extracted Balgavies Loch sediment core Ba-B.

depth (cm)	Cu (mg kg^{-1}) fractions I	II	III	IV	V
0-1	BDL	BDL	BDL	BDL	30
1-2	"	"	"	"	32
2-3	"	"	"	"	32
3-4	"	"	"	"	30
4-5	"	"	"	"	30
5-6	"	"	"	"	32
6-7	"	"	"	"	32
7-8	"	"	"	"	36
8-9	"	"	"	"	34
9-10	"	"	"	"	37
10-11	"	"	"	"	34
11-12	"	"	"	"	34
12-13	"	"	"	"	34
13-14	"	"	"	"	30
14-15	"	"	"	"	36
15-16	"	"	"	"	34

Table 6.12 Fe, Mn and Pb concentrations in porewaters from Balgavies Loch sediment cores Ba-C and Ba-D, water overlying the sediment and water column samples.

water column depth (m)	Fe (mg l^{-1})		Mn (mg l^{-1})		Pb (mg l^{-1})	
surface (0)	0.018	(0.077)	0.19	(0.19)	BDL	(BDL)
1	0.016	(0.075)	0.19	(0.19)	"	"
2	0.013	(0.078)	0.19	(0.19)	"	"
3	0.014	(0.088)	0.19	(0.19)	"	"
4	0.014	(0.108)	0.26	(0.28)	"	"
5	0.014	(0.210)	0.57	(0.76)	"	"
overlying water						
Ba-C	0.048	(1.15)	0.84	(0.84)	"	"
Ba-D	0.080	...	1.49	(4.01)	"	(0.009)
Ba-B	0.38	(0.44)	1.00	(1.24)	"	BDL
porewater depth (cm)	Ba-C	Ba-D	Ba-C	Ba-D	Ba-C	Ba-D
0-1	4.5	5.0	5.3	4.2	BDL	BDL
1-2	5.7	9.0	5.5	3.9	0.006	"
2-3	4.7	...	4.2	...	BDL	"
3-4	3.2	...	2.8	...	"	"
4-5	2.2	9.0	1.6	4.4	"	"
5-6	1.9	4.0	1.5	2.8	"	"
6-7	1.5	4.0	1.1	2.7	"	"
7-8	1.3	6.5	1.4	3.5	"	"
8-9	1.1	...	1.1	...	"	"
9-10	0.6	7.5	0.9	2.7	"	"
10-11	...	...	0.9	...	"	"
11-12	...	7.7	0.9	3.1	"	"
12-13	...	...	0.9	...	"	"
13-14	...	5.0	0.8	2.3	"	"
14-15	...	4.0	0.5	2.3	"	"
detection limits					0.003	

unfiltered water concentrations in brackets ( ).

Table 6.13 Zn, Cu and Cd concentrations in porewaters from Balgavies Loch sediment cores Ba-C and Ba-D, water overlying the sediment and water column samples.

water column depth (m)	Zn ($mg\ l^{-1}$)		Cu ($mg\ l^{-1}$)		Cd ($mg\ l^{-1}$)	
surface (0)	0.002	(≤blank)	BDL	(BDL)	BDL	(BDL)
1	≤blank	(0.002)	"	"	"	($3x10^{-4}$)
2	"	(0.001)	"	"	"	(BDL)
3	"	(≤blank)	"	"	"	"
4	"	(")	"	"	"	"
5	0.002	(0.009)	"	"	"	"
overlying water						
Ba-C	0.029	...	0.014	(0.022)	"	(BDL)
Ba-D	0.018	(0.031)	BDL	(0.019)	"	($6x10^{-4}$)
Ba-B	0.004	(0.010)	0.013	(0.013)	"	BDL
porewater depth (cm)	Ba-C	Ba-D	Ba-C	Ba-D	Ba-C	Ba-D
0-1	0.093	≤blank	0.020	0.013	BDL	BDL
1-2	0.19	0.045	0.064	0.020	$7x10^{-4}$	"
2-3	0.033	0.075	0.026	0.031	BDL	"
3-4	0.048	0.18	0.026	0.060	"	$2x10^{-4}$
4-5	0.087	0.11	0.031	0.028	"	BDL
5-6	0.081	0.11	0.031	0.020	"	"
6-7	0.10	0.04	0.054	0.030	"	"
7-8	0.075	0.10	0.039	0.029	"	$2x10^{-4}$
8-9	0.024	...	0.069	0.034	"	...
9-10	0.072	0.05	0.029	0.023	"	BDL
10-11	0.060	...	0.031	...	"	"
11-12	0.10	0.15	0.030	0.031	...	"
12-13	...	...	0.146	...	BDL	"
13-14	...	0.16	0.092	0.030	...	"
14-15	...	0.24	0.114	0.033	...	"
detection limits	blank = 0.005		0.01		$1x10^{-4}$	

unfiltered water concentrations in brackets ( ).

6.4 Discussion

6.4.1 Sediment core characteristics

Porosities in sediment cores Ba-A and Ba-B (Tables 6.4 and 6.5) are similar, ranging from 94.2% (14-15 cm, core Ba-B) to 98.0% (0-1 cm, core Ba-A), and while the porosities decrease with depth, the overall decrease is not marked. Total carbon contents for core Ba-A (Table 6.4) do not vary greatly, ranging from 14.5% to 15.5% C, and probably contain some carbonate, since this is a hard water loch. The C/N ratios also remain constant and show no evidence of organic matter degradation (Table 6.4).

6.4.2 Radionuclide data

^{210}Pb data

Total ^{210}Pb concentrations range from 100-197 Bq kg^{-1} (Table 6.6, Fig. 6.2) but show no systematic decrease downcore, indicating highly efficient mixing of the sediment over the sampled depth range 0-16 cm. Alternatively, this ^{210}Pb distribution could have been produced by very rapid sediment accumulation or slumping and the radiocaesium results will be useful in determining which is the most likely process.

The total ^{210}Pb inventory for this core is 1.58 kBq m^{-2} and, if steady state conditions are assumed, a flux of 49 Bq m^{-2} y^{-1} is implied (inventory x λ), which is a minimum value, since unsupported ^{210}Pb was still detectable in the deepest sampled section (15-16 cm). The ^{210}Pb profile (Fig. 6.2) is similar to the highly mixed profile of site 1 in Loch Lomond (Chapter 4), where low levels of unsupported ^{210}Pb were observed to 8 cm, followed by a sudden decrease to non-detectable levels below 9 cm, indicating intense mixing to 8 cm. In sediment core Ba-A however, the bottom of the mixed zone has not been reached at the maximum sampled depth.

A sedimentation rate and core chronology for this site cannot be calculated using the ^{210}Pb data obtained.

Radiocaesium data

^{137}Cs concentrations (Table 6.7, Fig. 6.3) range from 144-321 Bq kg^{-1} and 15-30 Bq kg^{-1} for ^{134}Cs. Maximum ^{137}Cs concentration (321 Bq kg^{-1}) is in the section at 7-8 cm, above and below which the ^{137}Cs concentration decreases. The radiocaesium data also provide strong evidence of sediment mixing in this core with

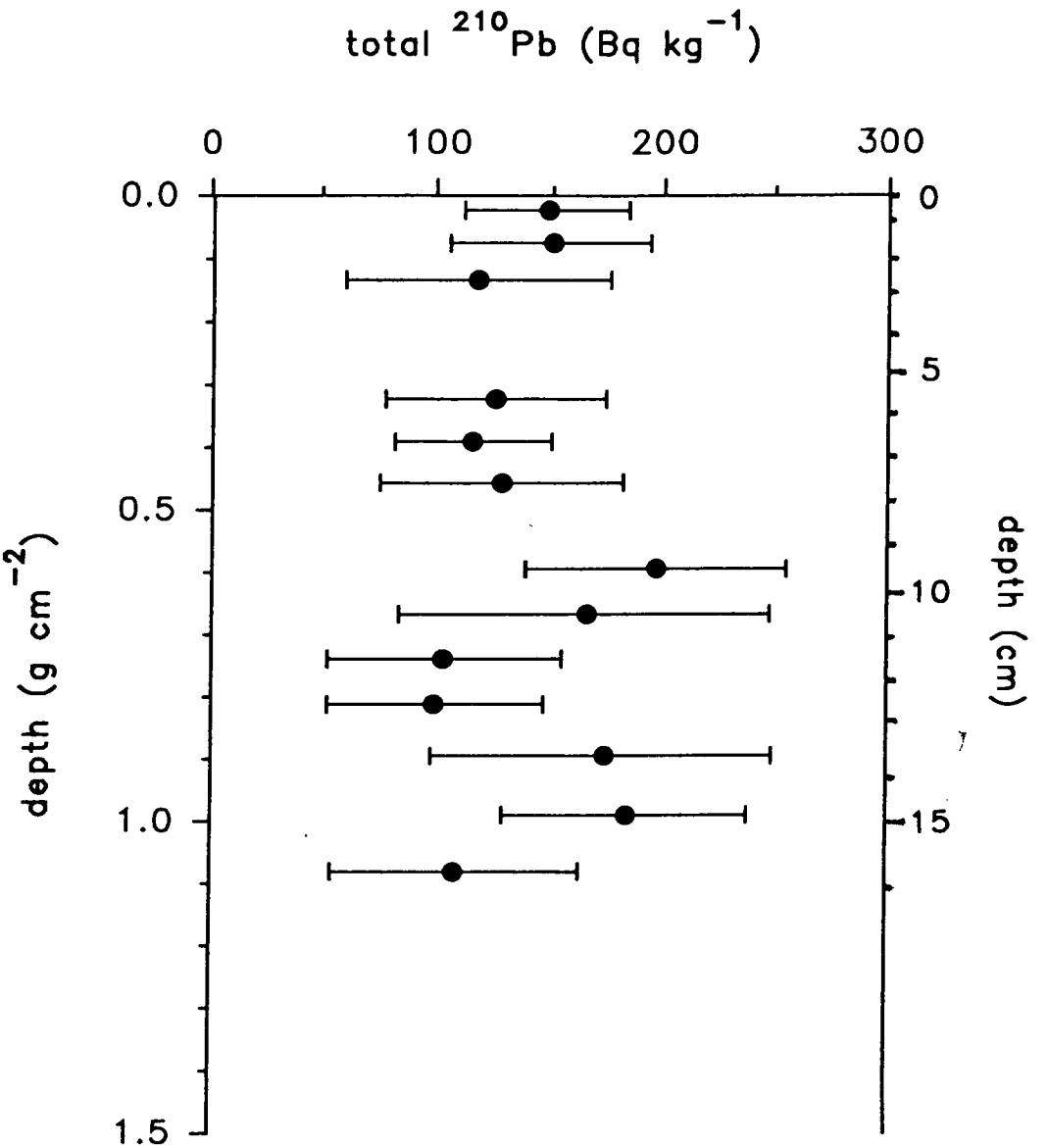

Fig. 6.2 Plot of total ^{210}Pb concentration against depth (weight/area) in Balgavies Loch sediment core Ba–A

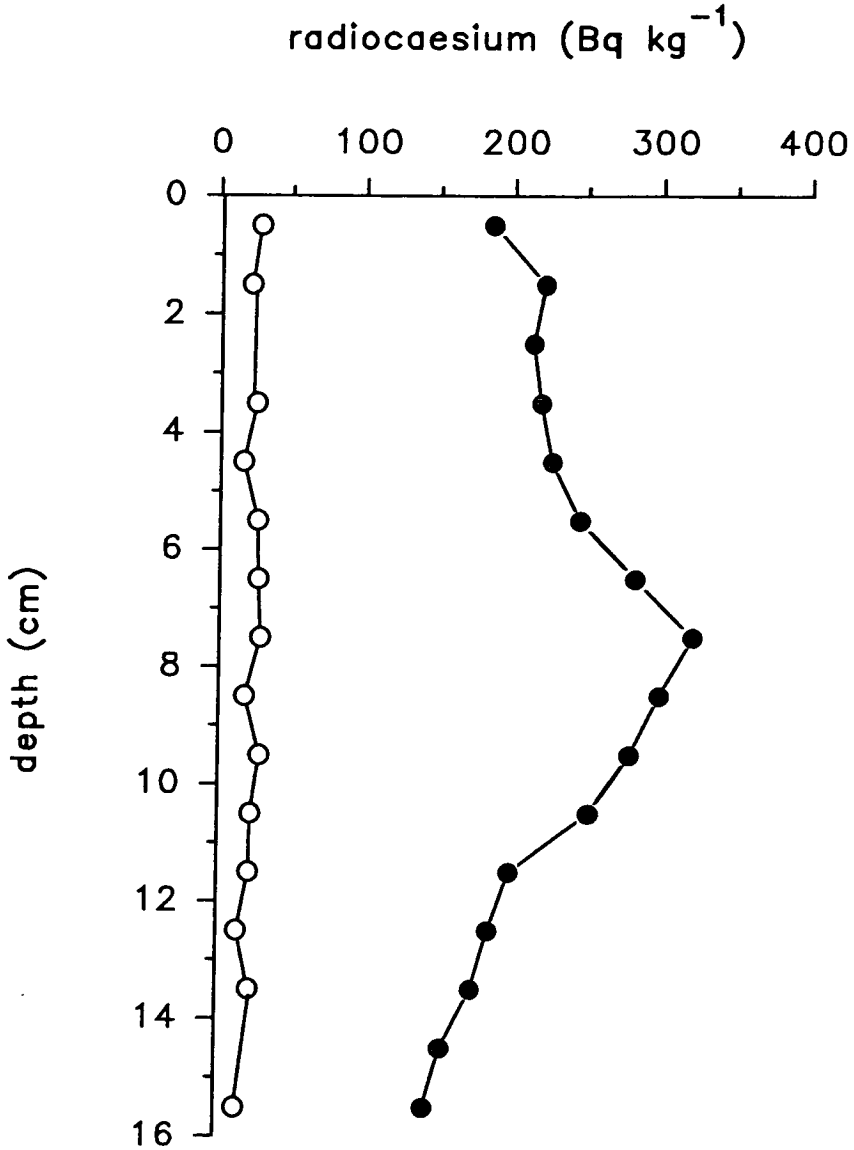

Fig. 6.3 ^{134}Cs (o) and ^{137}Cs (•) concentrations in Balgavies Loch sediment core Ba–A

^{134}Cs, from the input of Chernobyl fallout in 1986, being detected to the base of the core (16 cm) and the $^{134}Cs/^{137}Cs$ activity ratios (Table 6.7) indicate that, in fact, most of the radiocaesium is of Chernobyl origin. This suggests that mixing has occurred to a depth of at least 16 cm over a five year period.

The $^{134}Cs/^{137}Cs$ ratios (Table 6.7) are, with the exception of sections 4-5 cm and 8-9 cm, within error of the ratio of Chernobyl fallout radiocaesium (0.10 after correction for decay since 1.5.86). A decay-corrected Chernobyl fallout ^{137}Cs inventory of 2.68 ± 0.06 kBq m^{-2} is obtained, which is within the range of values reported for atmospheric Chernobyl fallout deposition 1-5 kBq m^{-2} for this area (Clark and Smith, 1988). A small contribution of weapons testing fallout ^{137}Cs to the radiocaesium inventory can be calculated (Appendix 1), giving a decay-corrected inventory of 0.23 ± 0.08 kBq m^{-2}, which is low compared with the recorded deposition of 2.8 kBq m^{-2} radiocaesium from weapons testing fallout to the area (Peirson *et al.*, 1982). This is unsurprising in view of the intense mixing in this core, which means there is probably radiocaesium of weapons testing origin below 16 cm (especially since Chernobyl radiocaesium was detected to the base of the core, Appendix 1).

In summary, the radionuclide data show that intense sediment mixing has occurred at this site, causing a uniform ^{210}Pb profile shape and Chernobyl radiocaesium detectable to the base of the core. The radiocaesium data with a small, but detectable weapons testing component are not explicable in terms of high sedimentation rate or sediment slumping, suggested as a possible cause of the ^{210}Pb concentration profile pattern. Sediment porosities at this site are high: 93-98% (Tables 6.4 and 6.5, Section 6.4.1), showing that even at depths of 15-16 cm, the sediment is fairly uncompacted and may therefore be readily mixed, probably by water movement at this relatively shallow coring site (5.5 m), during periods with no water column stratification. The relatively constant porosities, little variation in carbon content and C/N ratios (Section 6.4.1), and uniform core colour to almost the maximum core depth (Section 6.2) provide further supporting evidence of the intense mixing in this core.

6.4.3 Metal data

A historical interpretation of the metal data is not feasible at this site, due to the impossibility of establishing a sedimentation rate and a core chronology. For discussion of metal profiles, therefore, it is important to consider the intense mixing

shown by the radionuclide data. Acid digest profiles for all the metals will be considered initially, followed by partitioning and porewater data.

Metal concentration profiles in HNO_3/HCl acid digested sediment

Concentration profiles of metals in HNO_3/HCl acid digested sediment core Ba-B (Table 6.8 and Fig. 6.4) show little change with depth for all metals, except Mn, consistent with the apparently intense sediment mixing. The Pb profile shows a trend of increasing concentration downcore, though the increase is slight, 47 mg kg^{-1} (0-1 cm) to 57 mg kg^{-1} (14-15 cm) and a sub-surface minimum of 41 mg kg^{-1} is observed at 5-6 cm. The shape of the Cu profile is similar to that of Pb, with concentrations of 34 mg kg^{-1} (0-1 cm) to 38 mg kg^{-1} (15-16 cm) and a minimum of 30 mg kg^{-1} at 4-5 cm. A sub-surface Zn peak of 165 mg kg^{-1} is present at 1-2 cm, below which the concentration drops to 137 mg kg^{-1}, increasing slightly downcore to a maximum of 166 mg kg^{-1} at 15-16 cm. Cd concentrations are close to the detection limit and in the 0-1 cm section Cd is below the detection limit ($\leq$ 0.6 mg kg^{-1}). At depths greater than 1 cm there is a slight downcore increase and the concentration range is 0.7-1.0 mg kg^{-1}. Co and Ni also show fairly uniform concentration profiles ranging from 12-15 mg kg^{-1} (Co) and 38-44 mg kg^{-1} (Ni).

Since concentration profiles of pollutant metals Pb, Zn, Cu and Cd show no decrease to constant values at depth, a background (non-anthropogenic) value cannot be taken from this data set. However, concentrations of the (largely) 'non-pollutant' metals Fe, Co and Ni are similar in this sediment to those obtained in Loch Leven (Chapter 5), only 60 km south of Balgavies Loch, which together with the absence of known point-source pollutant metal inputs for either loch implies similar atmospheric inputs of pollutant metals. The total (*i.e.* anthropogenic + background) Pb, Zn and Cu concentrations in Loch Leven are also similar to those in Balgavies Loch and so background values from Loch Leven were used to estimate 'excess' inventories for pollutant metals (Table 6.14). These represent minimum values due to the intense mixing in this core, since there is a component of the pollutant metal input below the maximum sampled depth.

The concentration profiles of Pb, Zn, Cu, Cd, Co and Ni in acid digested sediment appear to be dominated by sediment mixing, indicated by the uniform concentration profile shapes, as found for ^{210}Pb. Possible causes of the slight sub-surface peaks/minima (Pb, Zn and Cu profiles) will however be examined with the solution phase and partitioning data.

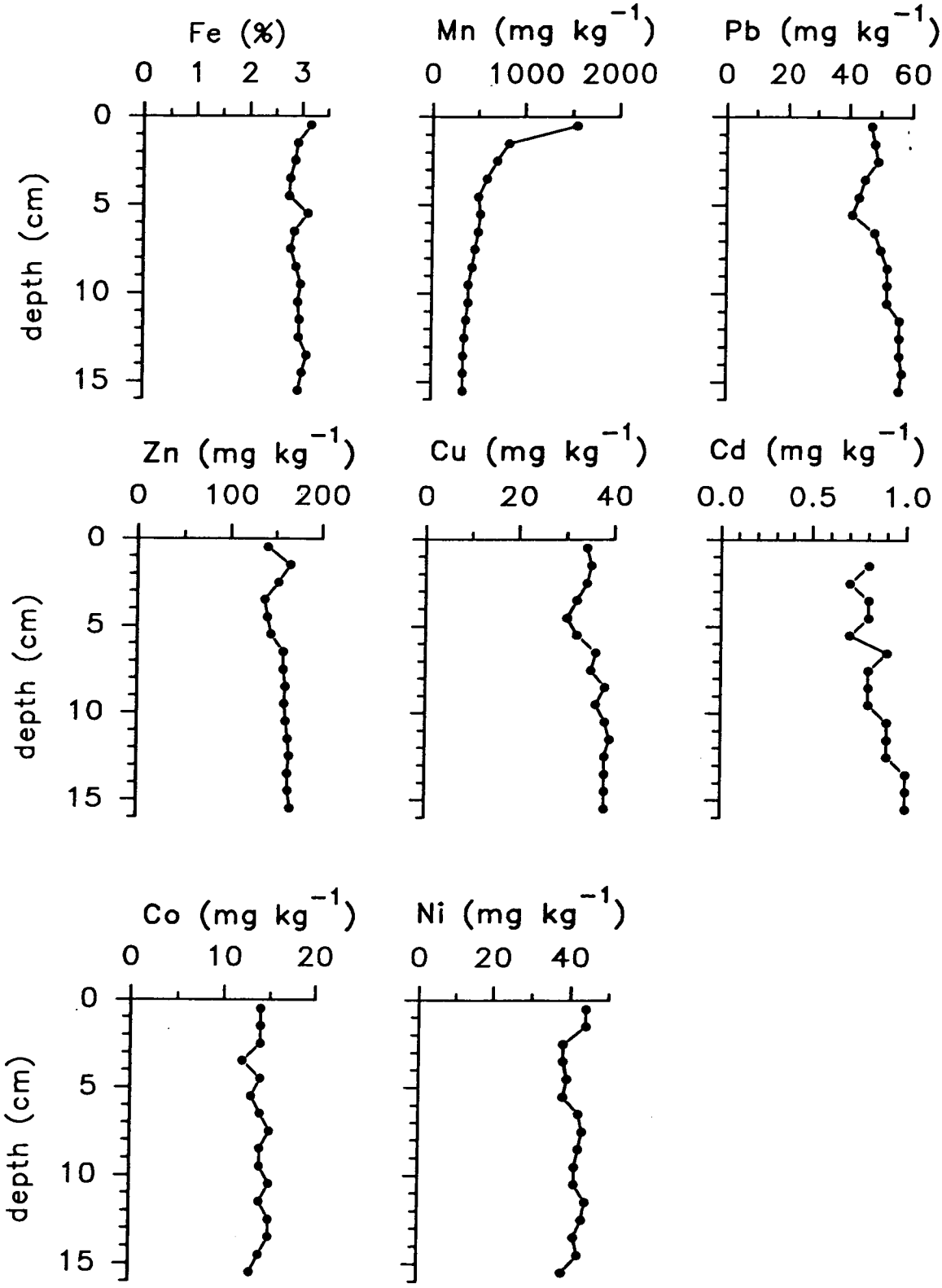

Fig. 6.4 Metal concentrations in HNO_3/HCl acid digested Balgavies Loch sediment core Ba–B

Table 6.14 'Excess' inventories of pollutant metals Pb, Zn and Cu in Balgavies Loch sediment core Ba-B

depth (cm)	Pb	Zn	Cu
background (Loch Leven) ($mg\ kg^{-1}$)	17	96	23
'excess' inventory for sediment core Ba-B ($g\ m^{-2}$)	0.47	0.84	0.18

Iron and manganese concentration profiles in HNO_3/HCl acid digested sediment

Fe concentrations (2.8-3.2%) show little downcore change (Table 6.8, Fig. 6.4). Highest concentrations are found in the sections at 0-1 cm, 5-6 cm, (which corresponds to the section with the minimum Pb concentration) and 13-14 cm.

The maximum Mn concentration (1,540 mg kg^{-1}) occurs in the 0-1 cm section, followed by a decrease below this to a constant 340 mg kg^{-1} below 13 cm (Table 6.8, Fig. 6.4). The Mn concentration profile, compared with the other metal profiles, is exceptional, in that it shows a definite concentration trend, despite the effects of mixing dominating all the other metal profiles. The surface peak overlying progressively diminishing concentrations suggests a redox-driven diagenetic enhancement of Mn (although the peak is not as pronounced as was observed for example in the Mn profiles of Loch Lomond, Chapter 4), which would require very rapid movement of Mn to compete with mixing. This will be discussed further with the partitioning and solution phase data.

Iron and manganese partitioning data

Fe is associated mostly with fraction V (Table 6.9, Fig. 6.5) and concentrations show an increase below around 12 cm to 2% Fe, indicating that Fe forms more stable mineral associations with depth. Fe concentrations in fraction IV gradually decrease from 0.62% at the surface (0-1 cm) to 12 cm and then more rapidly to a minimum of 0.11% at the base of the core (15-16 cm), indicating that Fe oxides/hydroxides are being reduced to some extent, which is consistent with redox cycling causing a slight enhancement of Fe in fraction IV in the surface sediment. Fe concentrations are relatively low in fraction III (ranging from 0.14-0.02%) and decrease gradually to 6 cm and then markedly, as for fraction IV, below 12 cm. This pattern is probably attributable to a removal of Fe oxides/hydroxides by fraction III (easily reducible) extractants and therefore mirrors the trends (though with lower concentrations) in fraction IV. Fe concentrations in fractions I and II also change below 12 cm, decreasing to the base of the core. Overall, the sum of Fe concentrations in fractions I-IV decreases rapidly below 12 cm, contrasting with fraction V which shows increasing Fe concentrations below this depth. It is possible that the sulphate reduction zone (Chapter 1) commences at 12 cm, below which Fe sulphide concentrations (fraction V) increase.

In the top 10 cm, Mn concentrations are highest in fraction I (Table 6.9, Fig. 6.6), decreasing rapidly from a maximum of 747 mg kg^{-1} at the surface (0-1 cm) to 304 mg kg^{-1} by 1-2 cm, below which a progressively more gradual decrease downcore is observed to 55 mg kg^{-1} at 15-16 cm. In fraction II Mn concentrations

range from a surface peak of 420 mg kg^{-1} (0-1 cm) to 98 mg kg^{-1} at 4-5 cm, overlying concentrations which decrease slightly to constant concentrations below 9 cm (mean concentration = 71 mg kg^{-1}). Fraction III shows a slight enhancement of Mn at the surface (84 mg kg^{-1}), below which concentrations are similar to Mn in fraction IV, decreasing to constant levels below 8 cm (mean = 12 mg kg^{-1} in fraction III and 13 mg kg^{-1} in fraction IV). Mn concentrations in fraction V show little variation downcore (96-128 mg kg^{-1}).

Iron and manganese solution phase data

Filtered water column Fe concentrations (Table 6.12, Fig. 6.5) are a mean 0.015 mg l^{-1} with unfiltered concentrations 4-15 times higher than this, illustrating that a significant portion of the Fe is associated with particulates in the water column. Concentrations of Fe in overlying water range from 0.048 to 0.38 mg l^{-1} for cores Ba-B, Ba-C and Ba-D and this range is likely to be due to variations in sampling height above the sediment-water interface.

A sub-surface Fe maximum at 1-2cm of 5.7 mg l^{-1} is observed in the porewater concentrations from core Ba-C, below which concentrations decrease to a minimum 0.6 mg l^{-1} at 9-10 cm (no data are available below this). This profile shape (Table 6.12, Fig. 6.5) is characteristic of redox-driven diagenesis causing reduction and dissolution of Fe oxides, coincident with the porewater maximum, below which concentrations decrease due to formation of authigenic associations (consistent with the partitioning data showing increasing concentrations of Fe in fraction V below 13-14cm). The same pattern is not observed in the higher Fe concentrations of core Ba-D with maxima of 9 mg l^{-1} at 1-2 cm and 3-4 cm and concentrations remaining high as deep as 11-12 cm (7.7 mg l^{-1}). It seems likely that some of the porewaters obtained from Ba-D have been 'contaminated' by particulates passing through the membrane filter into the sample, since there is no evidence from the solid phase data to suggest a reason for this irregular profile shape. In this case, a similar situation might be expected for the other metal concentrations in core Ba-D.

Filtered water column Mn concentrations (Table 6.12, Fig. 6.6) are a mean 0.24 mg l^{-1} to 4 m and 0.29 mgl^{-1} if the concentration at 5 m (0.57 mg l^{-1}) is included. Porewater concentrations are a mean 1.3 mg l^{-1} (Table 6.12, Fig. 6.6), about five times higher than those in the water column. A similar enhancement factor occurs between the overlying water and the mean peak values of 5.4 mg l^{-1} in sections 0-2 cm of core Ba-C. Below the peak concentrations to 2 cm, porewater concentrations in core Ba-C decrease downcore to a minimum of 0.5 mg l^{-1} at 14-15 cm.

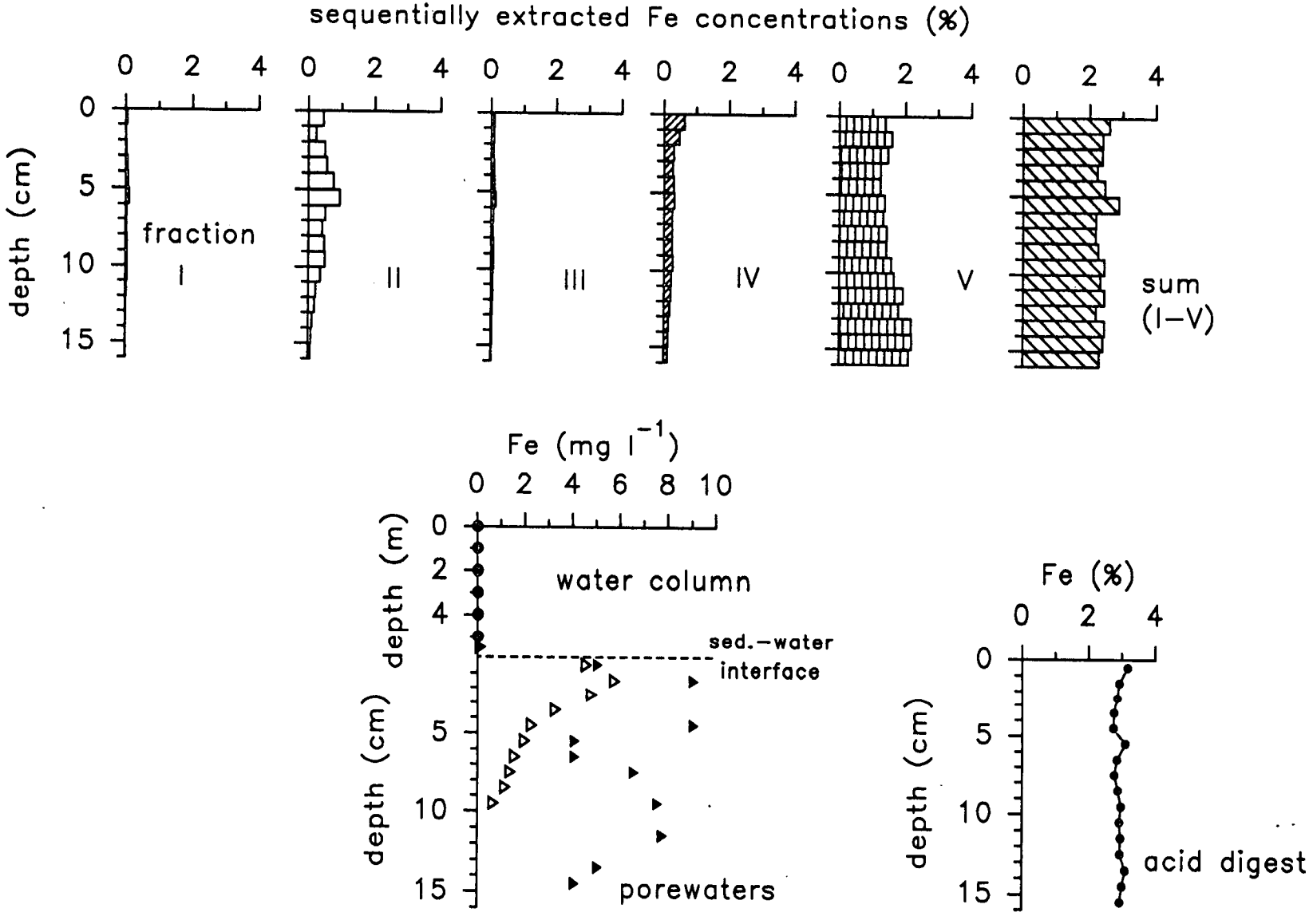
sequentially extracted Fe concentrations (%)
0 2 4
depth (cm)
0
5
10
15
fraction
I
II
III
IV
V
sum
(I–V)
Fe (mg l^{-1})
0 2 4 6 8 10
depth (m)
depth (cm)
water column
sed.–water
interface
porewaters
Fe (%)
acid digest

sequentially extracted Mn concentrations (mg kg^{-1})
0 1000
0 1000
0 1000
0 1000
0 1000
0 1000 2000
depth (cm)
0
5
10
15
fraction
I
II
III
IV
V
sum
(I–V)

Mn (mg l^{-1})
0 2 4 6
depth (m)
0
2
4
water column
sed.–water
interface
depth (cm)
5
10
15
porewaters

Mn (mg kg^{-1})
0 1000 2000
depth (cm)
0
5
10
15
acid digest

The thermal stratification at this site (Table 6.3) has resulted in near-anoxic bottom waters, around 50 cm above the sediment-water interface, in which case the solution phase maxima for the redox-sensitive metals Fe and Mn would be expected to be detected in the water column (Davison, 1981). This is however not the case, Fe and Mn solution phase concentration profiles for core Ba-C show maxima in the sediment porewaters at 1-2 cm (Fe) and 0-2 cm (Mn), below which concentrations decrease with depth. This can be explained by seasonal anoxia in the bottom waters. During periods of oxic bottom water conditions, redox-driven Mn enrichment occurs, giving rise to the solid phase peak in the surface sediment. During periods of anoxic (or near-anoxic) bottom waters, as when the sampling was carried out, Mn from the surface enhancement is released to the porewater, giving rise to the observed maximum in the porewaters. Supporting evidence for this is the high concentration of Mn in fraction I in the near-surface sediment, indicating Mn lability at the surface and not, as is generally observed for redox-driven enhancements, in fraction III (Chapter 4, Loch Lomond). In Balgavies Loch the solid phase profiles observed at the time of sampling may be transient features, in which the porewater peak is close to the previously produced (during oxic conditions) solid phase peak. Presumably if sampling had taken place during conditions of oxic bottom waters, Mn concentrations in the sequentially extracted enhanced layer at 0-2 cm would have been highest in fraction III. The porewater Mn profile indicates loss of Mn from the sediment to the water column (concentrations decrease from the surface sediment section to the water column) and the decreasing concentrations with depth imply some downwards diffusion from the surface peak into the sediment, although the partitioning data do not show a corresponding increase in any of the fractions with depth, which would be expected if Mn was forming solid phase associations with depth. Again, the seasonally anoxic bottom water conditions could explain this, because the partitioning results indicate that dissolution of fractions I-IV occurs (*i.e.* decreasing downcore concentrations) and that Mn is removed from the system at depth. If the porewater profiles observed are a transient response to reducing conditions in the bottom waters, then during periods of oxic bottom waters the maximum point of Mn release would be at greater depth in the sediment and the solid phase concentrations may be a reflection of these previous conditions. Additionally, the effects of mixing on the profile should not be ignored, despite the fact that Mn concentrations do vary (unlike the other metal profiles), because the Mn enhancement is not especially pronounced compared with the redox-driven diagenetic enhancement of Mn in the surface sediment of Loch Lomond (Chapter 4). As with Fe in the porewaters of core Ba-D, the Mn profile from this core shows

irregularities, which cannot be interpreted in the same way as the concentration profile of core Ba-C. Below 4 cm, Mn porewater concentrations are higher in core Ba-D than Ba-C, further indicating that these results are questionable.

Lead, zinc and copper partitioning data

The sum of concentrations in all fractions (Table 6.10, Figs. 6.7 and 6.8) for Pb and Zn are similar to concentrations in acid digested sediment at corresponding depths.

Within the different fractions, Pb concentrations change very little. Pb was not detectable in fractions I and III, but is associated mostly with fraction IV, with concentrations ranging from 30-35 mg kg^{-1} (mean contribution to the sum of fractions I-V = 56%). Concentrations in fraction V (12-24 mg kg^{-1}) are slightly greater than in fraction II (11-14 mg kg^{-1}, below detection limit between 3 and 16 cm), but there is no noticeable trend in either fraction. The lack of trends in the Pb partitioning data is consistent with previously discussed acid digest and radionuclide data in showing the effects of sediment mixing to the base of the core.

Zn was undetectable in fraction I and is mainly associated with fractions IV and V. Fraction IV Zn concentrations remained fairly constant (mean = 52 mg kg^{-1}), while in fraction V, there was a slight depletion of Zn at 0-2 cm (mean = 62 mg kg^{-1}) relative to the underlying constant concentrations (mean = 78 mg kg^{-1}). Zn concentrations in fractions II and III are higher in the top two sections (0-2 cm), at 20 mg kg^{-1} and 8 mg kg^{-1} respectively, below which a mean of 10 mg kg^{-1} (fraction II) and 4.8 mg kg^{-1} (fraction III) is observed. This change in Zn association (fractions II, III and V), albeit slight, between the surface sediment and that below 2 cm, indicates that there may be some process causing post-depostional mobilisation and redistribution of Zn, the effects of which are apparent despite sediment mixing.

Cu was only detectable in fraction V (Table 6.11, Fig. 6.9) with fairly constant concentrations, similar to those obtained by acid digestion of sediment.

Lead, zinc, copper and cadmium solution phase data

Pb is below the detection limit of 0.003 mg l^{-1} (Table 6.12) in all unfiltered water column samples, all porewater samples from core Ba-D and most from core Ba-C (in which Pb was detectable at a low concentration in three samples, all $\leq$ 0.006 mg l^{-1}). These results suggest that Pb is not mobile in the sediment.

Zn was only reliably detectable in two water column samples, the remaining samples being similar to the blank concentration of 0.005 mg l^{-1} (Table 6.13, Fig. 6.8). The overlying water Zn concentrations from cores Ba-C and Ba-D are similar

(0.029 and 0.018 mg l^{-1} respectively), around ten times higher than the two water column concentrations. Porewater Zn concentrations (Table 6.13, Fig. 6.8) from the two cores (Ba-C) and (Ba-D) show similar trends. A sub-surface peak concentration of 0.19 mg l^{-1} is observed in core Ba-C at a depth of 1-2 cm, as for Fe and Mn, and for Ba-D the peak (0.18 mg l^{-1}) is at a depth of 3-4 cm. Concentrations below this are between 0.024 and 0.102 mg l^{-1}, with increasing values towards the base of the core, reaching a maximum of 0.24 mg l^{-1} (core Ba-D) at 15-16 cm. The sub-surface Zn peaks, similar to those observed for Fe and Mn in core Ba-C, could be a result of Zn being associated with Fe or Mn oxyhydroxides, which would release Zn to the porewaters upon dissolution under reducing conditions.

Filtered water column Cu concentrations (Table 6.13) were below the detection limit of 0.01 mg l^{-1} and were detectable only in cores Ba-C and Ba-B in overlying water samples. Porewater Cu concentrations range from 0.013-0.146 mg l^{-1} in the two cores Ba-C and Ba-D (Table 6.13, Fig. 6.9). A sub-surface enhancement is observed in core Ba-C at 1-2 cm, as for Fe, Mn and Zn, but as with these metals, is not apparent in core Ba-D, in which an enhanced concentration occurs at 3-4 cm, as for Zn. A corresponding Cu enhancement in the solid phase at 1-2 cm could indicate redox-driven release, although the partitioning data provide no evidence of an association of Cu with redox-sensitive Fe or Mn oxyhydroxides.

Cd was below the detection limit ($1x10^{-4}$ mg l^{-1}) in all filtered water column and overlying water samples (Table 6.13). Cd was only detectable in three porewater samples (Table 6.13), including 1-2 cm (core Ba-C) and 3-4 cm (core Ba-D), that is, a similar pattern of higher values at 1-2 cm and 3-4 cm as found for Zn and Cu, but not suggestive of post-depositional Cd mobility in this core.

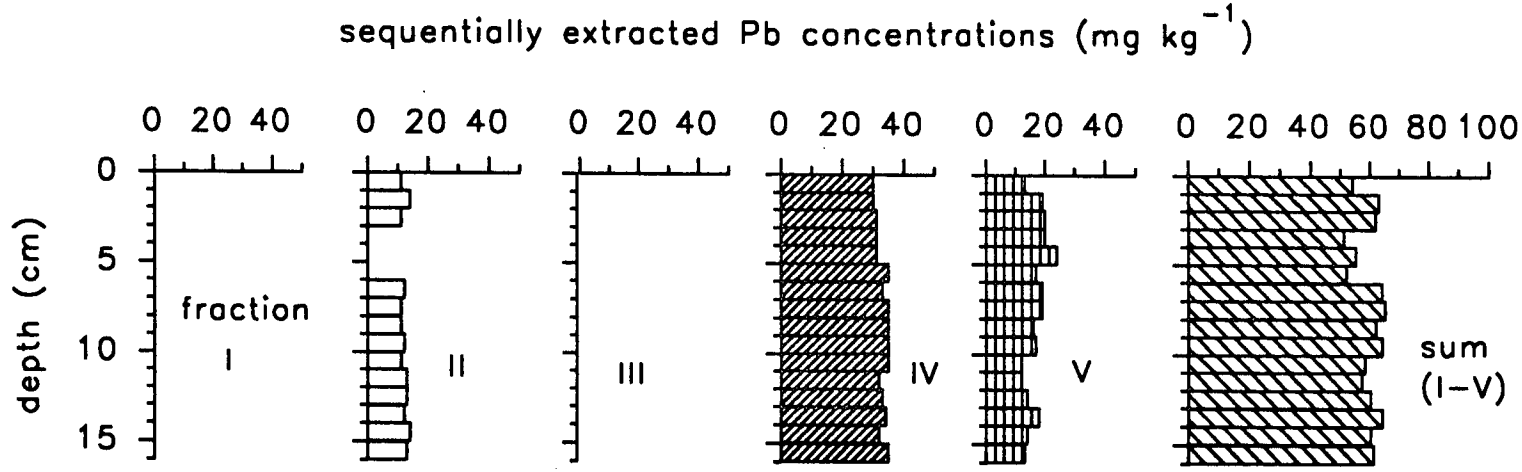
sequentially extracted Pb concentrations (mg kg^{-1})
0 20 40
0 20 40
0 20 40
0 20 40
0 20 40
0 20 40 60 80 100
depth (cm)
0
5
10
15
fraction
I
II
III
IV
V
sum
(I–V)

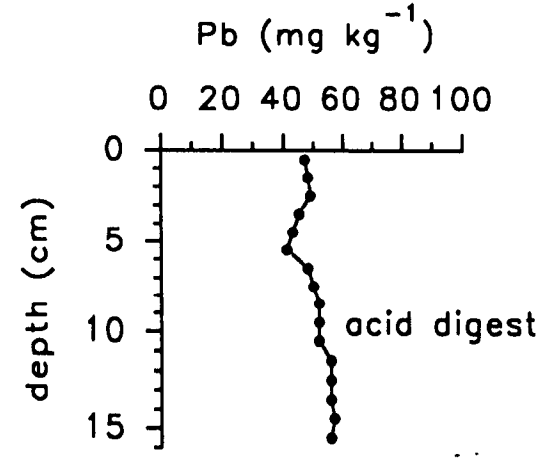
Pb (mg kg^{-1})
0 20 40 60 80 100
depth (cm)
0
5
10
15
acid digest

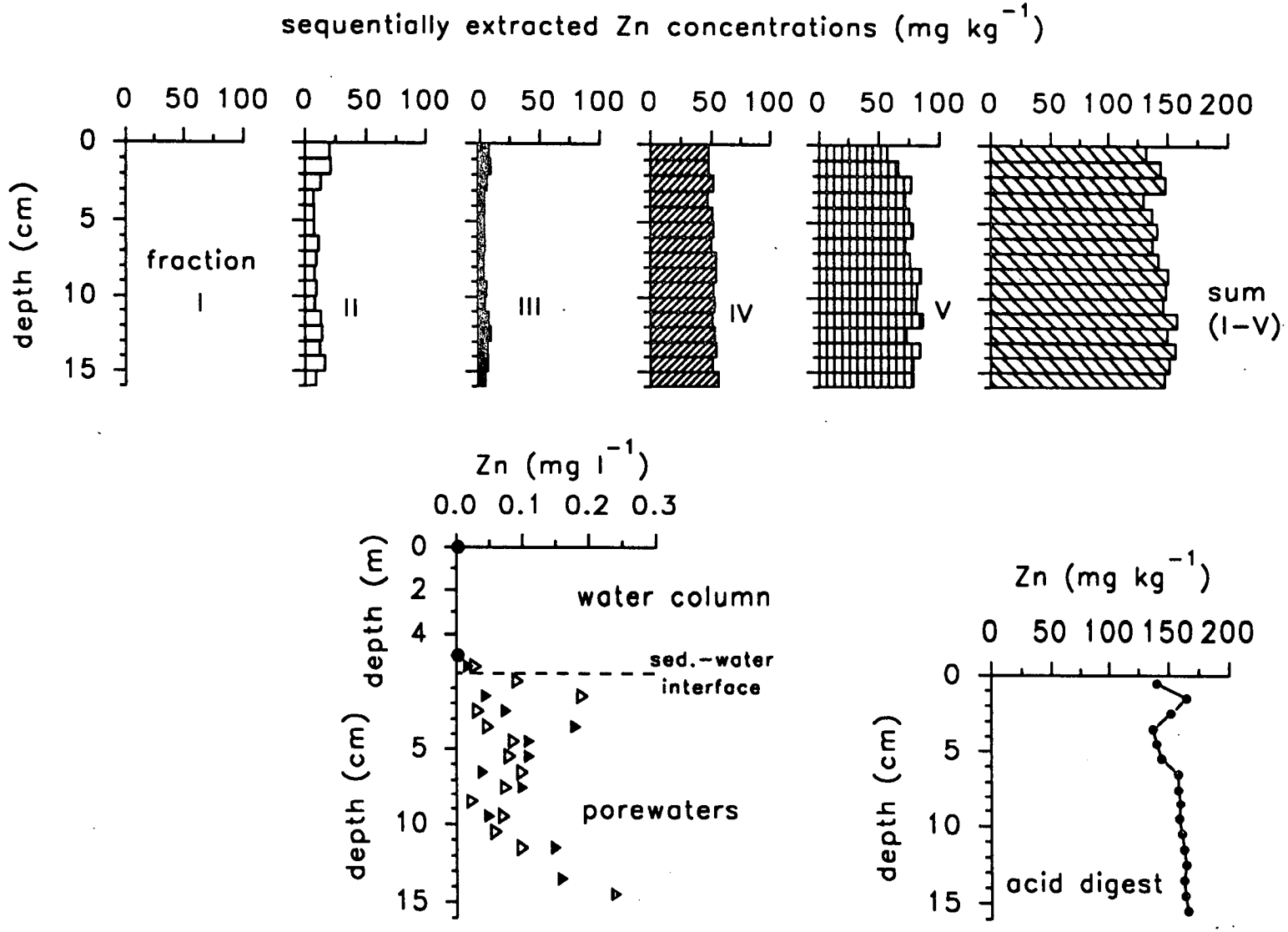
sequentially extracted Zn concentrations (mg kg^{-1})
0 50 100
0 50 100
0 50 100
0 50 100
0 50 100
0 50 100 150 200
depth (cm)
0
5
10
15
fraction
I
II
III
IV
V
sum
(I–V)
Zn (mg l^{-1})
0.0 0.1 0.2 0.3
depth (m)
depth (cm)
0
2
4
5
10
15
water column
sed.–water
interface
porewaters
Zn (mg kg^{-1})
0 50 100 150 200
depth (cm)
0
5
10
15
acid digest

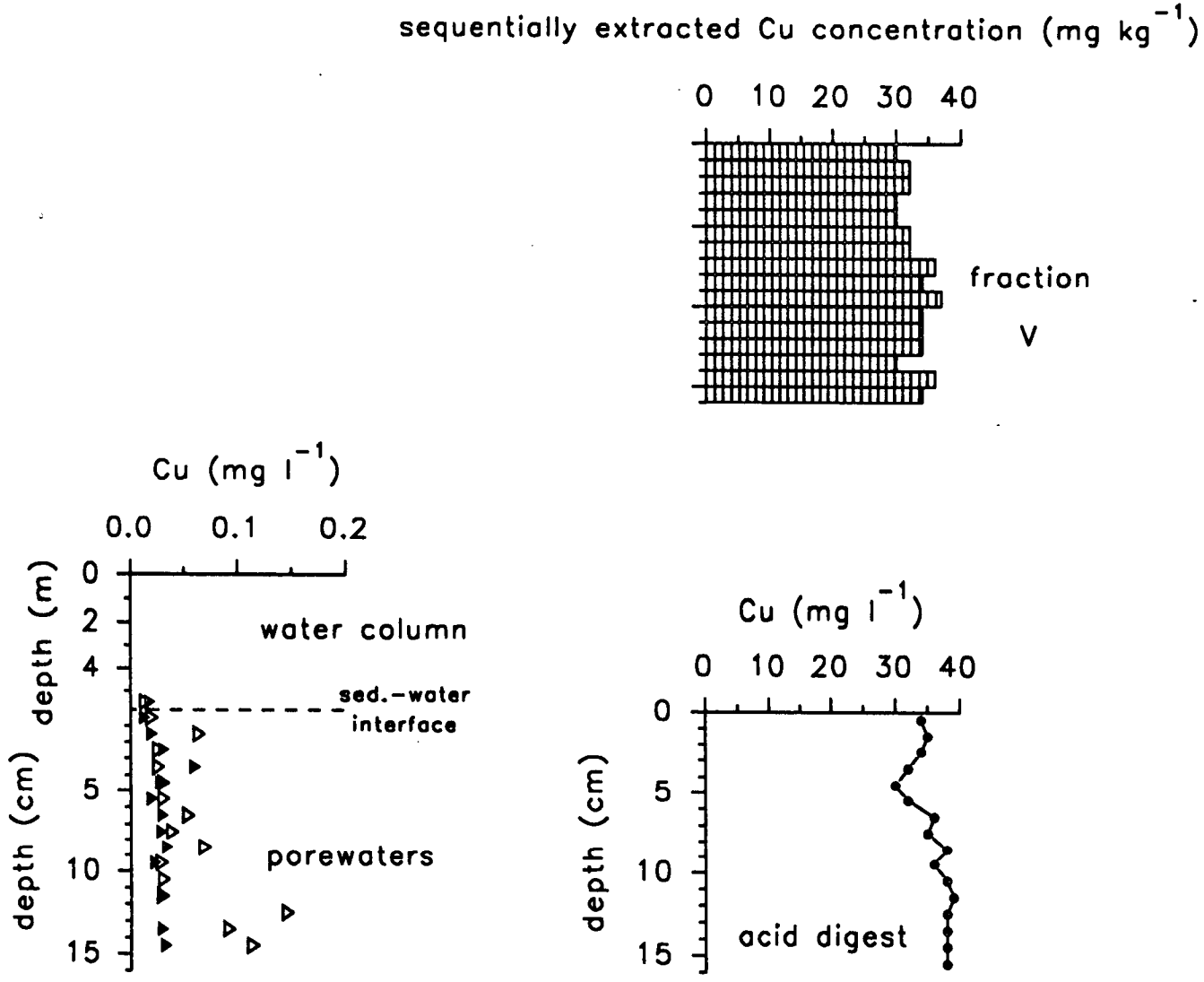
sequentially extracted Cu concentration (mg kg^{-1})
0 10 20 30 40
fraction V
Cu (mg l^{-1})
0.0 0.1 0.2
depth (m)
depth (cm)
0 2 4 5 10 15
water column
sed.–water interface
porewaters
Cu (mg l^{-1})
0 10 20 30 40
depth (cm)
0 5 10 15
acid digest

6.5 Conclusions

1. A uniform ^{210}Pb concentration profile and radiocaesium from Chernobyl fallout to the base of the core indicate intense mixing over the sampled depth (to 16 cm) at this site. Further support for this conclusion is provided by the uniform sediment colour, little downcore variation in %C and C/N ratios, and high sediment porosities throughout the core.
2. The calculated ^{137}Cs inventory due to Chernobyl fallout is within the range of reported values for ^{137}Cs deposition to the area from Chernobyl sources. The weapons testing ^{137}Cs inventory is rather low compared with reported deposition, which may well be due to the intense mixing in the core transporting some of the ^{137}Cs deposited to the loch from weapons testing below the maximum sampled sediment depth.
3. Profile shapes for Pb, Zn, Cu, Cd, Co and Ni in acid digested sediment are explicable in terms of sediment mixing, showing fairly constant concentrations downcore. Solution phase and partitioning data confirm the lack of Pb mobility. The Zn and, to some extent, the Cu data suggest some release from the solid phase and subsequent short-range mobility of these metals.
4. Fe and Mn are influenced by redox-driven diagenesis, as illustrated by the porewater data and, for Mn at least, partitioning and acid digest profiles. The apparent inconsistency between solid and solution phase results for the two metals respectively, with peak porewater concentrations occurring in the same sections as the solid phase enhancements, are explained by seasonal stratification in the water column of this loch, giving rise to transiently anoxic bottom waters. The porewater data are interpreted as a response to redox conditions at the time of sampling, whereas the profiles in the acid digested sediment are attributed to the previously oxic water column conditions. The Mn partitioning data reflect (to some extent) the change in Mn associations in response to the bottom waters becoming anoxic.

Chapter 7 Loch Coire nan Arr

7.1 Study Area

Loch Coire nan Arr is a clearwater loch lying at an altitude of 125 m on the Torridonian sandstones of the Applecross area in north-west Scotland (OS grid ref. NG 808 422). The loch lies in a deep sandstone corrie and has an extensive catchment area of 897 ha which receives high rainfall (2,800 mm y^{-1}). Catchment and loch characteristics are listed in Table 7.1 and Fig. 7.1 shows the loch bathymetry, which is simple with a single basin of maximum depth 12 m. Loch Coire nan Arr is part of the Acid Waters Monitoring Network (as is Round Loch of Glenhead; Chapter 3), but is one of the less acid sites. Palaeolimnological studies have shown that, although the loch is acid sensitive with a peaty catchment and low Ca levels, the surface waters have not been acidified and, historically, the pH has remained >6.0 (Battarbee, 1988). Catchment soils, mainly on the flatter ground on the floor of the corrie, are peats, while on the steeper terrain bare rock predominates. The catchment is unafforested (except for a small stand of conifers, which have failed to mature successfully) and vegetation is characterised by acid moorland species such as *Calluna, Molinia* and *Eriophorum*, which are grazed by sheep in the summer, but other than this there is little evidence of active land-management practices (Patrick *et al.*, 1991). The main inflow at the northern end of the loch is Allt Coire nan Arr, but the loch also receives drainage from a number of small precipitous inflows (Patrick *et al.*, 1991). Outflow is via Russell Burn which flows 2 km into the sea and the proximity of the loch to the coast is reflected in high Na^+ and Cl^- concentrations in the water. The sediments in the loch were observed to be sandy, dark brown and organic-rich (peaty), due to the nature of the catchment.

The ecology of Loch Coire nan Arr is typical of oligotrophic and circumneutral conditions. The macrophyte flora is characterised by *Littorella uniflora, Lobelia dortmanna, Isoetes lacustris* and *Juncus bulbosus* var. *fluitans*. *Myriophyllum alterniflorum* and *Potamogeton natans* are locally abundant offshore and there is a prolific growth of *Nitella flexilis* in deeper water. Benthic invertebrates are fairly diverse and abundant, typical of circumneutral conditions. Characteristic species include molluscs - *Lymnaea peregra* and mayflies - *Leptophlebia vespertina* and *Siphlonurus lacustris*. There appears to be a good population of brown trout (*Salmo trutta* L.) in the loch (Patrick *et al.*, 1991).

Table 7.1 Characteristics of Loch Coire nan Arr and its catchment (Patrick *et al.*, 1991)

Loch altitude	125 m
Maximum depth	12 m
Volume	0.56×10^6 m^3
Loch area	11.6 ha
Catchment geology	Torridonian sandstone
Catchment soils	peat
Catchment vegetation	99% moorland, <1% conifers
Catchment area	897 ha
Ratio catchment : loch area	77.3:1
Mean annual rainfall	*ca.* 2,800 mm (1988)
Wet deposited acidity	0.37 kg ha^{-1} y^{-1} (1988)
Wet deposited non-marine sulphate	5.18 kg S ha^{-1} y^{-1}

Fig. 7.1 Loch Coire nan Arr bathymetry and sampling location (•). Contour depths in metres.

7.2 Sampling and analysis

Three sediment cores were collected on 6.11.91 in the centre of Loch Coire nan Arr (Fig. 7.1) at a water depth of 11 m, using a Jenkin Surface-Mud Sampler (Chapter 2). Table 7.2 shows core codes and purpose of core collection. Unsectioned core lengths were 12-16 cm and sediment was dark brown in colour with sandy particles observable.

Core LCA-A was sectioned in air at 1 cm vertical intervals (Chapter 2). Cores LCA-B and LCA-C were sectioned in a N_2-purged glovebox (Chapter 2): core LCA-B was sectioned at 1 cm intervals and the sediment sealed tightly in polythene bags, which were placed into 125 ml plastic tubs with screw-top lids and further sealed with insulating tape. After removal from the glovebox, the tubs were kept at 4°C until opened for HNO_3/HCl digestion of sediment and sequential extraction, which was carried out under N_2 (Chaper 2).

Porewater samples were collected by sectioning core LCA-C at 1 cm intervals and then succesively filtering samples via 0.45 μm and 0.1 μm filters (Chapter 2), using syringes with teflon stoppers. Porewaters were stored in 30 ml plastic Nalgene 'low metal' bottles. Water overlying the sediment in the core tube was collected with a syringe and sub-samples passed via a 0.1μm filter. All samples were acidified (Chapter 2).

Water column samples were collected at 1 m intervals with a Friedinger sampler to a depth of 10 m and were transferred into acid-washed, sample-rinsed plastic Nalgene bottles. Sub-samples were filtered via 0.45 μm filters. All samples were acidified (Chapter 2). Measurements of surface-water and overlying core water (core LCA-B) characteristics (Table 7.3) were made using the Checkmate meter. pH readings have been excluded due to the questionable results obtained (*i.e.* anomalously low values).

Table 7.2 Core codes, sampling dates and purpose of core collection from Loch Coire nan Arr

core code	sampling date	core purpose
LCA-A	6.11.91	γ-spectrometry
LCA-B	6.11.91	chemical digestion
LCA-C	6.11.91	porewater analysis

Table 7.3 Water column characteristics at the time of sampling

	T. (°C)	O_2 (%)	conductivity (μS)
surface water	6.1	103	80
overlying core water	...	98	106

7.3 Results

Results for Loch Coire nan Arr are listed in Tables 7.4-7.13 and Figures illustrating some of the data are presented in the Discussion (Section 7.4).

1. Tables 7.4 and 7.5 contain wet and dry sediment section weights, mid-section cumulative weights (g cm^{-2}), porosities and, where measured, carbon content and C/N ratios. Porosities were calculated using an assumed solid sediment density of 2.39 g cm^{-3}.

2. Total ^{210}Pb and mid-section cumulative weights are listed in Table 7.6. ^{226}Ra was not detectable.

3. Radiocaesium concentrations and $^{134}Cs/^{137}Cs$ ratios are presented in Table 7.7. ^{134}Cs peaks at the 605 keV γ line were used to calculate concentrations, since counting errors were significantly higher at 796 keV.

4. Table 7.8 contains metal concentrations for HNO_3/HCl acid digested sediment core LCA-B and, for the same core, metal concentrations in sequentially extracted sediment are presented in Tables 7.9-7.11, in which column headings I-V refer to the following fractions and extractants:

I. 1M ammonium acetate, pH7, 20°C (exchangeable fraction)

II. 1M sodium acetate, pH5 with acetic acid, 20°C ("carbonate bound"/specifically sorbed)

III. 0.1M hydroxylammonium chloride/0.01M nitric acid, 20°C (easily reducible)

IV. 1M hydroxylammonium chloride/4.4M acetic acid, 20°C (moderately reducible)

V. 30% w/v hydrogen peroxide, pH2, 85+/-2°C; 3.2M ammonium acetate in 3.2M nitric acid (organic fraction/sulphides)

Sum I-V refers to the sum of metal concentrations in all fractions.

5. Metal concentrations in porewater samples in sediment core LCA-C, water overlying the sediment in the core tube (overlying water) and water column samples are listed in Tables 7.12 and 7.13. Unfiltered water column Zn concentrations (Table 7.13) were all less than, or equal to, the blank concentrations ($\leq$ blank).

6. (BDL) is entered where samples were below detection limit, and (...) where a result was not available.

Table 7.4 Some physical characteristics, carbon content and carbon/nitrogen ratios of Loch Coire nan Arr sediment core LCA-A.

section depth (cm)	wet section weight (g)	dry section weight (g)	mid-section cumulative weight (g cm^{-2})	porosity (%)	carbon content (%)	C/N ratio
0-1	31.257	2.519	0.034	96.5	12.0	15.4
1-2	35.149	4.464	0.127	94.3	11.0	16.4
2-3	42.200	5.654	0.262	93.9	10.6	15.1
3-4	37.364	5.570	0.412	93.2	7.5	15.6
4-5	42.186	6.257	0.571	93.2	8.5	17.0
5-6	40.693	6.476	0.741	92.7	8.9	16.3
6-7	40.119	7.436	0.927	91.3	6.7	17.2
7-8	39.054	7.228	1.123	91.3	10.8	17.4
8-9	41.058	7.641	1.322	91.3	12.4	19.1
9-10	37.511	7.567	1.525	90.4	11.1	17.6
10-11	33.348	8.022	1.734	88.3	...	...

Table 7.5 Some physical characteristics of Loch Coire nan Arr sediment core LCA-B.

section depth (cm)	wet section weight (g)	dry section weight (g)	mid-section cumulative weight (g cm^{-2})	porosity (%)
0-1	29.026	1.164	0.016	98.3
1-2	33.911	3.163	0.073	95.9
2-3	35.283	4.526	0.176	94.2
3-4	39.044	4.836	0.301	94.4
4-5	36.502	4.569	0.427	94.4
5-6	43.264	6.154	0.571	93.5
6-7	40.910	6.059	0.734	93.2
7-8	46.015	7.532	0.916	92.4
8-9	42.059	7.539	1.117	91.6
9-10	41.548	6.892	1.310	92.3
10-11	50.504	9.445	1.529	91.2
11-12	44.710	7.614	1.757	92.1
12-13	37.487	7.465	1.958	90.6
13-14	33.836	7.582	2.160	89.2

core cross-section area = 37.39 cm^2

Table 7.6 ^{210}Pb concentrations for Loch Coire nan Arr sediment core LCA-A (6.11.91)

section depth (cm)	mid-section cumulative weight ($g\ cm^{-2}$)	total ^{210}Pb ($Bq\ kg^{-1}$)
0-1	0.034	664 ± 58
1-2	0.127	445 ± 39
2-3	0.262	815 ± 55
3-4	0.412	600 ± 56
4-5	0.571	380 ± 53
5-6	0.741	361 ± 38
6-7	0.927	147 ± 41
7-8	1.123	124 ± 39
8-9	1.322	175 ± 43
9-10	1.525	91 ± 31
10-11	1.734	BDL

Table 7.7 Radiocaesium concentrations and $^{134}Cs/^{137}Cs$ activity ratios for Loch Coire nan Arr sediment core LCA-A (6.11.91)

section depth (cm)	^{137}Cs ($Bq\ kg^{-1}$)	^{134}Cs 605keV ($Bq\ kg^{-1}$)	$^{134}Cs/^{137}Cs$
0-1	255 ± 8	12 ± 5	0.046 ± 0.021
1-2	252 ± 5	6 ± 2	0.024 ± 0.008
2-3	456 ± 11	BDL	
3-4	511 ± 2	"	
4-5	627 ± 13	"	
5-6	470 ± 9	"	
6-7	234 ± 8	"	
7-8	102 ± 6	"	
8-9	58 ± 6	"	
9-10	28 ± 4	"	
10-11	22 ± 4	"	

core cross-section area = 37.39 cm^2

Table 7.8 Fe, Mn, Pb, Zn, Cu, Cd, Co and Ni concentrations in HNO_3/HCl digested Loch Coire nan Arr sediment core LCA-B

depth (cm)	Fe %	Mn mg kg^{-1}	Pb mg kg^{-1}	Zn mg kg^{-1}	Cu mg kg^{-1}	Cd mg kg^{-1}	Co mg kg^{-1}	Ni mg kg^{-1}
0-1	7.7	4,100	39	49	14	0.9	26	BDL
1-2	4.3	917	33	37	7.7	0.3	11	4.6
2-3	1.9	345	36	36	6.9	0.2	6.6	4.5
3-4	1.9	326	50	70	8.5	0.4	9.7	7.2
4-5	1.9	294	53	47	8.6	0.5	17	5.3
5-6	1.7	252	47	41	7.9	0.6	11	4.7
6-7	1.7	242	49	42	8.1	0.5	8.0	4.9
7-8	1.6	242	44	40	8.3	0.5	9.1	4.3
8-9	1.5	221	37	38	7.8	0.4	7.9	4.9
9-10	1.4	221	39	40	7.6	0.5	6.6	4.3
10-11	1.3	208	32	37	6.9	0.4	7.4	4.4
11-12	1.4	248	41	34	8.4	0.4	8.8	5.2
12-13	1.3	209	32	32	7.2	0.3	7.3	4.5
13-14	1.2	205	29	26	7.4	0.3	5.5	4.2

Table 7.9 Fe and Mn concentrations in sequentially extracted Loch Coire nan Arr sediment core LCA-B

	Fe (%) fractions						Mn (mgkg^{-1}) fractions					
depth (cm)	I	II	III	IV	V	sum I-V	I	II	III	IV	V	sum I-V
0-1	0.005	0.43	0.21	1.86	5.62	8.13	795	873	959	908	1,070	4,600
1-2	0.009	0.16	0.09	0.62	2.76	3.64	240	157	45	36	282	760
2-3	0.006	0.09	0.06	0.27	0.91	1.34	113	78	20	13	48	272
3-4	0.003	0.07	0.06	0.24	0.92	1.29	105	73	19	13	50	260
4-5	0.002	0.10	0.06	0.30	0.96	1.42	93	69	20	14	45	241
5-6	0.003	0.07	0.05	0.24	0.91	1.28	92	69	21	15	46	243
6-7	0.004	0.07	0.05	0.23	0.80	1.15	92	65	20	15	42	234
7-8	0.003	0.07	0.05	0.23	0.69	1.04	86	60	19	13	36	214
8-9	0.002	0.06	0.05	0.20	0.64	0.95	86	57	17	11	34	205
9-10	0.004	0.07	0.05	0.24	0.65	1.01	99	65	19	13	36	232
10-11	0.002	0.06	0.05	0.20	0.52	0.84	82	62	19	13	31	207
11-12	0.005	0.08	0.06	0.23	0.60	0.97	111	61	18	13	38	241
12-13	0.006	0.07	0.05	0.20	0.52	0.85	90	54	16	11	39	210
13-14	0.008	0.07	0.05	0.17	0.51	0.80	97	51	15	11	41	215

Table 7.10 Pb and Zn concentrations in sequentially extracted Loch Coire nan Arr sediment core LCA-B

depth (cm)	Pb (mg kg^{-1}) fractions I	II	III	IV	V	sum I-V	Zn (mg kg^{-1}) fractions I	II	III	IV	V	sum I-V
0-1	BDL	BDL	BDL	21	18	39	BDL	5.4	2.5	14	20	42
1-2	"	"	"	15	23	38	"	2.8	1.9	6.0	12	23
2-3	"	7.3	"	16	12	35	"	2.1	0.99	8.0	13	24
3-4	"	9.2	"	18	12	39	"	3.3	1.4	14	16	35
4-5	"	9.4	"	23	17	49	"	3.6	1.6	14	18	37
5-6	"	9.1	"	21	16	46	"	2.1	1.3	13	22	38
6-7	"	9.0	"	20	17	46	"	1.2	0.90	11	25	38
7-8	"	7.0	"	17	14	38	"	1.2	0.80	7.4	22	31
8-9	"	6.2	"	14	14	34	"	1.3	0.74	8.3	22	32
9-10	"	7.5	"	17	16	40	"	1.3	0.85	9.9	26	38
10-11	"	5.6	"	13	13	32	"	0.8	0.58	8.3	22	32
11-12	"	6.9	"	17	14	38	"	1.2	0.55	8.0	24	34
12-13	"	5.7	"	14	12	32	"	1.0	0.48	7.0	21	29
13-14	"	4.3	"	12	11	27	"	1.0	0.40	4.5	18	24

Table 7.11 Cu concentrations in sequentially extracted Loch Coire nan Arr sediment core LCA-B

depth (cm)	Cu (mgkg^{-1}) fractions I	II	III	IV	V
0-1	BDL	BDL	BDL	BDL	8.2
1-2	"	"	"	"	6.9
2-3	"	"	"	"	5.3
3-4	"	"	"	"	4.1
4-5	"	"	"	"	6.1
5-6	"	"	"	"	4.2
6-7	"	"	"	"	5.5
7-8	"	"	"	"	5.7
8-9	"	"	"	"	5.9
9-10	"	"	"	"	6.8
10-11	"	"	"	"	5.5
11-12	"	"	"	"	6.5
12-13	"	"	"	"	6.0
13-14	"	"	"	"	5.6

Table 7.12 Fe, Mn and Pb concentrations in porewater samples from Loch Coire nan Arr sediment core LCA-C, water overlying the sediment and water column samples

water column depth (m)	Fe (mg l^{-1})		Mn (mg l^{-1})		Pb (mg l^{-1})	
surface (0)	0.014	(...)	0.006	(0.006)	BDL	BDL
1	0.012	(0.035)	...	(...)	"	"
2	0.018	(0.034)	0.006	(0.006)	"	"
3	0.016	(0.037)	...	(...)	"	"
4	0.014	(0.036)	0.006	(0.007)	"	"
5	0.028	(0.033)	...	(...)	"	"
6	0.013	(0.037)	0.005	(0.007)	"	"
7	0.011	(0.038)	...	(...)	"	"
8	0.013	(0.037)	0.005	(0.006)	"	"
9	0.014	(0.060)	...	(...)	"	"
10	0.018	(0.038)	0.005	(0.006)	"	"
core water	0.165	(...)	...	(...)	"	"
porewater depth (cm)						
0-1	0.13		0.03		BDL	
1-2	0.098		0.05		"	
2-3	0.14		0.04		"	
3-4	0.18		0.08		"	
4-5	0.12		0.06		"	
5-6	...		0.09		"	
6-7	0.078		0.09		"	
7-8	0.11		0.10		"	
detection limits					$5x10^{-3}$	

unfiltered water concentrations in brackets ( )

Table 7.13 Zn, Cu and Cd concentrations in porewater samples from Loch Coire nan Arr sediment core LCA-C, water overlying the sediment and water column samples.

water column depth (m)	Zn (mgl^{-1})		Cu (mgl^{-1})		Cd (mgl^{-1})	
surface (0)	≤ blank	(0.004)	BDL	BDL	BDL	BDL
1	"	(")	"	"	"	"
2	"	(0.005)	"	"	"	"
3	"	(")	"	"	"	"
4	"	(0.003)	"	"	"	"
5	"	(")	"	"	"	"
6	"	(0.002)	"	"	"	"
7	"	(")	"	"	"	"
8	"	(0.002)	"	"	"	"
9	"	(")	"	"	"	"
10	"	≤ blank	"	"	"	"
core water	"	"	"	"	"	"
porewater depth (cm)						
0-1	0.004		BDL		BDL	
1-2	0.008		"		"	
2-3	0.028		"		"	
3-4	0.032		"		"	
4-5	0.014		"		"	
5-6	0.008		"		"	
6-7	0.015		"		"	
7-8	0.018		"		"	
detection limits	blank = 0.006		$8x10^{-3}$		$1x10^{-4}$	

unfiltered water concentrations in brackets ( ).

7.4 Discussion

7.4.1 Sediment core characteristics

Porosities for sediment cores LCA-A and LCA-B are similar, ranging from 89-98% (Table 7.4 and 7.5) and showing a steady decrease with depth. The carbon content (Table 7.4) decreases downcore from a surface (0-1 cm) value of 12%C to 7.5% at 3-4 cm, which is consistent with bacterial degradation of organic carbon. Below 4 cm however, the carbon content changes little and then abruptly increases to 10.8-12.4%C between 7 and 10 cm. This indicates a change in sediment type, with a greater proportion of inorganic matter between depths of 3 and 7 cm. The change in %C content, with an abrupt increase below 7 cm, around 60 years ago (Section 7.4.2), suggests a change in the sediment source, perhaps because of disturbance to the catchment. The ^{210}Pb concentration (Section 7.4.2) in the 8-9 cm section is slightly higher than in the sections above and below, which could be interpreted as an increased input of catchment material due to catchment disturbance. The catchment is largely unafforested but on the eastern slope a small block of conifers has been planted (at an unknown date) (Patrick *et al.*, 1991) and this could perhaps account for the change in sediment at the depths described.

The C/N ratios for core LCA-A (Table 7.4) are fairly high throughout the core, reflecting the peaty organic matter (having a higher C/N ratio than planktonic matter). Although the ratios are generally lower in the upper sections of the core (mean to 4 cm = 15.6), compared with a mean ratio of 17.4 below 4 cm, the change is not great, probably because this is an oligotrophic loch, with low planktonic productivity.

7.4.2 Radionuclide data

^{210}Pb data

Total ^{210}Pb concentrations (Table 7.6, Fig. 7.2) range from 91-815 Bq kg^{-1} and fall below a detection limit of 70 Bq kg^{-1} in the deepest sampled section at 10-11 cm. ^{226}Ra was not detectable in this core and, since the total ^{210}Pb concentrations have not decreased to a constant level at depth (maximum depth of ^{210}Pb detection was 10 cm), the supported ^{210}Pb component is apparently too small to quantify and can legitimately be ignored. A low ^{226}Ra content is unsurprising in these sediments since the bedrock is sandstone, laid down in oxidising conditions during which uranium (^{226}Ra is a decay product of ^{238}U, Fig. 1.8) would have been in the highly soluble 6^+ oxidation state. Consequently deposition of uranium would have been minimal and

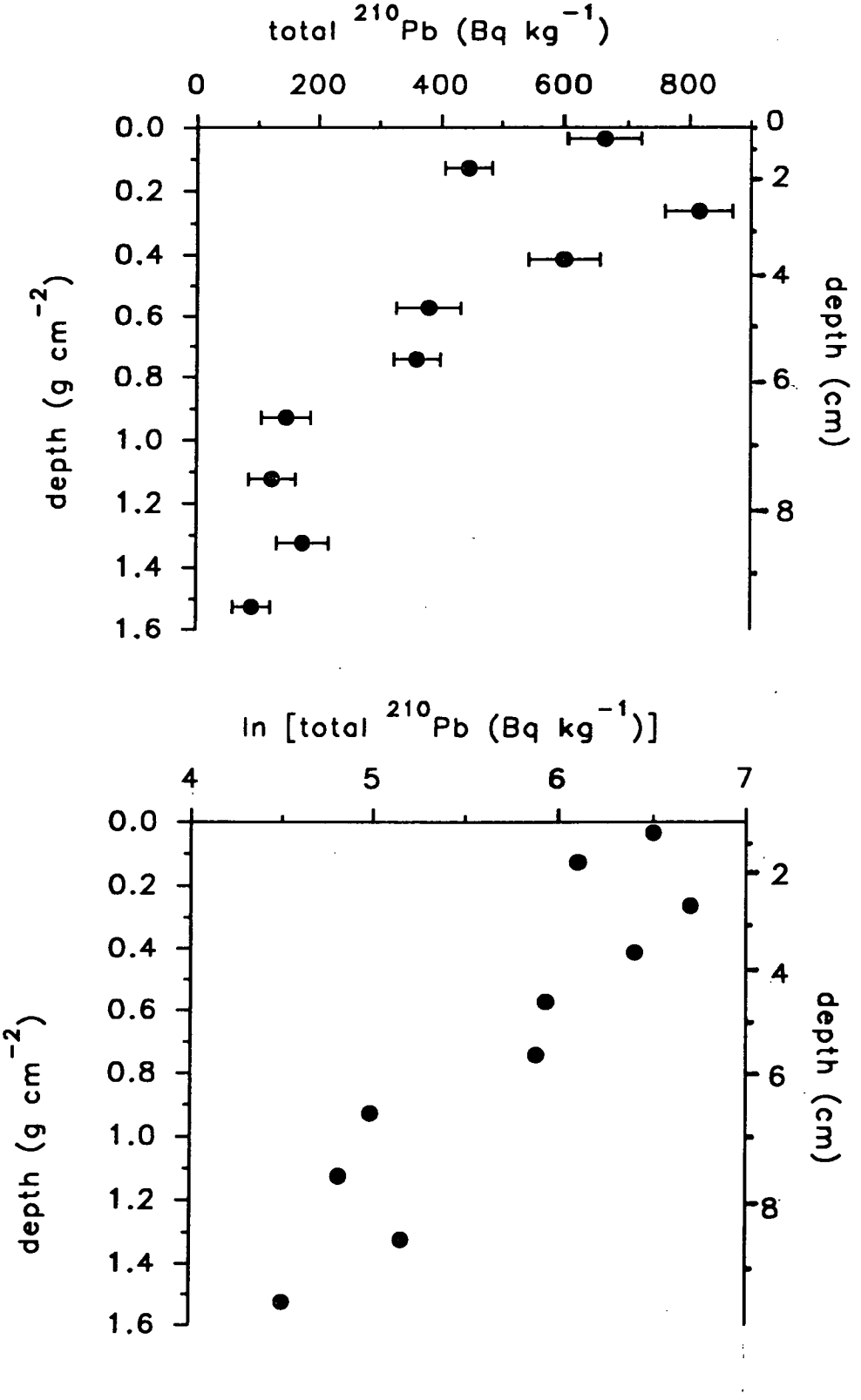

Fig. 7.2 Plot of total ^{210}Pb and ln (total ^{210}Pb) against depth in Loch Coire nan Arr sediment core LCA–A.

the dominant mineral in the sandstone is quartz, which has a low uranium content. In view of this, total ^{210}Pb values were used to calculate a sedimentation rate and Fig. 7.2 shows ln total ^{210}Pb concentration against depth (as cumulative weight/area to compensate for sediment compaction). The profile shows the maximum ^{210}Pb concentration (815 Bq kg^{-1}) at a depth of 2-3 cm, below which a steady decrease to 8 cm occurs. Below 8 cm the concentration increases slightly again at 8-9 cm before decreasing to the maximum depth of ^{210}Pb detection at 10 cm. The profile shape from the surface to 3 cm (*i.e.* no steady decrease in concentration) indicates sediment mixing to a depth of 3 cm.

Linear regression of ln ^{210}Pb concentrations against depth (g cm^{-2}) between the base of the mixed zone (2-3 cm) and 8 cm gives a sedimentation rate of 16.4 ± 2.4 mg cm^{-2} y^{-1}, which was used to obtain a core chronology (Table 7.14). A ^{210}Pb flux of 168 Bq m^{-2} y^{-1} is implied if steady-state conditions are assumed (inventory x λ), which compares well with ^{210}Pb fluxes calculated by Appleby *et al.* (1990), for sites in the north-west of Scotland, of 130 Bq m^{-2} y^{-1} (Lochan Dubh) and 222 Bq m^{-2} y^{-1} (Loch Doilet) and by Sugden (1993) of 150 Bq m^{-2} y^{-1} for a peat core from North Uist, Outer Hebrides. For Round Loch of Glenhead (Chapter 3), a site of similar rainfall to Loch Coire nan Arr, values of 82-95 Bq m^{-2} y^{-1} were obtained.

Radiocaesium data

Radiocaesium data are presented in Table 7.7 and are shown graphically in Fig. 7.3. ^{134}Cs is detectable to 2 cm (maxiumum 12 Bq kg^{-1} at 0-1 cm) and ^{137}Cs to 11 cm, with concentrations ranging from 22-627 Bq kg^{-1} (maximum at 4-5 cm). ^{134}Cs was only detectable in the top 2 cm, indicating the radiocaesium from Chernobyl fallout only occurs in significant amounts to this depth. The $^{134}Cs/^{137}Cs$ activity ratios (Table 7.7), when compared with the characteristic Chernobyl-emitted $^{134}Cs/^{137}Cs$ ratio of 0.13 (corrected for decay to the time of sampling), show that there is still radiocaesium of weapons testing origin present in the surface sediment and that all of the ^{137}Cs below 2 cm is from weapons testing fallout. This is consistent with the sediment mixing implied by the ^{210}Pb data and is further supported by the shape of the ^{137}Cs concentration curve increasing from the relatively constant value in the 1-2 cm section to the peak at 4-5 cm. Using the sedimentation rate of 16.4 mg cm^{-2} y^{-1}, the ^{137}Cs peak corresponds to a mid-section date of 1957 and an upper section limit of 1962, which is in close agreement with the maximum in weapons testing fallout deposition in 1963. Again, this is consistent with the ^{210}Pb-based evidence of partial sediment mixing, with the surface Chernobyl-derived ^{137}Cs peak and underlying peak attributable to weapons testing being maintained, though damped

Table 7.14 ^{210}Pb-derived chronology for Loch Coire nan Arr sediment cores LCA-A and LCA-B

	LCA-A		LCA-B	
depth	mid-section	base-section	mid-section	base-section
(cm)	date	date	date	date
0-1	1989	1987	1990	1990
1-2	1984	1980	1987	1984
2-3	1975	1971	1981	1977
3-4	1966	1962	1973	1969
4-5	1957	1952	1965	1962
5-6	1946	1941	1957	1952
6-7	1935	1929	1947	1942
7-8	1923	1917	1936	1929
8-9	1911	1905	1923	1917
9-10	1898	1892	1912	1906
10-11	1886	1879	1898	1890
11-12			1884	1878
12-13			1872	1866
13-14			1860	1853

based on a sedimentation rate of 16.4 mg cm^{-2} y^{-1}.

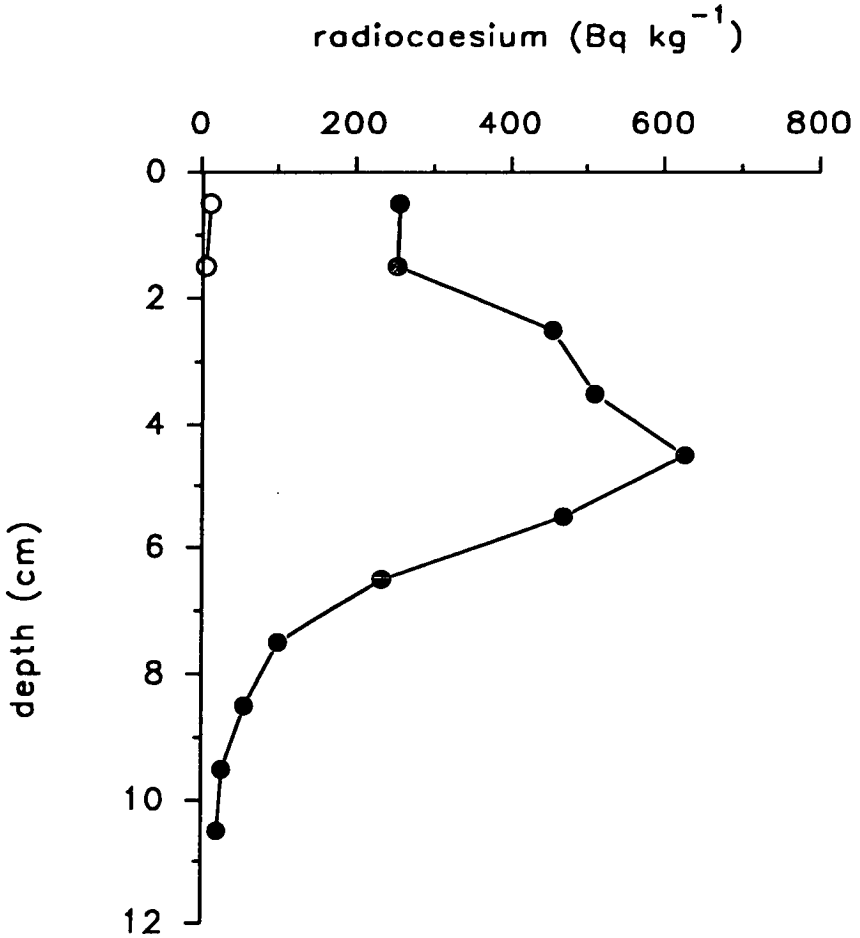

Fig. 7.3 ^{134}Cs (o) and ^{137}Cs (•) concentrations in Loch Coire nan Arr sediment core LCA–A.

and broadened due to the combined effects of mixing and burial in the sediment. The possibility of the radiocaesium peak being due to a change in sediment type should be examined, because of the downcore change in carbon content indicating a change in sediment type (Section 7.4.1, Table 7.4), with a greater proportion of inorganic matter between depths of 3 and 7 cm. However, the change observed in the radiocaesium profile does not correspond to depths over which changes in the %C content occur and is therefore unlikely to be attributable to a change in the sedimentary carbon content. The porosity values in this core (Section 7.4.1, Table 7.4) show a steady decrease with depth and do not imply a sudden change in sediment type, further indicating that the ^{137}Cs peak at 4-5 cm is not due to an abrupt change in the sediment type.

Below 5 cm (Fig. 7.3) the ^{137}Cs concentration decreases exponentially downcore and was still detectable in the base section at 10-11 cm. On the basis of the sedimentation rate of 16.4 mg cm^{-2} y^{-1} and sediment mixing to the base of 3 cm, the date corresponding to the maximum depth of radiocaesium penetration is 1900, which is before the advent of nuclear technology and shows that radiocaesium must be subject to downwards movement in this part of the core via mixing and/or diffusion, in sediment with a mean total carbon content of 10% (Table 7.4).

Using the $^{134}Cs/^{137}Cs$ activity ratios (Table 7.4) to calculate the relative contributions of fallout from Chernobyl and weapons testing to the total ^{137}Cs inventory gives values of 0.13 kBq m^{-2} for Chernobyl radiocaesium (corrected for decay since 1.5.86) and 8.66 kBq m^{-2} from weapons testing fallout (corrected for decay since 1963). If all the ^{137}Cs in the 0-2 cm section was of Chernobyl origin, this would give an upper limit to the Chernobyl ^{137}Cs inventory of 0.52 kBq m^{-2} and a lower limit to the weapons testing fallout of 7.98 kBq m^{-2}. These inventories are compared in Table 7.15 with deposition values previously reported. The Chernobyl radiocaesium inventory obtained for Loch Coire nan Arr compares well with that recorded by Clark and Smith (1988) and the weapons testing inventory is slightly greater than the reported range (Peirson *et al.*, 1982), which may be a result of catchment inputs, as the catchment : loch area ratio in this loch is particularly high.

In summary the ^{210}Pb data indicate some mixing of the near-surface sediment and this is supported by the radiocaesium data. Although there is evidence of diffusional and/or mixing mobility of radiocaesium at depth in the core, the weapons testing radiocaesium concentration profile shape agrees well with the historical fallout deposition. The radiocaesium inventories estimated at this site are similar to reported deposition values for ^{137}Cs of Chernobyl and weapons testing origins.

Table 7.15 Estimated ^{137}Cs inventories of fallout from Chernobyl and weapons testing in Loch Coire nan Arr sediment core LCA-A compared with reported deposition values (Clark and Smith, 1988; Peirson *et al.*, 1982).

	Chernobyl (kBq m^{-2})	weapons testing (kBq m^{-2})
Loch Coire nan Arr	0.13 ± 0.04	7.98 ± 0.08
	→ 0.52 ± 0.01	→ 8.66 ± 0.11
reported value	0.1-1	2.8-6

7.4.3 Metal data

Lead, zinc, copper and cadmium in HNO_3/HCl acid digested sediment

Pb concentrations range from 29-53 mg kg^{-1} (Table 7.8, Fig.7.4), with the maximum concentration in the sediment section at 4-5 cm. Below 5 cm, the trend downcore is of decreasing concentrations. Above 4 cm the concentration is relatively constant (33-39 mg kg^{-1}), consistent with mixing to this depth as discussed in the previous section. While the Pb concentrations vary little above 3 cm, it could be argued that the profile shape in this area of the core (lowest at 1-2 cm) is similar to that of ^{210}Pb, with a depletion in the 1-2 cm section, perhaps implying dissolution of Pb (*i.e.* stable and ^{210}Pb) at this depth, which will be subsequently discussed. Straightforward consideration of the radionuclide data and the Pb peak at 4-5 cm, would mean a maximum pollutant input in the mid-1960's followed by a decrease since then, assuming the sedimentation rate has remained constant. This is consistent with global historical trends of a decrease in anthropogenic emission of Pb to the atmosphere, reflected for example in Greenland snows since the late 1960's (Boutron *et al.*, 1991) and in Loch Lomond (Chapter 4) where Pb concentrations decreased from the mid-1960's. Pb concentrations and fluxes in peat from the Outer Hebrides have been found to decrease since the 1950's (Sugden *et al.*, 1991b). Peak Pb concentrations in Loch Lomond (southern basin) (Chapter 4) and Round Loch of Glenhead (Chapter 3) occurred around 1930, *i.e.* earlier than in Loch Coire nan Arr, which is probably attributable to different sources of pollutant Pb to the lochs, the more southerly lochs perhaps being more heavily influenced by industrial sources of Pb (fossil fuel combustion, heavy industry). As Pb concentrations do not reach constant levels at the maximum sampled depth (14 cm), a pollutant 'excess' inventory cannot be calculated, but the total Pb inventory amounts to 0.89 g m^{-2}, which compares with values of around 0.4 g m^{-2} for Balgavies Loch and Loch Leven (Chapters 5 and 6) and the significantly higher 'excess' inventories for Round Loch of Glenhead and Loch Lomond (Chapters 3 and 4) of between 2 and 5 g m^{-2}. The lower inventory for Loch Coire nan Arr, relative to those for Round Loch and Loch Lomond, is unsurprising since this is a remote loch. Although it receives a high annual rainfall (Table 7.1), similar to the rainfall for Round Loch, the atmospheric input of pollutants is likely to be low for Loch Coire nan Arr as the prevailing winds are often from the Atlantic (reflected in high water column Na^+ and Cl^- concentrations, Patrick *et al.*, 1991) and are relatively unpolluted.

Using the ^{210}Pb-based sedimentation rate of 16.4 mg cm^{-2} y^{-1}, the estimated age of the sediment at the base of core LCA-B is 1854 (taking the downward smearing

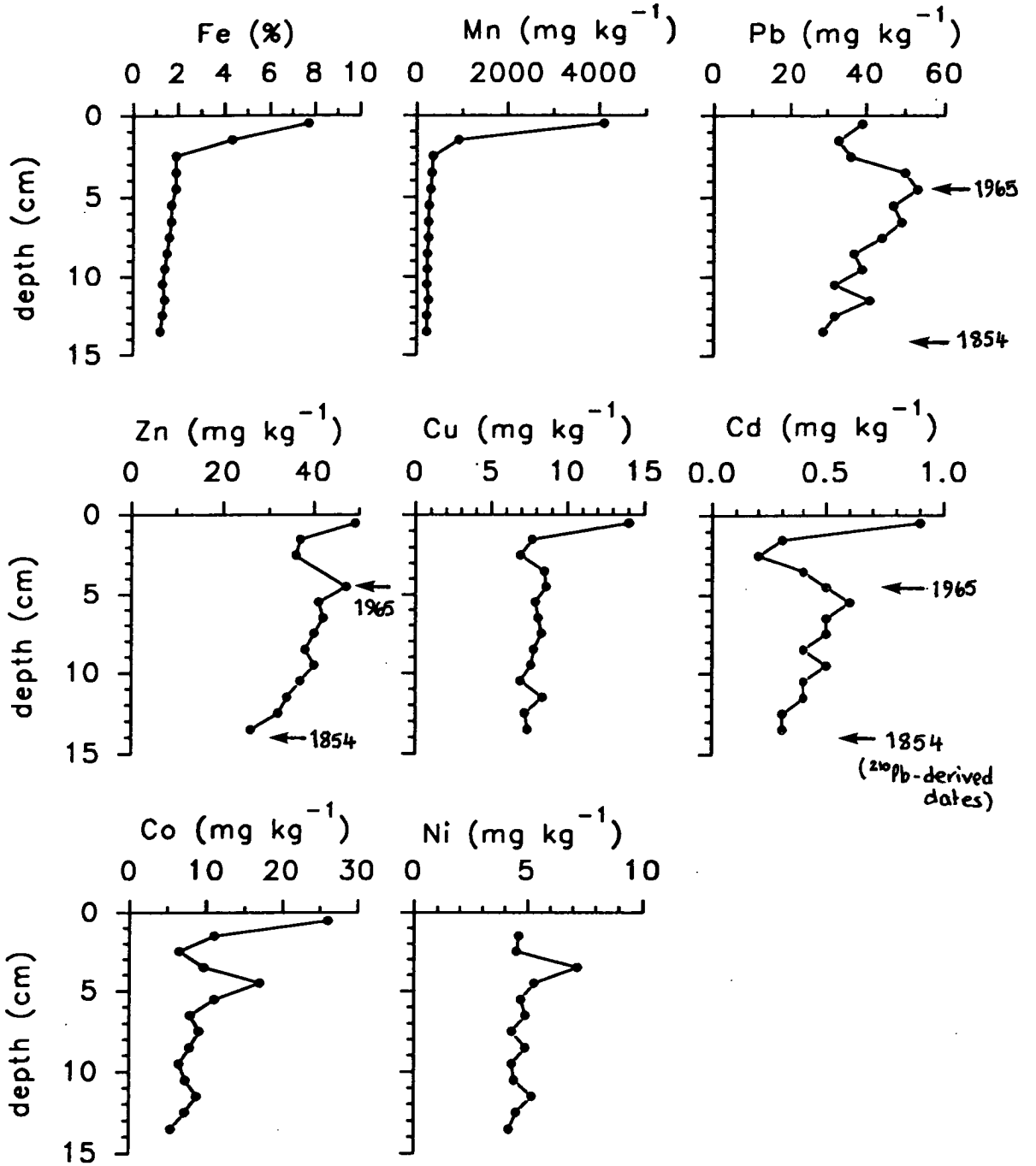

Fig 7.4 Metal concentrations in HNO_3\HCl acid digested Loch Coire nan Arr sediment core LCA–B

effects of mixing to 3 cm into account, by subtracting the cumulative weight/area at the base of 3 cm from that at the base of the deepest section), which means it is likely that around 50-100 years of pollutant metal profile occur below the maximum sampled depth of 14 cm, *i.e.* since the Industrial Revolution. Data from other lochs in this study (*e.g.* from Round Loch, Chapter 3 and the southern basin of Loch Lomond, Chapter 4) indicate that the pollutant metal concentrations (Pb, Zn and Cu) were increasing between the mid-18th and mid-19th centuries, but had not reached peak concentrations and so the 'loss' of this portion of the inventories for Loch Coire nan Arr is probably not significant. Background (non-pollutant) metal concentrations are likely to be fairly low at this site due to the low metal content of the underlying sandstone bedrock.

With the exception of a clear 0-1 cm enhancement of 49 mg kg^{-1} (Table 7.8, Fig. 7.4), a similar trend to Pb is observed for Zn (concentrations ranging from 26-49 mg kg^{-1}) with a high concentration at 4-5 cm (47 mg kg^{-1}), underlain by decreasing concentrations. It seems unlikely that the peak in Zn concentration at the surface is attributable to changes in atmospheric input of this metal, on the basis of the observed Pb concentration trends at this site, Zn concentration profile trends in Round Loch of Glenhead and Loch Lomond (Chapters 3 and 4) and in the absence of known recent high inputs of Zn to the area. Other factors should be examined to determine the cause of the surface enhancement. Interpretation of the profile shape below 4-5 cm in terms of changes in anthropogenic emissions of Zn does appear to be valid with an apparent increase in Zn deposition at least since the mid-19th century and the sub-surface Zn peak corresponding to a ^{210}Pb-derived date of 1965. Agreement between dates of the onset of decreasing Zn concentrations in cores from Loch Lomond and Round Loch and Loch Coire nan Arr is good. The maximum Zn concentration is earlier for Round Loch (around 1930), but in Loch Lomond is dated to around 1970. As for Pb, the Zn concentrations do not drop to constant background (non-anthropogenic) levels and the total Zn inventory is similar to that of Pb at 0.85 g m^{-2} and, again, much lower than the 'excess' pollutant inventory of 11.5 g m^{-2} obtained in the southern basin of Loch Lomond (Chapter 4), but is similar to pollutant Zn inventories in Round Loch (site 2), Loch Leven and Balgavies Loch (Chapters 3, 5 and 6 respectively).

The Cu concentration profile (Table 7.8, Fig.7.4) shows a surface maximum (analogous to Zn) of 14 mg kg^{-1} (0-1 cm), below which concentrations are around 8 mg kg^{-1} *i.e.* almost half the maximum concentration. The total Cu inventory is 0.18 g m^{-2}. Since global Cu emissions have not dramatically increased in the last decade (Nriagu, 1990) and evidence from other Scottish lochs (Round Loch of Glenhead, Chapter 3 and Loch Lomond, Chapter 4) does not indicate a recent dramatic increase

of Cu pollution in Scotland, the surface maximum is unlikely to be a historical feature, as concluded for the Zn surface peak, and this will be discussed later. Below 1 cm the Cu concentrations stay relatively constant (unlike Pb and Zn concentrations), suggesting either that anthropogenic Cu inputs were not sufficient to cause a noticeable change in the total Cu concentration or that post-depositional processes have influenced the concentration profile and obscured any trend due to historical changes in Cu input. The total Cu inventory at this site (0.18 g m^{-2}) is lower than the inventory for Loch Lomond (Chapter 4), although the difference is not as marked as with the Pb and Zn inventories for the two lochs. Similar or slightly lower Cu inventories were observed for the other lochs sampled in this study.

In contrast to Cu, the Cd concentration profile (Table 7.8, Fig.7.4) has a similar pattern to that seen in the Pb and Zn profiles, with concentrations increasing from the base of the core to the surface (0-1 cm) maximum of 0.9 mg kg^{-1}, closely resembling the pattern in the Zn profile and indicating similar behaviour of Cd and Zn in this loch. The onset of a decrease in concentration above 5 cm, corresponds to the mid-1960's. The total Cd inventory in the core is 9.5×10^{-4} g m^{-2}, less than 'excess' Cd inventories obtained for Round Loch and Loch Lomond (southern basin).

Cobalt and nickel in HNO_3/HCl acid digested sediment

Concentrations of Co (Table 7.8, Fig. 7.4) range from 5.5-26 mg kg^{-1} with a maximum at 0-1 cm overlying much lower concentrations below this, except for a peak at 4-5 cm (17 mg kg^{-1}). Ni concentrations range from undetectable in the surface section (though this was ≤12 mg kg^{-1} due to the low sample weight) to 7.2 mg kg^{-1} at 3-4 cm (Table 7.8, Fig. 7.4) and, with the exception of the surface concentration, which cannot be commented on due to the high detection limit, shows a profile shape similar to Co, though for Ni the sub-surface peak is positioned slightly higher, at 3-4 cm.

Since the historical trend in anthropogenic emissions of these metals has not been one of sudden change (increase) during the early 1970's (Nriagu, 1990) and in the absence of known recent inputs to this loch, the patterns observed in these profiles must be due to other factors causing an enhancement in Co at two depths in the core and Ni at least at 3-4 cm, possibly also at the surface. Balistrieri (1992,b) found that Co was associated with Mn cycling in the water column of Lake Sammamish, Washington, and Shaw *et al.* (1990) reported an association of Co and, to a lesser extent, Ni with Mn oxides in cores collected from offshore basins in the Southern California Borderland. The detection limit of Ni in the surface section prevents comparison of Co and Ni at this depth, but the sub-surface peaks suggest parallels at

this site in the behaviour of these geochemically similar elements. Whilst the surface peak in Co concentration is most likely due to redox-driven diagenesis, the sub-surface peaks are not immediately explicable. As discussed for the radiocaesium data, %C values from the adjacent core (LCA-A) and the porosity values from this core (LCA-B, Table 7.5) do not indicate a change in sediment type around the depth 4-5 cm, which could be causing the enhancement. Furthermore, the fact that the Ni enhancement is slightly higher than that of Co is perhaps evidence that this feature is due to a chemically related difference in the behaviour of these metals, rather than a change in the sediment type.

Manganese and iron concentrations in HNO_3/HCl acid digested sediment

Concentrations of Mn (Table 7.8, Fig. 7.4) increase dramatically from a mean of 251 mg kg^{-1} below 2 cm to 4,100 mg kg^{-1} in the 0-1 cm section, a 16-fold enhancement. The pattern in the Fe concentration profile (Table 7.8, Fig.7.4) is similar to that of Mn with concentrations increasing very slightly from the maximum depth to 2 cm and then increasing from a mean concentration of 1.6% below 2 cm to a maximum of 7.7% in the 0-1 cm section, a 4-5 fold enhancement.

The patterns observed in the Fe and Mn profiles, of surface enhancements overlying fairly constant, low values at depth, are typical of those caused by redox-driven release of Fe and Mn to the porewaters (below 2 cm), followed by upward migration and reprecipitation in the surface sediment. The differences between the profiles of the two elements are also consistent with redox cycling: Mn is more rapidly reduced and is reduced nearer the sediment surface compared with Fe, and Mn has a sharper peak, mainly in the surface (0-1 cm) section, whereas Fe shows significant enhancement in both sections from 0-2 cm.

Manganese and iron partitioning data

Concentration profiles of Mn in sequential extraction fractions I-V (Table 7.9, Fig. 7.5) all show the same pattern downcore as the HNO_3/HCl digest concentration profile, with maximum concentrations in the surface (0-1 cm) section overlying lower and fairly constant concentrations at depths below 2 cm. Although the Mn concentrations in each of the individual fractions in the surface section are broadly similar, concentrations are highest in fraction V (1,070 mg kg^{-1}), followed by fraction III (959 mg kg^{-1}). The presence of significant amounts of Mn in fraction IV (moderately reducible) suggests that, at this site, not all the Mn oxides/hydroxides (generally associated with fraction III) have been reduced and that the more vigorous extractants of fraction IV are required for this. If this is the case, and fraction IV

contains Mn hydroxides, then the sum of Mn in both fractions becomes the most important contribution to the surface peak and is explicable in terms of redox cycling, with authigenic oxides of Mn present in the enhanced surface layer, overlying low concentrations in the reducing sediment below 2 cm. Mn concentrations are enhanced 52 and 70 times relative to mean underlying concentrations in fractions III and IV respectively. Despite the enhancement of surface values relative to underlying mean concentrations being greatest in fractions III and IV, all fractions show the same pattern and, therefore, appear to be influenced by the redox cycling.

The sum of Mn concentrations in fractions I-V is similar to, or greater than, the HNO_3/HCl acid digest concentration, showing that there is little or no Mn in more resistant fractions than those extracted by the sequential extraction reagents. Where the sum of fractions has a higher concentration than the acid digested concentration in samples from the same core, this can be accounted for by cumulative errors in determining the Mn concentration for each fraction, or non-homogeneity of wet sediment compared with the ground, dried sediment used for the acid digestion.

Fe is predominantly associated with fraction V, especially in the surface (0-1 cm) section where a peak of 5.6% Fe comprises 69% of the sum of fractions I-V (Table 7.9, Fig. 7.6). The concentration profile of Fe in fraction V is the same shape as that of the sum of fractions I-V, with a surface peak overlying slightly decreasing concentrations below 2 cm (from 0.5-0.9%). Fraction IV contains 1.9% Fe in the surface section and concentrations fall to around 0.2% below 2 cm. The Fe concentration profiles for fractions IV and V are consistent with redox cycling, as for Mn, and although fraction V appears to be involved in the remobilisation-reprecipitation process, the importance of Fe in fraction V in the surface section may also be due to direct precipitation of Fe with humic substances from the water column to the sediment.

As for Mn, the sum of concentrations is similar to, or greater than, the acid digested concentrations, showing that little or no Fe is present in more chemically resistant fractions. This means that the difference in the extent of surface enhancement between Fe and the more pronounced Mn peak is not due to a greater availability of Mn in fractions susceptible to remobilisation, but is probably because of the kinetic and thermodynamic properties of the two metals, *i.e.* that Mn^{4+} is more readily and rapidly reduced to Mn^{2+} than Fe^{3+} is to Fe^{2+} and that reoxidation of Mn^{2+} to Mn^{4+} is slower (Chapter 1) than Fe^{2+} to Fe^{3+}.

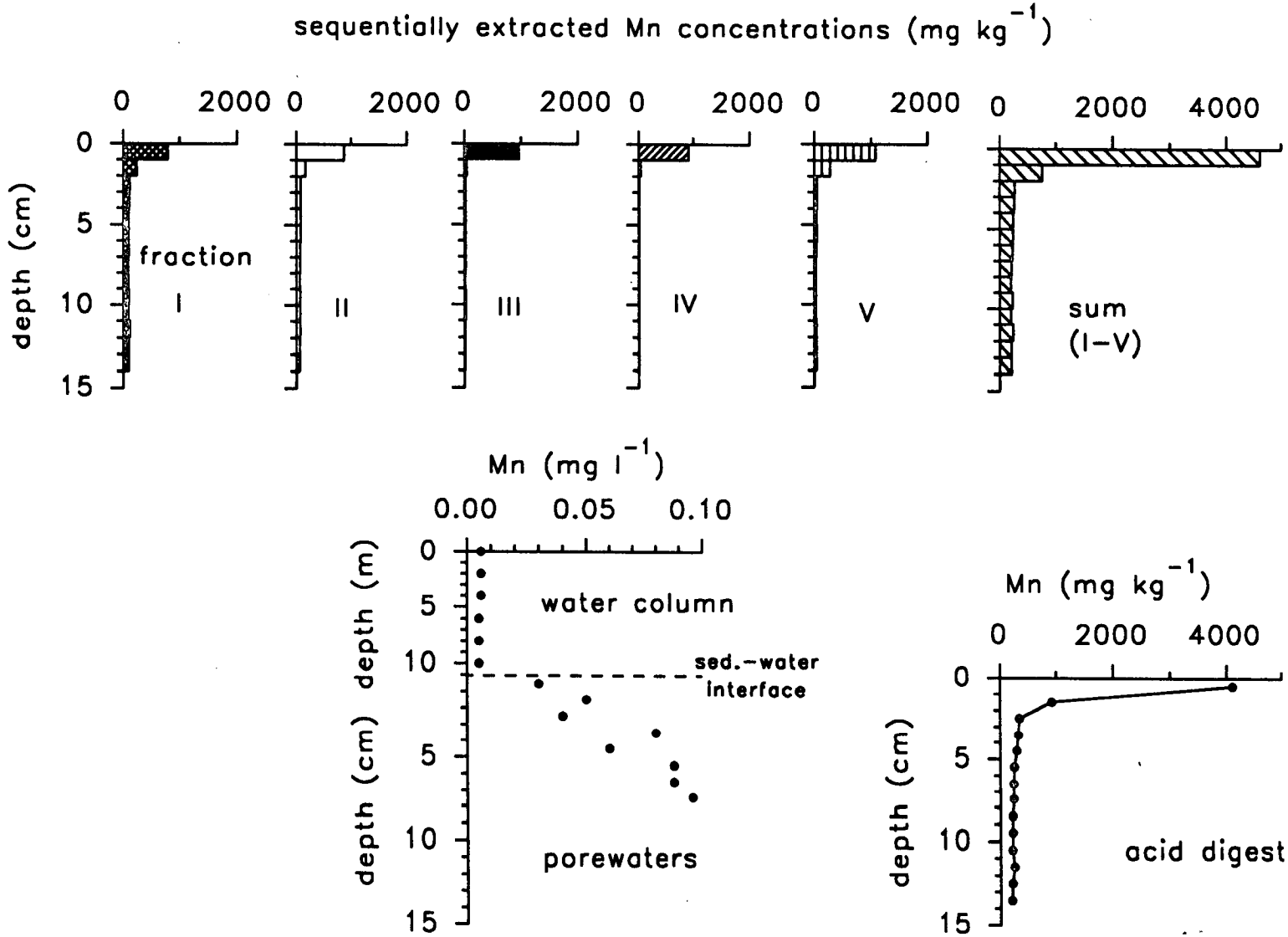
sequentially extracted Mn concentrations (mg kg^{-1})
0 2000 0 2000 0 2000 0 2000 0 2000 0 2000 4000
depth (cm)
0
5
10
15
fraction
I
II
III
IV
V
sum
(I–V)
Mn (mg l^{-1})
0.00 0.05 0.10
depth (cm) depth (m)
water column
sed.–water
interface
porewaters
Mn (mg kg^{-1})
0 2000 4000
depth (cm)
acid digest

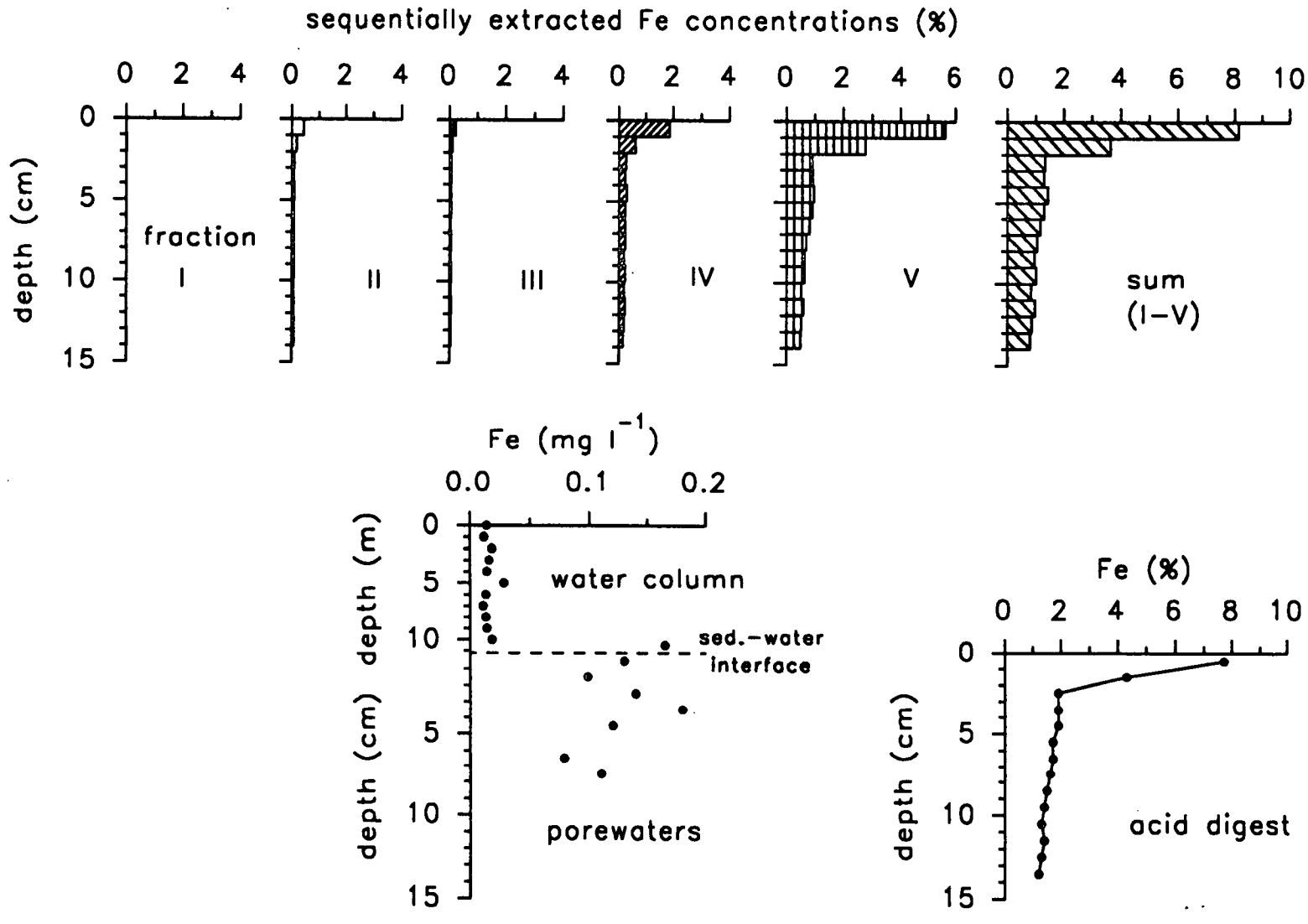
sequentially extracted Fe concentrations (%)
depth (cm)
fraction
I
II
III
IV
V
sum
(I–V)
Fe (mg l^{-1})
depth (m)
depth (cm)
water column
sed.–water
interface
porewaters
Fe (%)
acid digest

Manganese and iron solution phase data

Concentrations of dissolved Mn in the water column (Table 7.12, Fig. 7.5) are similar to those in unfiltered water column samples, showing that Mn is not significantly associated with particulates in the water column. Dissolved Mn concentrations show little variation in the water column to 10 m (0.005-0.006 mg l^{-1}). The porewater concentrations (Table 7.12, Fig. 7.5) range from 0.03-0.10 mg l^{-1} with a general trend of increasing concentration with depth. This pattern is consistent with the redox-driven remobilisation of Mn, indicated by the solid phase data with Mn released to the porewaters upon dissolution in the reducing sediment, diffusing upwards to reprecipitate at the surface with much lower and constant concentrations in the water column. The absence in this core of the generally observed (Chapter 1) decrease in porewater Mn concentration, due to the formation of new associations at depth in sediments with active redox-cycling in the near-surface sediment, is likely to be a result of sampling to only 8 cm, with the maximum point of dissolution probably occurring at a greater depth than this.

Fe concentrations are relatively constant (mean = 0.016 mg l^{-1}) in the filtered water column samples to 10 m (Table 7.12, Fig.7.6). Below this, at the sediment-water interface, the concentration of Fe in the water overlying the sediment core is ten times greater than in the water column (0.165 mg l^{-1}). Fe concentrations in unfiltered water column samples are 2-3 times higher than the corresponding filtered samples, indicating that, unlike Mn, Fe is significantly associated with particulates in the water column.

Porewater Fe concentrations range from 0.078-0.18 mg l^{-1} (Table 7.12, Fig. 7.6). Below the sediment-water interface there is a decrease in concentration (relative to the water directly overlying the sediment) to the section at 1-2 cm, followed by an increase to the maximum peak value of 0.18 mg l^{-1} in the 3-4 cm section. The concentration then decreases, with a slight (though probably insignificant) increase in the bottom section (7-8 cm). The peak at 3-4 cm is further evidence of the redox-driven diagenesis indicated by the solid phase data. The peak corresponds to the zone of maximum Fe release to the porewaters with diffusional movement of Fe occurring both upwards (to reprecipitate as oxides) and downwards (to associate with different fractions, *e.g.* sulphides, although there is no change in the concentrations at depth of fraction V, *i.e.* the organically bound Fe and Fe sulphides). However, this somewhat contradicts the interpretation of the Mn porewater profile, in which the point of maximum Mn dissolution (which might be anticipated to occur further upcore than Fe) was thought not to have been reached by 8 cm. The high Fe concentration in the core water would result in downwards movement of Fe from the water column to the

sediment and this supports the idea of Fe precipitating as humic substances from the water column. The low Fe concentrations in the water column from the surface to 10 m relative to the overlying water concentration can be accounted for by the process of advection/eddy diffusion dispersing the Fe in the water column (Chapter 1). To summarise, the porewater and water column data for Fe suggest two processes influencing its behaviour, *i.e.* redox-cycling and Fe precipitation with humic substances, which is similar to the conclusion drawn for Fe behaviour in the organic-rich sediments of acidified Round Loch of Glenhead (Chapter 3).

While the shape of the Mn porewater profile alone could be explained in terms of redox-cycling and the maximum sampled depth being insufficient to show the point of maximum Mn dissolution (Chapter 1), porewater Fe data, which show a peak in Fe at 3-4 cm, suggest that the Mn peak should occur above 3 cm. The Mn porewater profile does not exhibit this and bears some resemblance to the porewater profile for two of the porewater profiles from Round Loch of Glenhead (Chapter 3, Figs. 3.9 and 3.11), in which the concentration also increases downcore. In Round Loch, however, there was an increase in the solid phase concentration with depth, providing a source for Mn dissolution from the base of the core. Since this is not observed in the solid phase profile for Loch Coire nan Arr, unequivocal interpretation of the solution phase Mn, in the light of the Fe profile, is not straightforward. The differences between the Fe and Mn porewater profiles, with a sub-surface peak in Fe and increasing Mn concentration with depth, has also been observed in the Santa Monica Basin of the Southern California Borderland (Shaw *et al.*, 1990), where it was attributed to compression of the profiles so that evidence of the Mn reduction zone was eliminated, while the Fe reduction zone was much more pronounced.

Lead, zinc and copper partitioning data

Pb was not detectable in fractions I and III, but is mainly associated (and to a similar extent) with fractions IV and V (Table 7.10, Fig. 7.7). The profile shapes of the two fractions are alike and the concentrations in the respective fractions are slightly less than 50% of the sum of concentrations in all fractions, with Pb in fraction II comprising the remainder of the total Pb removed by the sequential extraction scheme. Downcore concentrations of Pb in fractions IV and V vary, as do the acid digest concentrations, previously explained by historical changes in anthropogenic Pb emissions.

Zn was removed mainly in fraction V (Table 7.10, Fig. 7.8), a peak of 20 mg kg^{-1} occuring in the surface section (0-1 cm), below which there is a gradual increase to 11-12 cm, perhaps a result of ZnS formation with depth. The increase in Zn in

sequentially extracted Pb concentrations (mg kg^{-1})
depth (cm)
0
5
10
15
0
20
40
60
fraction
I
II
III
IV
V
sum
(I–V)

Pb (mg kg^{-1})
depth (cm)
0
5
10
15
0
20
40
60
acid digest

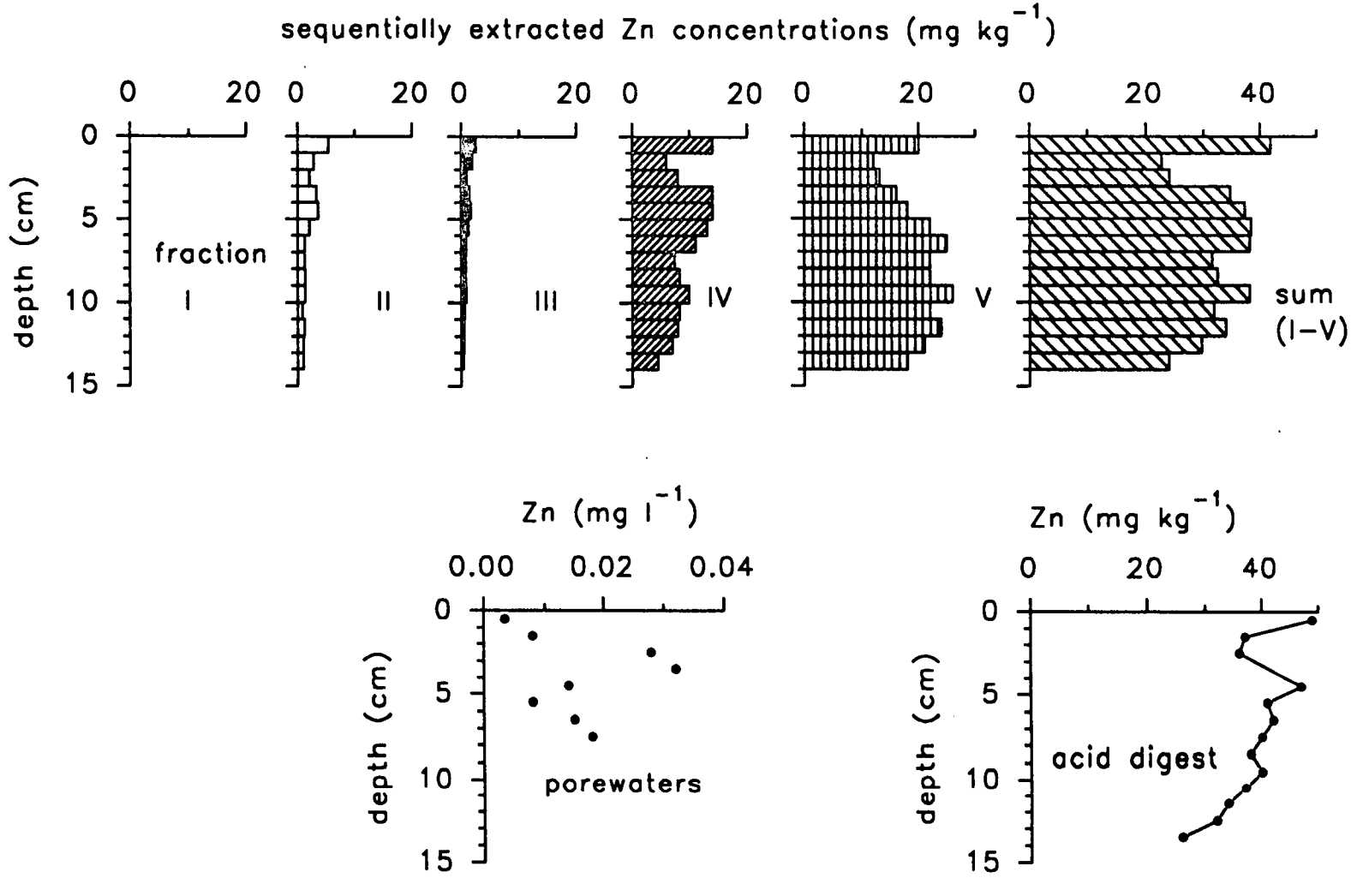
sequentially extracted Zn concentrations (mg kg^{-1})
0 20
0 20
0 20
0 20
0 20
0 20 40
depth (cm)
0
5
10
15
fraction
I
II
III
IV
V
sum
(I–V)
Zn (mg l^{-1})
0.00 0.02 0.04
depth (cm)
porewaters
Zn (mg kg^{-1})
0 20 40
depth (cm)
acid digest

fraction V with depth contrasts with the pattern in fraction IV, showing decreasing Zn concentrations from 4 cm downcore. The concentrations in the sum of fractions I-V are similar to the acid digested concentrations implying little or no Zn in resistant mineral lattices. The enhancement in the 0-1 cm section is due to Zn in both fractions IV and V and this suggests a link between post-depositional Zn mobility and Fe cycling, since the surface Fe peak was also observed in fractions IV and V.

Cu was only detectable in fraction V (Table 7.11) with a maximum of 8.2 mg kg^{-1} in the surface (0-1 cm) section. Apart from this section,where the acid digest concentration is higher (14 mg kg^{-1}), the concentrations in fraction V are similar to those obtained by sediment acid digestion. The surface peak in fraction V may be partly due to release of Cu from biogenic material as it is buried and degraded, followed by rapid reassociation with undegraded organic matter at the surface and, to account for the higher peak in the acid digested sediment, perhaps also reassociation with oxides/hydroxides of Mn or Fe.

Zinc solution phase data

Zn porewater concentrations range from a minimum at the surface (0-1 cm) of 0.004 mg l^{-1} to a maximum of 0.032 mg l^{-1} at 3-4 cm. The peak at 3-4 cm implies release of Zn from the solid to solution phase at this depth, which could be due to a change in redox conditions and upwards and downwards diffusion of Zn in the porewaters, as implied for Fe by the porewater profile. Together with the sequential extraction data, which, in fraction IV (moderately reducible, Fe oxides/hydroxides) clearly exhibit low concentrations between 1 and 3 cm, above the maximum in the porewater profile (3-4 cm), and an enhancement in the surface section, coincident with the minimum porewater concentration, this strongly suggests that Zn release and short-range mobility results from the redox-related process controlling the cycling of Fe. While this has apparently not completely obscured the historical record of Zn pollution to the area, the remobilisation of Zn would cause a damping of Zn concentrations below the surface layer, which contains enhanced Zn levels not attributable to changes in the atmospheric input of pollutant Zn. The peak observed in the surface of the Cd profile is probably explicable in the same manner as Zn, which is geochemically similar.

The Pb partitioning data show that fraction IV is more important for Pb than Zn, although for both metals, fractions IV and V are the predominant fractions. This implies that processes controlling their behaviour are similar and contrasts with the situation at Round Loch of Glenhead. The slight Pb enhancement in fraction IV from 0-1 cm, overlying depleted concentrations to 3 cm, indicates that although solution

phase Pb was below the detection limit, Fe cycling may, to a limited extent, also be influencing the Pb profile. Further evidence pointing to this conclusion is the resemblance between the stable Pb and ^{210}Pb concentration profiles above 3 cm, with a minimum at 1-2 cm and a slight surface enhancement.

7.5 Conclusions

1. ^{210}Pb data indicate mixing of sediment to a depth of 3 cm, but a sedimentation rate of 16.4 ± 2.4 mg cm^{-2} y^{-1} is obtained from results for sections below the mixing zone. A relatively high estimated ^{210}Pb flux of 168 Bq m^{-2} y^{-1} reflects the high annual rainfall at this site.

2. Radiocaesium information supports the conclusions made for the ^{210}Pb results, indicating partial sediment mixing. The weapons testing fallout peak correlates well to the date of atmospheric deposition maximum in weapons testing fallout, using the ^{210}Pb-derived sedimentation rate and if mixing is taken into account. Radiocaesium is detectable in sediment from the deepest sampled section, corresponding to a ^{210}Pb-based date of 1900 and providing evidence of some diffusional and/or mixing mobility of radiocaesium at this site.

3. Radiocaesium inventories estimated for fallout from Chernobyl and weapons testing agree with literature values for inventories from the two sources for this area.

4. Redox cycling dominates the Fe and Mn sedimentary solid phase profiles. Solution phase Fe concentrations support this, but interpretation of the Mn solution phase concentrations is not straightforward. Co, and probably Ni, also appear to be affected by the redox cycling of Fe and/or Mn, but other post-depositional processes are also operating to cause sub-surface peaks in HNO_3/HCl acid digested Co and Ni concentration profiles. Additionally, Fe behaviour at the sediment-water interface is influenced by its association with organic matter, probably humic substances.

5. Pb, Zn and Cd show historical trends in the acid digested concentration profiles, generally agreeing with observed trends in Round Loch of Glenhead and Loch Lomond. Zn appears to be additionally influenced by the redox cycling of Fe, which is supported by both solid and solution phase results. The profile shape of Cd concentrations in the acid digested sediment bears a close resemblance to that of Zn, indicating that the same processes are controlling the behaviour of these metals. The observed similarity between the partitioning data for Pb and Zn and, significantly, the ^{210}Pb and stable Pb profiles above 3 cm, indicates that some Pb may be released to the porewaters and reprecipitated at the sediment surface as a result of Fe cycling. However, there is no direct porewater evidence for this and changes in the stable Pb concentration profile below 3 cm are attributable to historical changes in pollutant Pb deposition, so any post-depositional Pb mobility must be short-range.

6. Cu does not show a noticeable historical trend and post-depositional processes involving organic-matter associations are implicated as the cause of a surface concentration enhancement.

Chapter 8 Summary and overview

8.1 Metal behaviour

The following section describes and compares the behaviour of metals in the five lochs sampled in terms of the processes, described in the Introduction (Chapter 1), which have been reported or suggested as playing important roles in determining metal behaviour in lakes.

8.1.1 Redox cycling

Iron and manganese

Evidence for redox-driven remobilisation and reprecipitation was found in the sediments of all lochs sampled, despite their different characteristics. This evidence includes Mn and Fe concentration enhancements in the acid digested surface sediments of cores from Loch Lomond, Loch Leven, Balgavies Loch and Loch Coire nan Arr. In addition, partitioning data in the sections of enhanced concentrations generally showed the prominence of Mn in fraction III (easily-reducible) and Fe in fraction IV (moderately reducible), representing the authigenic oxides and hydroxides of Fe and Mn. Fe was also often associated with fraction V (organics/sulphides) in the sections with enhanced concentrations and this was thought to be a result of organic matter associations, whereas an increase of Fe in fraction V with depth was more likely due to the formation of Fe sulphides in the sulphate reducing zone. In sediment sections below the peak Mn concentrations, an increase in Mn lability was generally indicated by an increase in the Mn concentrations of fraction I. Porewater Fe and Mn concentration profiles, however, were not always solely interpretable in terms of redox cycling.

In Balgavies Loch intense sediment mixing to the maximum sampled depth was evident from the radionuclide data. Here, the solid phase Mn concentration profile and, to a lesser extent, that of Fe, showed greater concentrations in the surface sediment, contrasting with the concentration profiles of the other metals and the radionuclides, which showed generally uniform concentrations downcore. The patterns in the Fe and Mn concentration profiles, interpretable in terms of redox-driven diagenesis, indicated that the rate of remobilisation and reprecipitation was greater than the sediment mixing rate. Porewater profiles of Fe and Mn in Balgavies Loch were explicable by redox conditions at the time of sampling, *i.e.* anoxic waters in the water immediately overlying the sediment, whereas the solid phase data had not been

changed sufficiently to reflect these conditions. This highlighted the importance of obtaining porewater data, which rapidly display the effects of a change in the sediment or overlying water.

Greater surface sediment enhancements of Mn in sediment collected from eutrophic Loch Leven during the summer, compared with autumn and winter sampling, were explained by influences of higher temperature, and high pH and dissolved oxygen concentrations due to the biological activity during the summer, causing increased Mn sedimentation. For the enhanced concentration to be maintained, the increased Mn sedimentation must outweigh releases of Mn from the sediment to the water column during the summer.

Fe enhancements in acid digested sediment were not as pronounced in Loch Leven and Balgavies Loch compared with other lochs, which was attributed to some seasonal release of Fe from the sediment to the water column in the former two lochs, as well as a significant amount of Fe associated with fractions not available for remobilisation. As previously found in the sediments of Loch Lomond, Fe and Mn were both influenced by redox cycling, giving rise to concentration enhancements in the surface, or near-surface, sediment. In acidified Round Loch of Glenhead surface peaks of Fe were observed in the acid digested sediment, attributable both to redox-related processes, as well as pH-related enhancement of Fe precipitation with humic substances (indicated by the importance of Fe in fraction V in the section containing the overall peak Fe concentration). In contrast, enhancement of Mn was only observed in the surface sediment of the core collected during the summer, and not in sediment from the winter sampling, which was thought to be a seasonal effect. Redox-related enhancements of Fe and Mn were also found in the surface sediments of Loch Coire nan Arr, with Fe being additionally influenced, as at Round Loch, by precipitation with humic substances, contributing to the surface concentration peak.

Lead

Pb was detected in fraction IV (moderately reducible) in the sediments of all the sampled lochs and, in Loch Lomond (central and southern basins), Balgavies Loch and Loch Leven, was primarily associated with fraction IV throughout the cores. The importance of fraction IV indicates an association of Pb with the oxides of Fe and could perhaps imply an influence of redox-driven Fe cycling on the behaviour of Pb. However, there was no direct evidence in any of the lochs for significant remobilisation of Pb. In all the lochs, Pb concentrations in the porewaters were either very low, or below the detection limit, and the observed lack of change downcore in the relative contributions of different fractions to the sum of all five fractions, both

support the conclusion that Pb is not remobilised. In the absence of any physical or biological reworking of the sediment, the sediment core should provide an intact historical record of Pb deposition at the sampled sites.

Zinc

In sediment from the southern basin of Loch Lomond, Zn was mostly associated with fraction III in the 0-2 cm depth range and the increase in Zn concentration in fraction I between 1 and 26 cm was similar to trends in the Mn partitioning data. However, despite the apparently greater lability of Zn relative to Pb, the porewater data were not explicable in terms of Zn mobility associated with Mn cycling. The solid phase Zn concentration profile was more reasonably interpretable in terms of historical trends in anthropogenic inputs of Zn to the loch (Section 8.2). In the central basin sediments of Loch Lomond, Zn was most concentrated in fraction IV, but again, no supporting evidence from porewater data was found for redox-related cycling.

Zn was predominantly associated with fractions IV and V in the sediments of Loch Coire nan Arr and patterns in the partitioning data were similar to those observed for Fe. The porewater Zn concentration trends were also analogous to those of Fe, strongly suggesting that Zn release and short-range mobility was caused by the redox-related processes controlling the cycling of Fe. This however, had not completely obscured the historical record of atmospheric Zn pollution in the area.

Sub-surface peaks in the porewater concentrations of Zn in Balgavies Loch, in the same sections as those observed for Fe and Mn, and a slight change in Zn partitioning data below 2 cm, with higher Zn concentrations in fractions II and III, implied minor release of Zn from the solid phase, followed by short-range mobility.

Zn was detectable in all fractions in the sediment of Loch Leven, but was mainly associated with fraction V and showed no influence from the Fe and Mn redox-cycling, nor was there any evidence for this in Round Loch of Glenhead.

Copper, cadmium, cobalt and nickel

Cu was predominantly associated with fraction V (organic/sulphides) in the sediments from the five lochs, indicating the importance of organic matter associations for this element. A peak Cu concentration in the surface sediment of Loch Coire nan Arr was thought to be caused by post-depositional processes involving organic-matter associations. The similarity between porewater Cu concentrations and Fe and Mn concentrations suggested some post-depositional mobility associated with redox cycling, but there was no evidence from the partitioning data for this.

Cd concentrations in acid digested sediment were often near the detection limit and in Loch Lomond, Round Loch of Glenhead, Balgavies Loch and Loch Leven there was no evidence of redox-related mobility. This contrasted with Loch Coire nan Arr, where the similarity between the Cd and Zn concentration profiles, with a peak concentration in the surface sediment, and the evidence of short-range Zn mobility, related to Fe redox cycling, suggested that, to some extent, Cd too was affected by redox cycling at this site.

Co and Ni concentrations in acid digested sediment generally did not vary significantly downcore and, of all of the lochs sampled, Loch Coire nan Arr was the only one in which the behaviour of Co, and possibly Ni, was associated with the redox cycling of Fe and/or Mn.

8.1.2 Acidification

Iron and manganese

Surface water acidification has influenced the behaviour of Mn in the sediments of Round Loch of Glenhead, where an increase in solid phase Mn with increasing depth was observed. This pattern was not seen in the profiles of any of the other sampled lochs, but has been reported in other acid lakes, where it has been attributed to post-depositional leaching of Mn from the surface sediment by acidified surface waters or alternatively, to a pH-related decrease in the efficiency of Mn sedimentation. The data obtained from Round Loch suggested that both these mechanisms have influenced the Mn profile. The prominence of Fe in fraction V (organic/sulphides) in the enhanced surface section in Round Loch of Glenhead provided evidence that in addition to redox-related processes, deposition of Fe with humic substances is an important process and may well be an effect of surface water acidification since it has been reported to be more pronounced under acidic conditions. Concentrations of Fe in the surface sediment of Round Loch were enhanced to a much greater extent (relative to underlying concentrations) than Mn concentrations. This was not found in any of the other lochs (where Mn enhancements were more pronounced than those of Fe) and is probably a reflection of the effect of acidification on the two metals, with greater Mn solubility and a pH-related increase in the precipitation of Fe with humic substances.

Lead, zinc, copper, cadmium, cobalt and nickel

While the concentrations of Zn and Cd in the acid digested sediment of Round Loch of Glenhead show sub-surface enhancements which are broadly explicable in terms of historical pollution trends, as for Pb and Cu (Section 8.2), the sharply

decreasing concentrations of Zn and Cd towards the surface were explained by a pH-related decrease in the efficiency of Zn (and Cd) deposition to the sediment. Additionally, the importance of Zn in fraction V (organic/sulphides) in the zone of greater Zn concentrations, suggested an influence of downward diffusion of Zn from the water column to the sediment to form ZnS in the enhanced concentration zone.

There was no evidence of an effect of acidification on the behaviour of Pb, Cu, Co or Ni in either of the sites sampled in Round Loch of Glenhead.

8.1.3 Eutrophication

Iron and manganese

As discussed in Section 8.1.1, Fe and Mn both showed evidence of redox cycling in eutrophic Loch Leven and the greater surface enhancement in Mn concentration during the summer, relative to the autumn and winter, was attributed to the effects of the algal bloom. In Balgavies Loch, also nutrient-enriched, there was no direct evidence of effects on the behaviour of Fe and Mn, specifically attributable to eutrophication. However, deoxygenation of the bottom waters during stratification, which was found to influence the redox cycling of Mn and Fe, is related to the biological oxygen demand of the water column and surface sediment and is therefore dependent on the productivity of the loch, so the eutrophication of Balgavies Loch indirectly affects the behaviour of Mn and Fe.

Lead, zinc, copper, cadmium, cobalt and nickel

Although the prominence of Zn and Cu in fraction V indicated the importance of organic matter associations in the sediments of both Loch Leven and Balgavies Loch, there was no obvious influence of eutrophication on the behaviour of Pb, Zn, Cu, Cd, Co or Ni.

8.2 Heavy metal inventories and historical trends

Inventories of the pollutant metals Pb, Zn, (Cd) and Cu were calculated by subtracting the 'background' concentrations (constant concentrations at depth in the sediment) from the total concentrations in HNO_3/HCl acid digested sediment and multiplying by the dry section weights before summing. These 'excess' inventories are listed, for each loch, in Table 8.1, although values for Loch Coire nan Arr are based on total concentrations, since the background concentration had not been reached at the maximum sampled depth.

Table 8.1 Pollutant 'excess' metal inventories

		Inventories ($g\ m^{-2}$)			
		Pb	Zn	Cu	Cd
Round Loch of Glenhead					
	site 1	4.34	1.93	0.25	0.014
	site 2	2.24	0.95	0.12	0.006
Loch Lomond	site 1	1.59	3.10	...	...
	site 2	5.4	11.5	0.38	0.03
Loch Leven 1		0.56	0.78	0.13	...
2		0.45	0.70	0.072	...
3		0.39	0.60	0.082	...
Balgavies Loch		0.47	0.84	0.18	
Loch Coire nan Arr (total inventories)		0.89	0.85	0.18	9.5×10^{-4}

Inventories for Loch Leven and Balgavies Loch are in good agreement, which is a reflection of their proximity and, therefore, in the absence of point source pollutant inputs, the similarity in atmospheric pollutant input. Values for Pb and Zn in Loch Coire nan Arr are slightly higher because of using total metal inventories, since this is a remote loch, situated in the north-west of Scotland, which would not be expected to receive high pollutant inputs. Pb and Zn inventories are highest in Loch Lomond (southern basin), which is probably a reflection of the closeness of Loch Lomond to populated areas. The lower values in the central basin can be explained by coarser-grained sediment at this site (also reflected in the differences between the radiocaesium inventories at the two sites). The pollutant Pb inventories for Round Loch of Glenhead are relatively high, due to the high levels of atmospheric pollution received by this remote loch. In particular, deposition of industrial pollutants from fossil fuel combustion has been significant in this area and has contributed greatly to the acidification of lochs in the region. Cu inventories ranged between (g m^{-2}) 0.072 (Loch Leven, winter sampling) and 0.38 (Loch Lomond, southern basin).

Trends of metal pollutant concentrations in acid digested sediment were dated using ^{210}Pb-derived chronologies in the southern basin of Loch Lomond, Loch Coire nan Arr and Round Loch of Glenhead. The trends showed broad agreement with historical changes in atmospheric pollution, with concentrations of Pb and Zn increasing from between the mid-18th and mid-19th centuries, related to the start of the Industrial Revolution. Concentrations of Pb and Zn decreased from ^{210}Pb-based dates of the 1960's and mid-1970's onwards, due to the reduction in fossil fuel combustion and, for Pb, in the use of alkyl lead additives in petrol. In Round Loch of Glenhead and Loch Lomond (southern basin), maximum Pb concentrations occurred earlier (1930's) than peaks in Loch Coire nan Arr (mid-1970's). The Pb maxima in the 1930's for Round Loch and Loch Lomond may be a result of different pollution sources received by these lochs (*e.g.* a greater importance of Pb due to industrial sources relative to petrol-derived Pb).

Cd concentration trends were similar to those of Zn in Round Loch, Loch Lomond and Loch Coire nan Arr, which is unsurprising in view of the similar geochemical behaviour of these two metals and the fact that they are often emitted by the same pollutant sources. Cu concentration trends in Loch Coire nan Arr did not reflect changes in atmospheric pollutant deposition, whereas in Round Loch patterns were similar to those for Pb. In Loch Lomond (southern basin), the onset of increase in Cu concentration occurred about 100 years later than the onset of increase in Pb and Zn concentration.

Intense sediment mixing, in sediment from the central basin of Loch Lomond,

Balgavies Loch and Loch Leven, implied by the radionuclide data, meant that metal concentration profiles could not be interpreted in terms of historical trends because of distortion of the concentration profiles and the impossibility of establishing a sediment chronology at these sites. Nevertheless, increased concentrations of Pb, Zn and Cu towards the surface of the cores in Loch Lomond and Loch Leven were probably a result of relatively recent atmospheric pollutant inputs. Supporting evidence for this was found in the central basin of Loch Lomond, where an approximate sedimentation rate was derived, using the radiocaesium data, and peak concentrations of Pb and Zn were dated to the mid-late 1960's, before concentrations decreased towards the sediment surface.

8.3 Radionuclide data

Information from sedimentary ^{210}Pb and radiocaesium concentrations showed that mixing was taking place in the sediments of all the lochs sampled. However, the extent of mixing varied; in Round Loch of Glenhead, Loch Coire nan Arr and the southern basin of Loch Lomond, the mixing was restricted to the uppermost layers of sediment and the rate of accumulation must have been more rapid than the mixing rate, because historical trends in the pollutant metal profiles were not significantly distorted. Sedimentation rates and core chronologies were determined using the CIC model (Chapter 1) below the mixed zones of the sediment. For Round Loch (site 1) and Loch Lomond (southern basin), sedimentation rates were consistent with published data. Intense sediment mixing was evident in cores from Balgavies Loch, Loch Leven and the central basin of Loch Lomond. Balgavies Loch and Loch Leven were sampled at water depths of less than 6 m, *i.e.* relatively shallow areas, probably contributing to the extent of mixing at these sites. Physical mixing due to wave action is much more probable at a shallow site than in deeper areas, in addition to bioturbation, which may be more pronounced in eutrophic systems (*i.e.* Balgavies Loch and Loch Leven), where the greater availability of autochthonous detritus could perhaps lead to more dense populations of burrowing organisms. Although the coring site in the central basin of Loch Lomond was at the same water depth as the southern basin sampling site, the proximity of the former to a road suggests that catchment disturbance (*e.g.* road building) may have caused sediment mixing.

Of the lochs sampled, the unsupported ^{210}Pb flux (Table 8.2) was highest for Loch Coire nan Arr and this value compared well with reported fluxes for Lochan Dubh, also in north-west Scotland, and for a peat core from North Uist in the Outer Hebrides, off the coast of north-west Scotland. In the southern basin of Loch

Lomond the ^{210}Pb flux was only slightly lower than for Loch Coire nan Arr, but more than twice that of the central basin of Loch Lomond, a finding attributable to the finer-grained sediment in the southern basin. Estimated radiocaesium inventories of fallout from Chernobyl and weapons testing (Table 8.3) show a wide range of values for each of the fallout sources in the five lochs. While these differences are, in part, due to different atmospheric fallout inputs at the locations of the lochs, they are also attributable to varying behaviour of radiocaesium in the different lake systems.

The low estimated Chernobyl radiocaesium in the sediments of Round Loch of Glenhead, compared with the high fallout deposition to the area (Table 8.3), is explicable by loss of radiocaesium from the loch by hydraulic flushing, resulting from inefficient deposition of radiocaesium to the sediment and/or post-depositional losses from the highly organic sediment to the water column. Radiocaesium was highly mobile via downwards diffusion at site 1 in Round Loch, obscuring historical trends in the fallout deposition from the two sources. The radiocaesium at site 2 exhibited less mobility, but nevertheless, as at site 1, ^{137}Cs penetrated to depths dated at long before the onset of use of nuclear weapons. In Round Loch of Glenhead, therefore, radiocaesium was not useful for dating the sediment.

In Loch Coire nan Arr the estimated radiocaesium inventories (Table 8.3) were in broad agreement with the reported deposition values for the two fallout sources and concentration peaks were attributable to fallout maxima. However, there was some evidence of radiocaesium movement, probably due to diffusion and/or mixing effects.

Radiocaesium was efficiently bound in the clay-rich sediments of Loch Lomond, indicated by the high ^{137}Cs inventories (Table 8.3), and peaks in the ^{137}Cs concentration profile due to weapons testing and Chernobyl fallout were clearly discernible. In the southern basin there was excellent agreement between ^{210}Pb-derived dates and the positions of the ^{137}Cs maxima derived from resolution of the two fallout sources.

While the ^{137}Cs inventories from the two fallout sources for Loch Leven (Table 8.3) agreed well with reported values for fallout deposition, indicating efficient binding in the clay-rich sediments, the historical trend had been obscured and there was evidence of downward movement of radiocaesium, both being a consequence of the intense mixing at this site. Similarly, the historical record of fallout ^{137}Cs deposition to the area had been distorted in Balgavies Loch due to sediment mixing and though the estimated Chernobyl ^{137}Cs inventory was within the range of reported fallout values, the calculated weapons testing inventory was low, probably because mixing had moved some of the ^{137}Cs to greater depths in the sediment than the maximum sampled depth.

Table 8.2 Unsupported ^{210}Pb fluxes calculated from ^{210}Pb inventories in sediment cores from the five sampled lochs

		unsupported ^{210}Pb flux ($Bq\ m^{-2}\ y^{-1}$)
Round Loch of Glenhead	site 1	95
	site 2	83
Loch Lomond	site 1	72
	site 2	152
Loch Leven		15
Balgavies Loch		49
Loch Coire nan Arr		168

Table 8.3 Estimated ^{137}Cs inventories of fallout from Chernobyl and weapons testing in the five sampled lochs, compared with reported deposition values (Clark and Smith, 1988; Peirson *et al.*, 1982; Baxter *et al.*, 1989)

		Inventories ($kBq\ m^{-2}$)			
		weapons testing fallout		Chernobyl fallout	
		calculated	reported	calculated	reported
Round Loch of Glenhead				4.68 ± 0.03 →	
	site 1	1.53 ± 0.05	2.8	5.13 ± 0.04	20-38
	site 2	1.20 ± 0.18	"	7.37 ± 0.12	"
Loch Lomond	site 1	10.22 ± 0.22	6-8	2.64 ± 0.05	1-5
	site 2	14.41 ± 0.10	"	6.85 ± 0.05	"
Loch Leven		1.46 ± 0.12	2.8	0.78 ± 0.06	0.1-1
Balgavies Loch		0.23 ± 0.08	"	2.68 ± 0.06	1-5
Loch Coire nan Arr		7.98 ± 0.08	2.8-6	0.13 ± 0.04 →	0.1-1
		→8.66 ± 0.11		0.52 ± 0.01	

Table 8.4 Main conclusions

	Round Loch of Glenhead		Loch Lomond		Loch Leven	Balgavies Loch	Loch Coire nan Arr
	site 1	site 2	central basin	southern basin			
Metal data							
Redox-driven diagenesis of Fe and Mn	yes	yes	yes	yes	yes	yes	yes
Redox-related remobilisation of other metals (Pb, Zn, Cu, Cd, Co, Ni)	no	no	no	no	no	ltd. mobility of Zn (related to Fe and/or Mn cycling)	ltd. mobility of Zn and Cd (related to Fe cycling) and Co (related to Mn cycling)
Effects of acidification on metal behaviour (Round Loch)	Mn concs. inc. with depth in sediment; enhanced precipitation of Fe with humics; sharply dec. concs. of Zn and Cd towards sediment surface;						
Effects of eutrophication on metal behaviour (Loch Leven and Balgavies loch)					enhanced precipitation of Mn in surface sediment	indirect effect of eutrophication on Mn and Fe, due to dexygenation of bottom water	
Pollutant metal inventories	high Pb inventory, due to deposition from fossil fuel combustion		Pb and Zn inventories lower than for site 2, due to coarser sediment at site 1	max. Pb, Zn and Cu inventories cf. all other lochs, reflects proximity to industrialised/ urban areas	similar Pb, Zn and Cu inventories, due to proximity of these lochs; relatively low inventories, due to situation on east coast of Scotland;		

Table 8.4 cont.

	Round Loch of Glenhead		Loch Lomond		Loch Leven	Balgavies Loch	Loch Coire nan Arr
	site 1	site 2	central basin	southern basin			
Historical trends	inc. in Pb, Zn and Cd concs. related to onset of Industrial Revolution; dec. concs. from 1960's-mid 1970's onwards; maximum Pb conc. in 1930's indicates industrial Pb sources > important cf. Loch Coire nan Arr;		historical interpretation not possible; inc. upcore concs. of Pb, Zn and Cu indicate input of pollutant metals	as for Round Loch	as for Loch Lomond, central basin	historical, interpretation not possible; no trends observed in sediment Pb, Zn, Cu and Cd concs.	as for Round Loch, except Pb conc. max. in mid-1970's: > importance of petrol-derived Pb
Radionuclide data							
Evidence of sediment mixing	partial mixing to 4cm (both sites)		intense mixing to 8cm	partial mixing to 6cm	intense mixing to at least 5cm	intense mixing to base of core (16cm)	partial mixing to 3cm
^{210}Pb-derived sedimentation rate (mg cm^{-2}y^{-1})	7.2-12.3 (12.3 found to be > appropriate)	8.0	could not be determined (intense mixing)	32.0	could not be determined (intense mixing)	could not be determined (intense mixing)	16.4
Evidence of radiocaesium movement in the sediment	yes, diffusive movement and historical trends obscured at site 1		yes, but separation of fallout peaks clear	yes, but ltd. and good agreement with historical fallout trends	yes, historical trends obscured	yes, historical trends obscured	yes, but weapons testing ^{137}Cs conc. profile related to historical fallout trends
calculated ^{137}Cs inventories relative to reported deposition values	Chernobyl (and weapons testing) ^{137}Cs inventories low cf. reported values, due to inefficient deposition of ^{137}Cs to organic-rich sediment and/or post-depositional loss from sediment, followed by loss from lake system		inventories from both sources within, or slightly > than, reported values; efficient binding of radiocaesium in clay-rich sediment		inventories from both sources within reported range; efficient binding of Cs in clay-rich sediment;	Chernobyl ^{137}Cs inventory within reported range; weapons inventory low due to sediment mixing;	broad agreeement of both inventories with reported values

8.4 Discussion of conclusions

The following Section is a discussion of the main conclusions of this study (summarised in Table 8.4) in the context of the findings of others, to illustrate the contribution made to knowledge in the research area.

Redox cycling

The redox cycling of Fe and Mn in lake systems is a well-established process (Mortimer, 1941, 1942; Davison *et al.,* 1982; Farmer and Lovell, 1986) and has been reported in lakes with pH values between 4.0 and 8.4 (Belzile and Tessier, 1990). This study has also shown that, despite the lake system diversity, redox related diagenesis of Fe and Mn occurs in all sampled lochs. However, there was only limited evidence of redox-related short-range mobility of other metals, followed by reprecipitation in Loch Coire nan Arr (Zn, Cd, Co and Cu) and Balgavies Loch (Zn). The lack of significant redox-related mobility of Zn, Cu and Cd in Round Loch of Glenhead, Loch Lomond, Loch Leven and Balgavies Loch (Cu and Cd) is consistent with findings in seasonally anoxic Esthwaite Water (Morfett *et al.,* 1988) and Lake Sammamish, Washington (Balistrieri *et al.,* 1992a, 1992b). In contrast, Co and Ni behaviour has been linked to seasonal changes in redox conditions (Balistrieri *et al.,* 1992a, 1992b; Shaw *et al.,* 1990).

The observed Pb immobility in the lochs sampled, agrees with the work of Crusius and Anderson (1989 and 1990) and Morfett *et al.* (1988). However, in some studies, Pb mobility has been linked to the diagenetic cycling of Fe (Gobeil and Silverberg, 1989) and, additionally, of Mn (Benoit and Hemond, 1990). The conclusion that Pb is not mobile in the sediments of the Scottish lochs sampled is therefore relevant to a subject where there is still some controversy and supports the fundamental assumption of Pb immobility in the use of ^{210}Pb for sediment dating (Krishnaswami *et al.,* 1971; Appleby and Oldfield, 1978).

Acidification

The increase in Mn concentration with depth in the sediments of acidified Round Loch of Glenhead has not been previously documented in the acidified lochs in Scotland. However, other studies have shown similar results, for example, in a Black Forest Lake (Steinberg and Högel, 1990), in Lake Gårdsjön, Sweden (Renberg, 1985) and in Clearwater Lake, Canada (Carignan and Nriagu, 1985). A decrease in the surface water pH of Darts Lake decreased deposition of Mn to the sediments (White and Driscoll, 1987b). The greater enhancement of Fe, relative to Mn, found

only in the surface sediment of Round Loch, agrees well with the work of Bendell-Young and Harvey (1992) who attributed this to a combination of redox-driven diagenesis and dissolution of the diagenetic Mn enhancement by acidic surface water in four lakes in Canada. The prominence of Fe in the organic phase of the surficial sediments of the same Canadian lakes (ibid.), due to a pH-related increase in the precipitation of Fe with humic substances (Tipping, 1981), was also found in the sediments of Round Loch.

The observed sharp decrease in Zn (and Cd) concentrations towards the surface of Round Loch of Glenhead sediments has been attributed to a reduction in anthropogenic Zn input (Battarbee *et al.*, 1989; Rippey, 1990), although the possibility of an influence of surface water acidification was not ruled out. Suggested mechanisms for the depletion of Zn and Cd in the surface sediments of acidified lakes include: post-depositional leaching of Zn and Cd from the sediment (Trefry and Metz, 1984; Arafat and Nriagu, 1986), less efficient transfer of particulate Zn to the sediment (Schindler *et al.*, 1980; Renberg, 1985) and downward diffusion of Zn from the water column to the sediment to precipitate as ZnS in a sub-surface zone of enhanced Zn concentration (Carignan and Tessier, 1985; Tessier *et al.*, 1989). In view of the possibility of in-situ alkalinity generation in the porewaters of acid lakes (Rudd *et al.*, 1986; Norton *et al*; 1990), post-depositional leaching of Zn and Cd from the sediment to the water column seems least likely and the latter two mechanisms were used to explain the more pronounced decrease in Zn and Cd concentrations, relative to Pb, towards the surface sediment of Round Loch.

Acidification has been reported to cause leaching of other metals from the sediment, such as Cu, Ni and Co (Schindler *et al.*, 1980; Arafat and Nriagu, 1986), but this was not apparent in Round Loch. The observed lack of effect of acidification on the behaviour of Pb in Round Loch is consistent with the laboratory experiments of Davis *et al.* (1982) and Trefry and Metz (1984) at pH values > pH 3 and > pH 4 respectively. Again, this finding is important with respect to the use of ^{210}Pb for sediment dating.

Eutrophication

The high pH and oxygen conditions, associated with an algal bloom, causing enhanced deposition of Mn to the surface of eutrophic Loch Leven sediments, were thought to cause Mn nodule formation in eutrophic, freshwater Lake Oneida, New York (Dean and Greeson, 1979; Dean *et al.*, 1981) and enhanced fluxes of Mn to sediment traps during the summer in Lake Windermere (Hamilton-Taylor, 1984). Reynolds and Hamilton-Taylor (1992) found that algal cycling influenced the transfer

of Zn to the sediments, but had little effect on the cycling of Cu. While no obvious effect of eutrophication on Pb, Zn, Cu, Cd, Co or Ni was found during this study, further work on these metals in the water column would be useful (Section 8.5).

Historical trends and inventories

The broad agreement between dated Pb, Zn and Cd concentration trends in Round Loch, Loch Lomond (southern basin) and Loch Coire nan Arr, and historical changes in atmospheric pollution, is consistent with published trends of Pb and Zn concentrations in sediment from other sites in Round Loch (Battarbee *et al.*, 1989; Rippey, 1990) and of Pb, Zn and Cd concentrations in the southern basin of Loch Lomond (Farmer *et al.*, 1980; Baxter *et al.*, 1981; Sugden *et al.*, 1991a). Calculated 'excess' inventories for Pb, Cu and Cd and pollutant fluxes of Pb, Zn and Cd in Loch Lomond (southern basin) in this study were similar to those reported for a sediment core collected from a nearby site (Farmer *et al.*, 1980) and atmospheric deposition fluxes of Pb, Zn and Cd to the Clyde Sea area (Cambray *et al.*, 1975). The decreases in Pb, Zn and Cd concentrations since the 1960's-1970's observed in sediment from Round Loch, Loch Lomond (southern basin) and Loch Coire nan Arr are consistent with global historical trends of decreasing pollutant inputs of these metals to the atmosphere, reflected in Greenland snows (Boutron *et al.*, 1991) and, for Pb, in peats and loch sediments from Scotland, using Pb isotope ratios (Sugden, 1993).

Radionuclide data

Radiocaesium mobility and the low ^{137}Cs inventories for Chernobyl and weapons testing fallout in the organic-rich sediments of Round Loch are consistent with various studies showing mobility of radiocaesium in sediments with a low clay content (Evans *et al.*, 1983; Davis *et al.*, 1984; Torgersen and Longmore, 1984). In contrast, the efficient binding of radiocaesium by clay-rich sediments (Benes *et al.*, 1989; Petersen *et al.*, 1990) was reflected in the general agreement between reported fallout deposition values and calculated ^{137}Cs inventories for both fallout sources in Loch Lomond (southern basin) and Loch Leven, and for Chernobyl-derived ^{137}Cs in Balgavies Loch. In the southern basin of Loch Lomond, the excellent agreement between ^{137}Cs peaks, separated into the two fallout sources, and ^{210}Pb-derived dates of fallout deposition maxima, supports the findings of Pennington *et al.* (1973) and Edgington *et al.* (1991), who found that ^{137}Cs-derived sedimentation rates closely matched rates obtained using ^{210}Pb data.

8.5 Suggestions for future work

1. Further sampling within each lake system to determine the variability of conditions within the lochs; Sampling of other acidified lochs in the vicinity of Round Loch of Glenhead; Water column studies on eutrophic systems, before, during and after an algal bloom, to establish effects of algal cycling on metals - possible use of sediment traps for this.
2. Fine resolution sediment sectioning (<5mm intervals) to increase detail in metal concentration profiles; More porewater sampling, using the glovebox method, which proved to be the most reliable technique in this study.
3. Determination of further elements in the samples collected, *e.g.* alkali metals, to establish whether changes in the rate of catchment erosion have occurred, and other pollutant metals, such as V and Hg.
4. Further characterisation of the sediment: mineralogy (*e.g.* by X-ray diffraction), grain size (*e.g.* by laser granulometry) and differentiation between organic and inorganic carbon.

References

ALLOTT T.E.H., HARRIMAN R. and BATTARBEE R.W. (1992) Reversibility of lake acidification at the Round Loch of Glenhead, Galloway, Scotland. *Environ. Pollut.* **77**, 219-225.

ANDERSON J.M. (1981) *Ecology for Environmental Sciences: Biosphere, Ecosystems and Man (Resource and Environmental Science Series).* Edward Arnold Publishers.

ANDREAE M.O. (1986) Chemical species in seawater and marine particulates. In: *Speciation in environmental processes.* (eds. M. Bernhard, F.E. Brinckman, and P.T. Sadler) Dahlem Konferenzen, Springer Verlag.

APPLEBY P.G. and OLDFIELD F. (1978) The calculation of ^{210}Pb dates assuming a constant rate of supply of unsupported ^{210}Pb to the sediment. *Catena* **5**, 1-8.

APPLEBY P.G. and OLDFIELD F. (1983) Assessment of ^{210}Pb from sites with varying sediment accumulation rates. *Hydrobiol.* **103**, 29-35.

APPLEBY P.G., OLDFIELD F., THOMPSON R. and HUTTUNEN P. (1979) ^{210}Pb dating of annually laminated lake sediments from Finland. *Nature* **280**, 53-54.

APPLEBY P.G., RICHARDSON N., NOLAN P.J. and OLDFIELD F. (1990) Radiometric dating of the UK SWAP sites. *Phil. Trans. R. Soc. Lond.* B. **327**, 233-238.

ARAFAT N. and NRIAGU J.O. (1986) Simulated mobilization of metals from sediments in response to lake acidification. *Wat. Air Soil Pollut.* **31**, 991-998.

BAILEY-WATTS A.E. and KIRIKA A. (1987) A reassessment of phosphorus inputs to Loch Leven (Kinross, Scotland): rationale and overview of results on instantaneous loadings with special reference to runoff. *Trans. Roy. Soc. Edin.: Earth Sciences* **78**, 351-367.

BAILEY-WATTS A.E., MAY L. and KIRIKA A. (1991) *Nutrients, phytoplankton and water clarity in Loch Leven following phosphorus loading reduction.* Final report to the Scottish Development Department.

BALISTRIERI L.S., MURRAY J.W. and PAUL B. (1992a) The cycling of iron and manganese in the water column of Lake Sammamish, Washington. *Limnol. Oceanogr.* **37**, 510-528.

BALISTRIERI L.S., MURRAY J.W. and PAUL B. (1992b) The biogeochemical cycling of trace metals in the water column of Lake Sammamish, Washington: Response to seasonally anoxic conditions. *Limnol. Oceanogr.* **37**, 529-548.

BATTARBEE R.W. (1988) The Acidification of Scottish Lochs. *Chapter 9, Symposium Proceedings, 8. Nov. 1988, Scottish Development Department, Edinburgh.*

BATTARBEE R.W., STEVENSON A.C. and RIPPEY B. (1985) Lake acidification in Galloway: a palaeoecological test of competing hypotheses. *Nature* **314**, 350-352.

BATTARBEE R.W., STEVENSON A.C., RIPPEY B., FLETCHER C., NATKANSKI J., WIK M. and FLOWER R.J. (1989) Causes of lake acidification in Galloway, south-west Scotland: A palaeoecological evaluation of the relative roles of atmospheric contamination and catchment change for two acidified sites with non-afforested catchments. *J. Ecol.* **77**, 651-672.

BAXTER M.S., COOK G.T. and MCDONALD P. (1989) *An assessment of artificial radionuclide transfer from Sellafield to south-west Scotland, United Kingdom.* D.O.E. Report No. DOE/RW/89/127. UK Department of the Environment, London.

see Corrigenda, page 365

BAXTER M.S., CRAWFORD R.W., SWAN D.S. and FARMER J.G. (1981) ^{210}Pb dating of a Loch Lomond sediment core by conventional and particle track methods and some geochemical observations. *Earth Planet. Sci. Lett.*, **53**, 434-444.

BELZILE N., LECOMTE P. and TESSIER A. (1989) Testing readsorption of trace elements during partial chemical extractions of bottom sediments. *Environ. Sci. Technol.* **23**, 1015-1020.

BELZILE N. and TESSIER A. (1990) Interactions between arsenic and iron oxyhydroxides in lacustrine sediments. *Geochim. Cosmochim. Acta* **54**, 103-109.

BENDELL-YOUNG L.I. and HARVEY H.H. (1992) Geochemistry of Mn and Fe in lake sediments in relation to lake acidity. *Limnol. Oceanogr.* **37**, 603-613.

BENDELL-YOUNG L.I., HARVEY H.H., DILLON P.J. and SMITH P.J. (1989) Contrasting behaviour of manganese in the surficial sediments of thirteen south-central Ontario lakes. *Sci. Tot. Environ.* **87/88**, 129-139.

BENES P., LAMRAMOS P. and POLIAK R. (1989) Factors affecting interaction of radiocaesium with freshwater solids. I. pH, composition of water and the solids. *J. Radioanal. Nucl. Chem. Articles* **133**, 359-376.

BENOIT G. and HEMOND H.F. (1990) ^{210}Po and ^{210}Pb remobilisation from sediments in relation to iron and manganese cyling. *Env. Sci. Technol.* **24**, 1224-1234.

BERNER R.A. (1980) *Early Diagenesis - A Theoretical Approach.* Princeton University Press.

BOUTRON C.F., GÖRLACH U., CANDELONE J-P., BOLSHOV M.A. and DELMAS R.J. (1991) Decrease in anthropogenic lead, cadmium and zinc in Greenland snows since the late 1960s. *Nature* **353**, 153-156.

BRINKHURST R.O., CHUA K.E. and BATOOSINGH E. (1969) Modifications in sampling procedure as applied to studies on the bacteria and tubificid oligochaetes inhabiting aquatic sediments. *J. Fish. Res. Bd Can.* **26**, 2581-2593.

CALVERT S.E. (1974) Distribution of bottom sediments in Loch Leven, Kinross. *Proc. Roy. Soc. Edin.* B **74**, 69-80.

CAMBRAY R.S., JEFFERIES D.F. and TOPPING G. (1975) *An estimate of the input of atmospheric trace elements into the North Sea and the Clyde Sea (1972-3).* AERE-R 7733. HMSO, London.

CAMBRAY R.S., PLAYFORD K. and LEWIS G.N.J. (1982) *Radioactive fallout in air and rain: Results to the middle of 1981.* United Kingdom Atomic Energy Authority, Harwell Report AERE-R 10485. HMSO, London.

CAMPBELL P.G.C. and TESSIER A. (1989) Biological availability of metals in sediments: Analytical approaches. In: *Proc. 7th Internat. Conf. on Heavy Metals in the Environment.* **1**, 516-525.

CARIGNAN R. (1984) Interstitial water sampling by dialysis: methodological notes. *Limnol. Oceanogr.* **29**, 667-670.

CARIGNAN R. and NRIAGU J.O. (1985) Trace metal deposition and mobility in the sediments of two lakes near Sudbury, Ontario. *Geochim. Cosomochim. Acta* **49**, 1753-1764.

CARIGNAN R., RAPIN F. and TESSIER A. (1985) Sediment porewater sampling for metal analysis: a comparison of techniques. *Geochim. Cosmochim. Acta* **49**, 2493-2497.

CARIGNAN R. and TESSIER A. (1985) Zinc deposition in acid lakes: the role of diffusion. *Science* **228**, 1524-1526.

CLARK M.J. and SMITH F.B. (1988) Wet and dry deposition of Chernobyl releases. *Nature* **332**, 245-249.

COMANS R.N.J., MIDDELBURG J.J., ZONDERHUIS J., WOITTIEZ J.R.W., DE LANGE G.J., DAS H.A. and VAN DER WEIJDEN C.H. (1989) Mobilisation of radiocaesium in pore water of lake sediments. *Nature* **339,** 367-369.

CRAIB J.S. (1965) A sampler for taking short undisturbed marine cores. *J . Cons. perm. int. Explor. Mer.* **30**, 34-39.

CRANK J. (1956) *The mathematics of diffusion.* Clarendon Press, Oxford.

CRUSIUS J. and ANDERSON R.F. (1989) Resolving discordant ^{137}Cs and ^{210}Pb chronologies using laminated sediments and additional radionuclides. In: *Proc. 7th Internat. Conf. on Heavy Metals in the Environment.* **1**, 467-470. CEP, Edinburgh.

CRUSIUS J. and ANDERSON R.F. (1990) Immobility of ^{210}Pb in Black Sea sediments. *Geochim. Cosmochim. Acta* **55**, 327-333.

CULMO R.F. (1988) *Principle of operation - The Perkin-Elmer PE 2400 CHN elemental analyzer.* Perkin-Elmer Corporation, USA.

DAVE G. (1992) Sediment toxicity and heavy metals in eleven limed reference lakes of Sweden. *Wat., Air, Soil Pollut.* **63**, 187-200.

DAVIS R.B., HESS C.T., NORTON S.A., HANSON, D.W., HOAGLAND K.D. and ANDERSON D.S. (1984) ^{137}Cs and ^{210}Pb dating of sediments from soft-water lakes in New England (USA) and Scandinavia; a failure of ^{137}Cs dating. *Chem. Geol.* **44**, 151-185.

DAVISON W. (1985) Conceptual models for transport at a redox boundary. In: *Chemical Processes in Lakes* (ed. W. Stumm) 31-53. Wiley, New York.

DAVISON W., GRIME G.W., MORGAN J.A.W. and CLARKE K. (1991) Distribution of dissolved iron in sediment pore water at sub-millimetre resolution. *Nature* **352**, 323-324.

DAVISON W. and WOOF C. (1984) A study of the cycling of manganese and other elements in a seasonally anoxic lake, Rostherne Mere, UK. *Water Res.* **18**, 727-734.

DAVISON W., WOOF, C. and RIGG E. (1982) The dynamics of iron and manganese in a seasonally anoxic lake; direct measurement of fluxes using sediment traps. *Limnol. Oceanogr.* **27**, 987-1003.

DAVISON W., WOOF C. and TURNER D.R. (1982) Handling and measurement techniques for anoxic interstitial waters. *Nature* **295**, 582-583.

DEAN W.E. and GREESON P.E. (1979) Influences of algae on the formation of freshwater ferromanganese nodules, Oneida Lake, New York. *Arch. Hydrobiol.* **86**, 181-192.

DEAN W.E., MOORE W.S. and NEALSON K.H. (1981) Manganese cycles and the origin of manganese nodules, Oneida Lake, New York, USA. *Chem. Geol.* **34**, 53-64.

DESMET G. and SINNAEVE J. (eds.) (1992) *Evaluation of data on the transfer of radionuclides in the food chain: post-Chernobyl action.* CEC report EUR 12550.

DICKSON J.H., STEWART D.A., THOMPSON R., TURNER G., BAXTER M.S., DRNDARSKY N.D. and ROSE J. (1978) Palynology, palaeomagnetism and radiometric dating of Flandrian marine and freshwater sediments of Loch Lomond. *Nature* **274**, 548-553.

DREVER J.I. (1982) *The Geochemistry of Natural Waters.* Prentice-Hall Inc.

EDGINGTON D.N., KLUMP J.V., ROBBINS J.A., KUSNER Y.S., PAMPURA V.D. and SANDIMIROV I.V. (1991) Sedimentation rates, residence times and radionuclide inventories in Lake Baikal from ^{137}Cs and ^{210}Pb in sediment cores. *Nature* **350**, 601-604.

EDMONDSON W.T. (1974) Book review. *Limnol. Oceanogr.* **19**, 284-291.

EG & G ORTEC (1993) *Instruments and systems for nuclear spectroscopy.* EG & G Nuclear Instruments, Oak Ridge, USA.

EL-DAOUSHY F. (1990) ^{210}Pb chronology of the Scandinavian SWAP sites. *Phil. Trans. R. Soc. Lond.* B. **327**, 239-242.
EMERSON S. (1976) Early diagenesis in anaerobic lake sediments: chemical equilibria in interstitial waters. *Geochim. Cosmochim. Acta* **40**, 925-934.
EVANS S., ALBERTS J.J. and CLARK R.A. (1983) Reversible ion-exchange fixation of ^{137}Cs leading to mobilisation from reservoir sediments. *Geochim. Cosmochim. Acta* **47**, 1041-1049.
FARMER J.G. (1991) The perturbation of historical pollution records in aquatic sediments. *Environ. Geochem. Health* **13**, 76-83.
FARMER J.G. and LOVELL M.A. (1984) Massive diagenetic enhancement of manganese in Loch Lomond sediments. *Environ. Technol. Lett.* **5**, 257-262.
FARMER J.G. and LOVELL M.A. (1986) Natural enrichment of arsenic in Loch Lomond sediments. *Geochim. Cosmochim. Acta* **50**, 2059-2067.
FARMER J.G., SWAN, D.S. and BAXTER S. (1980) Records and sources of metal pollutants in a dated Loch Lomond sediment core. *Sci. Tot. Environ.* **16**, 131-147.
FERGUSSON J.E. (1990) *The heavy elements: chemistry, environmental impact and health effects*. Pergamon Press.
FLOWER R.J. and BATTARBEE R.W. (1983) Diatom evidence for recent acidification of two Scottish lochs. *Nature* **305**, 130-133.
FLOWER R.J., BATTARBEE R.W. and APPLEBY P.G. (1987) The recent palaeolimnology of acid lakes in Galloway, south-west Scotland: Diatom analysis, pH trends and the role of afforestation. *J. Ecol.* **75**, 797-824.
FLOWER R.J., CAMERON N.G., ROSE N., FRITZ S.C., HARRIMAN R. and STEVENSON A.C. (1990) Post-1970 water chemistry changes and palaeolimnology of several acidified upland lakes in the UK. *Phil. Trans. R. Soc. Lond.* B **327**, 427-433.
FÖRSTNER U. (1980) Cadmium in polluted sediments. In: *Cadmium in the environment, I. Ecological cycling* (ed. J.O. Nriagu). Wiley, New York.
FOSTER I.D.L., CHARLESWORTH S.M. and KEEN D.H. (1991) A comparative study of heavy metal contamination and pollution in four reservoirs in the English Midlands, UK. *Hydrobiol.* **214**, 155-162.
FRIEDLANDER G., KENNEDY J.W., MACIAS E.S. and MILLER J.M. (1981) *Nuclear and Radiochemistry*, 3rd ed. John Wiley and Sons, Inc.
FROELICH P.N., KLINKHAMMER G.P., BENDER M.L., LUEDTKE N.A., HEATH G.R., CULLEN, D. and DAUPHIN P. (1979) Early oxidation of organic matter in pelagic sediments of the eastern equatorial Atlantic: sub-oxic diagenesis. *Geochim. Cosmochim. Acta* **43**, 1075-1090.
GIBSON M.J. and FARMER J.G. (1986) Multi-step sequential chemical extraction of heavy metals from urban soils. *Environ. Pollut.* **11**, 117-135.
GOBEIL C. and SILVERBERG N. (1989) Early diagenesis of lead in Laurentian Trough sediments. *Geochim. Cosmochim. Acta* **53**, 1889-1895.
GOBEIL C., SILVERBERG N., SUNDBY B. and COSSA D. (1987) Cadmium diagenesis in Laurentian Trough sediments. *Geochim. Cosmochim. Acta* **51**, 589-596.
GUBALA C.P., ENGSTROM D.R. and WHITE J.R. (1990) Effects of iron cycling on ^{210}Pb dating of sediments in an Adirondack lake, USA. *Can. J. Fish. Aq. Sci.* **47**, 1821-1829.
HAMILTON-TAYLOR J., WILLIS M. and REYNOLDS C.S. (1984) Depositional fluxes of metals and phytoplankton in Windermere as measured by sediment traps. *Limnol. Oceanogr.* **29**, 695-710.
HARPER D.M. and STEWART W.D.P. (1987) The effects of land use upon water chemistry, particularly nutrient enrichment, in shallow lowland lakes: comparative studies of three lochs in Scotland. *Hydrobiol.* **148**, 211-229.

HEM J.D. (1972) Chemistry and occurrence of cadmium and zinc in surface water and groundwater. *Water Resources Res.* **8**, 661-679.
HERLIHY A.T. and MILLS A.L. (1986) The pH regime of sediment underlying acidified waters. *Biogeochem.* **4**, 377-381.
HESSLEIN R.H. (1976) An in-situ sampler for close interval pore water studies. *Limnol. Oceanogr.* **21**, 912-914.
HOLDEN A.V. and CAINES L.A. (1974) Nutrient chemistry of Loch Leven, Kinross. *Proc. Roy. Soc. Edin.* B **74**, 101-121.
HORRILL A.D., LOWE V.P.W. and HAWSON G. (1988) *Chernobyl fallout in Great Britain.* D.O.E. Report No. DOE/RW/88.101. UK Department of the Environment, London.
JONES V.J., STEVENSON A.C. and BATTARBEE R.W. (1989) Acidification of lakes in Galloway, south-west Scotland: a diatom and pollen study of the post-glacial history of the Round Loch of Glenhead. *J. Ecol.* **77**, 1-23.
KERSTEN M. and FÖRSTNER U. (1987) Effect of sample pre-treatment on the reliability of solid speciation data of heavy metals - implications for the study of early diagenetic processes. *Mar. Chem.* **22**, 299-312.
KHEBOIAN C. and BAUER C.F. (1987) Accuracy of selective extraction procedures for metal speciation in model aquatic sediments. *Anal. Chem.* **59**, 1417-1421.
KIRBY R.P. (1974) The morphological history of Loch Leven, Kinross. *Proc. Roy. Soc. Edin.* B **74**, 56-67.
KRISHNASWAMI S., LAL D., MARTIN J.M. and MEYBECK M. (1971) Geochronology of lake sediments. *Earth Planet. Sci. Lett.* **11**, 407-414.
LIKENS G.E. (1989) Acid rain and its effects on sediments in lakes and streams. *Hydrobiol.* **176/177**, 331-348.
LIVENS, F.R. (1991) Chemical reactions of metals with humic material. *Environ. Pollut.* **70**, 183-208.
LIVETT E.A. (1988) Geochemical monitoring of atmospheric heavy metal pollution: theory and applications. *Adv. Ecol. Res.* **18**, 65-92.
LODER T.C., LYONS W.B., MURRAY S., MCGUINNESS H.D. (1978) Silicate in anoxic porewater and oxidation effects during sampling. *Nature* **273**, 373-374.
LOVELL M.A. (1985) Arsenic cycling in the freshwater sediments of Loch Lomond and some analytical speciation studies of arsenic metabolism. PhD thesis, University of Glasgow.
L'VOV B.V. (1991) A personal view of the evolution of graphite furnace atomic absorption spectrometry. *Anal. Chem.* **63**, 924-931A.
MACKENZIE A.B. and SCOTT R.D. (1984) Some aspects of coastal marine disposal of low level liquid radioactive waste. *Nucl. Engineer* **25**, 110-122.
MACKENZIE A.B., SCOTT R.D., MCKINLEY I.G. and WEST J.M. (1983) *A study of long term (10^3-10^4y) elemental migration in saturated clays and sediments.* Rep. Fluid Processes Unit Inst. Geol. Sci., FLBU 83-6
MACKERETH F.J.H. (1969) A short core sampler for sub-aqueous deposits. *Limnol. Oceanogr.* **14**, 145-151.
MAHAN K.I., FODERARO T.A., GARZA T.L., MARTINEZ R.M., MARONEY G.A. and TRIVISONNO M.R. (1987) Microwave digestion techniques in the sequential extraction of Ca, Fe, Cr, Mn, Pb and Zn in sediments. *Anal. Chem.* **59**, 938-945.
MAITLAND P.S. (ed.) (1981) The ecology of Scotlands largest lochs: Lomond, Awe, Ness, Morar and Shiel. *Monographiae Biologicae* **44**, 253-283. Dr W. Junk Publishers, The Hague.
MAITLAND P.S., LYLE A.A. and CAMPBELL R.N.B. (1987) *Acidification and fish in Scottish lochs.* ITE, Grange-over-Sands, Cumbria.

MARTIN P., NIREL P. and THOMAS A.J. (1987) Sequential extraction techniques: Promises and problems. *Mar. Chem.* **22**, 313-341.
MASON C.F. (1981) *Biology of Freshwater Pollution.* Longman Group Ltd.
MAULOOD B.K. and BONEY A.D. (1980) A seasonal and ecological study of the phytoplankton of Loch Lomond. *Hydrobiol.* **71**, 239-259.
METCALFE E. (1987) *Atomic absorption and emission spectroscopy.* John Wiley and Sons, Inc.
MOORE J.W. (1991) *Inorganic contaminants of surface water - Research and Monitoring Priorities.* Springer Verlag.
MORFETT K., DAVISON W. and HAMILTON-TAYLOR J. (1988) Trace metal dynamics in a seasonally anoxic lake. *Environ. Geol. Water Sci.* **11**, 107-114.
MORGAN N.C. (1972) *Productivity studies at Loch Leven (a shallow nutrient rich lowland lake).* Proc. of the IBP-UNESCO Symposium on productivity problems of freshwaters, Kazimierz Dolny, Poland, 1970.
MORGAN N.C. and MCLUSKY D.S. (1972/73) A summary of the Loch Leven IBP results in relation to lake management and future research. *Proc. Roy. Soc. Edin.* B **74**, 407-416.
MORTIMER C.H. (1941, 1942) The exchange of dissolved substances between mud and water in lakes: I and II. III and IV. *J. Ecol.* **30**, 147-201.
MURRAY E. (1989) Heavy Metals and fallout radionuclides in Loch Leven sediments. BSc Honours project, University of Edinburgh.
MURRAY J. and PULLAR L. (1910) *Bathymetrical survey of the Scottish freshwater lochs.* Edinburgh: Challenger Office.
NITTROUER C.A., DeMASTER D.J., McKEE B.A., CUTSHALL N.H. and LARSEN I.L. (1983/1984) The effect of sediment mixing on ^{210}Pb accumulation rates for the Washington continental shelf. *Mar. Geol.* **54**, 201-221.
NG A. and PATTERSON C.C. (1981) Natural concentrations of lead in ancient Arctic and Antarctic ice. *Geochim. Cosmochim. Acta* **45**, 2109-2121.
NORTON S.A., KAHL J.S., HENRIKSEN A. and WRIGHT R.F. (1990) Buffering of pH depressions by sediments in streams and lakes. In: *Advances in Environmental Science. Acidic precipitation vol. 4, Soils, aquatic processes and lake acidification.* S.A. Norton, S.E. Lindberg and A.L. Page (eds.). Springer Verlag, New York.
NRIAGU J.O. (1979) Inventory of natural and anthropogenic emissions of trace metals to the atmosphere. *Nature* **279**, 409-411.
NRIAGU J.O. (1990) Global metal pollution. *Environment* **32**, 7-11, 28-33.
NRIAGU J.O. (1991) Human influence on the global cycling of trace metals. In: *Proc. 8th Internat. Conf. on Heavy Metals in the Environment.* **1**, 1-5. CEP, Edinburgh.
NRIAGU J.O. and COKER R.D. (1980) Trace metals in humic and fulvic acids from Lake Ontario sediments. *Environ. Sci. Technol.* **14**, 443-446.
NRIAGU J.O. and PACYNA J.M. (1988) Quantitative assessment of worldwide contamination of air, water and soils by trace metals. *Nature* **333**, 134-139.
OAKLEY C.A. (1975) *The second city.* Blackie, Glasgow.
OLDFIELD F. and APPLEBY P.G. (1984) Empirical testing of ^{210}Pb-dating models for lake sediments. In: *Lake sediments and environmental history.* (eds. E.Y. Haworth and J.W.G. Lund)
OLDFIELD F., APPLEBY P.G. and BATTARBEE R.W. (1978) Alternative ^{210}Pb dating: results from the New Guinea Highlands and Lough Earne. *Nature* **271**, 339-342.
OHNSTAD F.R. and JONES J.G. (1982) *The Jenkin Surface-Mud Sampler user manual.* Freshwater Biological Association Occasional Publication No.15.

PATRICK S., WATERS D., JUGGINS S. and JENKINS. A (eds.) (1991) *The United Kingdom Acid Waters Monitoring Network: Site descriptions and methodology report.* ENSIS publishing, London.

PEIRSON D.H., CAMBRAY R.S., CAWSE P.A., EAKINS J.D. and PATTENDEN N. (1982) Environmental Radioactivity in Cumbria. *Nature* **300**, 27-31.

PENNINGTON W., CAMBRAY R.S. and FISHER E.M. (1973) Observations on lake sediments using fallout ^{137}Cs as a tracer. *Nature* **242**, 324-326.

PETERSEN W., KNAUTH, H-D. and PEPELNIK R. (1990) Vertical distribution of Chernobyl isotopes and their correlation with heavy metals and organic carbon in sediment cores of the Elbe Esturary. *Sci. Tot. Environ.* **97/98**, 531-547.

PICKERING W.F. (1986) Metal ion speciation - soils and sediments (a review). *Ore Geol. Rev.* **1**, 83-146.

RENBERG I. (1985) Influences of acidification on the sediment chemistry of Lake Gårdsjön, SW Sweden. *Ecol. Bull.* **37**, 246-250.

REYNOLDS G.L. and HAMILTON-TAYLOR J. (1992) The role of planktonic algae in the cycling of zinc and copper in a productive soft-water lake. *Limnol. Oceanogr.* **37**, 1759-1769.

REYNOLDSON T.B. (1987) Interactions between sediment contaminants and benthic organisms. *Hydrobiol.* **149**, 53-66.

RIDGWAY I.M. and PRICE N.B. (1987) Geochemical associations and post-depositional mobility of heavy metals in coastal sediments: Loch Etive, Scotland. *Mar. Chem.* **21**, 229-248.

RIPPEY B. (1990) Sediment chemistry and atmospheric contamination. *Phil. Trans. R. Soc. Lond.* B **327**, 311-317.

ROBBINS J.A. (1982) Stratigraphic and dynamic effects of sediment reworking by Great Lakes zoobenthos. *Hydrobiol.* 611-622.

ROBBINS J.A., KREZOSKI J.R. and MOZLEY S.C. (1977) Radioactivity in sediments of the Great Lakes: Post-depositional redistribution by deposit-feeding organisms. *Earth Planet. Sci. Lett.* **36** 325-333.

RUDD J.W.M., KELLY C.A., ST. LOUIS V., HESSLEIN R.H., FURUTANI A. and HOLOKA M.H. (1986) Microbial consumption of nitric and sulfuric acids in acidified north temperate lakes. *Limnol. Oceanogr.* **31**, 1267-1280.

SAAR R.A.Q. and WEBER J.H. (1982) Fulvic acid: modifier of metal-ion chemistry. *Environ. Sci. Technol.* **16**, 510-516A.

SALOMONS W. and FÖRSTNER U. (1984) *Metals in the hydrocycle.* Springer Verlag.

SCHAFRAN G.C. and DRISCOLL C.T. (1990) Porewater acid/base chemistry in near-shore regions of an acidic lake (the influence of groundwater inputs). *Biogeochem.* **11**, 131-150.

SCHINDLER D.W., HESSLEIN R.H. and WAGEMANN R. (1980) Effects of acidification on mobilisation of heavy metals and radionuclides from the sediments of a freshwater lake. *Can. J. Fish. Aq. Sci.* **37**, 373-377.

SCOTT C. (1990) Phosphorus fractionation in lake sediments. BSc Honours project, University of Edinburgh.

SHAW T.J., GIESKES J.M. and JAHNKE R.A. (1990) Early diagenesis in differing depositional environments: The response of transition metals in porewaters. *Geochim. Cosmochim. Acta* **54**, 1233-1246.

SLACK H.D. (1954) The bottom deposits of Loch Lomond. *Proc. Roy. Soc. Edin.* B **65**, 213-238.

SMITH I.R. (1974) The structure and physical environment of Loch Leven, Scotland. *Proc. Roy. Soc. Edin.* B **74**, 81-100.

STEINBERG C.E.W. and HÖGEL H. (1990) Forms of metals in a sediment core of a severely acidified northern Black Forest lake. *Chemosphere* **21**, 201-213.

STUMM W. and MORGAN J.J. (1981) *Aquatic Chemistry - An introduction emphasising chemical equilibria in natural waters*, 2nd ed. John Wiley and Sons, Inc.

SUGDEN C.L. (1993) Isotopic studies of the environmental chemistry of lead. PhD thesis, University of Edinburgh.

SUGDEN C.L., FARMER J.G. and MACKENZIE A.B. (1991a) Isotopic characterisation of lead inputs and behaviour in recent Scottish freshwater loch sediments. In: *Proc. 8th Internat. Conf. on Heavy Metals in the Environment* **1**, 511-514. CEP , Edinburgh.

SUGDEN C.L., FARMER J.G. and MACKENZIE A.B. (1991b) Lead and $^{206}Pb/^{207}Pb$ profiles in ^{210}Pb-dated ombrotrophic peat cores from Scotland. In: *Proc. 8th Internat. Conf. on Heavy Metals in the Environment* **1**, 90-93. CEP, Edinburgh.

TESSIER A., CAMPBELL P.G.C. and BISSON M. (1979) Sequential extraction procedure for the speciation of particulate trace metals. *Anal. Chem.* **51**, 844-851.

TESSIER A., CARIGNAN R., DUBREUIL B. and RAPIN F. (1989) Partitioning of zinc between the water column and the oxic sediments in lakes. *Geochim. Cosmochim. Acta* **53**, 1511-1522.

TIPPING E. (1981) The adsorption of aquatic humic substances by Fe oxides. *Geochim. Cosmochim. Acta* **45**, 191-199.

TIPPING E. (1993) Modelling the competition between alkaline earth cations and trace metal species for binding by humic substances. *Environ. Sci. Technol.* **27**, 520-529.

TORGERSEN T. and LONGMORE M.E. (1984) ^{137}Cs diffusion in the highly organic sediment of Hidden Lake, Fraser Island, Queensland. *Aust. J. Mar. Freshw. Res.* **35**, 537-548.

TREFRY J.H. and METZ S. (1984) Selective leaching of trace metals from sediments as a function of pH. *Anal. Chem.* **56**, 745-749.

TROUP B.N., BRICKER O.P. and BRAY J.T. (1974) Oxidation effect on the analysis of iron in the interstitial water of recent anoxic sediments. *Nature* **249**, 237-239.

TUREKEKIAN K.K., NOZAKI Y. and BENNINGER L.K. (1977) Geochemistry of atmospheric radon and radon products. *Ann. Rev. Earth Planet. Sci.* **5**, 227-255.

WHITTAKER R.H. (1975) *Communities and Ecosystems*, 2nd ed. Macmillan, New York.

WHITE J.R. and DRISCOLL C.T. (1985) Lead cycling in an acidic Adirondack lake. *Environ. Sci. Technol.* **19**, 1182-1187.

WHITE J.R. and DRISCOLL C.T. (1987a) Zinc cycling in an acidic Adirondack lake. *Environ. Sci. Technol.* **21**, 211-216.

WHITE J.R. and DRISCOLL C.T. (1987b) Manganese cycling in an acidic Adirondack lake. *Biogeochem.* **3**, 87-103.

Appendix 1 Derived concentrations of ^{137}Cs from Chernobyl and weapons testing fallout sources in sediment cores from Round Loch of Glenhead, Loch Lomond, Loch Leven and Balgavies Loch

	^{137}Cs concentrations (Bq kg^{-1}) from the two fallout sources on respective sampling dates									
	Round Loch of Glenhead		Loch Lomond				Loch Leven		Balgavies Loch	
sediment	site 2		site 1		site 2					
depth (cm)	Chernobyl	weapons	Chernobyl	weapons	Chernobyl	weapons	Chernobyl	weapons	Chernobyl	weapons
0-1	1702 ± 29		318 ± 41	88 ± 41	943 ± 13		56 ± 6		185 ± 7	
1-2	3499 ± 49		321 ± 14	46 ± 14	1366 ± 8		88 ± 3		221 ± 6	
2-3	4566 ± 56		185 ± 19	69 ± 19	1482 ± 8		113 ± 4		213 ± 8	
3-4	1605 ± 23		82 ± 16	79 ± 16	627 ± 20	162 ± 20	64 ± 11	22 ± 11	219 ± 8	
4-5	800 ± 60	103 ± 62		127 ± 2	41 ± 22	581 ± 22	45 ± 21	24 ± 21	168 ± 44	59 ± 44
5-6	363 ± 63	188 ± 64		201 ± 2		931 ± 6		37 ± 3.7*	246 ± 8	
6-7	297 ± 57	87 ± 57		221 ± 1		869 ± 5		50 ± 3	282 ± 5	
7-8	184 ± 46	86 ± 47		180 ± 2		503 ± 4		50 ± 3	321 ± 9	
8-9	115 ± 5	77 ± 5		100 ± 2		224 ± 4		46 ± 3	184 ± 49	115 ± 49
9-10	76 ± 4	51 ± 4		32 ± 1		100 ± 3	22 ± 7	15 ± 7	279 ± 8	
10-11	62 ± 2	42 ± 2		13 ± 1		37 ± 2	24 ± 8	11 ± 8	253 ± 6	
11-12	48 ± 2	32 ± 2		6 ± 1		18 ± 3	18 ± 6	8 ± 7	200 ± 7	
12-13	31 ± 2	21 ± 2		2 ± 1		10 ± 3		20 ± 2	186 ± 5	
13-14	20 ± 2	13 ± 2				5 ± 2		12 ± 1	175 ± 8	
14-15	13 ± 2	9 ± 2				7 ± 3		17 ± 1	155 ± 8	
15-16								8 ± 2	144 ± 7	

1. For Round Loch of Glenhead site 1 and Loch Coire nan Arr, derived ^{137}Cs concentrations are not listed, as ^{137}Cs inventories for the two fallout sources are based on estimations described in the text (Sections 3.4.2 and 7.4.2 respectively).
2. For Round Loch of Glenhead site 2, a weapons testing radiocaesium component of 30% was assumed below a depth of 8 cm, as low count rates and associated high errors in the $^{134}Cs/^{137}Cs$ activity ratios below 8 cm prevented calculation by $^{134}Cs/^{137}Cs$ ratios.

* estimated value, based on the mean of ^{137}Cs concentrations in sections 4-5 cm and 6-7 cm and 10% error

Appendix 2 Grain size data for Round Loch of Glenhead sediment

Grain size analyses were carried out by laser granulometry[1] to determine any differences between sediment particle sizes at the two sites sampled in Round Loch of Glenhead.
The following experimental conditions were used:

sample size:	0.28g
run length:	60 seconds
fluid:	water
optical model:	Fraunhofer

Sediment sections were grouped into depth ranges of 2-6cm, 8-12cm and 16-20cm from cores RLG1-C (site 1) and RLG2-2A (site 2). The results are summarised below (presented graphically on p.362):

site and core code	sediment depth range (cm)	grain size			
		mean (μm)	median (μm)	mode (μm)	mean/median
site 1 RLG1-C	2-6	174	75.4	853	2.3
	8-12	167	66.9	853	2.5
	16-20	246	124	853	2.0
site 2 RLG2-2A	2-6	157	60.3	65.1	2.6
	8-12	233	107	853	2.2
	16-20	241	120	853	2.0

The results do not show any significant difference in sediment grain size from the two sites. The skewness towards high particle diameters, shown in the histograms, indicates that large diameter particles (> 400 μm, and possibly > 1000 μm, since the instrument could not measure sizes greater than 1000 μm) are present in all the samples. These large particles are probably a result of plant material (observed throughought the core during sediment sectioning) in the sediment and, since the skewness appears to distort the particle size distribution of inorganic material, further investigation of the sediment grain size and mineralogy would be necessary to identify any differences between the sediment types at the two sites.

[1]Thanks to A.Mennim (Geology Department, Edinburgh University) for grain size analysis

Appendix 2 cont.

Particle size distribution in Round Loch of Glenhead sediment from sites 1 and 2

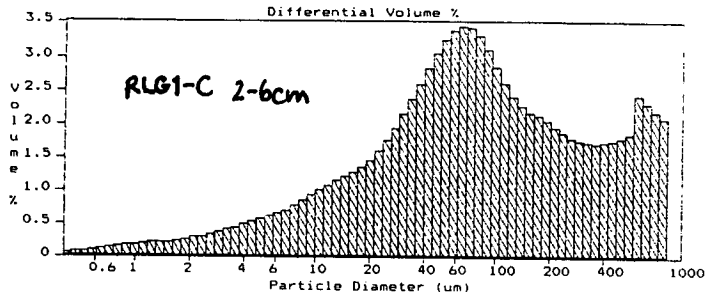

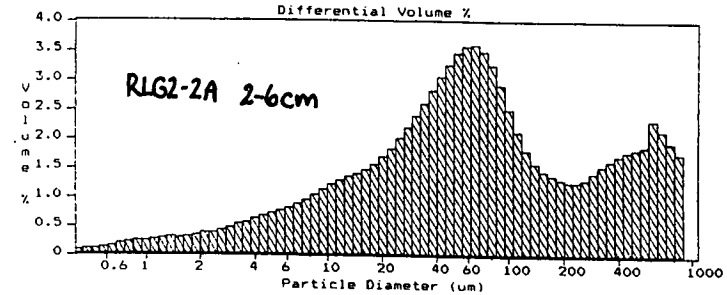

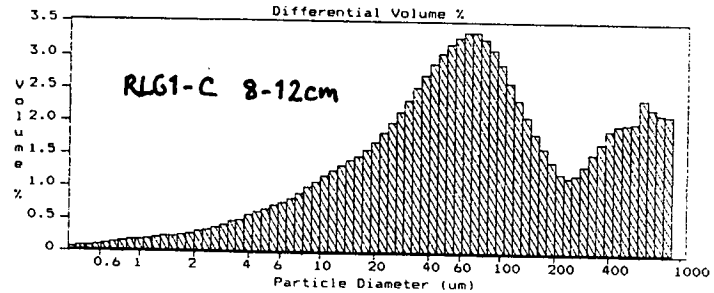

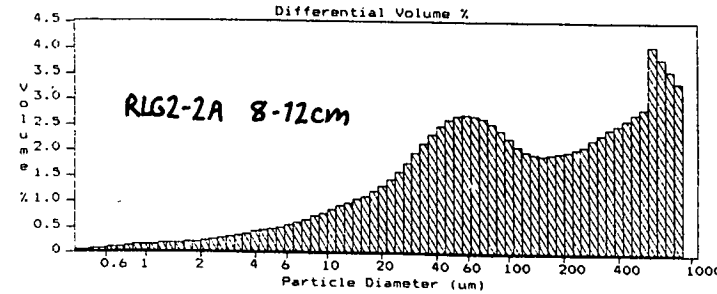

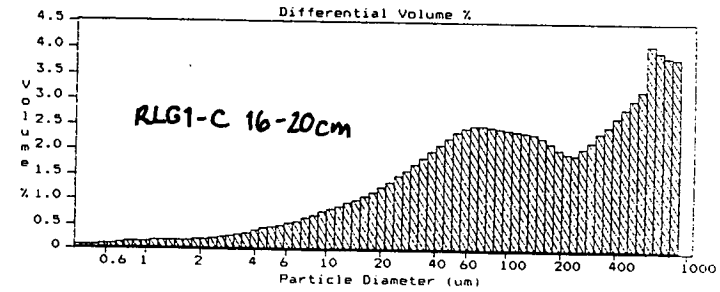

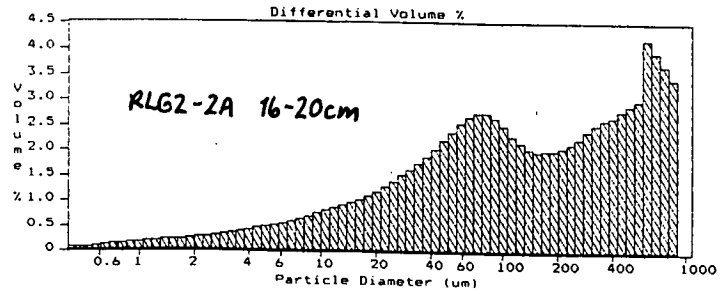

Lectures and conferences attended

Lectures

Final year environmental chemistry degree courses (1989-1990)

Analytical atomic absorption spectroscopy (4 lectures)

Sediments (3 lectures)

Radiochemistry (5 lectures)

COSHH regulations (Mr S. Luxen)

Health and safety and the law

New COSHH regulations

Applications of regulations to postgraduate research in chemistry

Chemistry department lectures, Edinburgh University

The development of substitutes for CFC's (Dr J. H. Steven, ICI Runcorn)

The sea as a waste-disposal site? (MAFF)

The role of RSC and the environment (Mr S. Luxen)

Dried, frozen or zapped? Detecting irradiated foods (Dr D. Sanderson, SURRC)

Health in the workplace (Dr . Robertson, IOM)

Metals, minerals and microbes: The biotechnology of metal extraction and recovery (Prof. M. Hughes, University of Columba)

Geology department lectures, Edinburgh University

CO_2, C flux, radiotracers - a new approach to an old problem (Dr G. Shimmield, Edinburgh University)

Conferences

SEGH (Society for Environmental Geochemistry and Health). Reading University, April 1990

Royal Society of Chemistry - Environmental radiation: Disposal of waste. Strathclyde University, 1990

Coger (Co-ordinating Group for Environmental Radioactivity)-London University (Royal Holloway and Bedford New College), December 1990

Postgraduate Palaeolimnology and Palaeoecology meeting - University College London, April 1991

Coger - Glasgow University, September 1991

8th International Conference on Heavy Metals in the Environment - Edinburgh, September 1991

SEGH - Edinburgh University, April 1992

Coger - Bangor University, September 1992

Publications

BRYANT C.L., FARMER J.G., MACKENZIE A.B., BAILEY-WATTS A.E. and KIRIKA A. (1991) The biogeochemistry of heavy metals in an acidified Scottish freshwater loch. In: *Proc. 8th Internat. Conf. on Heavy Metals in the Environmentt* **1**, 347-350. CEP , Edinburgh.

BRYANT C.L., FARMER J.G., MACKENZIE A.B., BAILEY-WATTS A.E. and KIRIKA A. (1993) Distribution and behaviour of radiocaesium in Scottish freshwater loch sediments. *Environ. Geochem. Health* **15**, 153-161.

Corrigenda

1. Page 8. Values for solubility products given by different authors for the same minerals are often considerably different, even of a few orders of magnitude (Stumm and Morgan, 1981). Reasons for this include: the composition and properties (*i.e.* reactivity) of the solids vary for different modifications of the same compound; species influencing the solubility equilibrium (*e.g.* species formed by complex formation) are overlooked (ibid.). The following are examples of solubility products (Log K) for some commonly occurring minerals (from Morel, 1983):

goethite	$\alpha FeOOH(s) + H_2O = Fe^{3+} + 3OH^-$	-41.5
rhodochrosite	$MnCO_3(s) = Mn^{2+} + CO_3^{2-}$	-10.4
siderite	$FeCO_3(s) = Fe^{2+} + CO_3^{2-}$	-10.7

Chemical speciation models may use such solubility data, for example to predict the fate/behaviour of metals within aquatic systems (Drever, 1982). However, their usefulness is limited by the variations in thermodynamic data, such as described above, and the difficulties in identifying and measuring all possible factors influencing equilibria, particularly measurement of the redox potential (ibid.).

2. Page 12. Mackereth (1965) reported that changes in the organic carbon content of sediment and alkali metal concentrations in long sediment cores (500 cm) from the Lake District were due to erosional changes in the catchments of lakes. Increases in mineral matter contents and potassium and sodium concentrations, with lower organic carbon contents were found to represent periods of greater erosion (ibid.).

3. Page 52, line 5-7 up should read: The corer is lowered into the water, causing the ball valves to lift and allowing water to escape from the anchor chamber.

4. Page 141. ....implies a higher sediment clay content at site 2, although initial grain size analyses did not confirm this and requires further investigation of sediment grain size and mineralogy.

5. **References**

ALLEN J.R.L., RAE J.E. and ZANIN P.E. (1990) Metal speciation (Cu, Zn, Pb) and organic matter in an oxic salt marsh, Severn Estuary, south-west Britain. *Mar. Poll. Bull.* **21**, 574-580.

DAVIS A.O., GALLOWAY J.N. and NORDSTROM D.K. (1982) Lake acidification: Its effect on lead in sediment of two Adirondack lakes. *Limnol. Oceanogr.* **27**, 163-167.

MOREL F.M.M. (1983) *Principles of aquatic chemistry*. John Wiley and Sons, Inc.

WETZEL R.G. (1975) *Limnology*. W.B. Saunders.